BERICHTE

aus dem MARUM und dem Fachbereich Geowissenschaften der Universität Bremen

No. 314

Bohrmann, G.,

Ahrlich, F., Bergenthal, M., Bünz, S., Düßmann, R,. Ferreira, Ch., Freudenthal, T., Fröhlich, S., Hamann, K., Hong, W.-L., Hsu, Ch.-W., Johnson, J., Kaszemeik, K., Kausche,A., Klein, T., Lange, M., Lepland, A., Malnati, J., Meckel, S., Meyer-Schack, B., Noorlander, K., Panieri, G., Pape, T., Reuter, M., Riedel, M., Rosiak, U., Schmidt, Ch., Schmidt, W., Seiter, Ch., Spagnoli, G., Stachowski, A., Stange, N., Wallmann, K., Wintersteller, P., Wunsch, D., Yao, H.

R/V MARIA S. MERIAN Cruise Report MSM57

Gas Hydrate Dynamics at the Continental Margin of Svalbard

Reykjavik – Longyearbyen – Reykjavik
29 July – 07 September 2016

Berichte, MARUM – Zentrum für Marine Umweltwissenschaften, Fachbereich Geowissenschaften, Universität Bremen, No. 314, 204 pages, Bremen 2017

ISSN 2195-9633

Berichte aus dem MARUM und dem Fachbereich Geowissenschaften der Universität Bremen

published by

MARUM – Center for Marine Environmental Sciences
Leobener Strasse, 28359 Bremen, Germany
www.marum.de

and

Fachbereich Geowissenschaften der Universität Bremen
Klagenfurter Strasse, 28359 Bremen, Germany
www.geo.uni-bremen.de

The "Berichte aus dem MARUM und dem Fachbereich Geowissenschaften der Universität Bremen" appear at irregular intervals and serve for the publication of cruise, project and technical reports arising from the scientific work by members of the publishing institutions.

Citation:

Bohrmann, G., Ahrlich, F., Bergenthal, M., Bünz, S., Düßmann, R,. Ferreira, Ch., Freudenthal, T., Fröhlich, S., Hamann, K., Hong, W.-L., Hsu, Ch.-W., Johnson, J., Kaszemeik, K., Kausche,A., Klein, T., Lange, M., Lepland, A., Malnati, J., Meckel, S., Meyer-Schack, B., Noorlander, K., Panieri, G., Pape, T., Reuter, M., Riedel, M., Rosiak, U., Schmidt, Ch., Schmidt, W., Seiter, Ch., Spagnoli, G., Stachowski, A., Stange, N., Wallmann, K., Wintersteller, P., Wunsch, D., Yao, H.: R/V MARIA S. MERIAN Cruise Report MSM57, Gas Hydrate Dynamics at the Continental Margin of Svalbard, Reykjavik – Longyearbyen – Reykjavik, 29 July – 07 September 2016. Berichte, MARUM – Zentrum für Marine Umweltwissenschaften, Fachbereich Geowissenschaften, Universität Bremen, No. 314, 204 pages. Bremen, 2017. ISSN 2195-9633.

An electronic version of this report can be downloaded from:
http://nbn-resolving.de/urn:nbn:de:gbv:46-MARUM9

Please place requests for printed copies as well as editorial concerns with reports@marum.de

BERICHTE AUS DEM MARUM UND DEM FACHBEREICH GEOWISSENSCHAFTEN
DER UNIVERSITÄT BREMEN

R/V MARIA S. MERIAN
Cruise Report MSM57

Gas Hydrate Dynamics at the Continental Margin of Svalbard

Reykjavik – Longyearbyen – Reykjavik
29 July – 07 September 2016

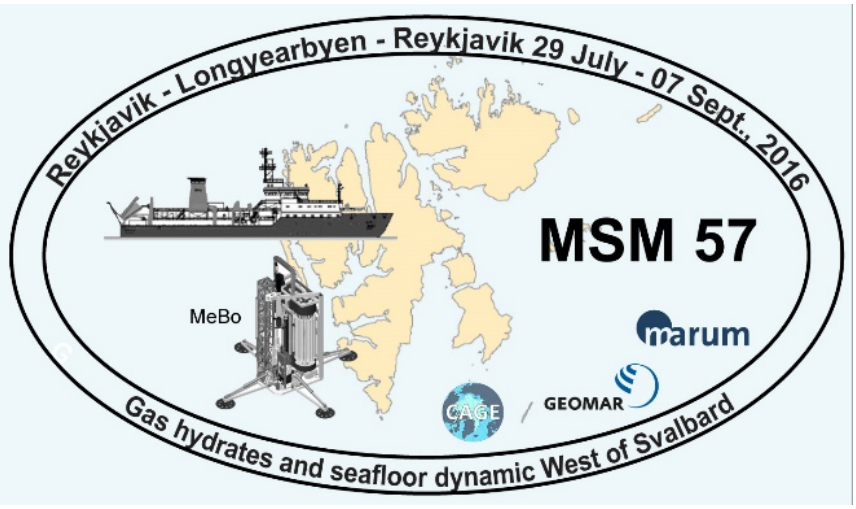

Cruise sponsored by Deutsche Forschungsgemeinschaft (DFG),
by MARUM,Center for Marine Environmental Sciences and by CAGE-Uit,
Centre for Arctic Gas Hydrate, Environment and Climate

Edited by
Gerhard Bohrmann and Greta Ohling
With contributions of cruise participants

marum

Universität Bremen

Table of Contents

1 Summary

Main objective during R/V MARIA S. MERIAN cruise MSM57 was to investigate gas hydrate systems and their dynamics at the continental margin of Svalbard. Gas hydrates have been documented by geophysical methods and by direct sampling in sediments of the margin. Samples have been retrieved from Vestnesa Ridge, an elongated sediment drift at the lower part of the continental margin. Along the crest of Vestnesa Ridge well defined chimney structures within a well-stratified sediment sequence and distinct pockmarks with active gas seepage were documented previously. Based on seismic 3D data six MeBo drill holes at three sites were performed inside and outside of the chimney structures in order to understand the distribution of gas hydrates. MeBo126 drilled a background sequence outside any influence of seepage down to 62.50 meter below seafloor. MeBo Holes 123, 124 and 125 drilled gas-hydrate-free sediments in the Lunde Pockmark, where no shallow disturbance in seismic data was observed. MeBo Holes 127, 128 and 138 were drilled at seep sites with high amplitude reflectors in seismic data. Seismic sections show gas invading from deeper along a faults zone to the south western part of the pockmark, rising to shallower levels as seabed gets shallower. Active gas emission was observed by acoustic flares in the water column. The high amplitude reflectors were drilled down to 23.95 mbsf and a sequence of gas-hydrate rich layers and seep carbonates were recovered, which seem to be typical for an active seepage environment. In addition, several gravity cores sampled shallow gas hydrates at Lunde and Lomvi Pockmarks and a series of heat flow measurements were performed over Vestnesa Ridge.

Drilling during Leg 2 was concentrated mostly at the uppermost part of the continental slope offshore Prins Karls Forland. Above the gas hydrate stability zone around 400 m water depth various methane emission sites were detected as acoustic plumes in echosounder recordings. One explanation interprets the methane emissions from hydrate decomposition due to a potential increase in water temperature of 1° C during the last 30 years. Such an increase of bottom water from 2° C to 3° C would cause a downward movement of the upper boundary of the gas hydrate stability of 38 m. Up to now no methane hydrates have been sampled in such shallow water depth off Svalbard and the hydrate melting hypothesis is highly questionable. In order to understand the hydrate dynamics of this depth interval between 300 – 500 m water depth 12 drill holes were performed at six sites between 340 m to 445 m water depth.

MeBo137 in 340 m water depth is located east of the gas flare accumulation isobaths and drilled glacigenic sediments down to 21.60 m. In 391 m three drill holes, MeBo133, 134 and 139, performed and drilled dropstone-rich diamictons down to 26.15 m. An authigenic carbonate layer was surprisingly intercalated at approximately 10 mbsf. Three sites were drilled around the upper boundary of the GHSZ. MeBo129-1 and -2 holes at 404 m water depth drilled up to 25.30 m glacigenic sediments. MeBo130, 131, 132 sampled sediments down to 20.30 m at 405 m water depth. MeBo140 was drilled 4 km north of the main seismic profile at 402 m water depth. Published seismic profiles have shown there bright-spot reflections which have been interpreted as gas-charged layers. The drilling could prove the free gas in 33.40 mbsf and sampled nearly 18 m of sediments. MeBo Holes 135 and 136 in 445 m water depth clearly drilled within the hydrate stability zone, however, methane hydrates have not been visually observed as it was the case for all drillings at the upper continental margin setting.

Additional to the Mebo drilling activities, 22 gravity cores have been taken, 11 T-lance deployments and seafloor mapping with PARASOUND and Multibeam EM122 was performed also at Svyatogor Ridge west of the Knipovich rift valley.

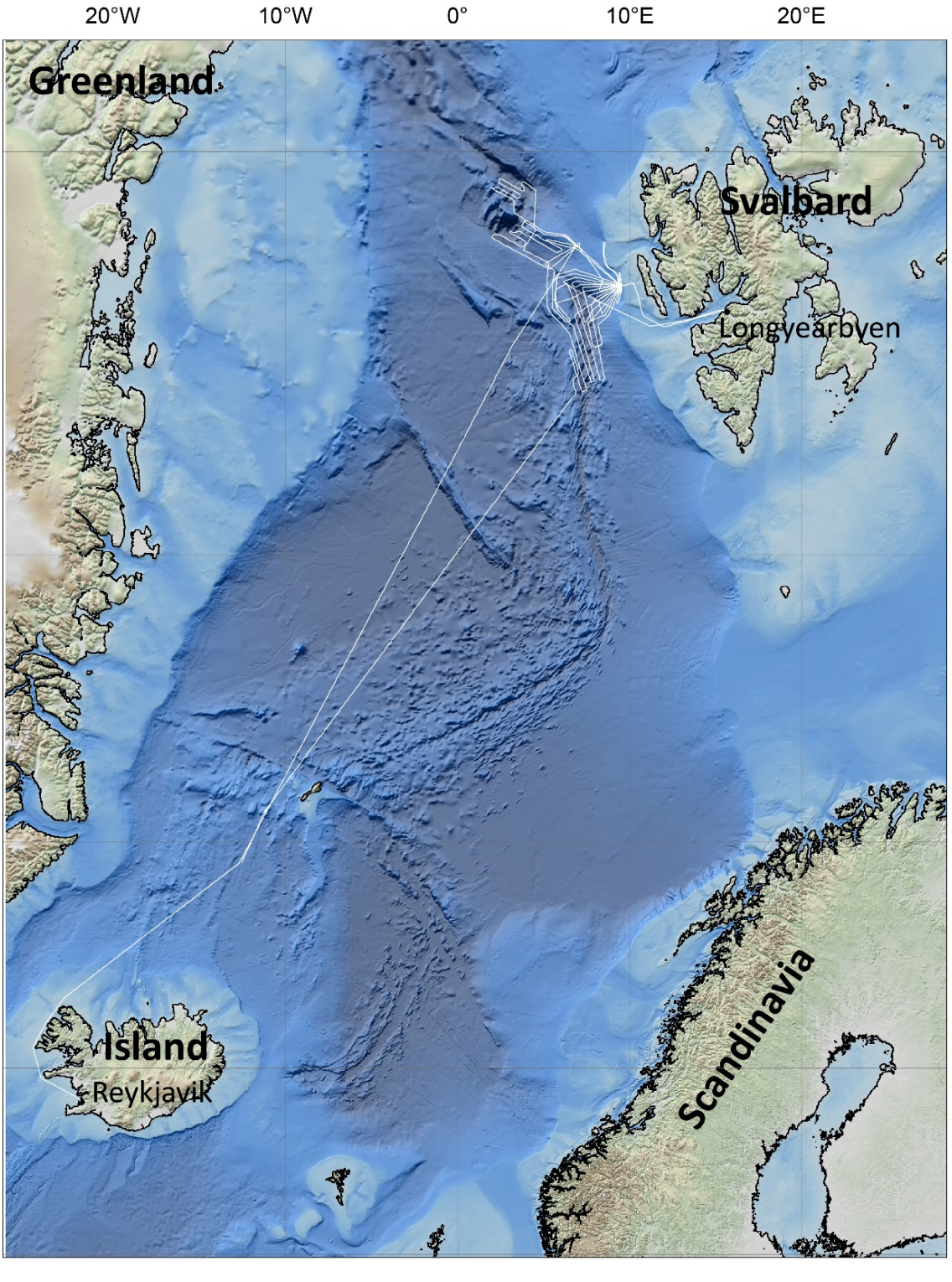

Fig. 1: Cruise track of R/V MARIA S. MERIAN Cruise MSM57 (29 July – 07 September 2016, Reykjavik – Longyearbyen - Reykjavik).

Fig. 2: R/V MARIA S. MERIAN at Ægisgarður Pier in the harbor of Reykjavik.

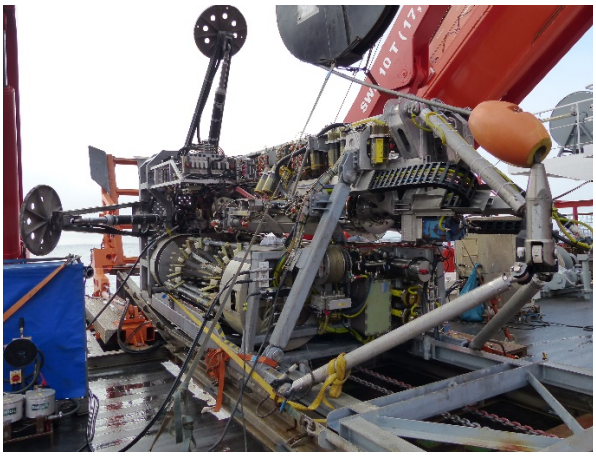

Fig. 3: The mobile drilling system MeBo onboard of R/V MARIA S. MERIAN .

Fig. 4: Heat flow lance from GEOMAR during its deployment during Cruise MSM57.

Fig. 5: Degassing of the autoclave core barrel (MDP) retrieved from MeBo drill site.

2 Participants

Table 1: Scientific crew

Name	Leg	Discipline	Affiliation
Ahrlich, Frauke	1+2	MeBo	MARUM
Bergenthal, Markus	2	MeBo	MARUM
Bohrmann, Gerhard	1+2	Co-chief scientist	FB5
Bünz, Stefan	1	Co-chief scientist	CAGE-UiT
Düßmann, Ralf	1+2	MeBo	MARUM
Ferreira, Christian	2	Data handling, hydroacoustics	FB5
Freudenthal, Tim	1	MeBo	MARUM
Fröhlich, Siefke	1	MeBo	MARUM
Hamann, Kristin	2	Pore water	GEOMAR
Hong, Wei Li	1+2	Pore water	CAGE-UiT
Hsu, Chieh Wei (Jeff)	1+2	Sediments, IR imaging	FB5
Johnson, Joel	2	Sediments	UoNH
Kaszemeik, Kai	2	MeBo	MARUM

Kausche,Arne	2	MeBo	MARUM
Klein, Thorsten	1	MeBo	MARUM
Lange, Mirko	2	Gas analyses	FB5
Lepland, Aivo	1	Sediments	CAGE-UiT
Malnati, Janice	1+2	Gas analyses	FB5
Meckel, Sebastian	2	MeBo	MARUM
Meyer-Schack, Birgit	2	Sediments, core handling	MARUM
Noorlander, Kees	2	MeBo	MARUM
Panieri, Giuliana	1	Sediments/stratigraphy	CAGE-Uit
Pape, Thomas	1	Autoclave sampling, gas analyses	FB5
Reuter, Michael	2	MeBo	MARUM
Riedel, Michael	1+2	Phys. props./T-Lance	GEOMAR
Rosiak, Uwe	1	MeBo	MARUM
Schmidt, Christopher	1+2	Pore water	GEOMAR
Schmidt, Werner	2	MeBo	MARUM
Seiter, Christian	1	MeBo	MARUM
Spagnoli, Giovanni	1	MeBo	Bauer
Stachowski, Adrian	1	MeBo	MARUM
Stange, Nikolas	2	MSCL, sediments	FB5
Wallmann, Klaus	2	Pore water	GEOMAR
Wintersteller, Paul	1	Hydroacoustics, GIS, IT	FB5
Wunsch, David	1	MeBo	Corsyde
Yao, Haoyi	1	Pore water	CAGE-UiT

MARUM Center for Marine and Environmental Sciences, DFG Research Center and Cluster of Excellence, University of Bremen, Postfach 330440, 28334 Bremen, **Germany**

FB5 Department of Geosciences, University of Bremen, Geo Building, Klagenfurter Str. 28359 Bremen, **Germany**

CAGE-UiT Centre for Arctic Gas Hydrate, Environment and Climate, Naturfagbygget, Dramsveien 201, 9010 Tromsø, **Norway**

GEOMAR Helmholtz-Zentrum für Ozeanforschung Kiel, Düsternbrooker Weg20/Wischhofstr. 1-3 , 24105 Kiel/24148 Kiel, **Germany**

Corsyde Corsyde International GmbH & Co. KG, Reuchlinstr. 10-11, 10553 Berlin, **Germany**

UoNH University of New Hampshire, Department of Earth Sciences, James Hall, 56 College Road, Durham, NH 03824, **U.S.A.**

Bauer BAUER Maschinen GmbH, Bauer-Str. 1, 86529 Schrobenhausen, **Germany**

Fig. 6: Scientific crew onboard R/V MARIA S. MERIAN during MSM57 Leg 1.

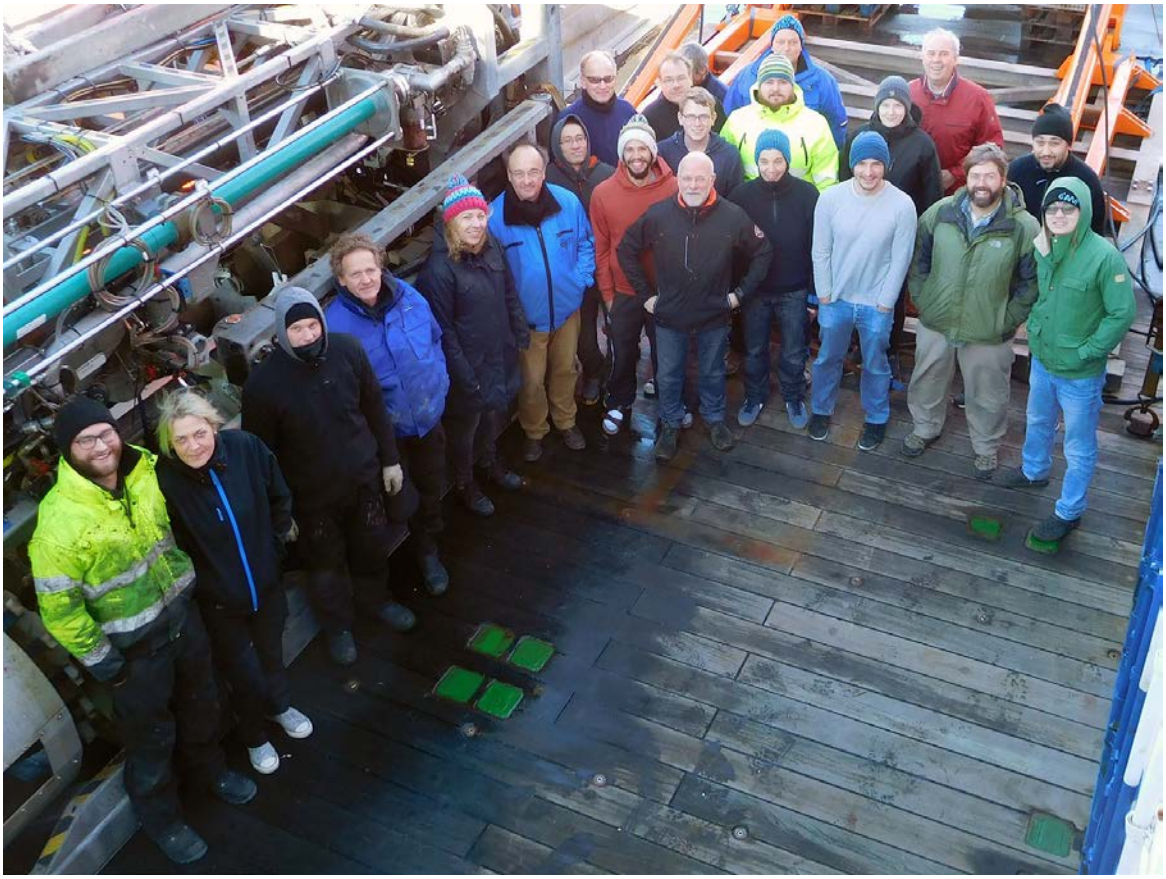

Fig. 7: Scientific crew onboard R/V MARIA S. MERIAN during MSM57 Leg 2.

Table 2: Crew members onboard.

Name	Discipline	Leg
Maaß, Björn	Master	1 + 2
Stegmaier, Eberhard	1st Officer	1 + 2
Griese, Theo	1st Officer	1 + 2
Janssen, Soeren	2nd Officer	1 + 2
Ogrognik, Thomas	Chief Engineer	1 + 2
Woltemade, David	2nd Engineer	1 + 2
Genschow, Steffen	3rd Engineer	1
Kasten, Stefan	3rd Engineer	2
Baumann, Frank	Electrician	1
Steffen, Martin	Electrician	2
Bauer, Boo	Ships doctor	1 + 2
Herrmann, Jens	Electronics	1 + 2
Maggiulli, Michael	System Operator	1 + 2
Wiechert, Olaf	Fitter	1 + 2
Sauer, Jürgen	Motorman	1 + 2
Bosselmann, Norbert	Bosun	1 + 2
Peschkes, Peter	Seaman	1 + 2
Peters, Karsten	Seaman	1
Vredenborg, Enno	Seaman	2
Papke, Rene	Seaman	1
		2
Wolff, Andreas	Seaman	1 + 2
Dembetzki, Torge	Seaman	1 + 2
Habel, Björn	Seaman	1 + 2
Bischeck, Olaf	Seaman	1 + 2
Arndt, Waldemar	Cook	1 + 2
Ennenga, Johan	2nd Cook	1 + 2
Seidel, Iris	Stewardess	1
Kluge, Sylvia	Stewardess	2

Shipping Operator: Briese Schiffahrts GmbH & Co KG, Abteilung Forschungsschifffahrt, Hafenstr. 12, 26789 Leer, **Germany**

3 Geological Setting of the Investigation Areas

3.1 Svalbard Continental Margin

The Norwegian-Svalbard continental margin is a highly dynamic area showing abundant evidence of fluid migration in the sediments, submarine mass wasting, normal faulting, hydrocarbon accumulation and sediment fan developing and gas hydrate formation (Vogt et al. 1999, Vanneste et al. 2005, Hustoft et al. 2009). This high-latitude gas hydrate accumulation area is dominated by major structural elements and underlain by young oceanic crust (Fig. 8). The Knipovich Ridge is a slowly and obliquely spreading northernmost extension of the Mid-Atlantic Ridge system, abutting the West-Svalbard margin in the Fram Strait (Thiede and Myhre, 1996). The presence of faults and rift escarpments further north suggest that the Knipovich Ridge is propagating as a buried feature. A series of transform faults like the Molloy Fracture Zone and short spreading centres, e.g. Molloy Ridge, ultimately connect the Knipovich Ridge with the Gakkel Ridge. Neotectonic activity is revealed by historical earthquakes and the earthquake loci are predominantly lined up along the active plate boundary (Vanneste et al. 2005). Deposited sediments on the western Svalbard margin are either glacigenic debris flows in trough-mouth fans beyond the shelf break or turbiditic, glaciomarine and hemipelagic sediments, in parts reworked by contour currents (Vorren et al. 1998). Vestnesa Ridge is a prominent ridge with fine-grained sediment drape on top, which is pierced by methane expulsions forming pockmarks on top (Petersen et al. 2010).

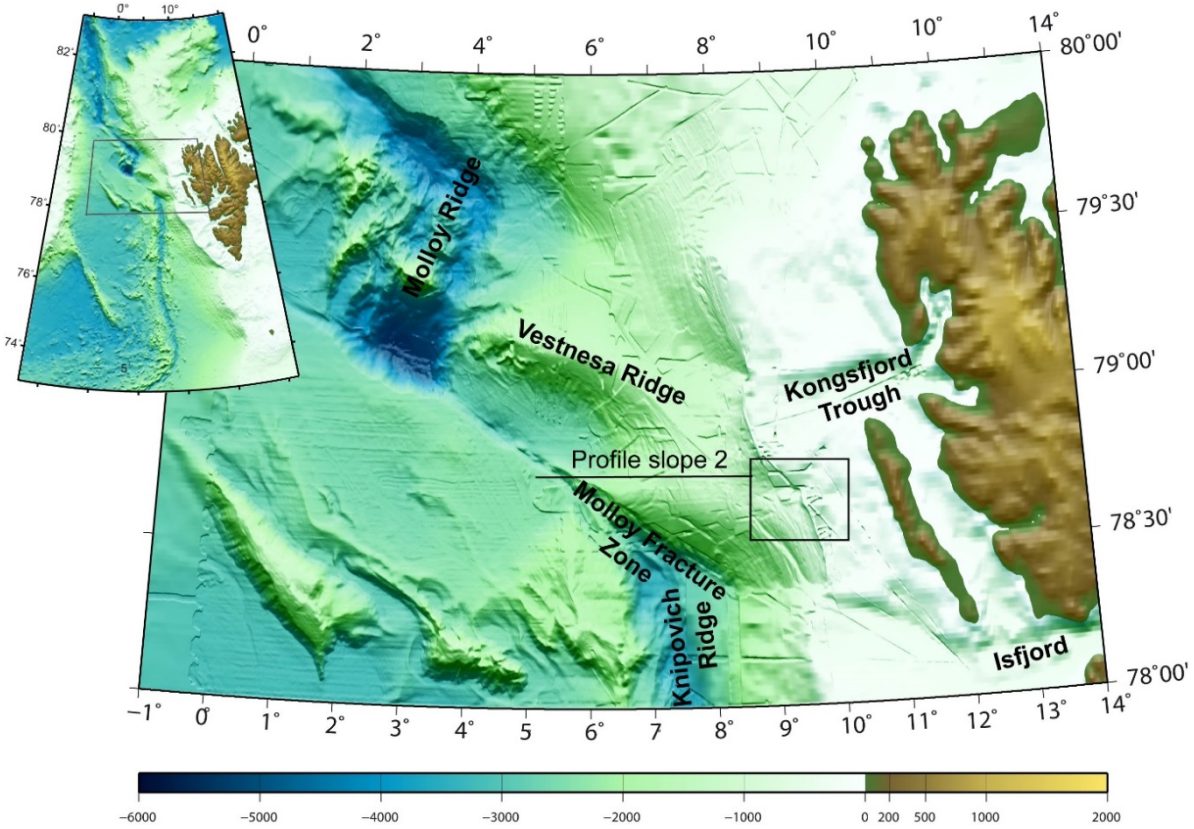

Fig. 8: Area of planned investigation (box) at the upper continental slope west of Spitsbergen. The location of seismic profile *slope 2* is also shown (bathymetry data are combined from AWI, NOC and IFM-GEOMAR).

The seismic profile *slope 2* (Figs. 8 and 9) crosses the ocean-continent transition and shows a prominent bottom seismic reflection from the upper slope at ca. 700 m water depth towards the Molloy Fracture Zone in approximately 2200 m water depth. Due to a higher heatflow close to the oceanic-continent transition the geothermal gradient is increasing towards the Molloy Fracture zone

which leads to a shallowing of the BSR instead a deepening, which should exist because of the higher hydrostatic pressure (Fig. 9). The BSR corresponds with a sharp drop in velocity, due to the presence of free gas in a 30 m thick interval underneath the BSR. The position of the BSR fits well with the base of the hydrate stability zone (BGHSZ), at the intersection of the methane hydrate phase boundary and the sub-bottom temperature (Vanneste et al. 2005). In shallower parts of the seismic line to the East the BSR is not seen (Fig. 9) which is also the case in all shallow seismic lines (Christian Berndt unpublished data). More recent calculations from seismic experiments predicts hydrate concentrations of up to 11% of pore space in a zone about 90 m-thick above the BSR, and an effective medium-based method predicts concentrations of up to 6%, if hydrate forms a connected framework, or 12%, if hydrate is both pore-filling and framework-forming (Westbrook et al. 2008).

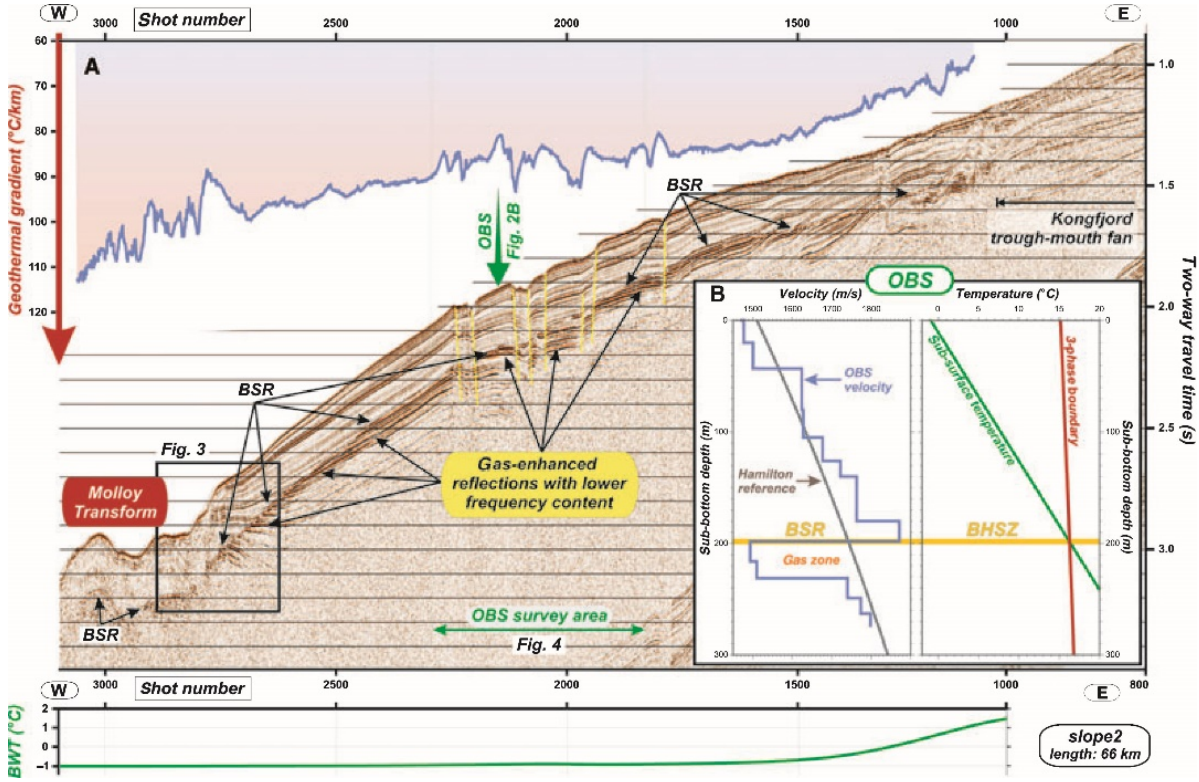

Fig. 9: Seismic reflection profile *slope 2* across the West Svalbard Margin (from Vanneste et al. 2005).

3.1.1 Vestnesa Ridge

The Vestnesa Ridge represents one of the northernmost gas hydrate provinces in the world. It is located on the western Svalbard margin in the eastern Fram Strait at ~79° N, north of the Knipovich Ridge (KR) and Molloy transform fault (MTF) (Fig. 10). The Vestnesa Ridge is a 100 km long submarine sediment drift situated on hot (>115 mW/m2) and relatively young (< 20 Ma) oceanic crust (Engen et al., 2008). The ridge elongates in a SE-NW (eastern segment) to EW (western segment) bending direction, where the crest of the ridge lies at 1200-1300 m water depth (Bünz et al., 2012; Plaza-Faverola et al., 2015).

A late Paleocene strike-slip along ancient shear zones marked the transition from a transpressional to an oblique divergent regime at ~36 Ma between Svalbard and northern Greenland (Engen et al., 2008). The separation of Svalbard from NE Greenland was initiated by the spreading and strike slip movements of the Arctic Gakkel Ridge along the W Svalbard shear zone during the Early Eocene. In addition to being compressive, the W Svalbard orogeny is a transpressive deformation with a dextral strike slip displacement between Greenland and Svalbard (Harland et al., 1997). In the Early Miocene,

sea floor spreading connected the North Atlantic mid-ocean ridge system (Mohns Ridge – Knipovich Ridge) with the Arctic Gakkel Ridge, causing the opening of the Fram Strait (Ritzmann and Jokat, 2003). The Fram Strait represents the final opening of the Atlantic-Arctic gateway, as a part of the non-glacial uplift and subsidence (Knies et al., 2014). An early shallow water connection existed through the Fram Strait during the late Oligocene (Jokat et al., 2008).

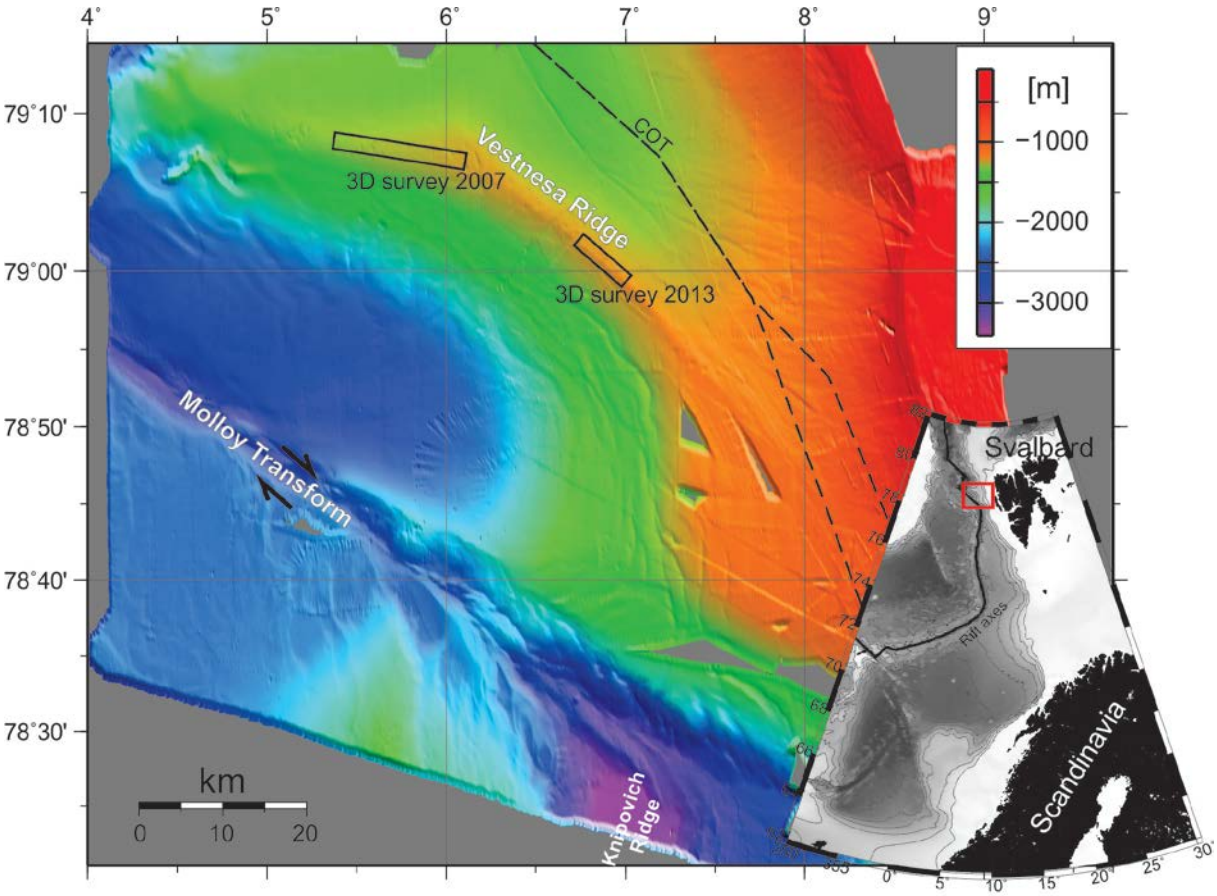

Fig. 10: Overview map of the Vestnesa Ridge area on the W-Svalbard margin. The two boxes indicate the location of high-resolution 3D seismic data.

There are two dominating sets of sediments on the western Svalbard margin; glacigenic debris flows in through mouth fans beyond the shelf break and turbiditic, glaciomarine and hemipelagic sediments, which are to some extent reworked by contour currents. During the Neogene, fast flowing ice-streams discarded thick glacial wedges from the western part of the shelf margin at the mouth of the cross-shelf troughs, forming delta-like extensions. The wedges are found to consist of stacks of glacial debris flow (Vorren and Laberg, 1997; Vorren et al., 1998). These large prograding wedges along the margin of the Atlantic-Arctic gateway region developed at ~2.7 Ma with the intensification of the northern hemisphere glaciation (Mattingsdal et al., 2013). At the W Barents Sea – Svalbard Margin this event occurred at a much later time, ~1.5 Ma (Andreassen et al., 2007b) when the Yermak Plateau was severely prone to glacial erosion.

The margins along the eastern flank of the Fram Strait were dominated by contourites during the late Miocene-Pleistocene (Mattingsdal et al., 2013). ODP sites at the Yermak Plateau showed that a major increase in sedimentation-rate occurred at ~2.7 Ma, which is attributed to the increase in glacial erosion at that time. Contour currents along the slope lead erosional sediments from the Barents Sea and Svalbard shelfs along the slope and deposit them in sediment drifts e.g. the Vestnesa Ridge

(Fohrmann et al., 2001). This sediment drift grows due to bottom-current controlled sediment dynamics (Eiken and Hinz, 1993). Several hundred meters of sediments are lying in close distance (40 km) to the 20 Ma young W-Svalbard margin, where the relatively warm and northward directed W-Spitsbergen current is shaping the morphology of the Vestnesa Ridge.

Eiken and Hinz (1993) established a three-sectioned sub-division of the eastern Vestnesa Ridge area: YP1, YP2 and YP3. YP1 is the unit at the bottom consisting of syn- and post-rift deposits. YP2 is mainly characterized by contourites, consisting of wedges thickening and down-lapping towards the west. Glacio-fluvial erosion during the latest Miocene – early Pliocene, deposited sandy sediments along the continental margin (Knies et al., 2014). The Plio-Pleistocene glaciations resulted in an unconformity between YP2 and the overlying YP3 unit. The boundary between the YP2 and YP3 units is dated to ~2.7 Ma by Knies et al. (2009), and represents the base of glacial deposits. The upper slope of YP3 mainly consists of glacial sediments in the Kongsfjorden through mouth fan. Howe et al. (2008) carried out sediment core analysis from the Vestnesa Ridge. The analysis revealed that Holocene sedimentation is dominated by muddy-silty contourites with abundant IRD (ice-rafted debris). This was deposited under the persistent flow of the West-Spitsbergen Current. The LGM (last glacial maximum) was dominated by silty turbidites, resulting from increased sediment supply. The mid-Weichselian section displayed both turbidites and contourites with abundant IRD. Further, Howe et al. (2008) calculated sedimentation rates at the Vestnesa Ridge to be 105 cm/kyr during the Mid to Late Weichselian and a decrease to <10 cm/kyr during the interval between the LGM to the Early Holocene.

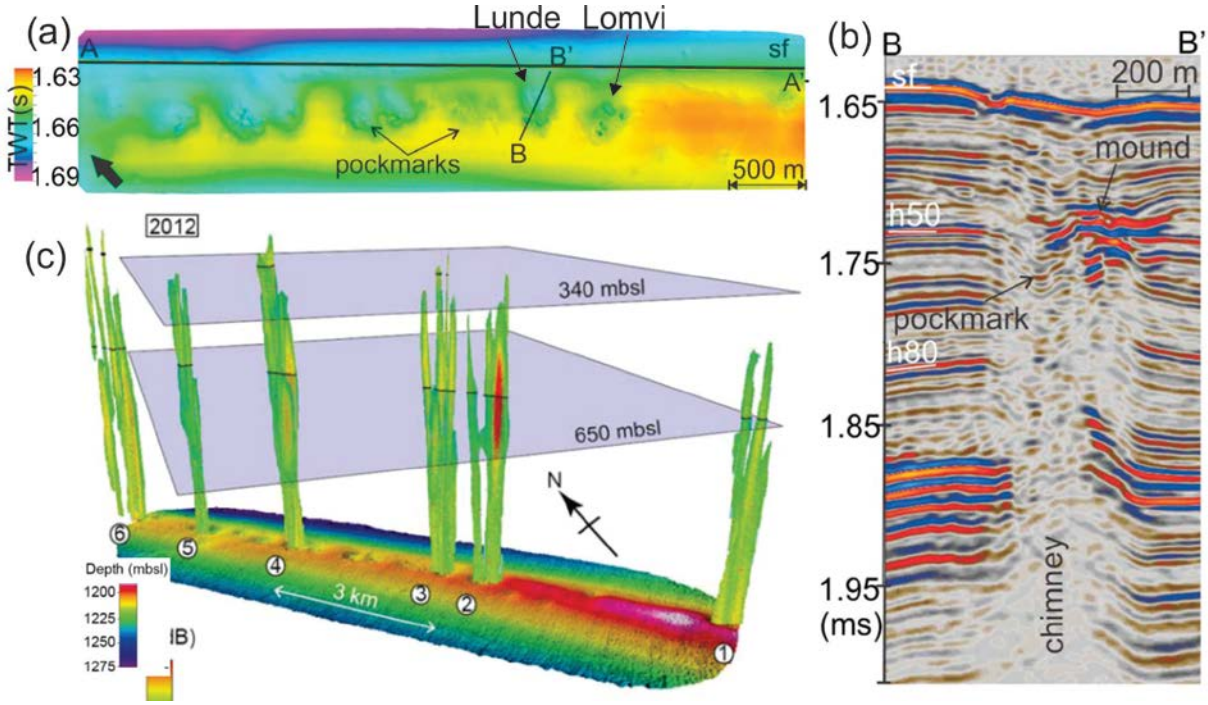

Fig. 11: (a) seafloor surface derived of high-resolution 3D seismic data from the eastern segment of the Vestnesa Ridge showing several pockmarks and highlighting the two most-studied pockmarks named Lomvi and Lunde. (b) seismic example of a chimney structure which resembles a vertical, focused fluid flow pathway underlying the pockmarks. (c) perspective view of the seafloor at the eastern segment of the Vestnesa Ridge showing hydroacoustic flares in the water column indicative of gas seepage. In this sub-figure pockmark 2 corresponds to Lomvi and 3 to Lunde, respectively. (Figures adapted from Smith et al. (2014) and Plaza-Faverola et al. (2015)).

The presence of a prominent gas-hydrate related BSR was revealed on seismic profiles in several seismic studies (e.g. Eiken and Hinz, 1993; Posewang and Mienert, 1999; Vanneste et al., 2005), which

indicates that gas hydrates and gas accumulations are common in the area. The BSR covers the whole of the Vestnesa Ridge, exhibiting a strong impedance contrast between hydrate-bearing and gas-charged sediments (Petersen et al., 2010; Bünz et al., 2012). Faults are identified on seismic profiles, stretching from the seafloor and through the BSR and control the ascend of fluids and the distribution of chimneys on the Vestnesa Ridge (Vanneste et al., 2005; Plaza-Faverola et al., 2015). In this setting very close to the mid-oceanic ridge the gas hydrate system is strongly influenced by the young and hot oceanic crust. Geothermal gradients increase gradually from 70 to 115°C/km towards the Molloy Transform Fault.

Vogt et al. (1994) mapped out a 1-3 km wide and 50 km long belt of pockmarks on the crest of the Vestnesa Ridge (Figs. 10, 11a). On a cruise in 2008, Hustoft et al. (2009) discovered acoustic flares in hydro-acoustic data documenting active seepage of gas from one pockmark at the eastern onset of the Vestnesa Ridge. Subsequent cruises in 2010 and 2012 found that active release of gas at the Vestnesa Ridge is more widespread than previously assumed (Fig. 11c, Bünz et al., 2012; Smith et al., 2014), although the actively-seeping pockmarks are confined to the eastern segment of the Vestnesa Ridge. Acoustic flares extend as shallow as <400 m below the sea surface corresponding to the upper limit of gas-hydrate stability for gas hydrates with thermogenic gases (Smith et al. 2014). Plaza-Faverola et al. (2015) suggest that the leakage of gas is tectonically controlled and is facilitated by numerous faults that extend to great depths beneath the Vestnesa Ridge. They further hypothesize that seepage has been going on for at least 1.5 Ma. Bünz et al. (2012) suggest that methane is generated at depths below the Vestnesa Ridge, rising vertically and then migrates along strata and along the base of gas-hydrate stability until the methane finally accumulates below the crest of the natural anticline formed by the ridge.

P-Cable 3D seismic data document complex and very heterogeneous, vertical conduits beneath the pockmarks (Fig. 11b, Petersen et al., 2010; Bünz et al., 2012; Plaza-Faverola et al., 2015). These focused fluid flow structures, also known as chimneys or pipes, pierce through the overburden sediments often linking with faults at greater depths and connecting the free-gas zone beneath the BSR with the seafloor. The high-resolution 3D seismic data show that chimneys resemble contorted structures with a highly variable internal reflection configuration. However, the chimneys associated with the active pockmarks are very wide and chaotic features and their acoustic character is different from those chimney structures at the western end of the Vestnesa Ridge (Petersen et al., 2010). The occurrence of amplitude anomalies within chimneys has previously been associated with the presence of gas hydrates and/or free gas, and possibly also carbonates in the upper few tens of meters (Petersen et al., 2010; Plaza-Faverola et al., 2010), but probably only drilling can resolve this ambiguity. Two of the most-studied pockmarks on the Vestnesa Ridge are Lomvi and Lunde (Fig. 11a). Gas hydrates have been recovered by gravity cores from both of these active pockmarks and $\delta^{13}C$ records indicate several leakage episodes during the last 23.5 ka (Panieri et al. 2014; Smith et al. 2014).

3.1.2 Upper Continental Margin West of Spitsbergen

The formation of the western Svalbard continental margin (Fig.8) dates back to Early Eocene resulting from the continental breakup in the Norwegian Sea followed by several rifting episodes in Late Paleocene/Early Eocene (Eldholm et al. 1987). The heterogeneous geomorphology of the area is mainly a result of glacial activity during the Pliocene and Pleistocene transition (Sohlheim et al. 1998, Knies et al. 2009). During this geological time, the Svalbard-Barents ice-sheet advanced and retreated

repeatedly reaching the shelf break. The analysis of prograding glacigenic sequences suggests that major glacier advances at the Svalbard continental margin happened at peak glaciations during the last 3.2 Million years (Chabert et al. 2011; Landvik et al. 1998; Rajan et al. 2012). The actual Svalbard continental shelf break marks the approximate maximum extent of the ice coverage (Landvik et al. 2005). The shelf was flooded as glacial ice retreated about 13,000 years ago. The sub-sea geomorphological features have been well characterized and reported by Rajan et al. (2012), Sarkar et al. (2012) etc. From high resolution bathymetry and seismic studies Sarkar et al. (2012) have reported plough marks, circular and elliptical crater-like depressions which have been formed by drifting icebergs. Furthermore the evidence of gas pockets right below a seepage area in form of negative-polarity bright spots, zones of low velocity and seismic attenuation and scattering have been found (Sarkar et al. 2012; Ker et al. 2014).

Widespread methane plumes have been observed at the upper continental margin in the water column between 80 and 415 m water depth (Sahling et al. 2014) revealing a maximum abundance around the 390/400 m contour line. This accumulation of gas emission sites was interpreted by Westbrook et al. (2009) to be the result of gas hydrate decomposition due to bottom water warming. In 2008 a multidisciplinary cruise with the RRS JAMES CLARK ROSS revealed more than 250 active plumes of gas bubbles emanating from the seabed in water depths shallower than 400 m (Fig. 12). Some of the plumes extend upward to within 50 m of the sea surface. Upward movements of gas bubbles were detected from echosounder records with rates of 80-250 mm/s. Repeated visits to the same plumes showed that they vary in strength over periods of a few days. Water samples from the plume areas showed increased methane concentrations (Fig. 13). Fissures and holes in the seabed, which are shown by high-resolution multibeam bathymetry and side-scan sonar images, locally control the positions of the plumes.

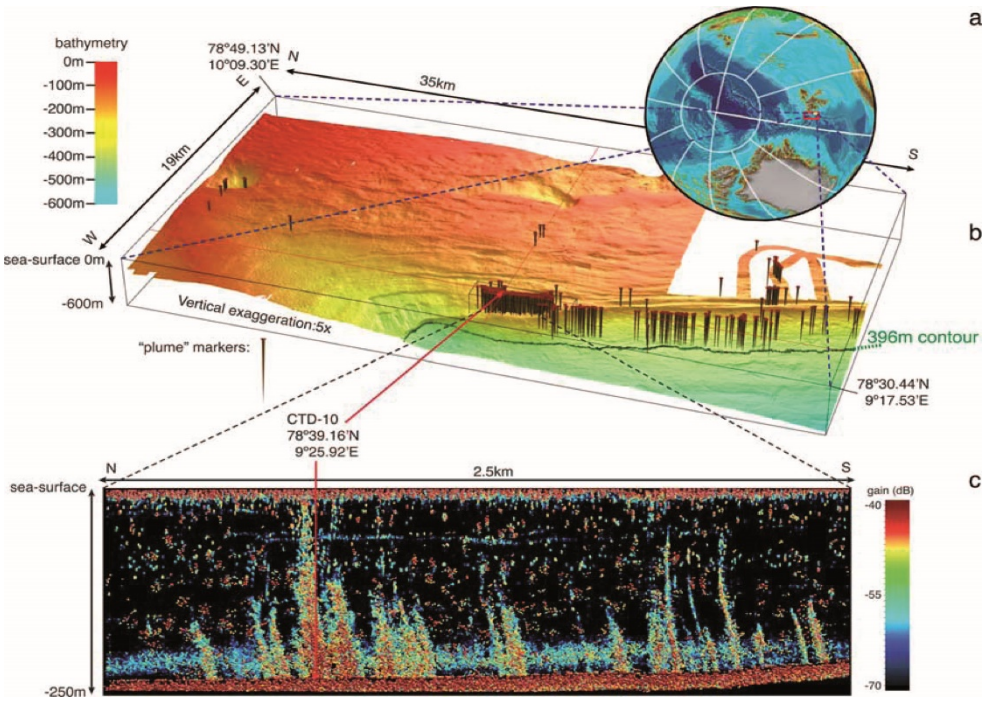

Fig. 12: Location of survey area west of Svalbard and position of plumes acoustically imaged with the EK60 sonar and part of the record from acoustic survey (from Westbrook et al. 2009).

Warming of the northward–flowing West Spitsbergen current by 1°C over the last 30 years (Schauer et al. 2009) is likely to have increased the release of methane from the seabed by reduction of the

extent of the gas hydrate stability zone, causing the liberation of methane from decomposing gas hydrates (Westbrook et al. 2009). Although the methane release from gas hydrates due to warming is not proved up to now, the implication that hydrate dissociation is potentially significant for a large portion of the Arctic continental slope, because the West-Spitsbergen current feeds into the Arctic Ocean, would be of global importance (Westbrook et al. 2009).

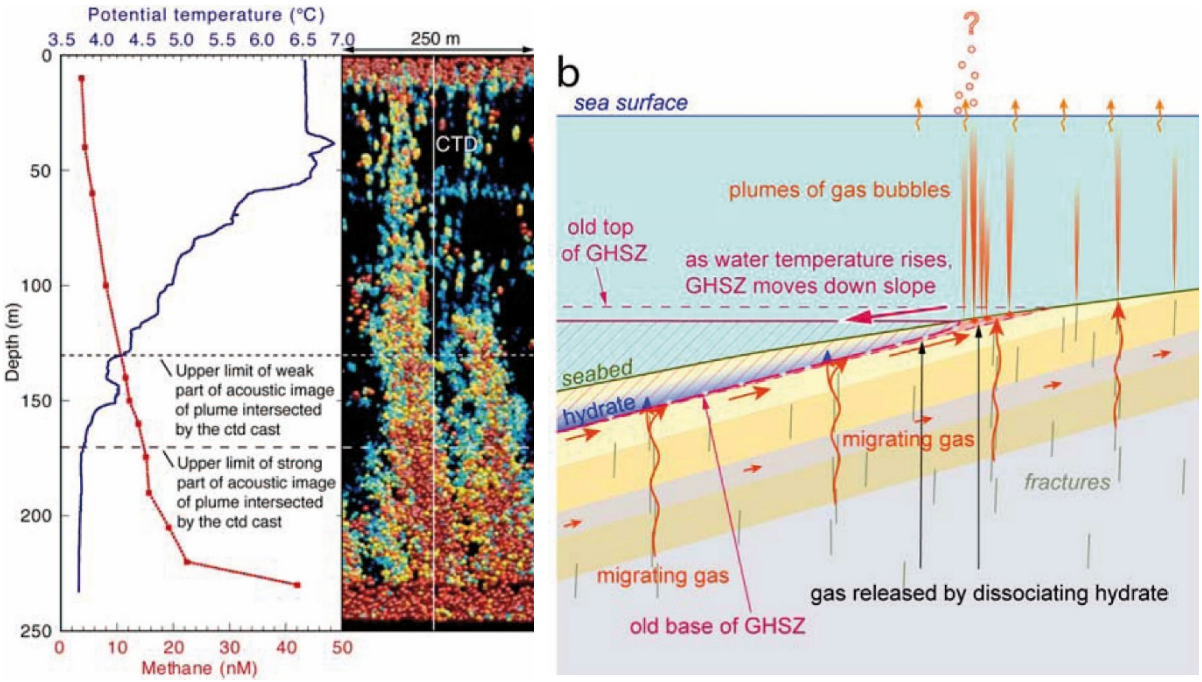

Fig. 13: Result from CTD cast 10, which intersects a bubble plume. Methane concentration increases consistently downwards and shows a strong increase in the lowermost 40 m of the water column. Beneath the area of the plumes seismic reflection sections show acoustic scattering that is typical of rising trains of gas bubbles, and down slope, beneath the GHSZ, the presence of free gas is indicated by negative polarity reflections, bright spots, attenuation of the high frequency content of the signal and velocity pull-down. Very few plumes occur where the seabed lies within the GHSZ, and, although plumes occur in shallower water on the shelf, the greatest concentration of them lies just landward of the edge of the GHSZ (left). Schematic diagram illustrates the downward shift in the GHSZ due temperature increase of bottom water. Where the GHSZ is removed entirely, all the released gas is free to move to the seabed, guided by local variation in lithology and structure (from Westbrook et al. 2009).

3.2 Objectives, Background Research Program

3.2.1 Objectives at Vestnesa Ridge

The overall aim of the was to obtain a better understanding of gas hydrate dynamics and fluid venting mechanism on the Vestnesa Ridge in relation to the stratigraphic and tectonic development of this area. In addition, stratigraphic and paleoceanographic analyses will provide more details and improve our understanding of environmental and climatic changes associated with the glacial-interglacial changes during the Middle to Late Pleistocene, possibly as far back as the debated timing of the onset of the full glaciation of the Barents Sea at around 1,1 – 1,5 Ma. Selected drilling sites focused on pockmarks with active seepage of gas from seafloor sediments and background sedimentation of Vestnesa Ridge outside seepage sites.

The individual objectives associated with drilling into these geological systems were:

- To identify the inner structure of chimneys and whether amplitude anomalies on high-resolution 3D seismic data relate to the presence of gas hydrates, free gas and carbonates.
- To identify and quantify the distribution of gas hydrates in shallow sediments and within focused fluid flow structures, whether they are widely disseminated or concentrated and whether they are occurring within chimney structures.
- To identify the mechanisms for gas migration through focused fluid flow structures, and what kind of open network and processes can sustain such a flow of fluids.
- To determine the geochemical composition of the hydrates and the gas that is seeping from the seafloor and to determine whether this gas is of biogenic or thermogenic origin in this relatively warm setting close to the mid-ocean ridge.
- To calibrate time-lapse seismic surveys such that we will be able to estimate the amount of gas that is expelled in this region.
- To determine the physical properties of sediments for rock physics and fluid flow models.
- To reconstruct palaeocenographic and climate changes over the Middle to Late Pleistocene.
- To obtain baseline information on fluid expulsion processes on the Vestnesa Ridge that allow an optimized design of a planned seafloor observatory to be deployed in this area.

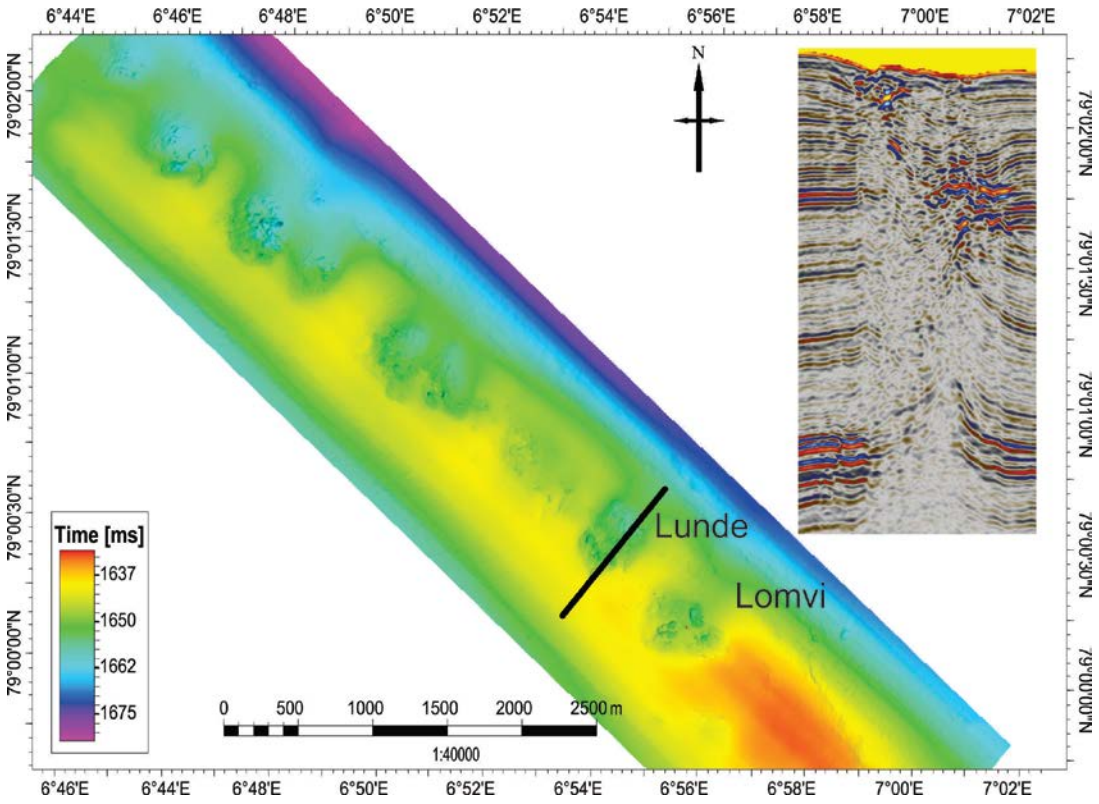

Fig. 14: Seafloor interpretation derived of the P-Cable 3D seismic data. The data clearly shows several pockmarks along the crest of the Vestnesa Ridge. The inset shows a seismic example of a chimney structure beneath the Lunde Pockmark. This high-resolution 3D seismic data forms an ideal basis for the selection of MeBo drilling locations.

High-resolution P-Cable 3D seismic data (Fig. 10 and 14) constitutes the basis for determining drilling locations in actively-seeping fluid flow structures (chimneys) and for sites away from fluid leakage, where such data exists. The P-Cable 3D seismic data used in planning the drilling locations has been acquired during a CAGE cruise with R/V HELMER HANSSEN in 2013 as part of a multi-year time-lapse

seismic study of fluid flow through vertical focused fluid flow structures. The 3D seismic data has a lateral resolution of 6,25 m and a temporal resolution of about 2-3 m. Chimney structures can be identified as vertical, semicircular zones of chaotic and disturbed seismic reflections (Fig. 14). Many of the chimney structures are variable in seismic characteristics. However, all of them show significant amplitude anomalies within the upper 50-100 m of the subsurface, i.e. well within reach of the MeBo drilling platform. Whether these anomalies are related to free gas, gas hydrates and/or carbonates is an interesting question in itself and will clearly help to better understanding how gas-rich fluids migrate through the subsurface.

3.2.2 Objectives at the Upper Continental Margin West of Svalbard

At the upper continental margin west of Spitzbergen the R/V MARIA S. MERIAN Cruise MSM57 primarily aimed to collect field data that will allow investigating the active interplay of fluid and gas flow processes from the sediments to the water column and the gas hydrate dynamics in relation to seawater temperature changes. There was evidence that an increase in bottom water temperature has already changed the gas hydrate stability zone and probably many active gas emission sites are caused by the gas liberation from methane hydrates (Westbrook et al. 2009).

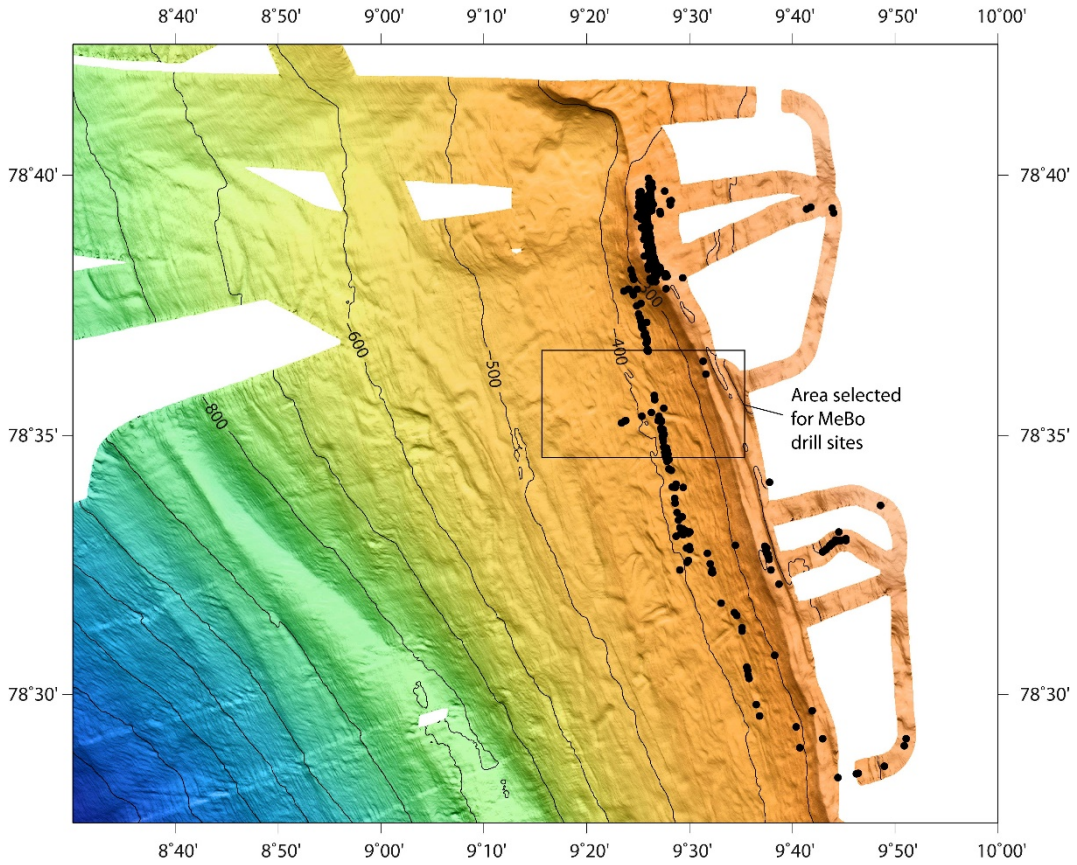

Fig. 15: Detailed bathymetric map from the area of planned investigation. Black dots show the locations of detected gas flares during the RRS JAMES CLARK ROSS (NOCS). The MeBo drill sites were planned in the black box area. Locations of drill sites are shown in Fig. 18.

In this situation it is important to understand how the gas hydrate reservoirs will react to future increases in the bottom-water temperature, and if future bottom-water warming might trigger the sudden release of large amounts of methane leading to accelerated climate warming. In a first step

hydrate dynamics have to be cored by sediment drilling and we therefore requested the use of the MeBo drilling system which can drill down to 50-60 m sediment depth and can cover the entire gas hydrate stability zone in such shallow water depths. By drilling several sites defined by gas flare positions (Fig. 15), the actual temperature field and seismic information we were addressing the following questions:

- How are hydrates distributed in the glacial and Holocene sediments of the slope in relation to the gas hydrate stability outcrop zone?
- Where are the hydrates concentrated? Do they occur close to the seabed or close to the base of the gas hydrate stability zone?
- How is the fabric of the hydrate in ration to the lithology? More massive hydrates? Dessiminated gas hydrates? Layers of hydrate parallel to stratification, lenses or fracture fillings?
- What is the detailed chemical composition of the hydrates; which gases are bound in the hydrate structure? Is there a fractionation in the gas composition in between the gas emanating at the seafloor and the gas in the hydrate structure?
- Beside structure I hydrate are there co-existing other structures (sh II, sh H) which influence the stability field of gas hydrates?
- Is it possible to recognise changes in the hydrate distribution? e.g. by gas hydrate carbonates? Clathrites?

Besides drilling we were interested to investigate the changes within the thermal regime at the sea floor. The key parameter that controls the propagation of bottom water temperature changes into the seafloor is the thermal conductivity of the sediment. Previous in situ thermal conductivity measurements conducted at five stations on the upper slope of the West Svalbard margin during the ARK-XXIV/2 cruise of R/V POLARSTERN in 2009 show unusually high thermal conductivity values of between 1.8 and 2.2 W/m/K (Feseker et al. 2008), which suggests rapid transport of heat from warming bottom waters into the seafloor. When gas hydrates close to the stability limit are present in the sediments, the consumption of latent heat during gas hydrate dissociation will delay the temperature increase. Depending on the rate of bottom water warming, the stabilization of the sediment temperature by the "gas hydrate thermostat" (Feseker et al., 2008) may lead to an inversion of the sediment temperature gradient above the dissociating gas hydrates.

4 Cruise Narrative

(G. Bohrmann)

Research vessel MARIA S. MERIAN sailed on **Friday, 29 July** 2016 at 1 p. m. local time from bunker pier of Icelandic port Reykjavik for a transit of four days to our research area at the western continental slope of Spitsbergen. Before, R/V MARIA S. MERIAN berthed at Ægisgarður Pier for an exchange of scientific crew and equipment of the cruises MSM56 and 57. For MSM57 the MARUM seafloor drill rig MeBo70 and many additional, mostly geological sampling devices were taken on board. In total eight 20' containers were discharged in addition to one 40' container by boatswain and crew. Especially the complex installation of MeBo70 prolonged the berthing time to four, instead of the usual three days.

Interestingly, MARIA S. MERIAN was not the only research vessel in the Icelandic port. On arrival of MERIAN, the British research vessel RRS DISCOVERY moored vis-à-vis at the same pier. After she sailed for oceanic measurements in Labrador Sea, the berth was taken by the Spanish research vessel SARMIENTO DE GAMBOA. On Tuesday, the new research vessel of Woods Hole Oceanographic Institution (WHOI), R/V NEIL ARMSTRONG, joined us in the same port basin, and finally, on Saturday, when we left our pier for bunkering, R/V POSEIDON of Helmholtz Centre for Ocean Research GEOMAR Kiel came to Reykjavik. Certainly, such a crowd of research vessels is quite rare and shows that the northernmost capital in Europe is an ideal starting port for research cruises to the North Atlantic.

Having left Reykjavik, MARIA S. MERIAN steamed along Iceland's west side, under coast protection, northwards across the Denmark Strait during **Saturday, 30 July**, crossed the active rift zone of Kolbeinsey Ridge and arrived on **Sunday, 31 July** at the Iceland Plateau, where we started to record data from the hydro-acoustic systems PARASOUND and the Multi-beam EM122 (Fig. 1). In principle the wind conditions with a force of just 5 to 6 on Beaufort scale were manageable; however, a groundswell existed constantly. During the first two days of transit we changed the time of the day for 2 hours from Iceland time to the time in Longyearbyen which is 2 hours ahead of UTC time. The vessel followed the direction of the Kolbeinsey Ridge to the north and crossed the Jan Mayen Fracture Zone west of the island Jan Mayen. The vessel steamed on **Monday, 1 August** through the Greenland Sea and crossed the Greenland Fracture on **Tuesday, 2 August** which is a remarkable elongated feature elevated from 3,900 up to 1,700 m water depth for a short distance along the track of the transect to the Boreas Basin (Fig. 1). We crossed the Molloy Transform Fault, which actively separates the Knipovich Ridge from the Molloy Ridge Area.

After we reached Vestnesa Ridge (Fig. 16), our target area for the first leg on Tuesday we started at 16:25 with a gravity corer at the potential MeBo drill site to recover a 577 cm sediment core (GC-1) of hemipelagic mud away from the pockmarks and gas chimneys in the seabed (Fig. 17). The temperature lance was afterwards launched together with the SVP slightly north of the ridge crest into the water column to calibrate the system and to measure a sound velocity profile of the area. Both were successful and a T-lance profile with 8 individual T-lance deployments were taken from stations in and around Lomvi and Lunde Pockmarks. On **Wednesday, 3 August** at 04:15 MeBo (MeBo123), the seafloor drill rig, was deployed for the first time during the cruise within the Lunde Pockmark at a location of relative flat seafloor (Fig. 17). The site was selected based on the 3D seismic data taken by P-cable measurements from University of Tromsø in 2007. In principle we tried to avoid large amplitude anomalies, which may represent free gas or gas hydrate/ free gas alternations close to the surface. Such features were expected in around 50 mbsf and have been observed at other locations of the pockmarks close to the seafloor. Unfortunately, MeBo stopped drilling after 3 hours due to technical

problems. Instead of MeBo drilling activities we took 2 gravity cores, one at the MeBo station to recover the uppermost meters of sediment which are difficult to sample by MeBo drilling. We recovered a 7.65 m-long core showing the uppermost sediment sequence in a very good quality. The second gravity core GC-3 sampled the sediment sequence again at the background station away from the pockmarks (Fig. 17). The following four-hour mapping activity covered the entire elongated 3D-seismic box of UiT whereas the profiles extended the NW and the SE rim of the box.

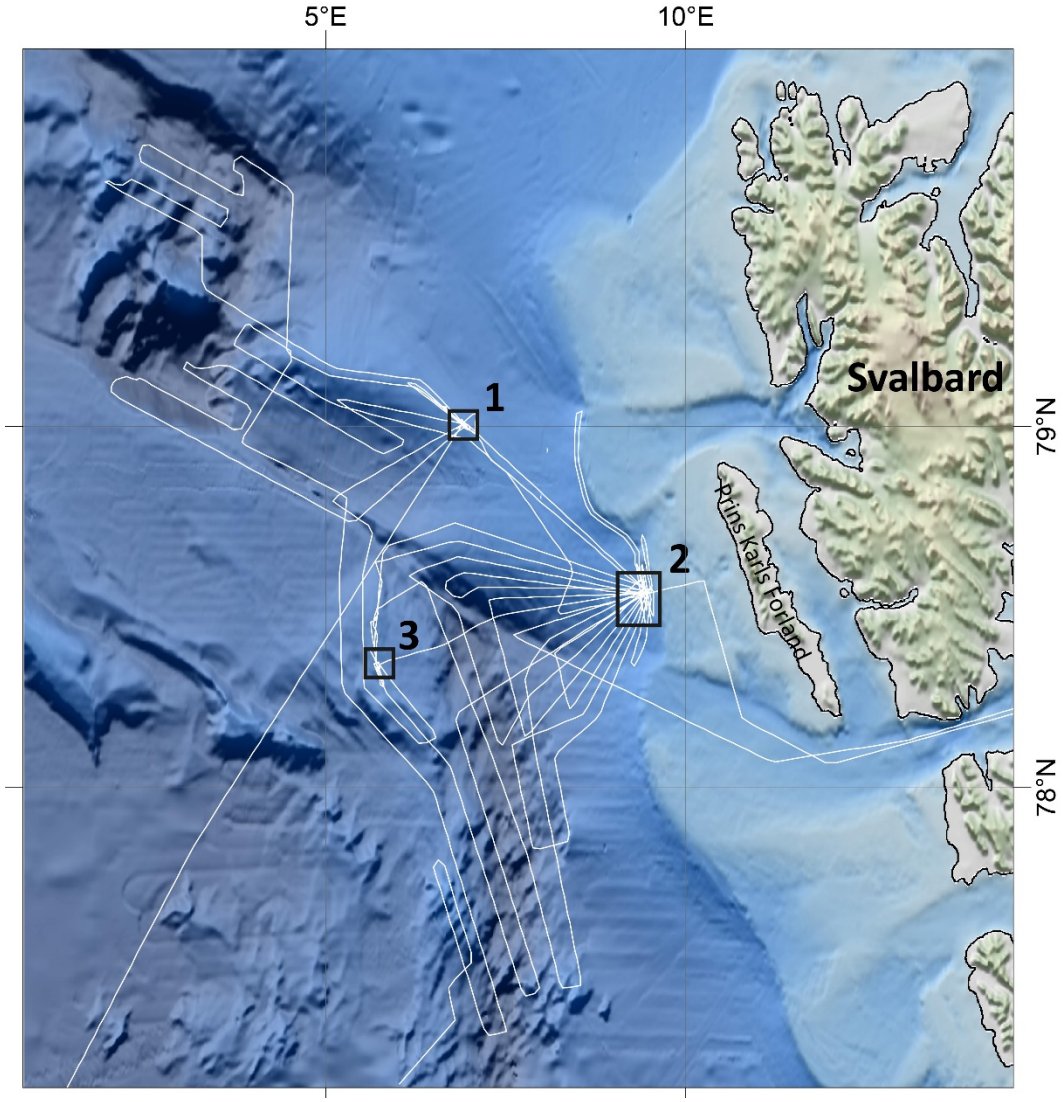

Fig. 16: Bathymetry of the Eastern Fram Strait with track lines of the Cruise MSM57. Three areas of research are indicated: 1 = Vestnesa Ridge (for details see Fig. 17), 2 = Upper continental margin of Prins Karls Forland (for details see Fig. 18), 3 = Svyatogor Ridge (for details see Fig. 19).

The presence of acoustic anomalies in the water column was recorded and the analysis of the data showed us the distribution of gas emission sites in relation to the pockmarks. A second T-lance profiling with eight individual stations on Vestnesa Ridge followed until the morning of **Thursday, 4 August** when MeBo (MeBo124) was launched at the same position in the Lunde Pockmark as before (Fig. 17). Due to the break of the hook for catching the core barrel, drilling had to stop and we had to recover the drill rig from the seafloor. Instead we took two gravity cores in the Lunde Pockmark to sample hydrates. For locations we were guided by the micro-bathymetry map recently taken by the UiT and we could define the sampled sites by very small-scaled morphological features. Gravity core GC-4 sampled 535 cm of the hemipelagic sediments and gravity core GC-5 recovered a 60 cm sequence with

gas hydrates. After the MeBo hook was repaired the seafloor drill rig (MeBo125) was deployed at the same position in the Lunde Pockmark as the two drilling attempts before (Fig. 17).

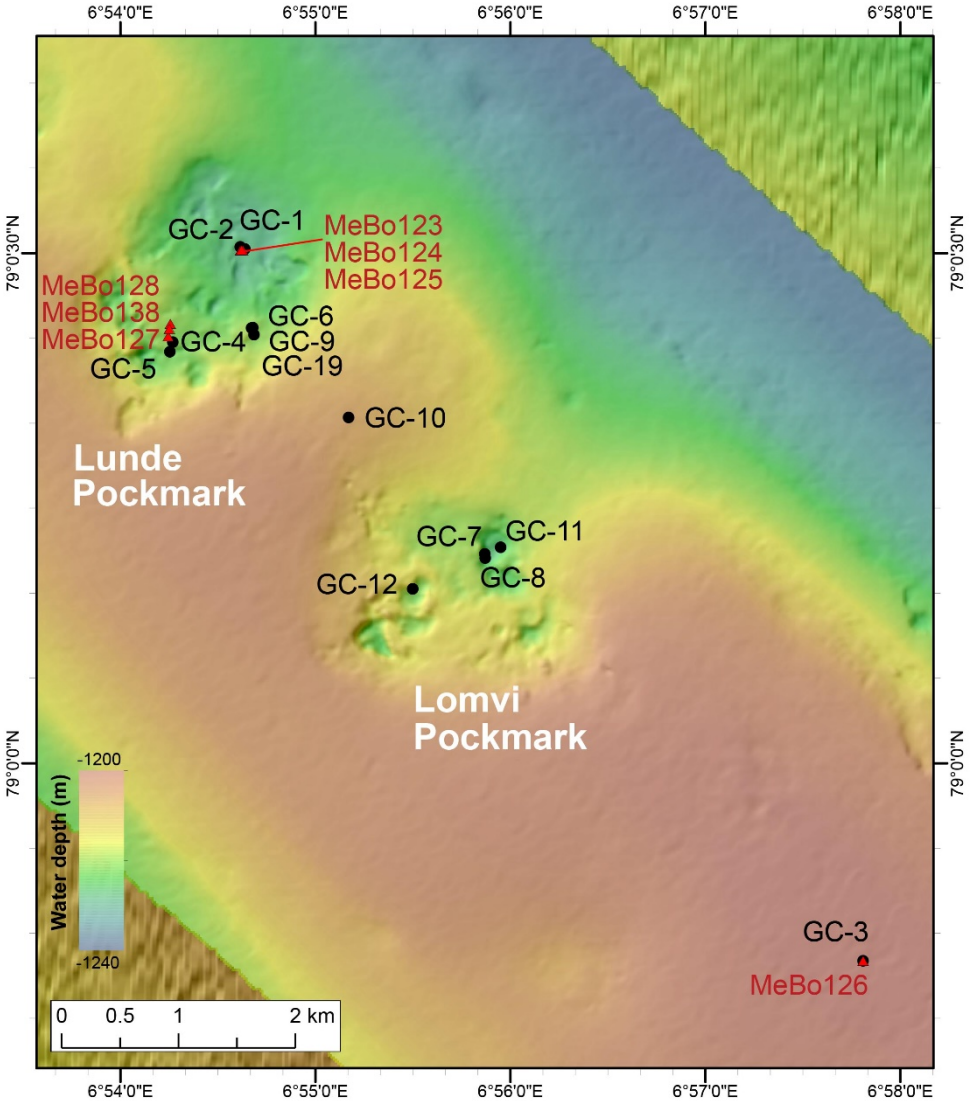

Fig. 17: Locations of seafloor sampling by MeBo drillings and gravity corer (GC) on Vestnesa Ridge during MARIA S. MERIAN Cruise 57. Besides sampling at Lunde and Lomvi Pockmarks a background station was selected by MeBo126 and GC-3 stations.

MeBo drilled over night until 06:00 on **Friday, 5 August** and drilling had to be stopped because a core barrel was cramped in the drill rod and it was not possible to pull it out with the wire-line system. The system drilled down to 22.90 mbsf and recovered 906 cm of core material. Several sediment intervals with chemosynthetic clam-remains were the highlight of the cores. Those clams live in symbiosis with microbes at the seafloor and were bound with gas seeps. So far those or similar chemo-synthetically living mussels had not been found at Vestnesa Ridge on the seafloor, and it is very interesting to know that this was different in the past. Perhaps these clams had lived in times of stronger methane emission? One clam shell layer so far was known from gravity cores, but now we know that there are several layers and that the methane release probably has varied several times. The chance, that MeBo had be rigged for the next drill site, was taken for ten more T-lance measurements predominantly within the Lunde Pockmark. A further gravity core (GC-6) sampled hydrate in a small pit of 30 m in diameter in the Lunde Pockmark (Fig. 17), before MeBo was deployed at the background station where we wanted to core the sediment sequence as deep as possible.

The position for drilling (MeBo126) was selected clearly away from the gas chimneys and a distinct fault in the deeper sediment sequence imaged by the 3D seismic data of UiT. Drilling was performed from Friday afternoon during **Saturday, 6 August** until **Sunday, 7 August** late morning. The drilling was the deepest one up to now during this cruise with a total penetration of 62.50 m and cored 26.42 m sediments (Fig. 17). First macroscopic investigations on the sediment cores showed that alternating layers of silty-sandy horizons with very clean, cohesive clay layers occur that could be a seal for fluid and gas emissions. A real highlight of this coring was the measured distribution of formation gases. The relation of methane to higher hydrocarbons as ethane, propane, butane, etc. is increasing continuously and should mainly be of thermogenic origin, whereas towards a lower sediment depth the part of biogenic methane continuously increases. The particular, steep gradient could be explained by the extremely bad routing because of the sealing clay. After drilling we deployed the temperature lance (TL05-1) to measure a 4.5 m temperature profile just at the same position as the MeBo drill site. Further 5 temperature lance measurements were taken within or outside pockmarks (TL06-1 to -5) and MeBo (MeBo127) started to drill a new site at Lunde Pockmark where high amplitude reflectors are seen close to the surface (Fig. 17). Drilling had to change from push coring to rotary coring around 5.75 mbsf where massive carbonates have been sampled. Due to technical problems the drilling had to be stopped much earlier at a drilling depth of 13.90 m. The deepest core was the autoclave tool core barrel (MDP) developed within the collaborative project SUGAR. The MDP was deployed three times during the drilling on Vestnesa Ridge. In all cases the formation pressure was kept by the tool that allowed a selective degassing and quantification of the gas amount in the formation. Unfortunately, one of the autoclave tools did not sample sediment; however, the other two autoclave deployments were more successful. MeBo127 had a total length of 3.52 m. Besides an autoclave core barrel (MDP) the borehole assembly was plugged at the end with a MeBoCORK (Circulation Obviation Retrofit Kit). Such CORKs have been developed by the scientific community within the international drilling program (ODP/IODP), and were installed inside submarine boreholes allowing to monitor in-situ pressure and temperature conditions. The CORK we used is equipped with a physical sensor package to measure temperature, pressure, and salinity. The MeBoCORK separates the inner borehole from the overlying ocean by using a plug to seal the drill pipe. The system is self-contained and includes data logger, batteries, thermistors and a differential pressure sensor. Data are planned to be recovered in 2018 during an ROV dive.

After the drilling activity on **Monday, 8 August** we took a gravity core (GC-7) at Lomvi Pockmark (Fig. 17) in the northeast pit and sampled gas hydrate. Unfortunately, the core barrel was bent and we had to take a second core at the same position. T-lance profiling (TL-7) was then performed during night inside and outside of Lomvi Pockmark. We recovered 16 temperature profiles until the morning of **Tuesday, 9 August**. A gravity core (GC-8) was taken in a small crater observed in the micro-bathymetry map and recovered gas hydrate as well at the base of the core (Fig. 17). A second gravity core (GC-9) was taken at the T-lance station TL02-5, where anomalies in conductivity have been found and comparisons with the lithology are planned. On **Tuesday, 9 August** the wind speed increased during late afternoon and the weather forecast predicted a sea state of Beaufort 7. We therefore decided to leave the area of Vestnesa Ridge and moved to the west to map the northern part of the Molloy Ridge area (Fig. 16). Although this area is only 60 nm away from Vestnesa Ridge, the weather was much better, due to extended ice fields. We performed east-west profiles which were cropped at its western ends, because of ice fields that slowed down our sailing speed. We reached the ice front around two degree of longitude east. We crossed through the sheet of floating ice and very much enjoyed the change in scenery.

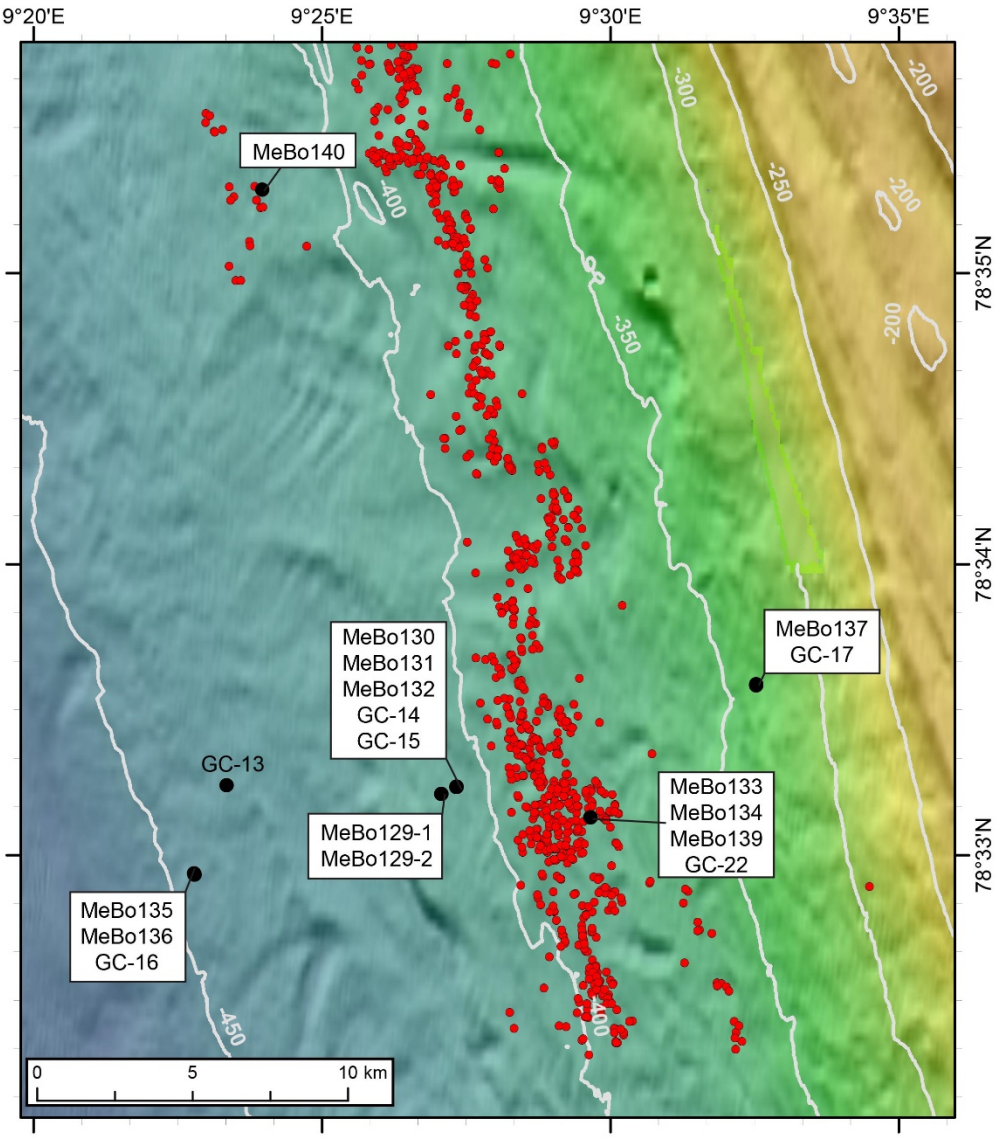

Fig 18: Location of the upper continental margin offshore Prins Karls Forland with gravity cores and MeBo drill sites performed during MARIA S. MERIAN Cruise 57. Red dots show the locations of gas seeps (Sahling et al. 2014).

Wednesday afternoon **10 August**, we moved back to Vestnesa Ridge, where the weather had calmed down as well and we were able to continue with MeBo drilling (MeBo128) at the seep site of Lunde Pockmark (Fig. 17). The drill hole was at the same spot as MeBo127 and should expand the knowledge on lithology with depth. Unfortunately, due to technical problems the drilling had to be stopped at 10.75 mbsf. An extensive profiling of the T-lance at 16 stations (TL08) followed northwest of the Lunde Pockmark and covered at least two more pockmarks that showed no activity by gas venting. Higher heat flux values were determined inside the pockmarks, and it appears that the higher heat flow values are not correlated to the gas-emission activity of the pockmarks. The T-lance program was finished on **Thursday** morning, **11 August,** and we took two gravity cores in small pits at Lomvi Pockmark (Fig. 17). Both cores (GC-11 and GC-12) sampled only a short sequence of sediments with distinct gas hydrate layers, which most probably stopped deeper penetration of the corer. During the last station of Leg 1 we deployed a sonar at the seafloor, close to the CORK position. The sonar will scan the water column and gas emissions during regular time intervals and will become recovered by ROV during a future expedition at the same time, when the data of the MeBoCORK will be downloaded.

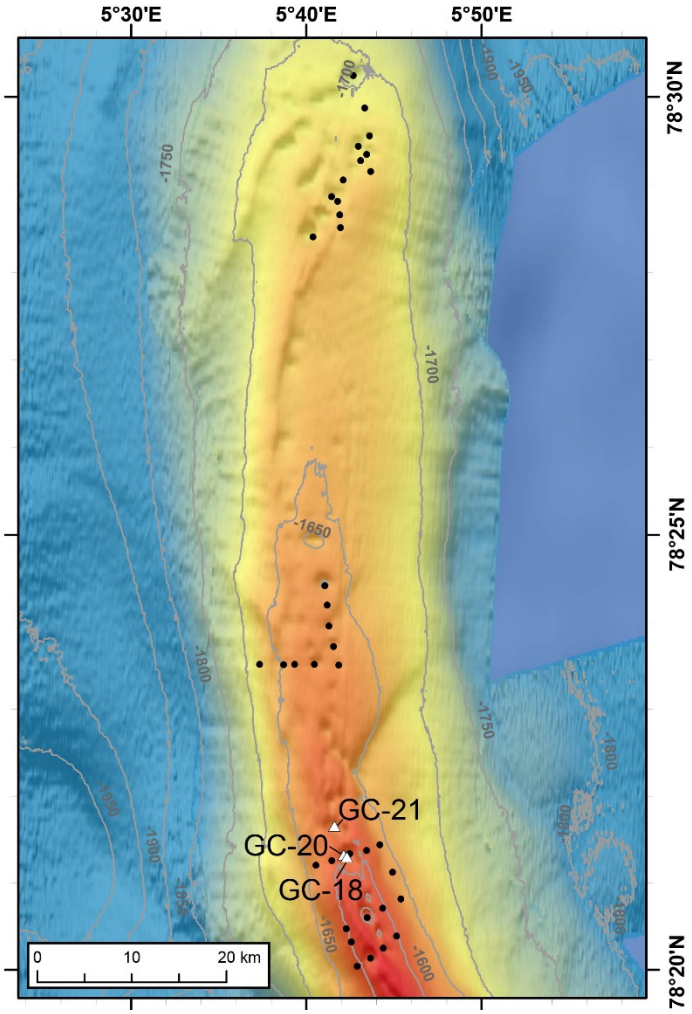

Fig. 19: Part of the crest of Svyatogor Ridge. Black dots show measurement locations of heat flow using the temperature lance. Three gravity cores (GC-18, -20, -21) were taken during Leg 2 of MARIA S. MERIAN Cruise 57.

On Thursday, R/V MARIA S. MERIAN started steaming to Longyearbyen. During the transit we performed seafloor mapping across Vestnesa Ridge and the continental slope, west of Svalbard (Fig. 16). During the night we reached the Isfjord, and berthed in the morning of **Friday, 12 August** at the coal mine pier of Longyearbyen directly at the airport. 14 scientists and 4 crew members were exchanged prior to Leg 2 of this cruise. Despite the rainy weather, many of us enjoyed the time to walk on land. R/V MARIA S. MERIAN left the coal mine pier on **Saturday** morning, **13 August** during sunny weather and continued mapping for the rest of the day and the night. After the crew-change in Longyearbyen we started our research studies at the western continental slope off Svalbard. Due to rough sea state we shifted the beginning of MeBo drilling (MeBo129-1) to the evening (Fig. 18). The location of the drill site in 405 m water depth was selected to drill into the glacigenic sediments at the slope of Spitzbergen and to penetrate a strong high amplitude reflector in 34-38 mbsf. The MeBo did two drill sites during the same deployment (MeBo129-1 and 129-2) which lasted from Sunday evening to Tuesday moring, **16 August 2016**. The first drill hole sampled sediments down to 12.39 m and the second hole recovered sediments down to 22.98 mbsf. We have realized after numerous attempts, that even MeBo has a hard time penetrating these sediment packages, mostly made up of boulder clay, which is a mix of fine grained mud with a variety of clasts and dropstones. After the MeBo was back on board we took a sound velocity profile (SVP-1) for calibration of the multi-beam.

Yet, the overall low wind speed and small sea state enabled us to conduct all station work safely. Only **Tuesday, 16 August**, sea state was too high to deploy MeBo, so we started an alternate science program to study the nearby Svyatogor Ridge, located west of the well-known Knipovich Rift (Fig. 16).

Svyatogor Ridge is a sediment drift complex formerly connected to Vestnesa Ridge. Due to lateral motion along the Molloy Transform Fault, both these ridges were separated from each other during the past 2 million years. The mapping program showed that the crest of Svyatogor Ridge is characterized by numerous pockmarks, similar to Vestnesa Ridge. Using the heat-probe we conducted temperature measurements at 16 stations overnight along three short transects across the ridge crest (Fig. 19). These measurements showed that the pockmarks are characterized by much higher heat flow compared to the regions outside these structures. Although we did not find any gas flares using the vessels' acoustic imaging tools, the increased heat flow is an indication of advection of warmer fluids from depths. Back at the shallow continental margin offshore Prins Karls Forland we took gravity core GC-13 during **Wednesday, 17 August** and started drilling a MeBo Site 130 close to MeBo129 at 405 m water depth (Fig. 18). Due to technical problems, we had to stop drilling at the early morning of **Thursday, 18 August**, and we took gravity core GC-14 at the same location. Afterwards, we started a new drilling attempt at the same position, which we had to stop 5 hours later because of a hydraulic leakage. The following drilling at the position in 405 m water depth (MeBo131) started at 08:00 on **Friday morning 19 August** and reached a drilling depth of 20.30 mbsf. MeBo drill Sites 133 and 134 continued drilling until **Sunday, 21 August** at the shallowest area at 340 m beyond the accumulation of recent gas seeps. Overnight mapping of the seafloor brought us back to the deepest drill site at 445 m water depth on **Monday morning, 22 August**. Between MeBo drilling sites 135 and 136 (Fig. 18) until **Wednesday morning, 24 August** mapping and gravity core GC-17 defined the station program.

After a short mapping survey, MeBo was again deployed Wednesday evening to start a new drill site in 340 m water depth (MeBo137), well outside the methane hydrate stability zone (Fig. 18). Drilling lasted until **Thursday morning 25 August** reaching a depth of 22 m. The cores revealed an interesting sequence of glacial deposits. Pore water and gas-compositions measured from this site outside the hydrate stability zone are an important constraint to better understand our previous results and establish a regional picture of the potential hydrate occurrences along the margin. An additional gravity core (GC-17) was taken at the same location, with a recovery of only 1 m, but allowing careful sub-sampling of the sediments closest to the seafloor. Due to changing weather condition further drilling became too challenging, and we left the shallow water margin sites to start a mapping program across the Knipovich Rift further to the South (Fig. 16). Weather conditions had turned drastically throughout the day.

While previously winds have been mostly from South to Southwest, we now faced strong northerly winds. Air temperatures dropped suddenly by 6° C to near the freezing point, accompanied by a snow storm. Initially, with the winds in our back, the mapping proceeded well despite the decrease in overall weather conditions. However, at the southern end of the profile and after a change in course of the MARIA S. MERIAN to a more northerly direction, the conditions worsened. With wind speed up to 22 m/s (Beaufort scale 9), however, the vessel became steadily slower, as swell increased considerably. Despite the storm over night, data quality was quite well and soon scientists began to investigate the multibeam data more closely. Due to the bad weather conditions, we started our sampling program on Svyatogor Ridge on **Friday 26 August** (Fig. 19). We first deployed the temperature lance along the northern portion of the ridge to investigate a series of pockmarks. A total of 13 stations (TL10) were completed. A gravity core (GC-18) was then taken within a pockmark that had shown the highest heat-flow value above the regional background trend (Fig. 19). After an additional short mapping survey, we reached Vestnesa Ridge and started drill site 138 at the seep site within Lunde Pockmark (Fig. 17)

in 1,200 m of water depth on **Saturday 27 August**. At this drill site we reached a total depth of nearly 24 m yielding a sediment sequence rich in methane hydrates and carbonate precipitates.

Seafloor mapping to the west brought us to the Molloy Deep on **Sunday, 28 August**, where sea ice coverage hindered us to map the westernmost part of the nodal deep (Fig. 16). Steaming back to Vestnesa Ridge to the East we took a gas hydrate-rich core (GC-19) at a seep site of Lunde Pockmark (Fig. 16) on **Monday morning 29 August**. Gas hydrate specimen were stored in liquid nitrogen and will be used for structural analysis in laboratories at home. At the same day we reached the upper margin offshore Prins Karls Forland and drilled a third drill hole at 391 m water depth (Fig. 18). This drilling was finished at the evening of **Tuesday, 30 August** at 26.15 mbsf. The over-night mapping brought us to Svyatogor Ridge, where we took two gravity cores (GC-20 and GC-21) and a T-lance profile (TL11) of nine stations (Fig. 19) on **Wednesday, 31 August**. During the following **Thursday, 1 September** we started to drill another site just below the methane hydrate stability zone in 402 m water depth and 4 km to the north of our main seismic profile. We were guided by a high-frequency seismic profile acquired by our French colleagues with the SYSIF deep-towed seismic tool. A bright spot reflection in around 30 mbsf, which was interpreted as gas-charged layer was one of the targets. We drilled down to 31.30m until **Friday morning, 2 September** and could confirm the presence of free gas in this horizon. Gravity corer GC22 followed afterwards and was the last station work performed during this cruise. Seafloor mapping for more than 26 hours was used to fill some gaps in the bathymetry maps and to extend the Knipovich Ridge data to the western rim of the rift valley (Fig. 16).

5 Hydroacoustic Mapping

(P. Wintersteller, Ch. Ferreira, M. Riedel, N. Stange)

5.1 Multibeam Echosounder (MBES)

5.1.1 Acquisition Devices and Settings

MBES surveys were conducted with the hull-mounted KONGSBERG EM122 MBES (KONGSBERG EM122, 2013). Only the shallow area west of Prins Karls Forland has been mapped in parallel with the shallow-water-MBES EM1002 (KONGSBERG EM1002, 2016), which is temporarily mounted in the moon-pool of the vessel.

The EM122 MBES is a well-known deep-sea system operating with 11.25 to 12.5 kHz. On-board R/V MARIA S. MERIAN, a beam width configuration of 2° (TX) by 2° (RX) is installed. A swath angle of up to 150 degrees and a maximum coverage of 5.5 times the water depth can be reached. During cruise MSM57, the maximum swath width was set to 120 degrees to improve data quality, reduce the amount of noisy data at the outer beams, and increase the ping rate.

The EM1002 MBES is a shallow to medium water system, operating with 95 kHz and a 2° beam width. Although it has just 111 beams, the specialty of this echosounder is its transducer array. It has a semicircular design and is used to both, transmit and receive and can provide very good measurement accuracy with precise phase and amplitude detection.

Sound velocity profiles (SVPs) were measured with XSV or AML-probe (see. Chapter 5.4) and applied to the raw data during acquisition via the SIS software from KONGSBERG.

The storage-intensive water column data have only be recorded if particular requested with respect to flare search during this cruise.

The settings used for both echosounders are shown in Table 3 and Table 4 below.

Table 3: EM122 Settings.

Runtime Parameters EM122	Setting	Reason
Swath Width	120°	Beyond 120° the outer beam quality is below our specs. Ping rate is higher the narrower the swath width.
Beam Spacing	HD EQST (high density equidistant mode)	432 soundings per ping, equidistant over the swath are achieved then
Ping Mode	Shallow or Medium AUTO	For flare-search surveys For bathymetric surveys
Dual Swath Mode	ON/AUTO	To increase the along track resolution
Pitch/Yaw stabilization	ON	Improvement of data quality

Table 4: EM1002 Settings.

Runtime Parameters EM1002	Setting	Reason
Swath Width	120°	Beyond 120° the outer beam quality is below our specs. Ping rate is higher the narrower the swath width.
Beam Spacing	EQST (equidistant mode)	111 beams per ping, equidistant over the swath are acquired
Ping Mode	AUTO	For bathymetric surveys
Dual Swath Mode	OFF	Not implemented
Pitch/Yaw stabilization	ON	Improvement of data quality

5.1.2 Processing Methods

While the EM1002-dataset has only been acquired but not processed during the cruise, EM122 bathymetry data were processed with the open source software package MB-System (vers. 5.5.2279; see Caress and Chayes, 1995). The following steps were carried out to the EM122 bathymetry-surveys:

- Converting the data to editable MB-format.
- Applying correct SVP if available.
- Applying tide correction based on the Tidal Prediction Software (OTPS; Oregon State University); integrated in MB-System (mbotps). Tides around Svalbard are part of the semidiurnal cycle around the main amphidromic point located in the central Arctic Ocean. The change in amplitude (max. up to 50 cm) and phase is due to Svalbard location between deep Arctic Ocean and shallow Barents Sea (Kowalik et al., 2015).
- Manual editing of the dataset.
- Correcting amplitude (aka backscatter) and sidescan (beam time series) values based on a function of grazing angle with respect to the seafloor (slope).
- Applying the changes to the raw files, creating processed files, grid the data by using netCDF (GMT) file format.

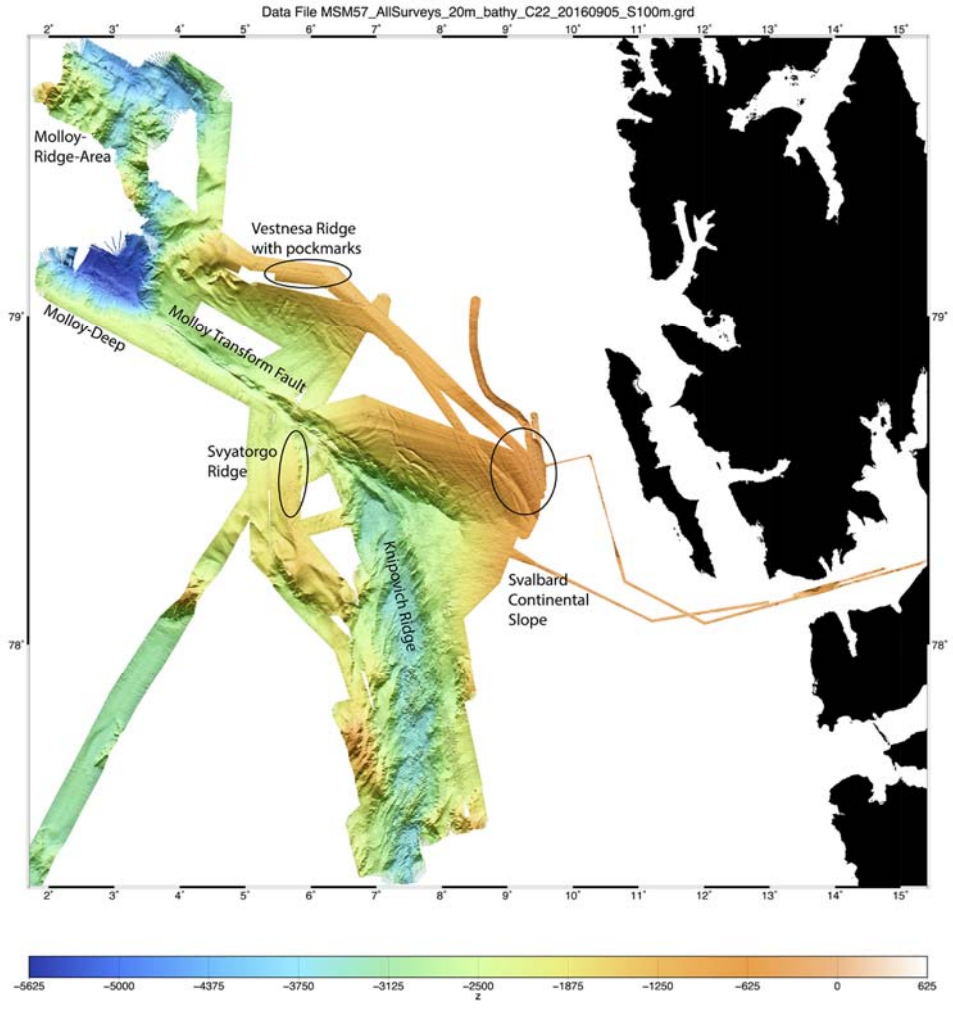

Fig. 20: EM122 bathymetric map of MSM57 (Leg 1 and 2) using a 20 meters grid cell size (smoothed to 100 m).

The generated bathymetry maps are presented in Chapter 5.1.3. ESRI ArcGIS vers. 10.3.1 was used to create maps and a sustainable spatial data management of the data obtained during the cruise. First detailed processing revealed sound velocity issues especially visible on Svalbard's continental slope (see Fig. 20).

5.1.3 Preliminary Results

In total about 8.2 Mill. beams were recorded during MSM57-2 with EM1002, within 165 survey-hours, a length of 496 km and an average speed of 1.6 knots. The data has not been processed yet. On a first glance the data seem to have lever arm or offset issues.

During MSM57 Leg 1 and 2 7,034 km and 861 hours of EM122 surveys were conducted, leading to an average speed of 4.4 knots.

The results of Leg 1 and 2 combined are presented in Fig. 20 showing bathymetry, and in Fig. 21 for the amplitude (backscatter). The latter shows a wrong scale-bar due to a number of amplitude-outliers. While sea-ice conditions impeded a complete mapping of the Molloy Ridge and Deep, the Molloy Transform Fault as well as the northern part of the Knipovich Ridge and the crests of Vestnesa and Svyatogor Ridge could be well mapped. The latter two show a number of pockmarks where coring and sampling were focused during this cruise. Both, bathymetry and backscatter reveal apparently fresh, uncovered volcanic areas, south of 78° latitude within the Knipovich Ridge (Fig. 20). This will be further investigated in the future.

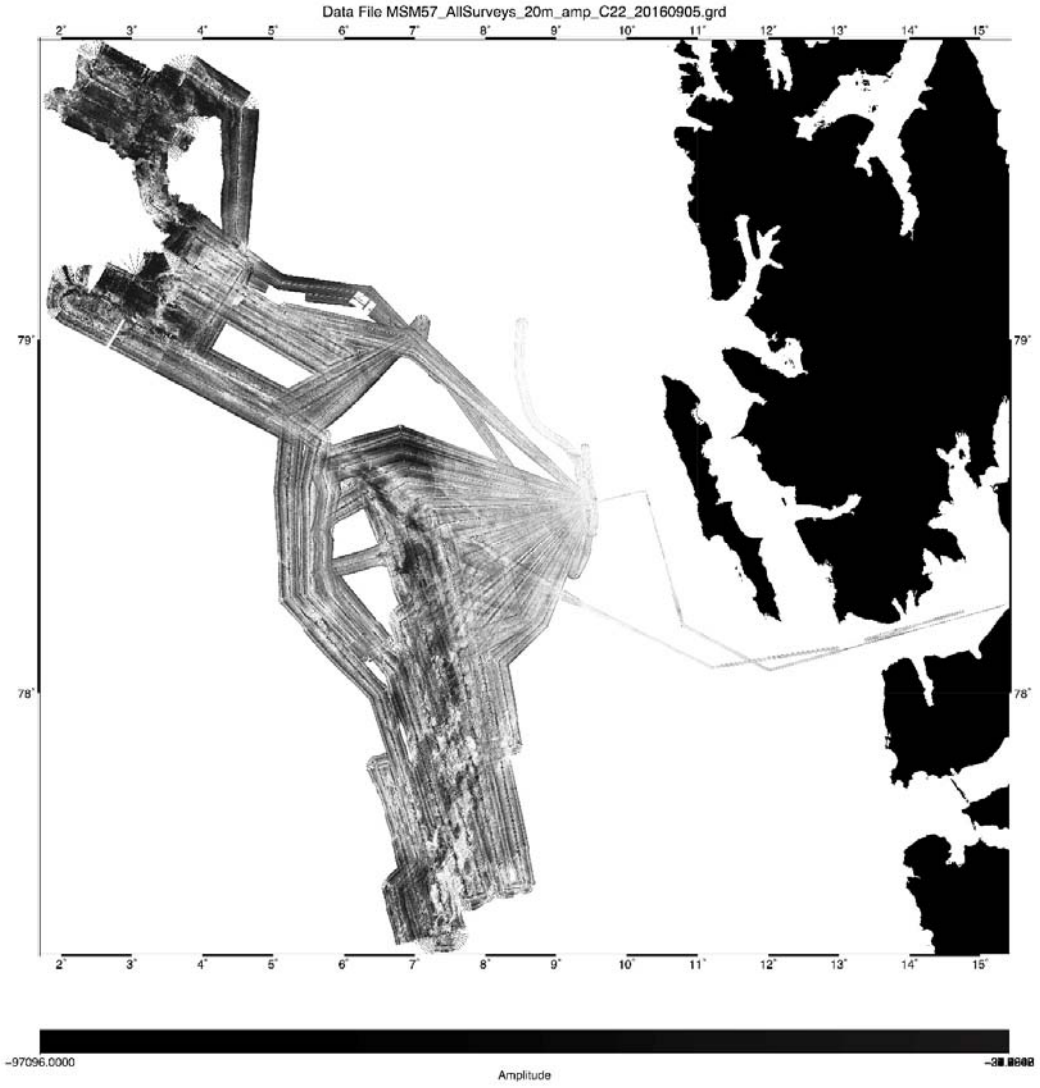

Fig. 21: Amplitude map of MSM57 (Leg 1 and 2) using 20 a meters' resolution. Bright values show a strong backscatter amplitude.

5.2 Sub-Bottom Profiler

5.2.1 Acquisition Device and Settings

The hull-mounted ATLAS PARASOUND P70 is a deep-sea parametric sub-bottom profiler (SBP) which utilizes the parametric effect based on non-linear relation of pressure and density during sonar propagation. Two high intensity waves with frequencies of ~18-20 kHz (a.k.a. primary high frequency, PHF) and a 22-24 kHz wave were used to create a so-called secondary high (about 40-42 kHz) and a secondary low frequency (SLF) of about 4 kHz. While the SLF is used for the sub-bottom profiling, the PHF signal can be recorded synchronously to image potential gas bubbles, plankton, fishes or nepheloid layers in the water column. The opening angle of the transducer array is 4 by 5, which corresponds to a footprint size of about 7% of the water depth. The data acquisition was performed with the real-time values of SSV measured close to the Tx/Rx-array (System C-Keel) and a static SVP of 1500 m/s (C-Mean). The program ATLAS PARASTORE is used for storing and displaying echograms, while the program ATLAS Hydromap Control (AHC) allows proper hydroacoustic settings during acquisition (shown in Appendix 5). During PARASOUND operations, data of the entire water column and sub-bottom are recorded and stored as vendor-specified *.asd files. The obtained data can be replayed in ATLAS PARASTORE software. Along with this raw files so-called *.ps3 and auxiliary data files were recorded for a certain given depth window.

5.2.2 Processing Methods

The above mentioned ps3-file format is used to further process and convert the data to SegY format or used to directly plot (and on-the-fly processed) profiles with the SeNT software (developed by H. Keil & V. Spiess, MTU-GeoB, University of Bremen, Germany).

5.2.3 Preliminary Results

During MSM57 Leg 1 and 2 the ATLAS PARASOUND was acquiring data in parallel to the EM122 MBES. Therefore around 7000 km of profiles were conducted. Fig. 22 shows an example of a cross-section over the Knipovich-Ridge. First analysis reveal a number of small sediment basins gradually deformed and tilted towards the center of the ridge were sediment coverage is strongly reduced or seems even absent.

5.3 Acoustic Doppler Current Profiler (ADCP)

Data were recorded from the two shipboard Acoustic Doppler Current Profiler (ADCP), the RDI Ocean Surveyor 38 and 75 kHz, both phased array. The systems are fully operational and require minimal operator interference. Data were acquired using the RDI software VMDAS (Vessel-Mount Data Acquisition). Operating parameters used during MSM57 are provided in Appendix 6. NOTE: The EA Heading alignment error in the OS75NBMSM57.txt is obviously wrong! Since 09.08.2016 the ADCP75kHz-settings were overwritten by the ADCP Alignment Correction (Edit Data Options) within the VMDAS software. According to the WTD (scientific technical service on board), the 75 kHz has no transducer misalignment whereas the 38 kHz transducer misalignment is 45° (clock wise rotated). During Leg 2 the ADCP38kHz has not been used. It is alternatively mounted to the EM1002 in the port-side moon-pool of the vessel.

5.4 Attributed Sensors (GPS/Navigation, Motion Reference Unit, Sound Velocity)

The ships position was calculated by the KONGSBERG SEAPATH 320 Inertial Navigation System (INS). Motion data (roll, pitch, heave) as well as heading and Differential Global Positioning System (DGPS) information was generated by the SEAPATH 320 in combination with the motion reference unit (KONGSBERG MRU 5+), and delivered to all hydroacoustic devices applied during MSM57. When using a SEAPATH 320 INS, the internal coordinate system refers to the approximate center of gravity (COG) of the vessel. This implies that lever arms and offsets to the DGPS antenna as well as the MRU are considered when referencing to an ideal plane at the COG. Every acoustic device on-board has its own lever arms or offsets between the given COG-plane and their own transceiver/receiver arrays or antennas, which are set by the different acquisition software packages. Positioning for ADCP, EM122, EM1002 and PS is provided by the SEAPATH 320 on R/V MARIA S. MERIAN. Posidonia USBL gets its position from DGPS1 via DSHIP (shipside-database). Surface sound velocity (SSV) is recorded in real-time (1/sec) by SV&P SMART probes, mounted starboard and redundant portside, near the transducer of the two MBES. Sound velocity profiles (SVP) were directly acquired with expendable sound velocity probes (XSV; n=2) and the AML-Oceanographic probe (n=3) which is lowered by one of the winches on board.

Relatively sparse SVPs were taken especially during leg two of the cruise, which leads to a more time consuming future processing of the data by modelling suitable SVPs to correct the bathymetry data. Currently still present residuals of wrong sound velocity can be seen in the bathymetric data, especially within the bathymetry of the continental slope (Fig. 20). Fig. 22 shows the influence of different water-masses of the Arctic and North-Atlantic and surficial glacial fresh-water inputs on sound velocity.

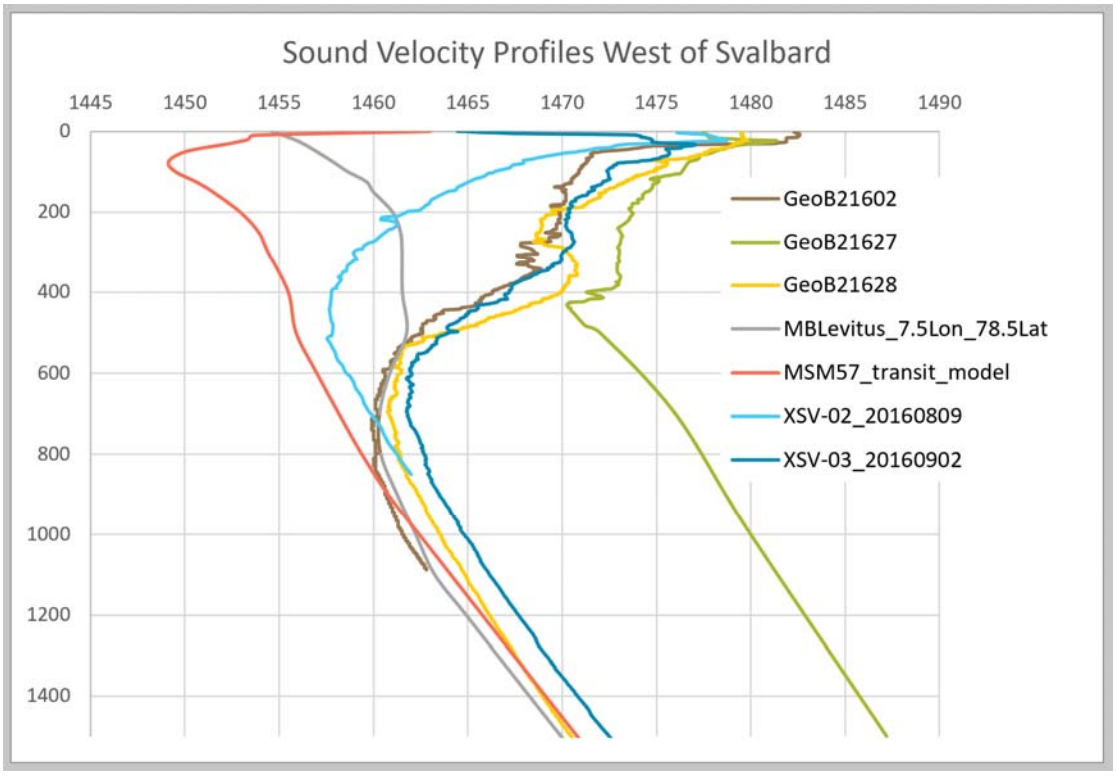

Fig. 22: Different sound velocities used during MSM57 show a very high dynamic within the first 400 m of the water column. GeoB21627 shows a clear offset down to 1500 m.

5.5 USBL Posidonia

IXSEA`s POSIDONIA 6000 is an ultra-short baseline (USBL) underwater navigation system and maintained by the scientific-technical service (WTD) on-board R/V MARIA S. MERIAN. The system is commonly mounted in the starboard-side moon pool. The last calibration of POSIDONIA has been conducted on 2nd of July, 2013. During the cruise, the system was used to supply navigation for MeBo deployments and positioning of heat-flow measurements as well as for gravity coring. To assure a proper refraction through the water column the SVP was updated for every area of investigation within the acquisition software ABYSS. The POSIDONIA spike-rejection filter was applied whenever using the device. It clearly enhances the position/depth output and avoids unrealistic jumps. On MARIA S. MERIAN DGPS support comes from DGPS1 via DSHIP. The system delivered very reliable and repetitive positions during the cruise.

5.6 Scientific Data Management (Hydroacoustic Data, GIS and DSHIP-Database)

Table 5 reveals the amount of storage needed during this cruise (about 35 days) for hydroacoustic data recording/processing as well as GIS and other scientific data. Water column data has been recorded only when gas flare search was required.

Table 5: Storage capacities needed for this cruise. NOTE: Please double or triple the size for backup copies.

Devices	RAW data	Processed data
EM1002	005	
EM122 Bathymetry	107	093
EM122 Water Column	053	
ADCP 38kHz	002	
ADCP 75kHz	008	
SBP Parasound P70	229	030
ESRI ArcGIS		010
Global Mapper GIS		053
Shipside Database export (DSHIP)	006	
Other scientific data	095	
Total GB	505	186

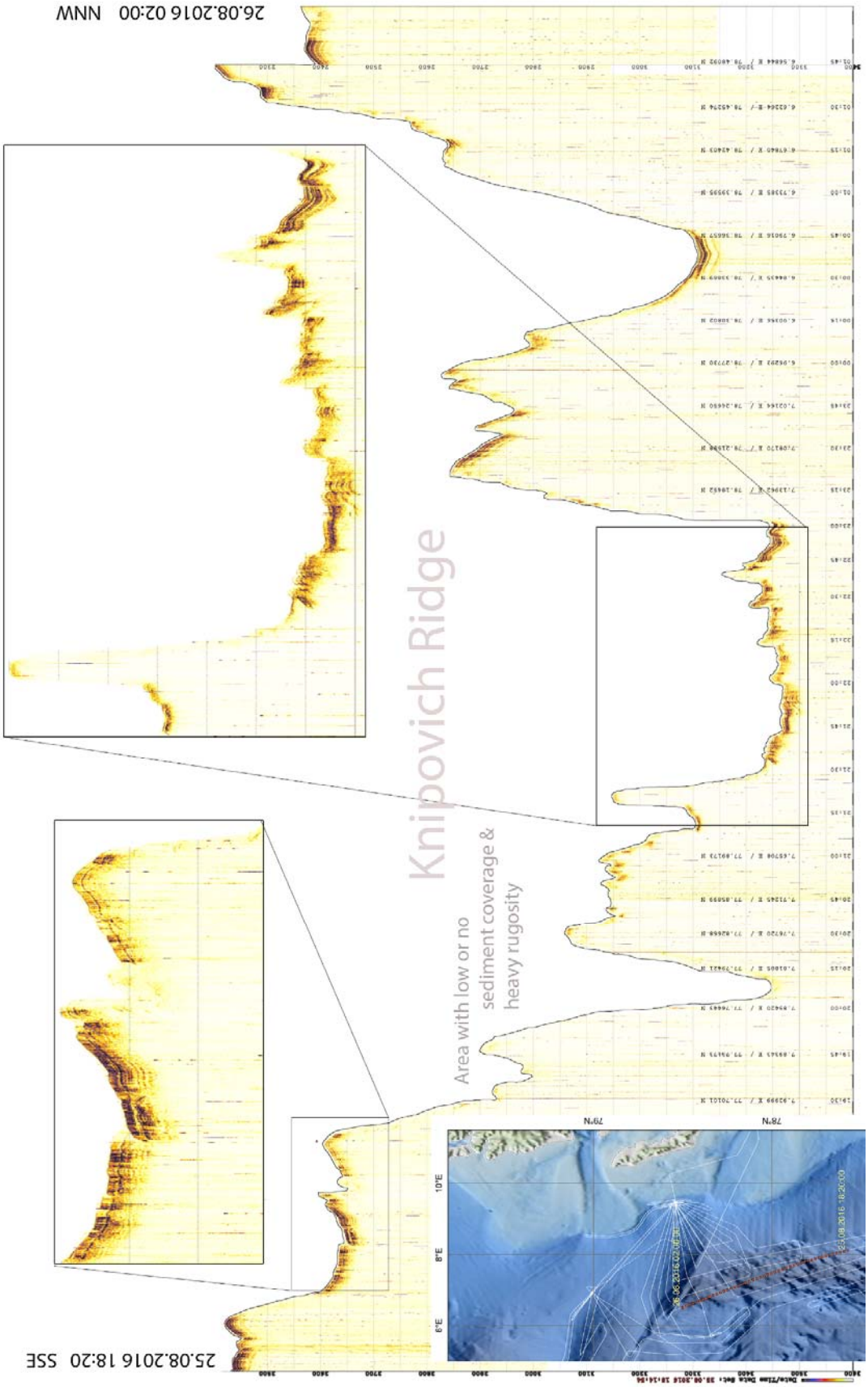

Fig. 23: PARASOUND sub-bottom-profile crossing the Knipovich-Ridge.

6 Measurement of in situ Geothermal Gradients and Thermal Conductivity

(M. Riedel, M. Bergenthal)

6.1 Introduction

During Cruise MSM57 we used two different techniques to define the subsurface geothermal regime. The majority of measurements were conducted with a heat flow probe, also called Giant Heat Flow (GHF) probe. This probe is capable to measure temperature within the upper 6 meter below seafloor. In order to define the deeper geothermal gradients, temperature measurements were made during MeBo drilling with a miniature temperature data logger (MTL) that is hydraulically pushed into the sediment. This new development was used for the first time regularly with MeBo during Cruise MSM57 and data acquisition and processing is still in the early phase and not routinely applied.

The mechanically robust GHF probe is designed for operation in pogo-style mode with a wide application range from 6000 m water depth to the upper continental slope. The 6 m long temperature sensor string allows measuring in situ temperature gradients, despite possible seasonal bottom water temperature variations. The heat-probe was used at several locations during Cruise MSM57, including active and inactive pockmark chains on the Vestnesa Ridge and Svyatogor Ridge to study fluid flow and gas hydrate formations. Previous heat-probe measurements were conducted on a regional scale across the study region (e.g. Crane et al., 1991), but no dedicated measurement campaign across the ridge was conducted prior to MSM57.

MeBo temperature measurements were conducted at drill sites on Vestnesa Ridge as well as in the shallow water regime of the continental margin near Prins Karls Forland. No GHF probe data were collected in this shallow-water region, as seafloor is typically covered with boulders and glacial debris, possibly damaging the tool. Also, this region has been intensely studied previously for the geothermal regime (e.g. Berndt et al., 2014) and included long-term monitoring at the MASOX and HYBIS sites.

6.2 Methods

6.2.1 Giant Heat Flow Probe

6.2.1.1 GHF Probe Tool Description

The heat probe (Fig. 24) is constructed in the classical “violin bow” design (e.g. Hyndman et al., 1979), with 22 thermistors distributed over an active length of 5.2 m in 0.26 m intervals inside an outer small tube (diameter of 14 mm) attached to the strength member (steel pipe of 130 mm diameter, Fig. 24). The sensor tube also contains a heater wire for the generation of high energy heat pulses typically on the order of 800 J/m for in situ thermal conductivity measurements according to the pulsed needle probe method (Lister, 1979). The data acquisition unit including power supply is housed in a single pressure case and mounted inside the probe’s weight stand. A second pressure case for the power supply used to generate the heat pulses is added in a second slot on the probe’s weight stand.

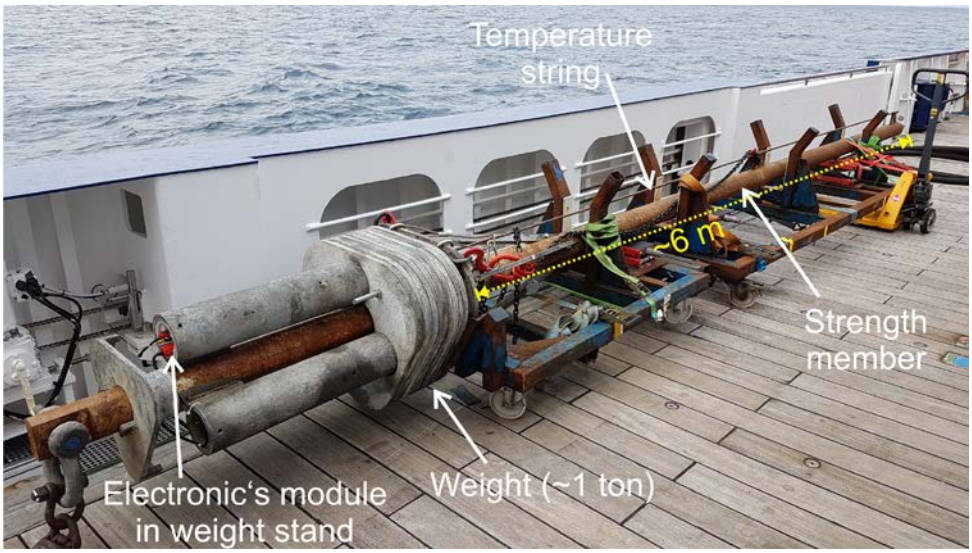

Fig. 24: Image of the heat-probe, secured in transportation carts on the starboard deck of MARIA S. MERIAN.

Fig. 25: Image of the deployment of the temperature probe on August 2nd at the starboard side of R/V MARIA S. MERIAN.

The signal of the temperature sensors is measured at a sample rate of 1 sec. A calibrated PT-100 seawater sensor on top of the weight stand allows to measure the bottom water temperature and to check the calibration of the sensor string in deep water with high accuracy. Tilt and acceleration of the probe is measured at a 1 sec sample rate to monitor the penetration process into the sediments and potential disturbances during the measurement time while the probe is in the sediment. The complete data set is stored in the probes' data acquisition unit. After each measurement campaign, the probe was brought back to the vessel, cleaned, and data were downloaded from the tool for post-processing.

6.2.1.2 Data Acquisition

The tool is deployed over the starboard side of the vessel using the main horizontal crane and the small starboard support crane (Fig. 25). After detaching the chains, the main crane lowers the tool to the seafloor. The acoustic pinger for positioning control with POSIDONIA was always mounted 60 m above the probe. Winch speed for penetration of the heat probe was ~1.0 m/s for maximum penetration into the sediment. During descent of the tool to the seafloor, we monitor winch-tension as main parameter to judge successful penetration. Once the tool fully penetrated and maximum relaxation of wire-tension was reached, a few meter of extra wire-length were paid out to prevent the tool from being accidentally pulled during swell. Upon recovery of the tool from the seafloor, we pulled at a speed of 0.2 m/s until the probe cleared seafloor. Maximum tension (pullout force) was recorded as an indicator of probe penetration depths. We have chosen a time of 7 - 8 minutes for temperature decay after initial penetration (from frictional heating) and the time for heat pulse decay observations was set to another 7 - 8 minutes. The heat probe position on the seafloor (and during descent) was monitored using the POSIDONIA positioning system available onboard the R/V MARIA S. MERIAN. Penetration of the heat probe into the upper meters of the soft sediments generates a thermal disturbance due to frictional heating. However, the probe will not have fully equilibrated at the end of this time. Therefore the temperature decay has to be fitted to a theoretical decay model. In situ thermal conductivity is measured with the heat pulse method (Lister, 1979) where the sensor string is heated up for typically 20 to 30 s and the thermal conductivity is derived from the shape of the temperature decay.

Since the probe was used in autonomous mode (no real-time monitoring), the probe was pre-programmed using three criteria to define conditions for generation of the heat-pulse. Those three criteria were set in a way that over a time period of 7 minutes after initial insertion into the sediment:

- tilt (in x and y-direction) had to be less than 0.3°,
- acceleration (z-direction) had to be less than 0.003 g,
- pressure differential (i.e. height of instrument) had to be > 100 dbar from previous insertion.

6.2.1.3 Data Processing Sequence

After device recovery the data stored on the acquisition unit has to be downloaded and converted to ascii-format. The entire data set of the time from programming, deployment, until recovery is then loaded into Matlab® for further processing. The codes for processing these data are provided by H. Villinger, University of Bremen. The individual penetration times, assumed onset of heat pulse and times for clearing the seafloor (see Appendix 2) are then used to split the data into individual “pen-files” representing each one separate penetration. Within each “pen-file” sequence, a portion of the temperature decay curves for each of the thermistors is used to find a best-fit temperature-decay curve. This modeled temperature decay curve then defines the equilibrium temperature. Onboard processing was done to generate initial thermal gradients and in situ thermal conductivity values to help guide sampling with MeBo and gravity cores. Additional processing is planned post-cruise.

6.2.1.4 Calibration of GHF Probe

Prior to using the probe in the sediments, calibration of the 22 thermistors is required. This is best done using the probe in deep water with a homogenous water-mass of uniform temperatures over the length of the probe (6 m). The location of the calibration was chosen in ~1200 m of water depth at the Vestnesa Ridge (see Table 6) with the average temperature of the water being around -0.8°C. The calibration is made by comparing each of the 22 temperature measurements to the standard measurement at the head of the probe (referred to as Pt100 in Fig. 26). The offsets of each sensor are stored in a separate file and applied during each data analysis procedure (see chapter 6.4). The portion of the data record used for calibration is shown in Figs. 27 and 28.

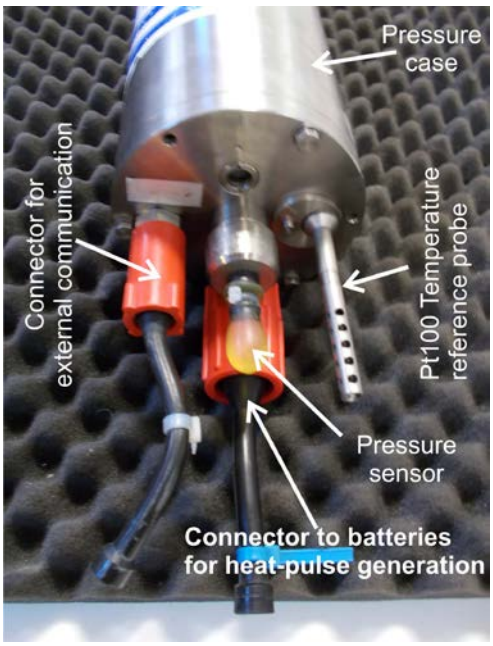

Fig. 26: Pressure case of temperature probe with reference Pt100 temperature probe and pressure sensor, used to guide heat-pulse generation.

Table 6: Calibration values for the temperature probe defined at Vestnesa Ridge.

Sensor	**S1**	**S2**	**S3**	**S4**	**S5**
T (°C)	-0.7615	-0.7046	-0.7216	-0.7343	-0.7259
Δ T(°C)	0.025	0.0819	0.0649	0.0522	0.0606
Sensor	**S6**	**S7**	**S8**	**S9**	**S10**
T (°C)	-0.8214	-0.8209	-0.8160	-0.8457	-0.7627
Δ T(°C)	-0.0349	-0.0344	-0.0295	-0.0592	0.0238
Sensor	**S11**	**S12**	**S13**	**S14**	**S15**
T (°C)	-0.7392	-0.7078	-0.7845	-0.7462	-0.7680
Δ T(°C)	0.0473	0.0787	0.0020	0.0403	0.0185
Sensor	**S16**	**S17**	**S18**	**S19**	**S20**
T (°C)	-0.7822	-0.7795	-0.7532	-0.7284	-0.8214
Δ T(°C)	0.0043	0.0070	0.0333	0.0581	-0.0349
Sensor	**S21**	**S22**	T of standard (PT100): -0.7865 °C		
T (°C)	-0.7500	-0.7135			
Δ T(°C)	0.0365	0.0730			

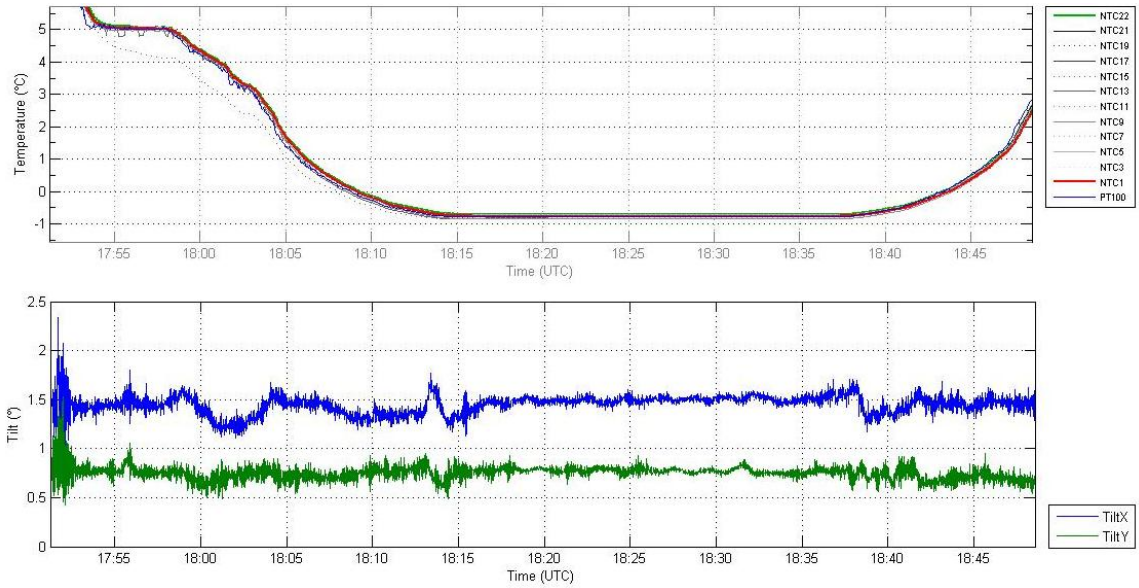

Fig. 27: Records of data from temperature calibration. Above panel shows temperature (as function of time) and lower panel shows the tilt (X, and Y-direction). A stable temperature record was reached at around 18:15 (UTC).

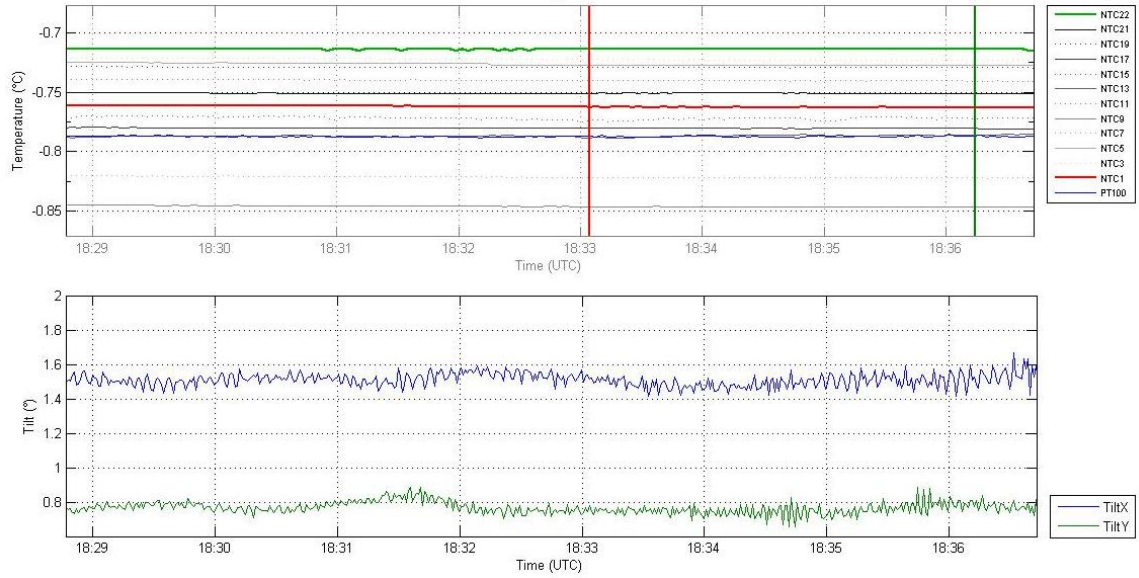

Fig. 28: Detailed view of the time interval used for defining offsets between each of the 22 thermistors to the standard temperature measurement. In the above panel, temperature is shown with the start and end times for defining average offsets shown as red and green bars, respectively. The lower panel shows the tilt of the instrument as function of time.

6.2.2 MeBo MTL

6.2.2.1 MTL Description

A miniature temperature data logger (MTL) built by 'Antares' (type 1854) was used for measuring temperature in situ with MeBo. The MTL was modified to fit into a pilot tube (Fig. 29). Initial testing of the technology was done during R/V SONNE Cruise 222 (Kopf et al., 2012). The electronics and battery of the MTL are located inside of a 16 mm diameter housing on top of a stainless steel tube (5 mm in diameter and ~100 mm long). The MTL is pre-programmed prior to loading into MeBo for deployment

and records data every 3 seconds for a total of 48 hours. The MTL was calibrated in the laboratory at MARUM prior to shipping.

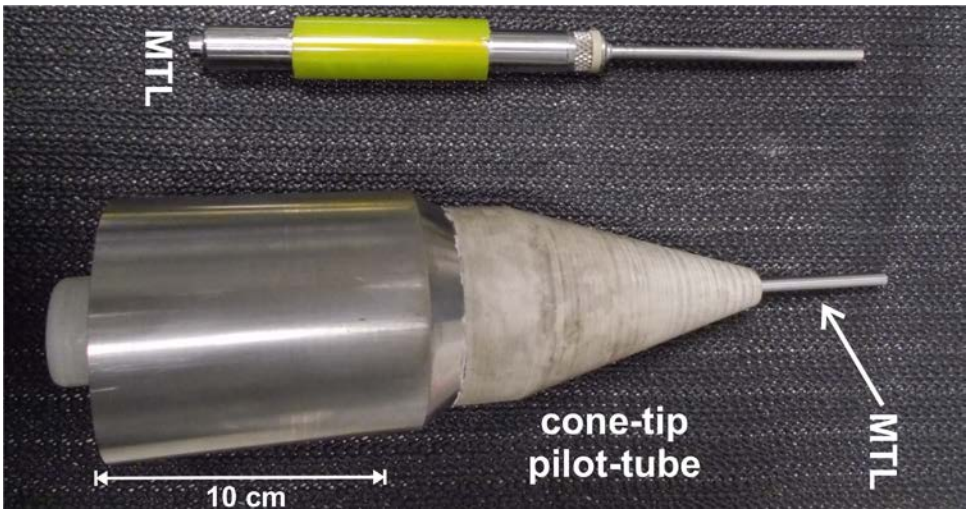

Fig. 29: Image of the MTL inside a pilot tube (lower) and the MTL itself (upper).

6.2.2.2 Data Acquisition Procedure

Data acquisition is autonomous inside the MTL for the duration of deployment. After recovery, data are downloaded from the MTL as continuous ascii-data record including a time-stamp, raw resistivity value, and converted values of temperature. At pre-defined drilling-depths, the MTL was inserted into the sediment, resulting in a frictional heating pulse (see Fig. 30) that then decays over time. As the probe is left in the sediments for up to 10 minutes, often temperatures almost reach equilibrium temperature of the formation. However, this is not always the case, and an additional first-order analysis-step is used onboard to extrapolate the incomplete temperature decay curve to the equilibrium stage using a plot of temperature as function of reciprocal time (Fig. 31). A liner fit to this data-curve then yields the equilibrium temperature as the intersection of the linear fit at reciprocal time “zero” (i.e. infinity).

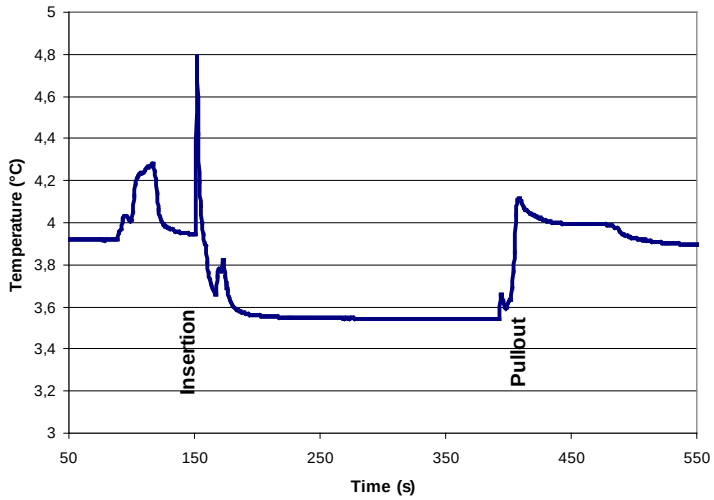

Fig. 30: Example of a temperature record from Station GeoB21643-1 (MeBo140) at a depth of 12.1 mbsf.

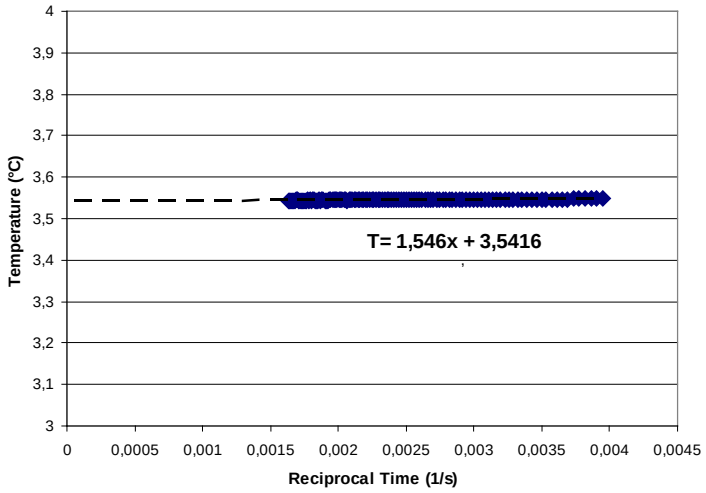

Fig. 31: Example of data analysis and extrapolation to establish equilibrium temperature (3.54° C) from the temperature record shown in Fig. 30.

6.3 Results

6.3.1 GHF Probe Data

During Cruise MSM57 a total of 10 individual deployment sequences of the GHF probe were conducted in different sub-regions of Vestnesa and Svyatogor Ridge, in addition to the calibration site. During these 10 sequences, a total of 102 individual probe-penetrations were completed. Only two of these did not yield useful information on the sub-seafloor geothermal regime due to incomplete penetration of the tool. Based on the record of rope-tension, we speculate that in both these instances the tool fell over as it could not penetrate deep enough into the sediment. Out of the 100 successful probe-insertions, 70 measurements included defining in situ thermal conductivities by employing the heat-pulse technique.

After the second deployment of the tool (TL-02, GeoB21603), we added a metallic segment to the 2nd mounting fin of the strength member to simplify tool deployment and recovery on deck. This metallic piece moved along the fin during tool-penetration into the sediment and was pushed closer to thermistor #16. In some cases, we noted unusually high in situ thermal conductivities near this sensor (relative depth below seafloor of ~3 m). The higher conductivity value is potentially related to the nearby metal (representing higher conductivity than the surrounding sediment). This modification was replaced with a more stable plate for the last deployment (TL-11, GeoB21642).

6.3.1.1 Vestnesa Ridge

At Vestnesa Ridge, we conducted a total of 65 probe penetrations (one unsuccessful, see Fig. 32 for overview map). These measurements focused on two active pockmarks called Lunde and Lomvi (Fig. 33) as well as adjacent northern, apparently inactive, unnamed pockmarks (Fig. 34). Additional data at 5 stations were taken across a fault-zone at the northern bend of the ridge (TL06, Fig. 32). We took 11 measurements around Lomvi Pockmark, and 30 stations were visited across Lunde Pockmark. Two stations were in between both these pockmarks. The adjacent inactive pockmarks were investigated with 15 stations. All results are listed in Tables 7 - 13. Finally a reference site (also MeBo Station 126) ~3 km south of Lomvi Pockmark has been conducted). The main result of the temperature measurements is a consistent difference in thermal gradients outside (average gradient of ~76° C/km)

and inside (average gradient of 95° C/km) of pockmarks. Also, the apparently inactive pockmarks north of Lunde (showing no gas flares) still show the same pattern, with stations inside a pockmark yielding an average thermal gradient of 85° C/km and stations outside a pockmark yielding an average gradient of 75° C/km.

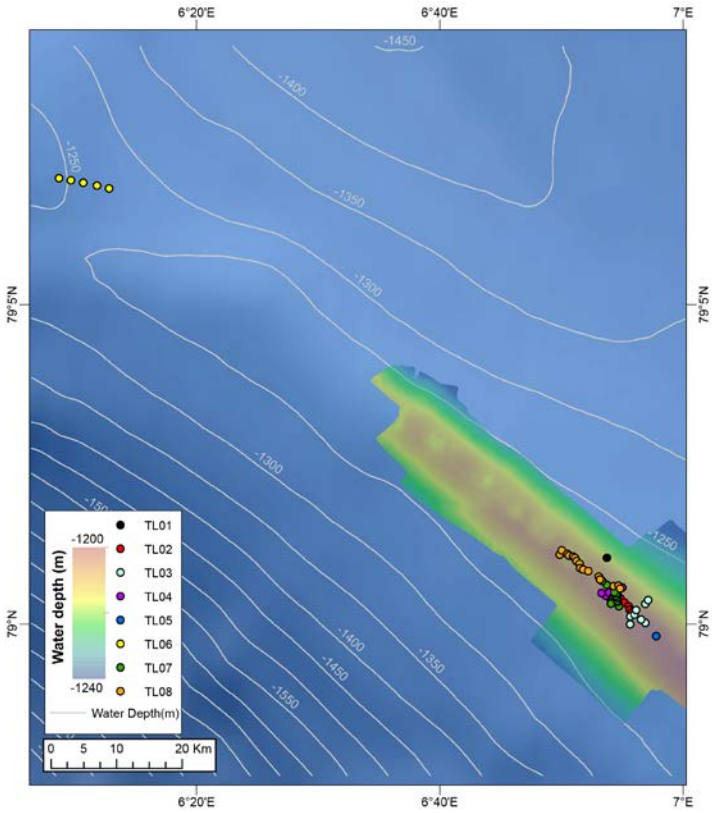

Fig. 32: Overview of all GHF deployment sites at Vestnesa Ridge.

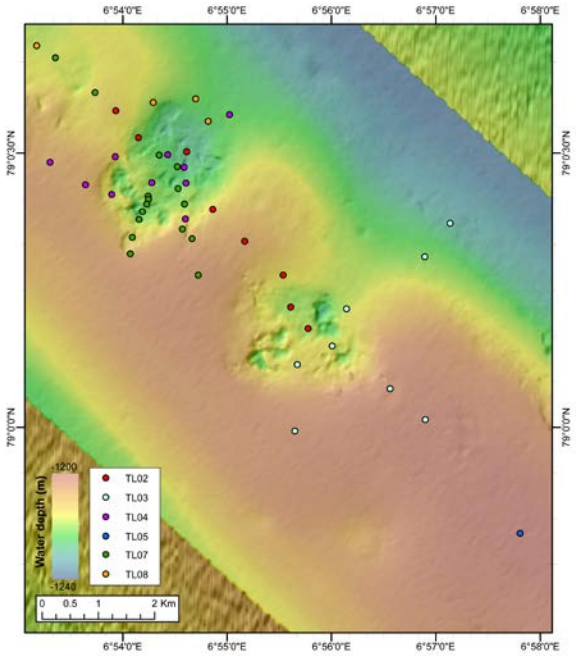

Fig. 33: Detailed image of deployment sites of the GHF probe at Lunde (northern pockmark) and Lomvi (southern pockmark). Bathymetry data are from P-cable 3D seismic data (courtesy S. Bünz, CAGE).

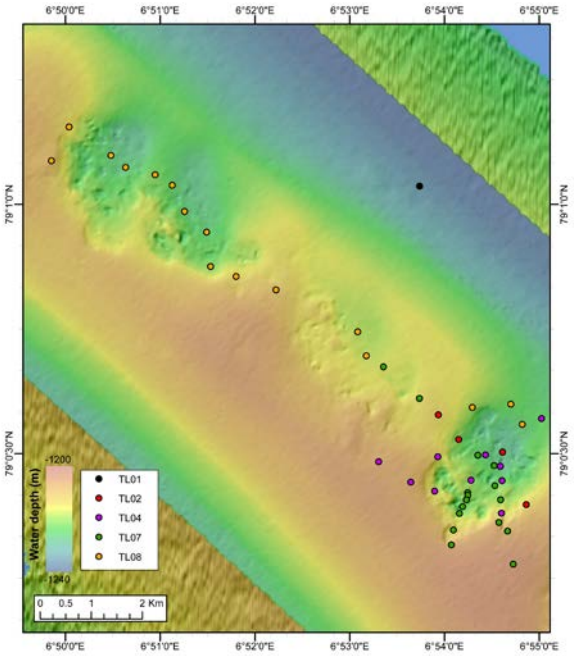

Fig. 34: Map showing locations of the deployment sites of TL08 (orange dots) across the apparently inactive chain of pockmarks north of Lunde Pockmark.

6.3.1.2 Svyatogor Ridge

Svyatogor Ridge had become a study focus after the discovery of possible abiotic methane as source-gas for methane hydrates (Johnson et al., 2015). Three deployments with the GHF probe were made (TL-09, -10, and -11) totaling 38 tool penetrations (one unsuccessful). Measurements were guided by previous gravity coring (Johnson et al., 2015). Three zones were chosen around prominent chains of pockmarks and fault outcrops (Fig. 35). The general pattern of higher thermal gradients inside pockmarks (115° C/km) relative to the region outside the depressions (95° C/km), already seen at Vestnesa Ridge, also holds true for Svyatogor Ridge. However, the geothermal gradients are overall much higher at Svyatogor Ridge, as the underlying crust is much younger (2 – 4 Ma) than at Vestnesa Ridge (> 10 Ma). Results are summarized in Tables 14 - 16. Three sub-regions were investigated: a southern cluster of pockmarks field (TL-09, Fig. 36), a northern field of pockmarks (TL-10, Fig. 37), and a central portion (TL-11, Fig. 38).

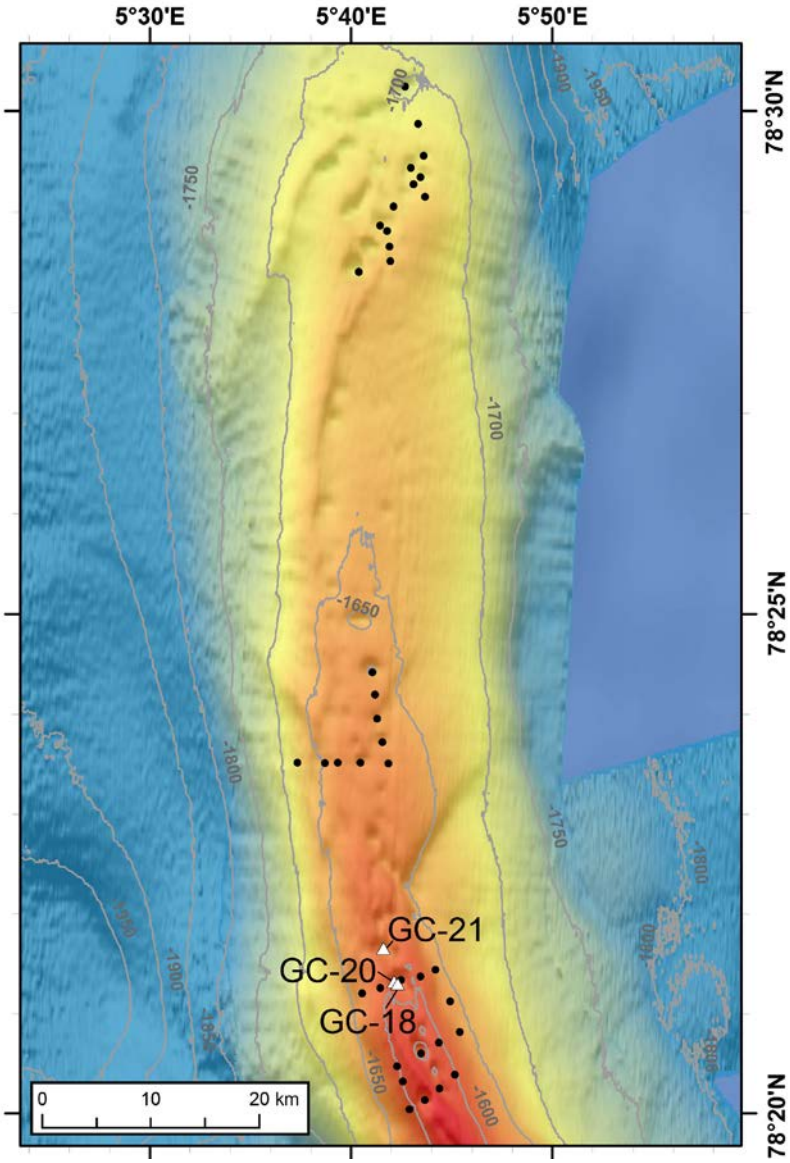

Fig. 35: Overview of GHF probe and gravity core stations along Svyatogor Ridge, including bathymetric data revealing prominent chains of pockmarks as well as fault outcrops.

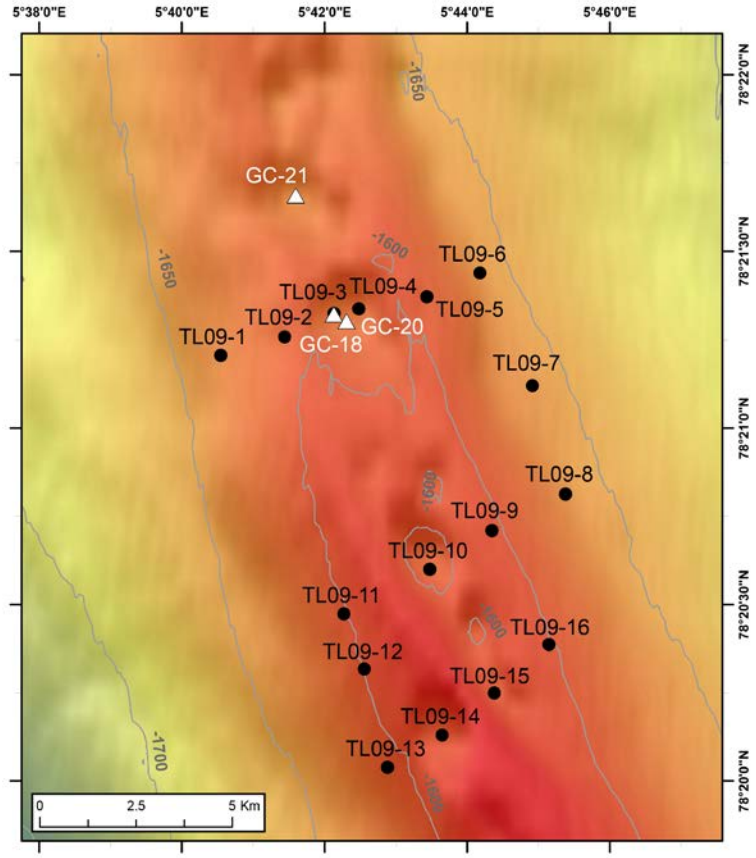

Fig. 36: Map of GHF probe stations of deployment TL-09 (and gravity cores) at the southern end of the Svyatogor Ridge

.

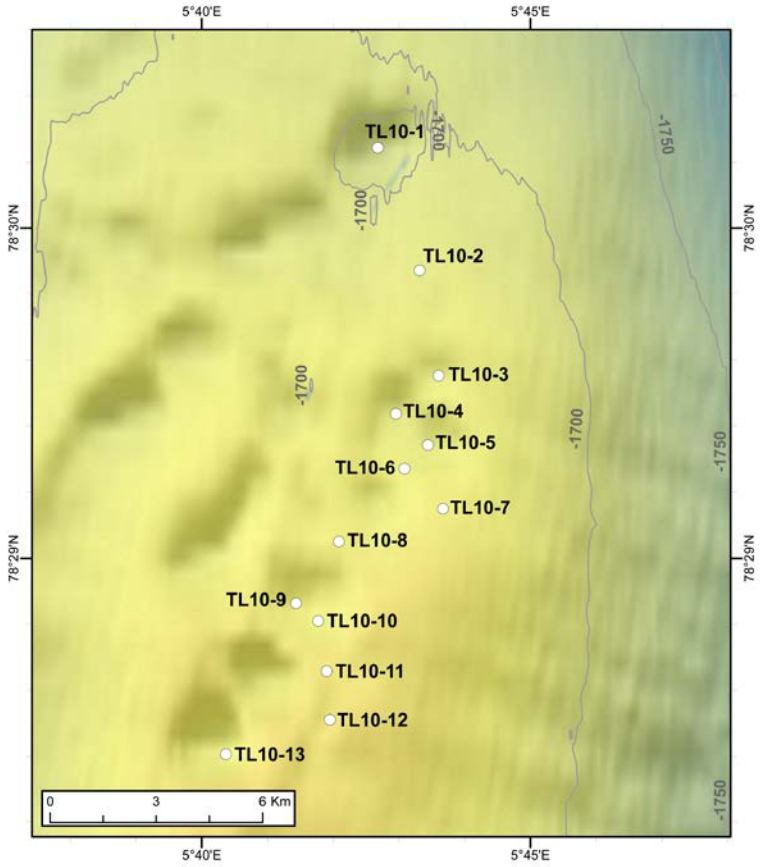

Fig. 37: Map of GHF probe stations of deployment TL-10 at the northern end of the Svyatogor Ridge.

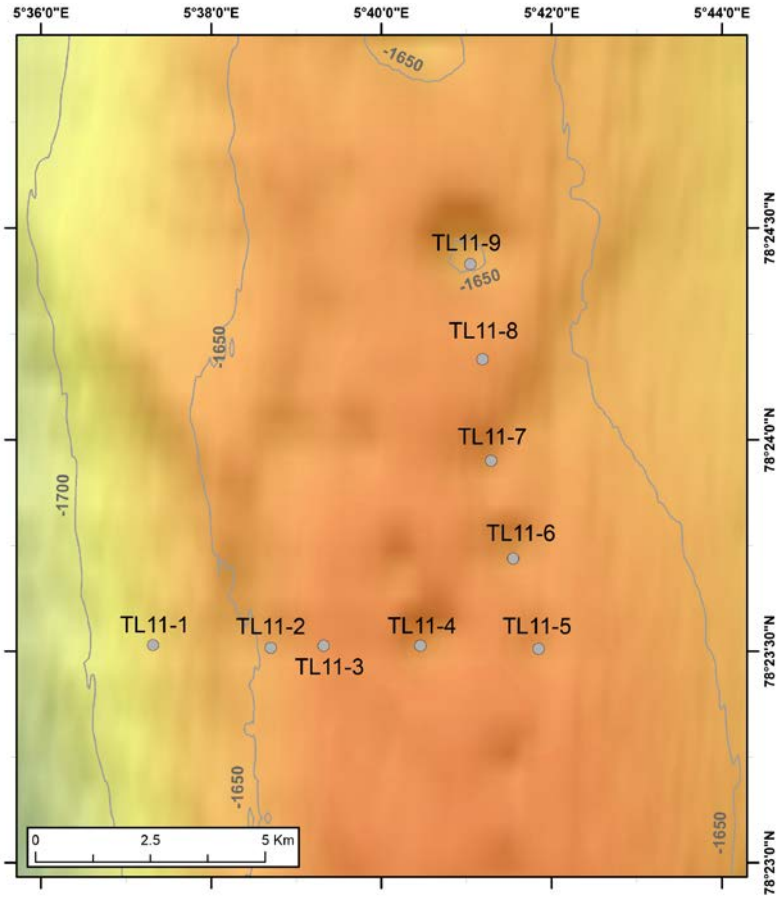

Fig. 38: Map of GHF probe stations of deployment TL-11 across the central portion of the Svyatogor Ridge.

Table 7: Results of measurements with the GHF probe for deployment TL02.

STN	Thermal gradient (°C/km)	Thermal Conductivity (W/m·K)	Heat Flow (mW/m²)
TL02-01	80,6	1,16	90,2
TL02-02	83,3	1.25 (assumed)	105
TL02-03	88,1	1,33	113,9
TL02-04	76,9	1.25 (assumed)	96
TL02-05	86,3	1,17	101,2
TL02-06	79,9	1.25 (assumed)	99,7
TL02-07	82,8	1,21	103,2
TL02-08	78,9	1,35	107,1

Table 8: Results of measurements with the GHF probe for deployment TL03.

STN	Thermal gradient (°C/km)	Thermal Conductivity (W/m·K)	Heat Flow (mW/m²)
TL03-01	77	1,25	96,8
TL03-02	74,3	1.25 (assumed)	92,7
TL03-03	77,1	1.25 (assumed)	96,1
TL03-04	83	1,25	108,3
TL03-05	80,2	1,23	99
TL03-06	78,9	1,17	93,5
TL03-07	78,2	1.25 (assumed)	97,6
TL03-08	80,8	1.25 (assumed)	101

Table 9: Results of measurements with the GHF probe for deployment TL04.

STN	Thermal gradient (°C/km)	Thermal Conductivity (W/m·K)	Heat Flow (mW/m²)
TL04-01	78,6	1,2	94,8
TL04-02	84	1,27	106,1
TL04-03	81,4	1.25 (assumed)	101,6
TL04-04	82,1	1.25 (assumed)	102,2
TL04-05	84,4	1,13	96,7
TL04-06	106	0,99	1035
TL04-07	73,8	1.25 (assumed)	92,4
TL04-08	76,3	1.25 (assumed)	95,1
TL04-09	78,8	1.25 (assumed)	100,3
TL04-10	81,5	1,27	103,1

Table 10: Results of measurements with the GHF probe for deployment TL05.

STN	Thermal gradient (°C/km)	Thermal Conductivity (W/m·K)	Heat Flow (mW/m²)
TL05-01	77,2	1,21	94,1

Table 11: Results of measurements with the GHF probe for deployment TL06.

STN	Thermal gradient (°C/km)	Thermal Conductivity (W/m·K)	Heat Flow (mW/m2)
TL06-01	90,7	1,1	101,5
TL06-02	90,5	1.25 (assumed)	113,1
TL06-03	95,8	1,24	121,8
TL06-04	85,3	1,12	98,8
TL06-05	86,6	1.25 (assumed)	107,7

Table 12: Results of measurements with the GHF probe for deployment TL07.

STN	Thermal gradient (°C/km)	Thermal Conductivity (W/m·K)	Heat Flow (mW/m²)
TL07-01	86,8	1,15	97
TL07-02	80,9	1,29	106,7
TL07-03	79,5	1,22	98
TL07-04	100	1,1	101,8
TL07-05	Failed attempt		
TL07-06	83,3	1,29	107,7
TL07-07	70,4	1.25 (assumed)	90
TL07-08	68,5	1,2	82,6
TL07-09	68,7	1,22	86,7
TL07-10	75,3	1,18	89,3
TL07-11	84,3	1,19	98,9
TL07-12	87,3	1,28	113,9
TL07-13	79,6	1.25 (assumed)	97
TL07-14	76,6	1.25 (assumed)	95,6
TL07-15	72,4	1,21	90,4
TL07-16	75,8	1,19	90,2

Table 13: Results of measurements with the GHF probe for deployment TL08.

STN	Thermal gradient (°C/km)	Thermal Conductivity (W/m·K)	Heat Flow (mW/m²)
TL08-01	72,3	1,2	88,6
TL08-02	75,7	1,16	89,5
TL08-03	83	1,16	96,1
TL08-04	78,2	1,2	95,3
TL08-05	76,4	1,15	89,2
TL08-06	78,2	1,25 (assumed)	98,1
TL08-07	89,9	1,18	110,6
TL08-08	78,6	1,16	94
TL08-09	85,6	1,14	97,8
TL08-10	77,1	1,25 (assumed)	95,8
TL08-11	75,1	1,24	93,7
TL08-12	92,6	1,55	138
TL08-13	83,3	1,25 (assumed)	103,4
TL08-14	81,1	1,37	115,0
TL08-15	76,7	1,25 (assumed)	95,8
TL08-16	77	1,28	104,2

Table 14: Results of measurements with the GHF probe for deployment TL09.

STN	Thermal gradient (°C/km)	Thermal Conductivity (W/m·K)	Heat Flow (mW/m²)
TL09-01	106,0	1,36	145,4
TL09-02	94,6	1,36	132,7
TL09-03	126,0	1,25 (assumed)	158,2
TL09-04	115,0	1,25 (assumed)	144,6
TL09-05	83,5	1,37	118,8
TL09-06	111,0	1,35	151,6
TL09-07	106,0	1,25 (assumed)	132,2
TL09-08	109,0	1,33	146,7
TL09-09	84,3	1,38	118,6
TL09-10	121,0	1,33	162,7
TL09-11	88,1	1,33	120,1
TL09-12	88,1	1,38	124,3
TL09-13	95,4	1,37	134,2
TL09-14	109,0	1,30	142,7
TL09-15	114,0	1,33	151,3
TL09-16	88,9	1,35	121,3

Table 15: Results of measurements with the GHF probe for deployment TL10.

STN	Thermal gradient (°C/km)	Thermal Conductivity (W/m·K)	Heat Flow (mW/m²)
TL10-01	131,0	1,32	175,0
TL10-02	95,0	1,29	121,0
TL10-03	104,0	1,32	139,0
TL10-04	106,0	1,21	128,0
TL10-05	73,0	1,25 (assumed)	73,0
TL10-06	98,0	1,30	131,0

TL10-07	111,0	1,35	148,0
TL10-08	94,0	1,37	129,0
TL10-09	121,0	1,29	154,0
TL10-10	105,0	1,42	147,0
TL10-11	90,0	1,37	120,0
TL10-12	110,0	1,24	138,0
TL10-13	115,0	1,33	150,0

Table 16: Results of measurements with the GHF probe for deployment TL11.

STN	Thermal gradient (°C/km)	Thermal Conductivity (W/m·K)	Heat Flow (mW/m²)
TL11-01	103,0	1,39	146,1
TL11-02	99,4	1,25 (assumed)	124,8
TL11-03	Failed attempt		
TL11-04	127,0	1,34	164,6
TL11-05	111,0	1,37	152,5
TL11-06	116,0	1,37	157,8
TL11-07	111,0	1,25 (assumed)	139,0
TL11-08	89,5	1,25 (assumed)	110,0
TL11-09	119,0	1,29	154,1

6.3.2 MeBo

6.3.2.1 Measurements at Vestnesa Ridge

At the Lunde Pockmark, a total of six MeBo drill-sites were established. Three sites are within the eastern depression (MeBo123, -124, and -125) and three within the western depression, closer to the active gas flares (MeBo127, -128, -138). Only two successful temperature measurements were made at these sites. In order to achieve a robust thermal gradient, these are combined and integrated with data from the GHF probe (Fig. 39).

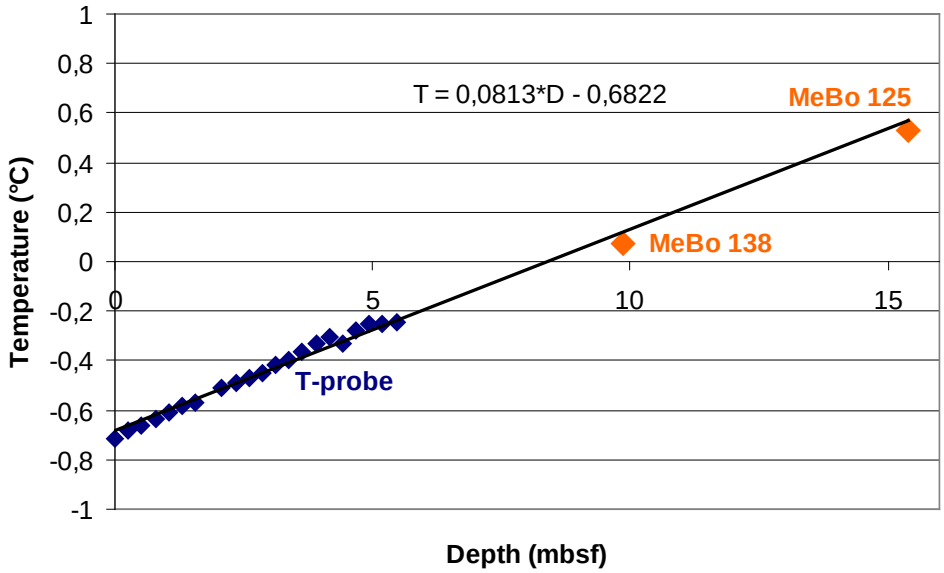

Fig. 39: Integration of temperature data from Lunde Pockmark. The combined data yield a thermal gradient of ~81°C/km. Note that all GHF data are below 0°C.

At the reference site drilled outside the pockmarks (MeBo126), five successful temperature measurements were made with MeBo. The data (without the near-seafloor data form the GHF probe) yield a thermal gradient of 80°C/km (Fig. 40). The near-seafloor data from the GHF suggest a gradient of ~77°C/km, and integrating all data yields a quite robust gradient of 78°C/km.

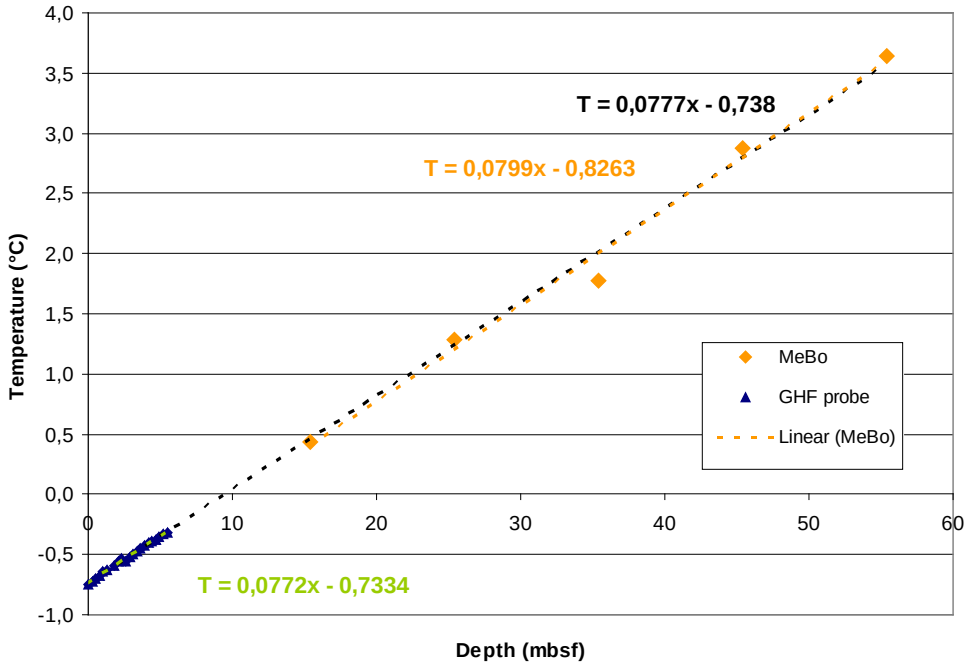

Fig. 40: Synthesis of temperature data from GHF probe at Station TL05-01 (blue) and MeBo measurements (orange) at the references Site of Vestnesa Ridge (GeoB21613-1, MeBo126). The black trend line is the integrated thermal gradient.

6.3.2.2 Measurements at the Continental Margin Sites

To investigate the deep thermal structure of the continental margin sites, a total of 13 successful temperature measurements were made with the MeBo MTL tool (Table 17). Three attempts were discarded for defining in situ temperatures. Combining data from the various drill sites and grouping those into three water-depth zones allowed the definition of thermal gradients for these zones (Fig. 41):

445 m: 37°C/km
405 m: 45°C/km
390 m: 49°C/km

A fourth location (MeBo140) in 402 meter water depth was drilled above a prominent seismic reflection, interpreted as gas-associated bright spot. The thermal gradient at this site is ~50°C/km.

Table 17: Temperature measurements with MeBo on the continental margin sites.

Station	Depth (mbsf)	Temperature (°C)	Comments	Depth-range (Fig. 41)
21632-2 MeBo134	10,3	3,46		390
	17,9	3,77		

21626-1,2 MeBo129-1,2	10,325	3,486		404
	10,325	3,546		
	17,925	3,796		
21631-1 MeBo130	12,82	not successful		405
21633-1 MeBo135	10,325	3,353		446
21633-3 MeBo136	10,325	3,375		446
	20,325	3,758		
	27,925	4,02		
21634-1 MeBo137	9,875	not successful		390
21639-1 MeBo139	12,75	not successful		390
	21,625	4,119		
21643-1 MeBo140	12,125	3,5654		402
	19,275	3,8165		
	26,325	4,366		

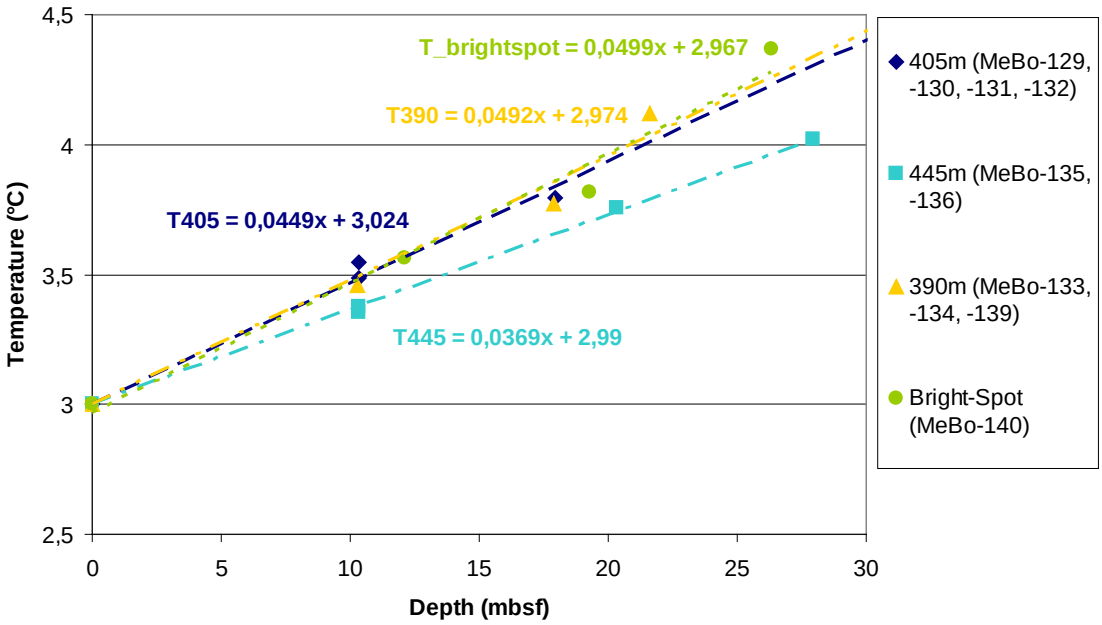

Fig. 41: All MeBo temperature measurements at the continental margin sites and respective calculated thermal gradients.

6.4 Outlook for Post-Cruise Analyses

Data processing onboard focused on quality control and defining first-order thermal gradients. Heat-flow values, the product of the measured (or assumed) average thermal conductivity with the thermal gradients, need to be further corrected for secondary effects, such as sedimentation rates (or erosion rates) as well as seasonal fluctuations in bottom-water temperatures. These will be conducted post-cruise. Further integration of the 6 m heat probe data with those MeBo acquired data will also be done post-cruise, including analyses of the respective thermal gradients and their influence on gas hydrate stability.

7 Seafloor Drilling with MeBo

(T. Freudenthal, M. Bergenthal, R. Düßmann, F. Ahrlich, T. Klein, C. Seiter, U. Rosiak, S. Froelich, A. Stachowski, G. Spagnoli, K. Kaszemeik, K. Noorlander, W. Schmidt, M. Reuter, A. Kausche, S. Meckel)

7.1 Technical Description

During R/V MARIA S. MERIAN Cruise MSM57, the seafloor drill rig MARUM-MeBo70 (Fig. 42) was used for getting long sediment cores. This device is a robotic drill that is deployed on the sea bed and remotely controlled from the vessel (Fig. 43). The complete MeBo system, including drill, winch, launch and recovery system, control unit, as well as workshop and spare drill tools is shipped within six 20' containers. A steel armoured umbilical with a diameter of 32 mm is used to lower the 10-tons heavy device to the sea bed where four legs are being armed out in order to increase the stability of the rig. Copper wires and fibre optic cables within the umbilical are used for energy supply from the vessel and for communication between the MeBo and the control unit on the deck of the vessel. The maximum deployment depth in the current configuration is 2000 m.

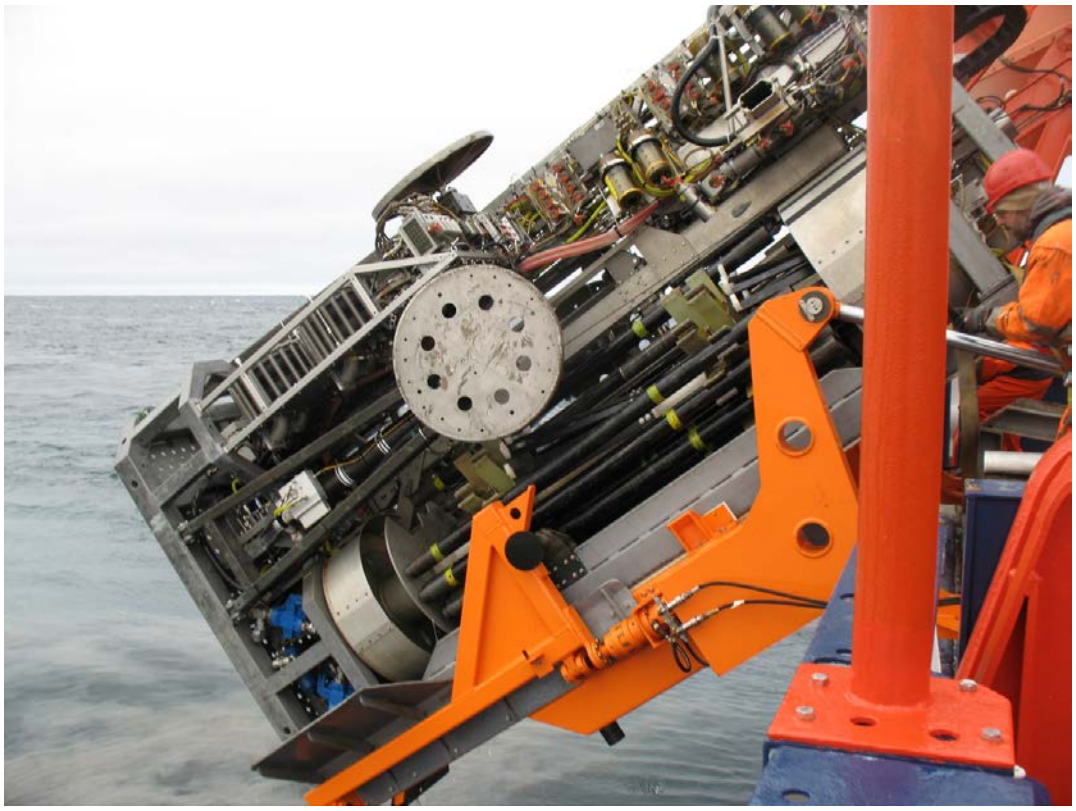

Fig. 42: The sea floor drill rig MARUM-MeBo70 on R/V MARIA S. MERIAN.

The mast with the feeding system forms the central part of the drill rig (Fig. 43). The drill head provides the required torque and rotary speed for rock drilling and is mounted on a guide carriage that moves up and down the mast with a maximum push force of 4 tons. A water pump provides sea water for flushing the drill string for cooling of the drill bit and for removing the drill cuttings. Core barrels and rods are stored on two magazines on the drill rig. We used wire-line core barrels (HQ) and hard metal drill bits with 55 mm (push coring) and 63 mm (rotary drilling) core diameter. The stroke length was 2.5 m (aluminum rods) or 2.35 m (steel rods). With complete loading of the magazines a maximum coring depth of more than 70 m can be reached. Station time can reach more than 24 hours per deployment.

A Spectrum Gamma Ray (SGR) probe was used for borehole logging. The probe is equipped with a 25 cm long scintillation crystal combined with a photo-multiplier. Light impulses that are generated by gamma ray collisions with the scintillation crystal are counted and analysed concerning the energy spectrum. The three naturally occurring gamma ray emitters - potassium, uranium and thorium - generate different energy spectra. A GeoBase software package is used to calculate a best fit for the spectra. By combining the results of the Spectrum fit with the gammy ray counts the concentrations of K, U, and Th are calculated.

The SGR-Memory is an autonomous tool that is used with the MeBo drilling system. When the maximum coring depth is reached the inner core barrel is replaced by the probe. The gravity point of the sensor is located about 125 cm above the drill bit and measures through the drill pipe. The probe is hooked up the bore hole together with the drill pipe during recovery of the drill string (logging while tripping). Tripping speed was about 0,6 m per minute.

A temperature probe was used for measuring formation temperature at different sediment depths. The temperature probe consists of a probe that replaces an inner core barrel for conducting temperature measurements at discrete depths. The lower end of the probe is located below the drill bit at the base of the drill string and is equipped with a miniaturized temperature data logger (MTL) with a 95 mm long tip. The temperature range of the MTL is -5 to 50°C with a resolution of about 1 mK. The absolute accuracy is about ±0.1K. The probe is pushed together with the drill string by 15 cm into the sediment. After 10 minutes measuring time the temperature probe is hooked up out of the drill string using the wire line technique and core drilling can proceed.

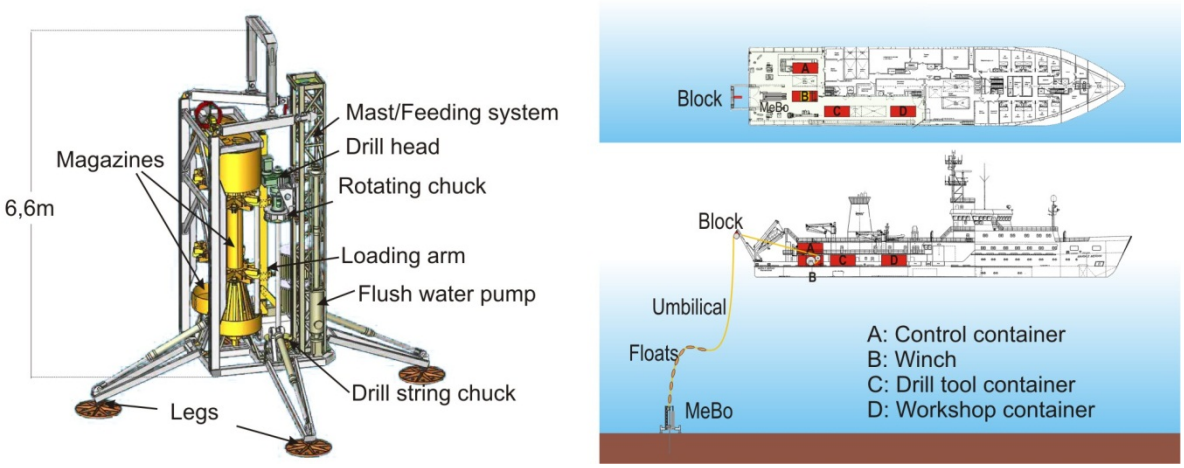

Fig. 43: Schematic overview on the MeBo drill rig (left) and its deployment from a research vessel (right)

7.2 Core Material Obtained

The MeBo was deployed 19 times to sample long cores in the investigation area west of Svalbard. In total, the MeBo was deployed for 333 hrs. 395 m were drilled. During several deployments the drill string was flushed through the upper meters since interest was only in cores below the penetration of gravity core deployments at these sites. In total 395 m were drilled of which 328 m were cored with an average recovery rate of 34 %. Altogether 25 temperature measurements at 12 stations were conducted. Bore hole logging with the SGR logging probe was conducted at one station. Detailed information on MeBo deployments and core recovery is summarized in the station list (Table 18).

Table 18: Station list for MeBo deployments.

Station GeoB No.	Deploy. duration [hrs:min]	Latitude [N]	Longitude [E]	Water depth [m]	Drill depth [cm]	Coring length [cm]	Total core recovery	Remarks
21604-1 #123	07:00	79°0,48'	6°54,54'	1214	280	260	100 cm 39%	
21608-1 #124	07:07	79°0,48'	6°54,57'	1213	530	510	161 cm 32%	
21610-1 #125	14:00	79°0,48'	6°54,57'	1215	2280	270	905 cm 45%	T (15,4 m)
21613-1 #126	41:50	79°59,84'	6°57,77'	1200	6250	1995	2465 cm 42%	T (15,4 m; 25,4 m; 35,4 m; 45,4 m; 55,4 m) SGR (59-0 m)l
21616-1 #127	21:37	79°0,45'	6°54,21'	1209	1390	5905	281 cm 26%	CORK (14 m)
21621-1 #128	08:30	79°0,46'	6°54,26'	1212	775	1075	447 cm 59%	
21626-1 #129-1	39:00	78°33,21’	9°27,06’	405	2290	1255	395 cm 32%	T (10,4 m; 17,7 m)
								10 m shift w/o recovery
21626-2 #129-2		78°33,21’	9°27,07’	405	2530	1980	254 cm 13%	T (10,4 m; 17,9 m)
21631-1 #130	10:58	78°33,24‘	9°27,34'	405	1530	745	53 cm 7%	T (12,9 m)
21631-3 #131	9:48	78°33,24‘	9°27,34'	405	1530	260	82 cm 32%	
21631-4 #132	13:09	78°33,24‘	9°27,33'	404	2030	270	116 cm 43%	
21632-1 #133	9:43	78°33,13‘	9°29,65'	395	1025	1005	268 cm 27%	
21632-2 #134	23:15	78°33,14‘	9°29,65'	395	1025	1005	283 cm 28%	T (10,4 m; 18 m)
21633-1 #135	11:13	78³32,94‘	9°22,79'	445	1775	1740	427 cm 25%	T (10,4 m)
21633-3 #136	25:49	78°32,94‘	9°22,78'	445	3800	3755	555 cm 15%	T (10,4 m; 20,4 m; 28 m)
21634-1 #137	14:40	78°33,59‘	9°32,53'	340	2160	2125	431 cm 20%	T (9,95 m)
21637-1 #138	26:14	79°00,43‘	6°54,24'	1201	2395	2360	870 cm 37%	T (9,95 m)
21639-1 #139	26:18	78°33,13‘	9°22,78'	390	2615	2565	1203 cm 47%	T (12,25 m; 21,7 m)
21643-1 #140	22:28	78°35,29‘	9°23,97'	402	3330	3250	1708 cm 53%	T (9,95 m; 12,2 m; 19,35 m; 26,4 m)
Total	**332:35**				**39540**	**32815**	**11203 cm 34%**	

7.3 MeBoPLUG (CORK) and CORK-Sonar

(A. Kopf, T. Fleischmann, P. Wintersteller, G. Bohrmann)

7.3.1 Methods: New Observatory Technologies That Monitor Gas Hydrate Stability

7.3.1.1 MeBoPLUG2 Borehole Observatory

The name MeBoPLUG of this second generation instrument is leant from the SmartPlug and GeniusPlug observatories, which also represent simple types of CORKs designed as extension to mechanical bridge plugs, but IODP drillhole-sized (Kopf et al., 2011). Instead of a bridge plug or CORK seal, we make use of the conical threads of the MeBo drill pipes and seal the pipe with a pair of additional o-rings (Figs. 44 and 45). The pressure housing is machined from stainless steel. At the top, a POM handle designed to specification of the ROV MARUM-QUEST manipulator was added. In the borehole-facing section, a thermistor as well as the downward-looking P port are situated (Fig. 44 inset on right).

Inside the housing we hosted standard "RBR Duo" data loggers (see www.rbr-global.com for detailed specifications) with Keller PD10 differential pressure transducers (500 kPa differential P range) for monitoring pressure transients in the boreholes (as a proxy for strain; Davis et al., 2006) relative to the seafloor pressure signal. With this approach we omit de-tiding of our data because all signals from wave action, etc. occur more or less simultaneously at the seafloor and in the shallow sub-seafloor formation. In the lowermost part of the instrument, pointing into the open MeBo borehole, we mounted a conductivity transducer (Sea&Sun 7-pole cell conductivity sensor). Given that only one thermistor was fitted into the so-called MeBoPLUG2, we are lacking a temperature record from the seafloor (i.e. upward-looking side of the MeBoPlug; see Fig. 44). In order to overcome this shortcoming, we have placed a temperature logger into the mooring next to the MeBo borehole.

Top of MeBoPLUG2 with POM handle for ROV recovery on top of the stainless steel P housing hosting the electronics

Inside view of the P housing showing the electronics with the KELLER pressure transducer and tubing, and also underwater plugs to connect to the conductivity sensor

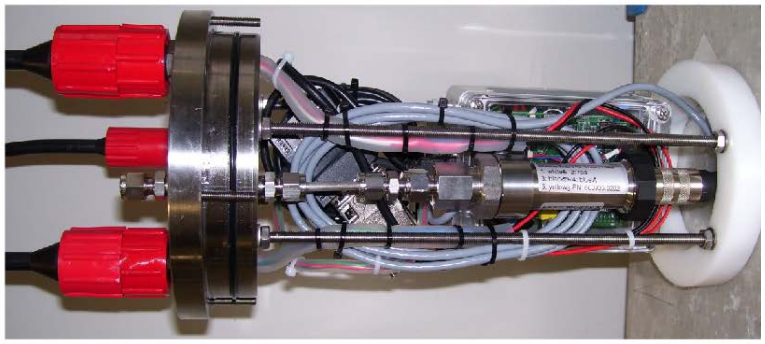

Lower portion of the MeboPLUG2 assembly showing the lower part of theP housing and its connection to the Sea & Sun conductivity sensor and thermistor

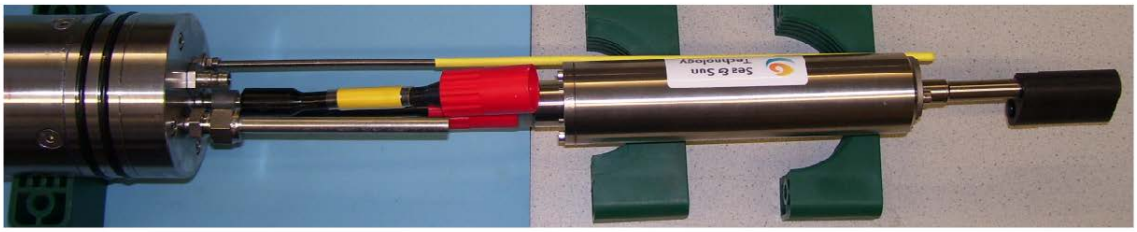

Fig. 44: MeBoPlug prior to being screwed into a MeBo drill pipe (left); right photograph shows bottom view into the borehole with ports for P (hole at left) and T (little pin at right) monitoring. See text.

Fig. 45: Picture of the system on board MERIAN prepared with fresh sealing to be mounted on an iron drill string.

7.3.1.2 Trawl-Safe "Sonar-CORK" to Quantify Seepage

We have designed a low-profile, self-contained mooring to monitor physical parameters indicative of fluid escape by recording pressure, temperature, electrical conductivity and quantifying methane bubbling. As main component, the moorings host an Imagenex 881 circumference sonar system that may be used for both bedform monitoring or gas bubble quantification. This system has been mounted at an upward-looking angle of appx 30° and is programmed to scan a window of 160° only. In addition, P-neutral seafloor batteries as well as a data acquisition and additional transducers for pressure (digitally interfaced Keller P33X) and temperature transducer placed in a P housing within the frame (see Fig. 46). Both transients in P and T, and more importantly freshening of the seawater as well as increasing amounts of methane bubbles over time will enable us to identify and quantify gas hydrate instability over time.

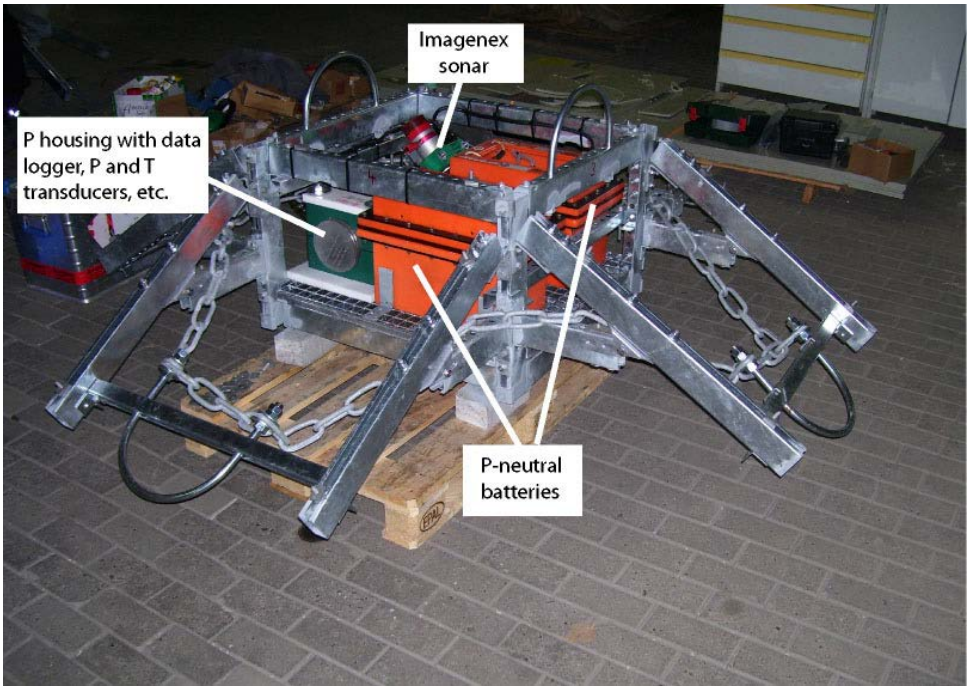

Fig. 46: Trawl-safe Sonar-CORK for gas hydrate stability monitoring, equipped with sonar system, P, T and el. conductivity transducers. Naked frame with batteries, electronics etc.

7.3.2 Deployment: Decisions and Positions

With respect to the documented and actual active venting at the Lunde pockmark in the direct vicinity of MeBo127 and the Sonar-CORK these sites were chosen to place the devices. The exact locations are shown in Fig. 48. Deployment of the CORK (MeBoPLUG2) took place on 7 August 2016. The device was placed on a 15 m long iron drill string. After a kind advice of our MeBo colleagues we used Aqua-Shield (http://aquashieldusa.com/) to seal the MeBoPLUG2 (Fig. 45) which should allow a later removal of the plug.

The Sonar-CORK was assembled on board about a day before deployment. Fittings and connections of two different metals were covered with zinc to avoid electrochemical corrosion (Fig. 47). The sonar was connected to the battery an hour before deployment. All the covers were tied up with additional ropes. Fig. 49 shows the Sonar-CORK during deployment.

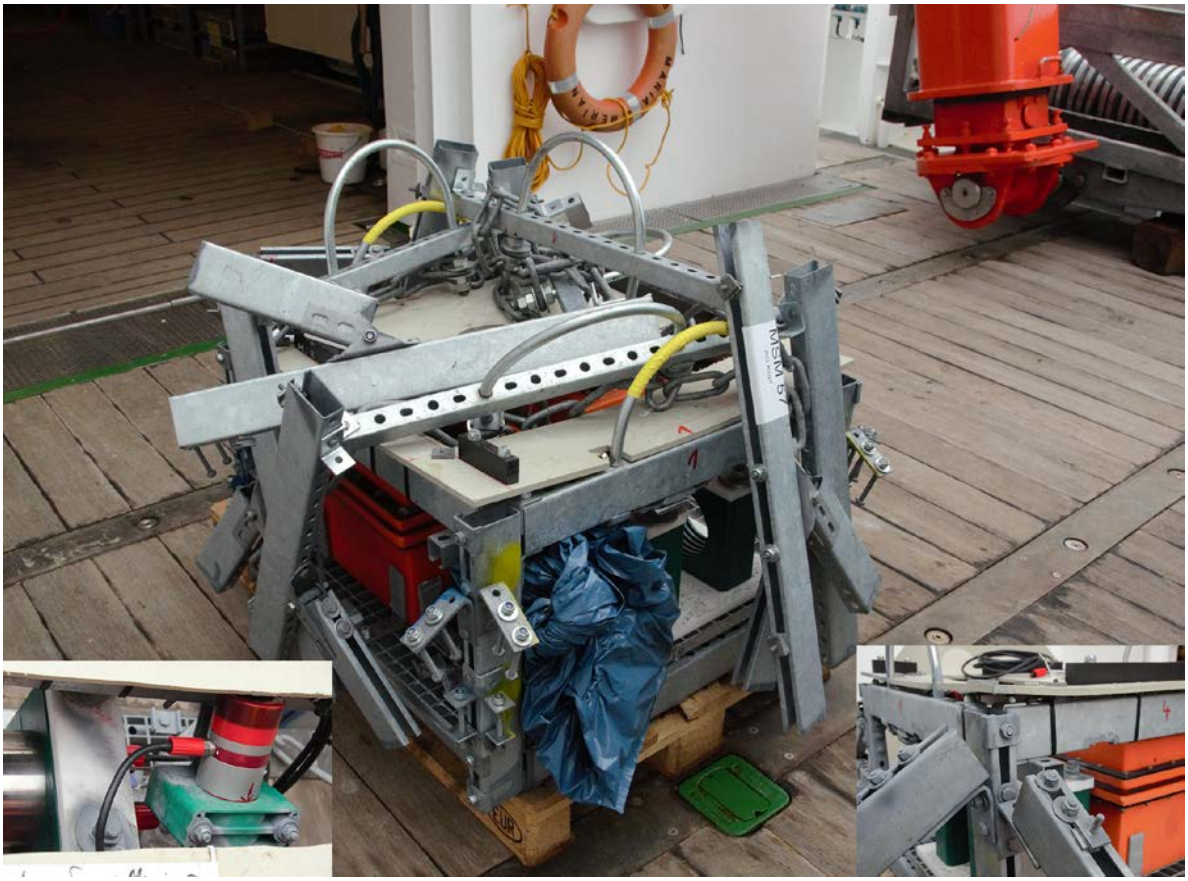

Fig. 47: Picture of the system on board MARIA S. MERIAN before assembling. Fittings and bi-metal connections got a zinc-protection.

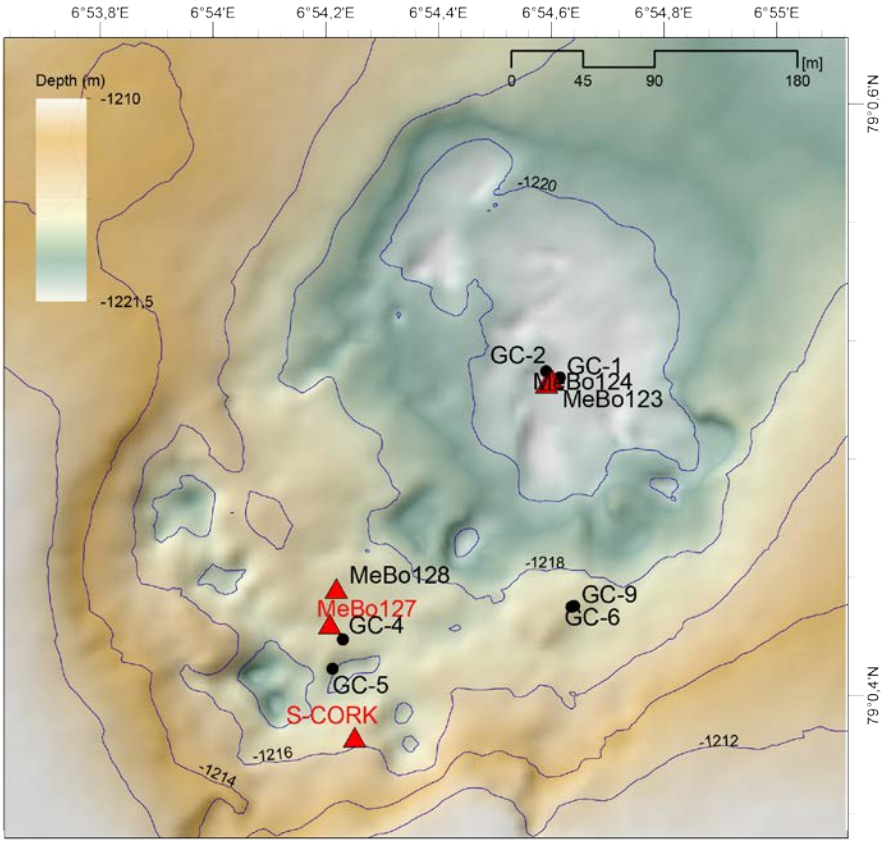

Fig. 48: Map of Lunde pockmark with the MeBo, GC and S-CORK positions.

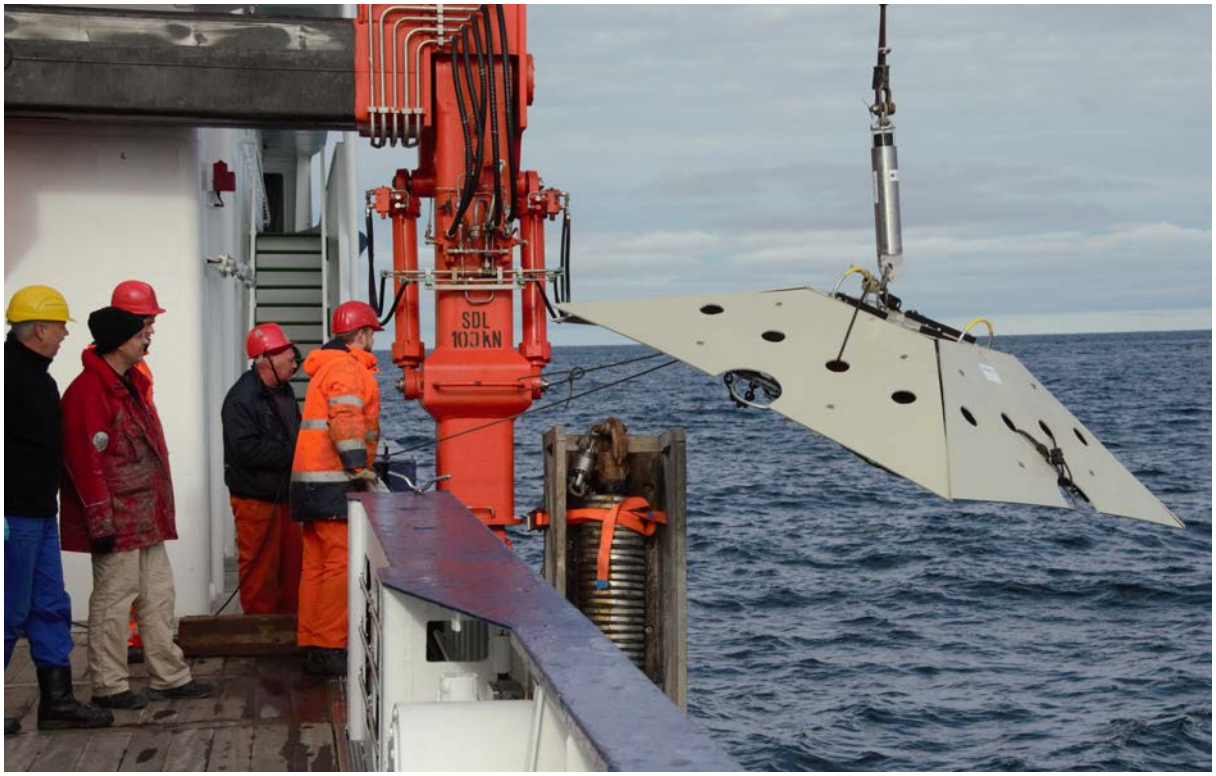

Fig. 49: Sonar-CORK deployment handling on board R/V MARIA S. MERIAN.

8 MeBo Drilling Sites

During R/V MARIA S. MERIAN Cruise MSM57 nine sites were drilled using the portable remotely operated drilling system MeBo70 (Freudenthal and Wefer, 2013). Drilling operation included 19 holes, from which seven holes were drilled at Vestnesa Ridge (Fig. 50), and 11 holes were drilled at the upper West Spitzbergen continental margin of (Fig. 54).

8.1 Vestnesa Ridge

(S. Bünz, G. Bohrmann)

Drilling on Vestnesa Ridge focused on gas hydrate presence, and dynamics of gas hydrate-related-processes inside and outside the pockmark structures. Pockmarks that are hundreds of meters in diameter and tens of meters in vertical relief occur along the ridge crest (Bünz et al. 2012; Hustoft et al. 2009). Gas bubbles were reported to emanate from some of the pockmarks using the 18 kHz signal of the Simrad EK60 echo-sounder (Hustoft et al. 2009) and show that free gas from below is actively passing the gas hydrate stability zone and reaches the seafloor. Chimneys in the sediment sequence, associated to the pockmarks are well expressed in high-resolution P-cable 3D seismic data by the occurrence of amplitude anomalies (Petersen et al. 2010; Plaza-Faverola et al. 2010; Bünz et al. 2012). Gas hydrates have been recovered by gravity cores from those pockmarks which are active by gas emissions (Fisher et al. 2011; Panieri et al. 2014; Smith et al. 2014; Hong et al. 2016).

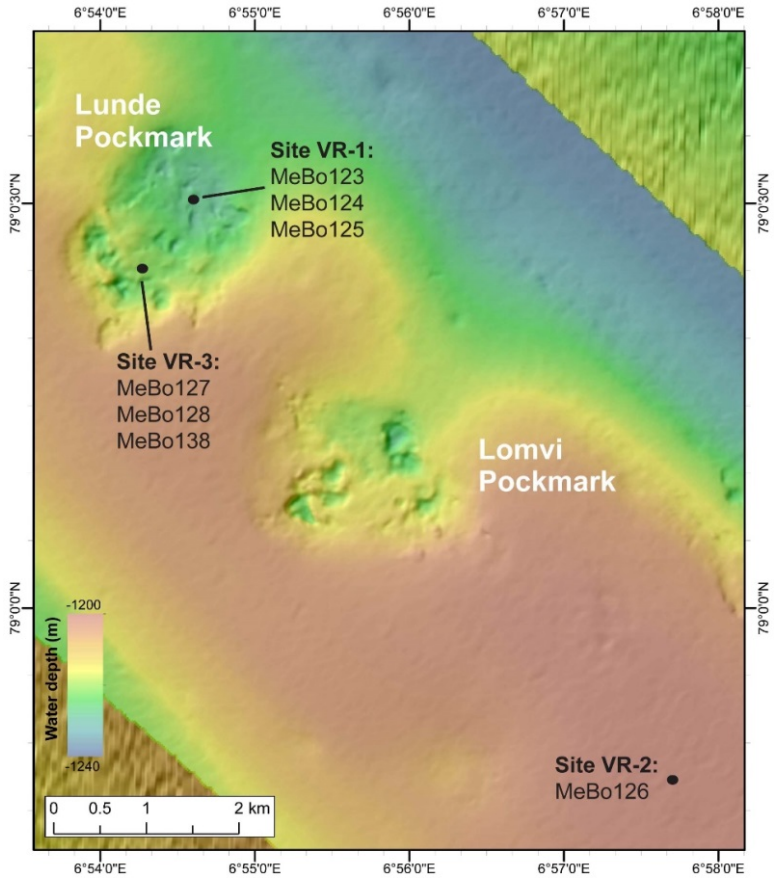

Fig. 50: Bathymetric map from a part of Vestnesa Ridge including two pockmarks known as Lunde and Lomvi Pockmark. Seven MeBo drill holes at three sites were drilled during MSM57.

During the cruise seven holes were drilled at three sites named Vestnesa Ridge 1-2 (VR 1-3) which differ in geological structure (Fig. 50; Tab. 19).

Table 19: MeBo Sites drilled during Cruise MSM57 at Vestnesa Ridge.

MeBo Drill sites	Water Depth [m]	Drilling Depth [mbsf]	Recovered sediment	Latitude [N]	Longitude [E]	Location
MeBo123	1213	2.80	1.00 m	79°00.50‘	06°54.625‘	VR-1: Lunde Pockmark, non-vent site
MeBo124	1212	5.30	1.61 m	79°00.502‘	06°54.615‘	VR-1: Lunde Pockmark, non-vent site
MeBo125	1212	22.80	9.05 m	79°00.503‘	06°54.621‘	VR-1: Lunde Pockmark, non-vent site
MeBo126	1198	62.50	24.65 m	78°59.806‘	06°57.808‘	VR-2: Vestnesa Ridge, background
Mebo127	1210	13.90	3.52 m	79°00.418‘	06°54.245‘	VR-3: Lunde Pockmark, vent site
MeBo128	1211	7.55	4.47 m	79°00.430‘	06°54.255‘	VR-3: Lunde Pockmark, vent site, CORK
MeBo138	1209	23.95	8.70 m	79°00426‘	06°54.246‘	VR-3: Lunde Pockmark, vent site

8.1.1 Non-seep Site at Lunde Pockmark VR-1

Lunde Pockmark (Fig. 50) is one of the pockmarks active by gas seepage documented by acoustic water column anomalies and the seismic data indicate that probably significant amounts of methane and methane hydrate are present within the chimney structure (Bünz et al. 2012). Drilling at VR1 addresses sediments within the pockmark, where no active seepage at the seafloor exist.

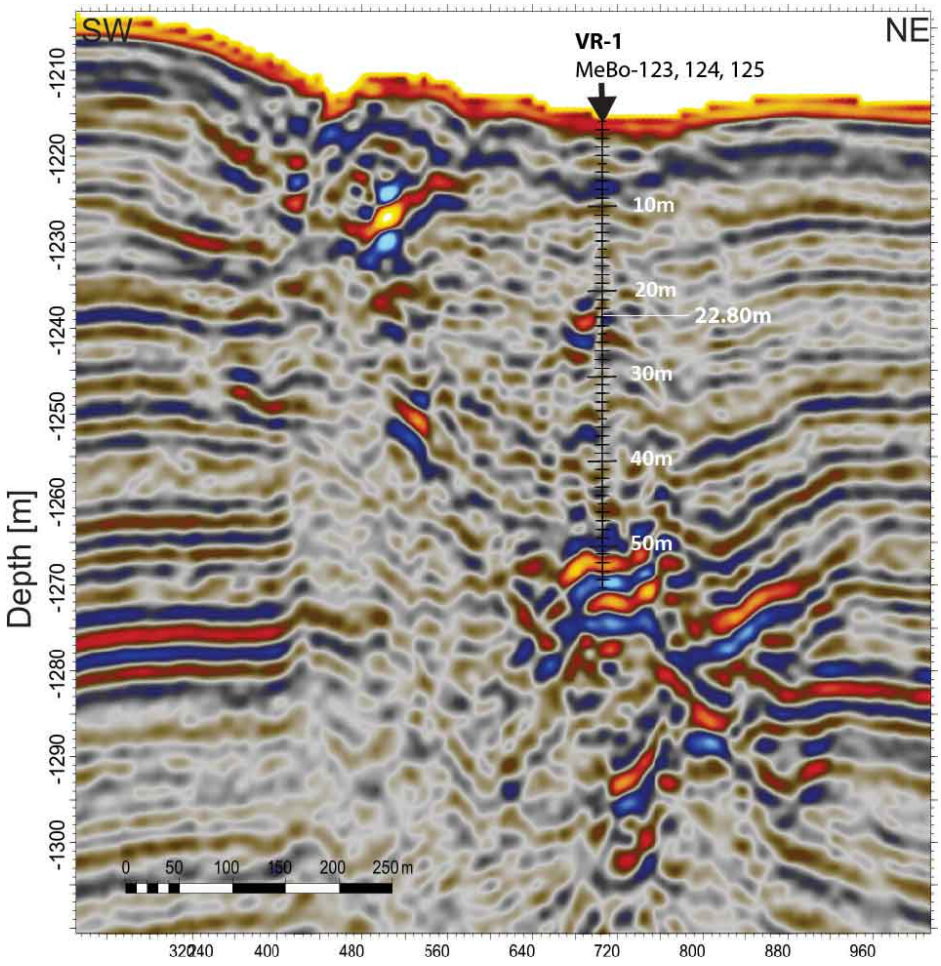

Fig. 51: High-resolution seismic data showing a profile from northeast to southwest over the MeBo drill site VR-1 within the Lunde Pockmark. The drilling location shows no seepage at the surface (P-Cable 3D seismic data from R/V HELMER HANSSEN (Bünz, 2013)).

Based on the 3D seismic data and the detailed bathymetry a location some tens of meters to the northeast of the center of the pockmark in 1212 m water depths was selected (Fig. 50). The plan was

to drill down to sediment depths deeper than 50 mbsf, where high amplitude anomalies have been documented. MeBo drillings 123 and 124 had technical problems and had to be stopped in 2.80 m and 5.30 m respectively. MeBo drilling 125 reached a drilling depth of 22.80 mbsf and sampled a sequence of sediments that differ in seismic pattern to structures outside of the pockmark, however, indications of methane saturation and gas hydrate occurrence have not been found in these uppermost sediments of the non-vent site.

8.1.2 Vestnesa Ridge Background Site VR-2

In order to drill the normal sediment sequence on Vestnesa Ridge that is not disturbed by any gas and fluid seepage we drilled MeBo Hole 126 at VR-2, a location approximately 8 km southeast of the Lunde Pockmark (Fig. 50). Based on the 3D-data (Fig. 52) from the P-cable cruise R/V HELMER HANSEN (Plaza-Faverola et al. 2015) a location was selected that was several hundred meters away from chimneys and vertical faults, which are normally present close to the crest of Vestnesa Ridge.

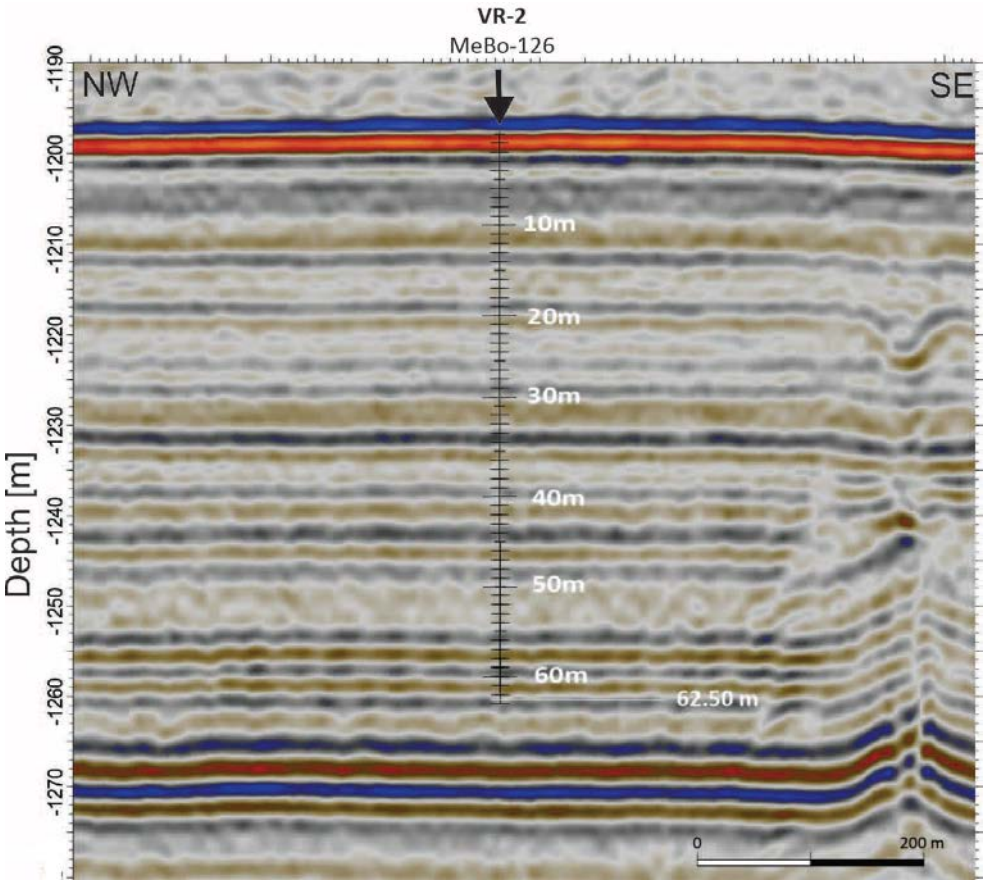

Fig. 52: High-resolution seismic line along the crest of Vestnesa Ridge (NW-SE direction). MeBo drill site VR-2 was selected in a sediment sequence where no indication of fluid or gas seepage was observed in seismic data (P-Cable 3D seismic data from R/V HELMER HANSSEN, (Bünz, 2013)).

Drill Hole MeBo126 at Site VR-2 is located in at 1,200 m water depth and drilled down to 62,50 mbsf (Fig. 52). Due to some large dropstones intercalated with the sediments, which hampered the drilling procedure, recovery rate was 42 %. Gas hydrates or any indications for methane hydrates have not been recovered. Nevertheless a sediment sequence that was never drilled before is now available and defines the background sequence outside the pockmarks.

8.1.3 Seep Site at Lunde Pockmark VR-3

Vestnesa Ridge Drill Site VR-3 was drilled at an active seep site at the southwestern part of Lunde Pockmark. The location was selected because high amplitude reflectors occur within the uppermost 25 mbsf and the active seepage is documented by continuously gas bubbling to a height of up to 1,000 m in the water column (Smith et al. 2014). The seepage site is connected in its deeper parts below 20 mbsf by steeply dipping reflections that are tilted to the northeast where higher amplitude reflections occur in 50 mbsf below Site VR-1 (Fig. 51). The tilted trace within the seismic line (Fig. 53) was interpreted as a fault responsible for gas transport from deeper in the chimney to the seafloor.

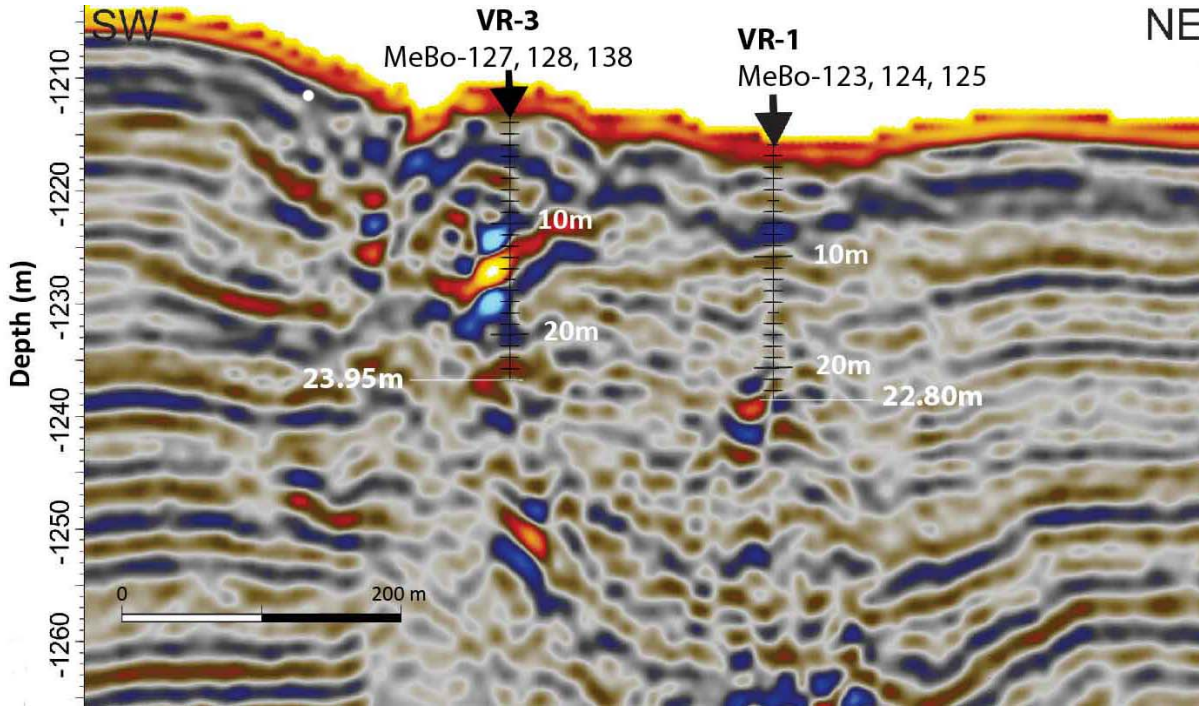

Fig. 53: High-resolution seismic line over Lunde Pockmark from northeast to southwest over the MeBo drill sites VR-1 and VR-3 within the Lunde Pockmark. VR-3 drilling location was performed where seafloor seepage occurs (P-cable data from R/V HELMER HANSSEN (Bünz, 2013))

A newly mapped micro-bathymetry of Lunde Pockmark showed that the former Drill Site VR-1 at a non-seep location was performed in a completely flat area. In contrast the seep location VR-3 was drilled at a small-scaled hilly ground. Water depths of the three drill holes MeBo127, 128, and 138 varied only between 1,209 m and 1,211 m, because we tried to avoid the seafloor landing of the MeBo device on the flank of seafloor pit and searched always for a flat area. Because of shallow-buried authigenic carbonates and gas hydrates we had to stop drilling in 13,90 mbsf (Mebo127) and 7.55 mbsf (MeBo128) respectively. During drilling of MeBo Hole 138 the drill bit could drill down to nearly 24 mbsf. Beside gas hydrates in most of the sediments massive light carbonates have been drilled below ca. 15 mbsf, where the highest amplitude anomaly exist in the seismic record (Fig. 53). These seep carbonates are dominantly composed of breccia of carbonate and clay clasts mixed with shells from chemosynthetic clams. The clasts are connected by thick pure carbonate rim-cements. Voids have been formerly filled by methane hydrates. Hole MeBo127 was closed by a CORK accompanied by a sonar observatory (see Chapter 7.3), which will be retrieved during an upcoming ROV cruise.

8.2 Upper Continental Margin

(G. Bohrmann)

Six sites were drilled at water depths between 340 m and 445 m at the upper continental margin west of Prinz Karls Forland, a north-south elongated Island west of Spitzbergen (Figs. 54 and 55). Numerous plumes of gas bubbles concentrated at water depths around 390 m have been interpreted as gas emissions probably released from gas hydrates at the upper boundary of the gas hydrate stability zone (Westbrook et al. 2009). Warming of the northward-flowing West Spitzbergen current by 1°C over the last 30 years was inferred from oceanographic data and was interpreted to have increased the release of methane from the seafloor by reducing the extent of the gas hydrate stability zone. A profile of five drill sites (Fig. 54: CM-1, CM-3, CM-4, CM-5 and CM-6) was planned to provide data from the sediments for supporting the hypothesis published by Westbrook et al. (2009).

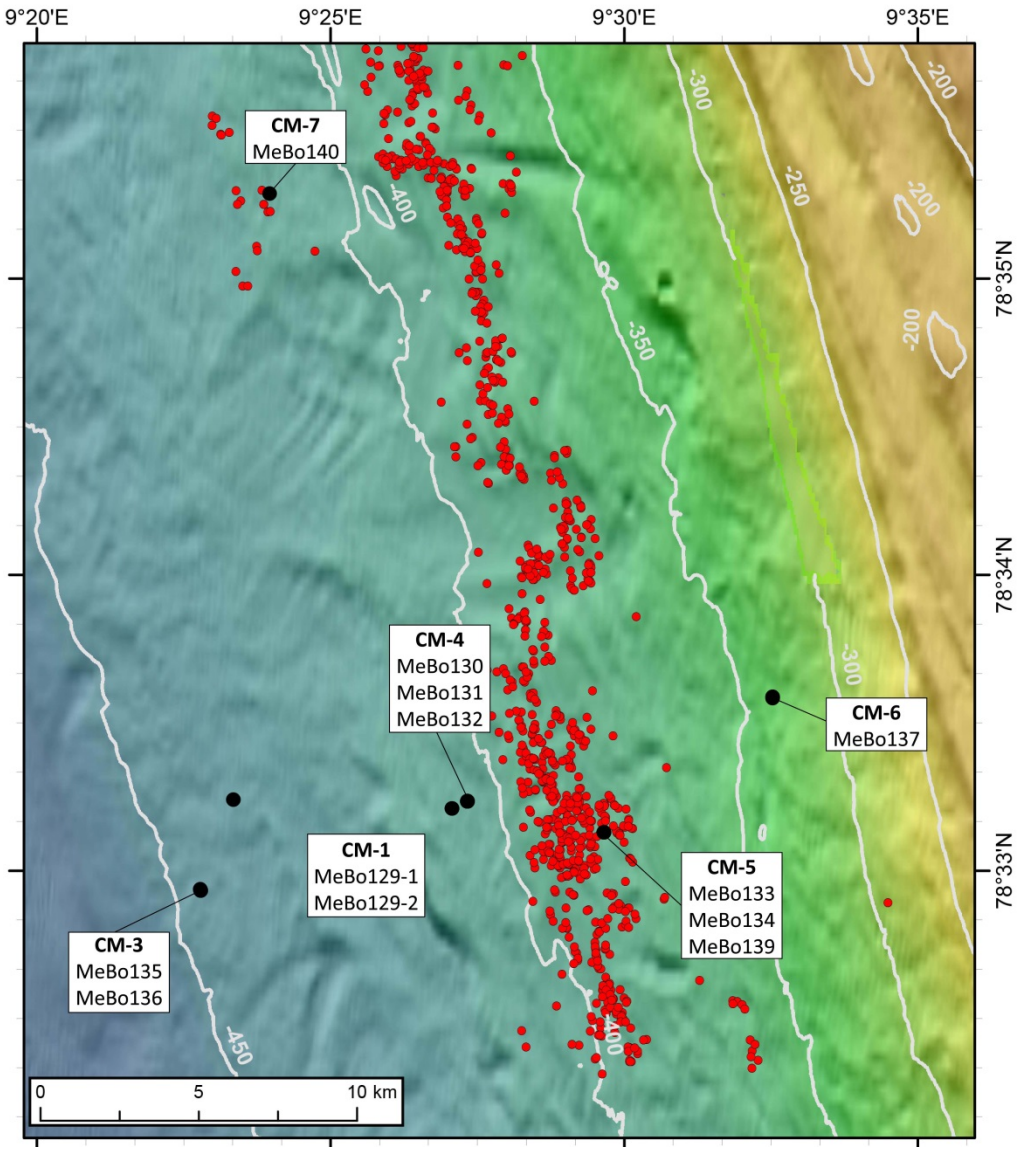

Fig. 54: Bathymetric map from a part of the upper continental margin west of Prins Karls Forland. MeBo holes from six sites drilled during MSM57 are shown. Gas emission sites (red circles) were taken from Sahling et al. (2014).

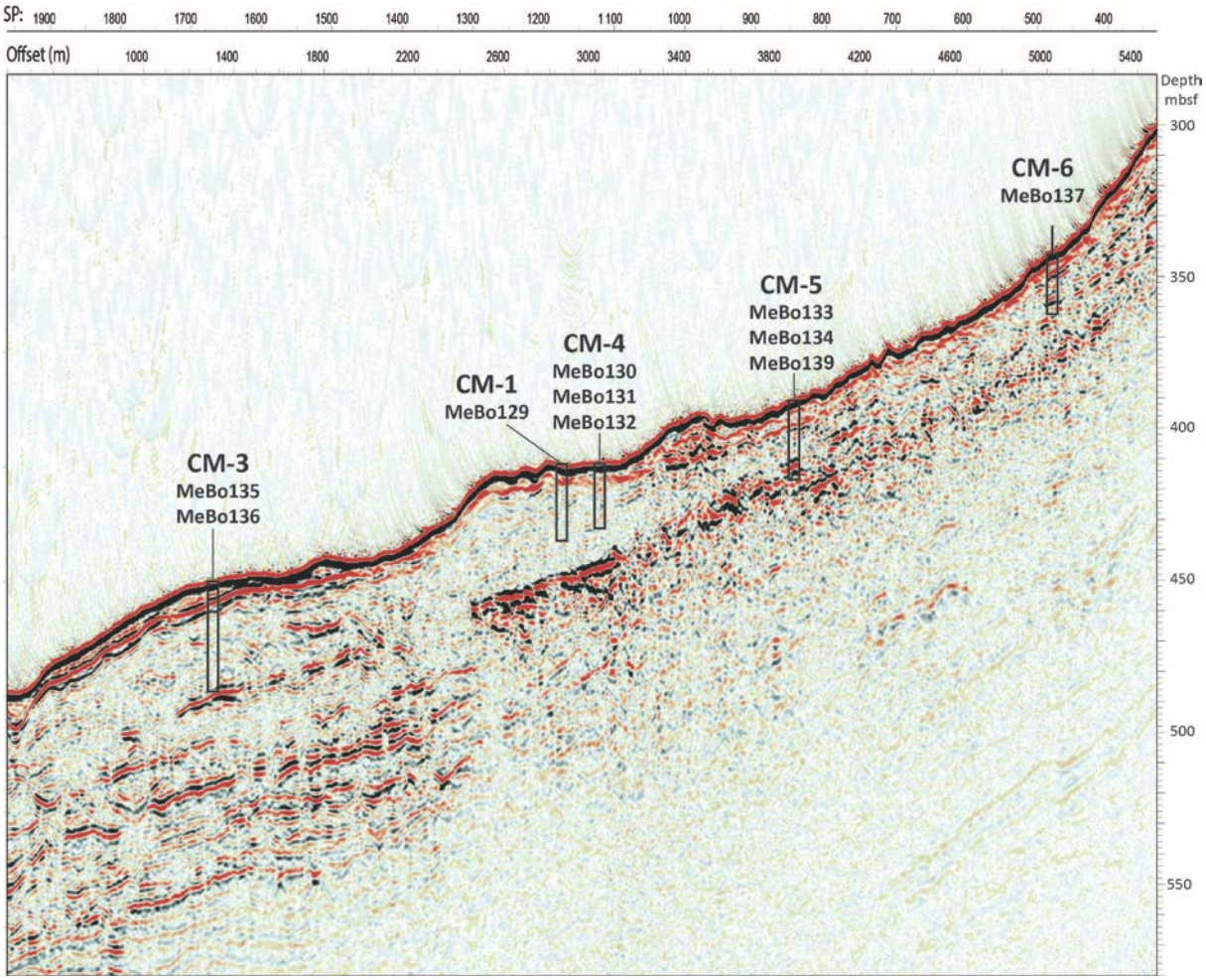

Fig. 55: Part of Seismic Line CAGE 14-5_HR2D_04 (from S. Bünz) with five MeBo drill sites from shallow water depth at 340 m (Site CM-6) downslope to deeper water depth at 445 m (Site CM-3). CM-5 was not drilled at the profile; position was projected to the profile.

Table 20: MeBo sites drilled during Cruise MSM57 at the upper continental margin West-Svalbard.

MeBo Drill sites	Water Depth [m]	Drilling Depth [mbsf]	Recovered sediment	Latitude [N]	Longitude [E]	Location
MeBo129-1	404	22.90	3.95 m	78°33.212‘	09°27.070‘	CM-1: Continental Margin, seep area
MeBo129-1	404	25.30	2.54 m	78°33.212‘	09°27.070‘	CM-1: Continental Margin, seep area
Mebo130	405	15.30	0.53 m	78°33.236‘	09°27.337‘	CM-4: Continental Margin, seep area
Mebo131	405	15.30	0.81 m	78°33.236‘	09°27.337‘	CM-4: Continental Margin, seep area
MeBo132	405	20.30	1.16 m	78°33.236‘	09°27.337‘	CM-4: Continental Margin, seep area
MeBo133	391	10.25	2.68 m	78°33.132’	09°29.653‘	CM-5: Continental Margin, seep area
MeBo134	391	25.30	2.83 m	78°33.132’	09°29.653’	CM-5: Continental Margin, seep area
MeBo135	445	17.75	4.27 m	78°32.935‘	09°22.790‘	CM-3: Continental Margin, GHSZ
MeBo136	445	37.95	5.55 m	78°32.935‘	09°22.790‘	CM-3: Continental Margin, GHSZ
MeBo137	340	21.60	4.31 m	78°33.585‘	09°32.528‘	CM-6: Continental Margin, non-seeps
MeBo139	391	26.15	12.03 m	78°33.132’	09°29.653’	CM-5: Continental Margin, seep area
Mebo140	402	33.30	17.08 m	78°35.357‘	09°24.939‘	CM-7: Continental Margin, bright spot

8.2.1 Site CM-6 at 340 m Water Depth

Continental Margin Site 6 (CM-6) was drilled at the shallow-most eastern end of the depth profile in 340 m water depth. MeBo Drill Hole 137 recovered glacial sediments down to nearly 24 mbsf. The

dropestone-rich sequence of fine-grained silty clay was intercalated by sand layers, probably responsible for slight reflections in the seismic record (Fig. 56). The location of the drill site is 50 m above the methane hydrate stability zone and no gas emission sites have been detected around the position.

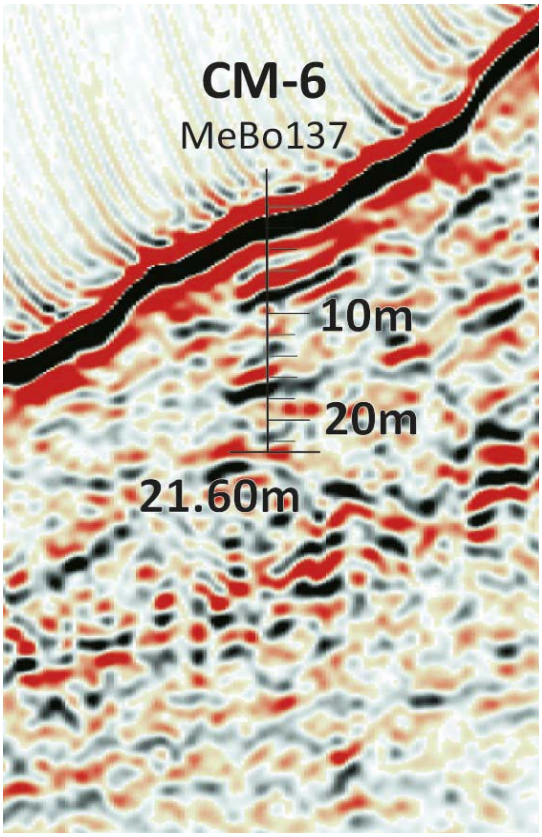

Fig. 56: Part of seismic line CAGE 14-5_HR2D_04 with MeBo Drill Site CM-6 (MeBo137) in 340 m water depth.

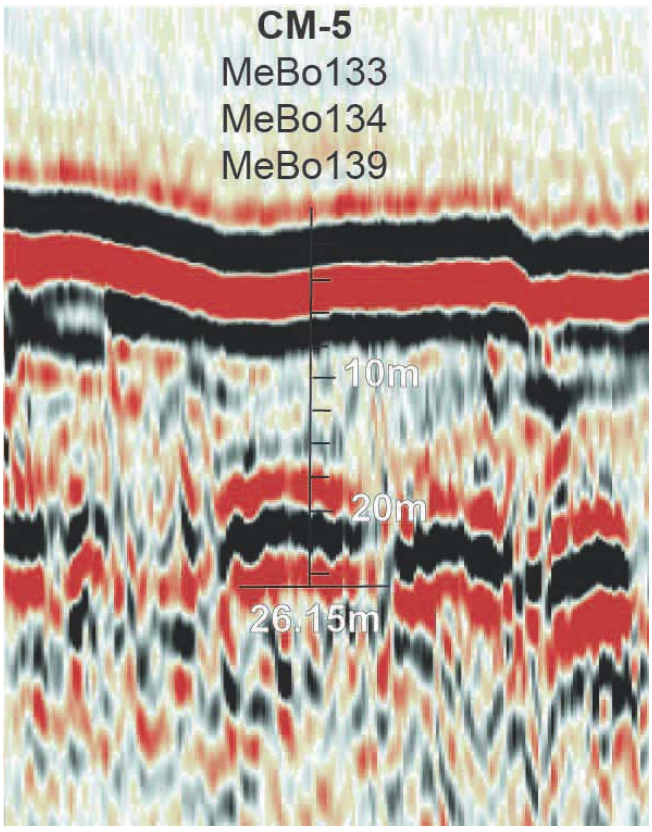

Fig. 57: Detail of seismic line PKF 2013_inline 54.

8.2.2 Site CM-5 at 391 m Water Depth

Continental Margin Site CM-5 in 391 m water depth lies at the upper boundary of the gas hydrate stability zone where numerous gas seeps exist. The location is found ca. 2 km southeast of the MASOX observatory (Berndt et al. 2014), and aside of the profile. The location was shifted away from the profile because a prominent reflector was much stronger there. During the drilling of three holes (MeBo133, 134, and 139) many acoustic anomalies known as flares have been detected in the vicinity of the drill site. The flares detected by using the EM122 multi-beam of the ship clearly represent gas emission sites constantly emitting methane in this area. Sediment depths of 10,25 mbsf (MeBo133, 134) and 26,15 mbsf (Mebo139) were reached and although big boulders exist recovery rates of up to 47% were achieved (Tab. 20). A distinct seismic reflector in 20 mbsf (Fig. 57) was penetrated, and seems to correlate with more sandy sediment material in the core. Temperature measurements could be successfully performed in several depth intervals (see Tab. 18).

8.2.3 Sites CM-1 and CM-4 at 404/405 m Water Depth

Continental Margin Sites 1 (CM-1) and 4 (CM-4) are lying 15 m downslope from CM-5 which is clearly in the gas hydrate stability zone based on the current bottom water temperature (Sahling et al. 2014). By drilling MeBo129-1 we tried to reach a strong reflector (Fig. 58) with negative polarity which marks a prominent depth level increasing with increasing water depth (Fig. 55) which is probably related to an unconformity in sediment sequence. At Drill Site CM-1 the reflector lies in ca. 35 mbsf and drilling trough sediments that showed a chaotic reflection pattern (Fig. 58) was not very successful and Drill Hole MeBo129 could not penetrate deeper than 25.30 mbsf. A slightly shift in northeastern direction to Drill Site CM-4, where the prominent reflector is around 5-7 m shallower was also not successful. Three drill holes there (MeBo130, 131, and 132) reached a maximum depth of 20.30 mbsf which is not deep enough to penetrate into the strong reflector. Indications of gas hydrates have not been found within the incomplete sampled sediment sequence

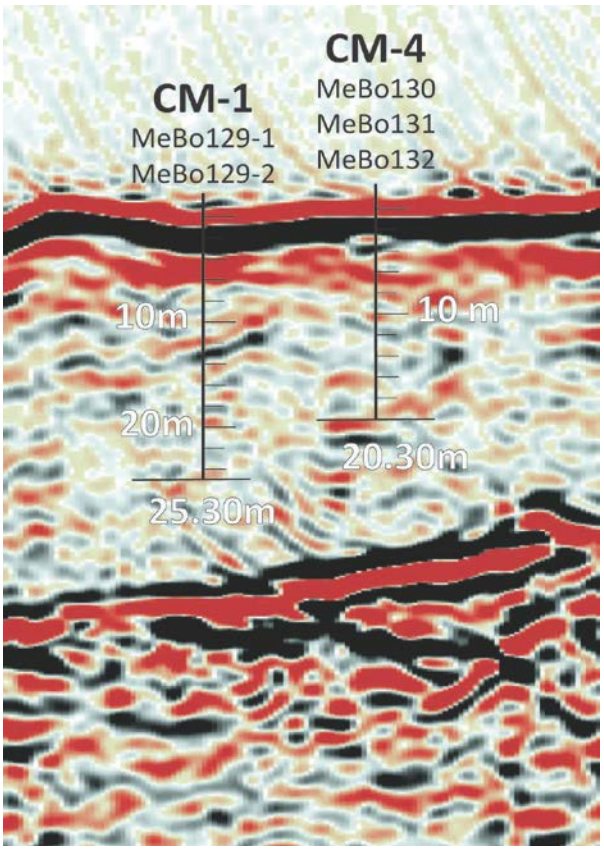

Fig. 58: Excerpt of seismic line CAGE 14-5_HR2D_04 showing the locations of MeBo Drill Site CM-1 and -4.

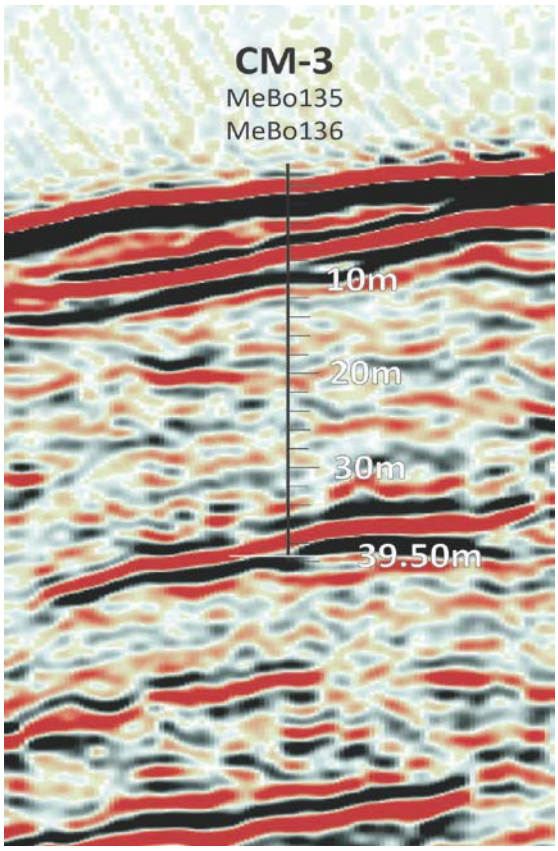

Fig. 59: Detail of seismic line CAGE 14-5_HR2D_04 showing MeBo Drill Site CM-3 location.

8.2.4 Site CM-3 at 445 m Water Depth

At continental margin Drill Site CM-3 two holes have been drilled (MeBo135 and MeBo136) representing the deepest water depth of 445 m which is 50 m within the gas hydrate stability zone and gas hydrates should be existing. The prominent reflector in 36 - 38 mbsf showing a negative polarity (Fig. 59) may represent the depth of the lower boundary of the GHZ where free gas could be responsible for the presence of the seismic reflector. MeBo Drill Hole 136 reached a depth of

39.50 mbsf and penetrated the reflector, where no free gas was detected. Based on recovered lithologies the interpretation of the reflector as an unconformity seems to be more likely. Indications for the presence of gas hydrates within the sediments have not been found.

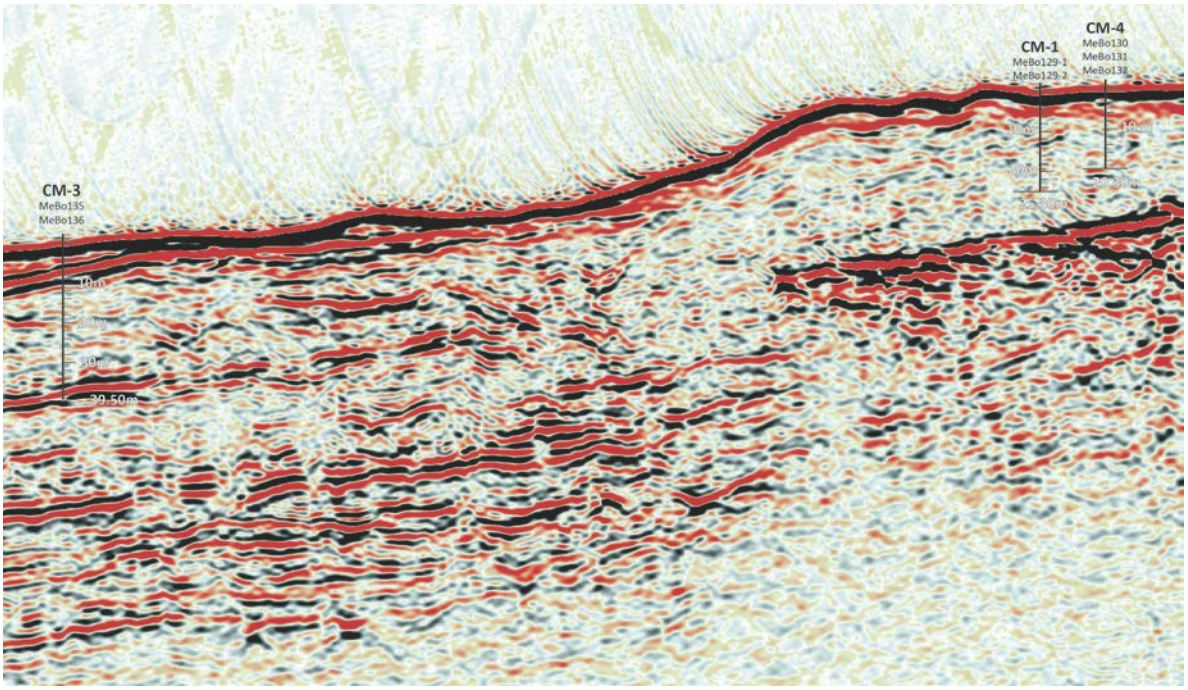

Fig. 60: Seismic line CAGE 14-5_HR2D_04 showing the locations of MeBo Drill Site CM-1, -3 and -4, representing the section close to the upper boundary of methane hydrates.

8.2.5 Site CM-7 at 402 m Water Depth

Continental margin Site CM-7 was drilled 20 km northwest of the profile in 402 m water depth (Fig. 54). The area is characterized by numerous flares separated from the band of gas emissions site following the slope to the north and reaching a water depth of 380 - 390 m at this latitude. CM-7 lies approximately 2—4 km west of the prominent band of gas flares. The separated field of gas flares around CM-7 indicated a special situation below the boundary for gas hydrate stability. More than 17 m fine-grained sediments associated with glacial pebbles have been drilled at this location revealing a recovery rate of 53%. Formation temperature measurements at four depths in MeBo Hole 140 have been successfully performed and calculated a thermal gradient of 50°C/km (see Chapter 6.3.2).

The basis for the selection of Drill Hole Mebo140 was the detailed seismic study of this area achieved by Ker et al. (2014). The authors took advantage of the source signature of the deep-towed high resolution SYSIF seismic device and demonstrated the value of the method for interpreting different types of gas-related reflections associated with sub-meter-scale distribution of gas. MeBo Drill Hole 140 drilled down to depth of 33.30 mbsf where the bottom hole assembly stopped in a sand layer charged with free gas. The gas ascended in the drill hole and released into the water column by forming a gas flare similar to the natural gas flares in the surrounding area.

High amplitude reflections of the bright spot have been seen in both low-frequency seismic profiles and high-frequency seismic records (Fig. 61) of the area and are clearly induced by a gas-charged layer, which was successfully drilled by MeBo.

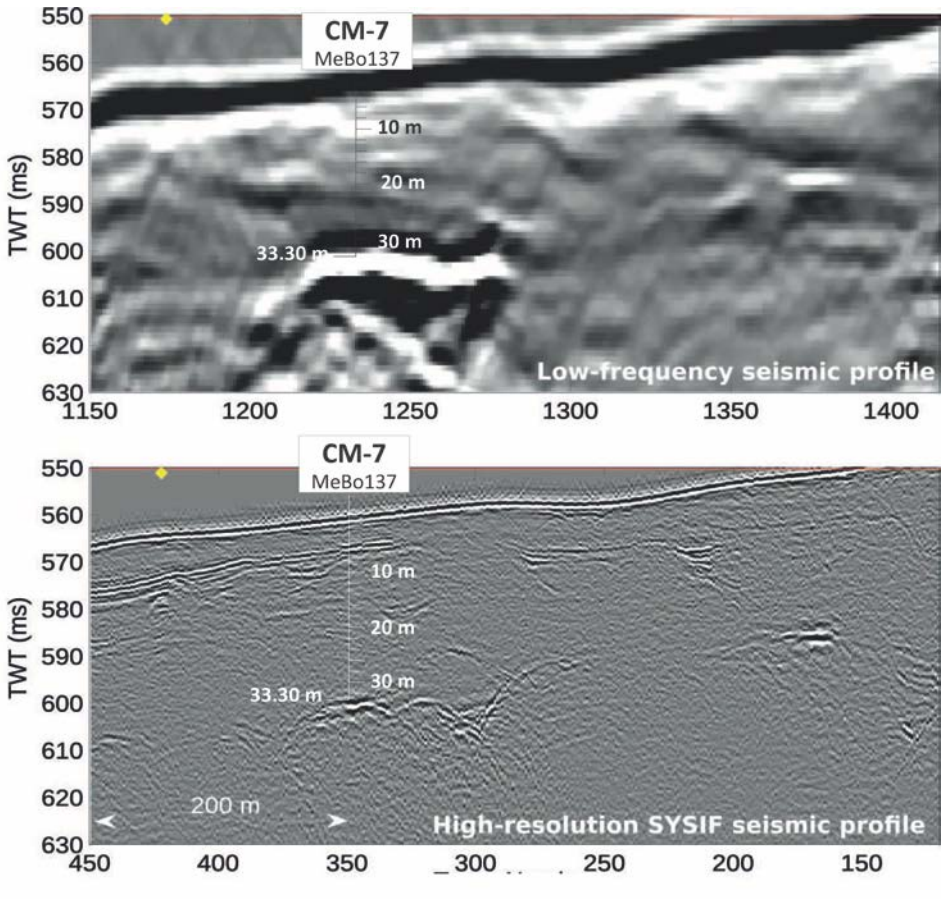

Fig. 61: Location of single MeBo Site CM-7 (MeBo Hole 137) ca. 18 km north of the MeBo-profile seismic line. Drill site is plotted in low-frequency seismic profile (above) and in a high-frequency seismic profile from Ker et al. (2014).

9 Sedimentology

(J. Johnson, G. Panieri, A. Lepland)

9.1 Introduction

The MSM57 Expedition recovered 19 MeBo drill cores and 22 gravity cores (Table 21) from multiple sites on the Western Svalbard margin (Figs. 16, 17, 18). The sites ranged in water depth from 340—1634 m. MeBo drill cores were either push cores (P) or rotary cores (R) depending on drilling conditions.

Gravity cores were collected with solid plastic core liners for most cores, however to enable rapid core splitting, plastic bags were used for cores intended to sample shallow seafloor gas hydrate. MSM57-Leg 1 was focused on the pockmarked crest of Vestnesa Ridge, where a well-developed free gas and gas hydrate system results in shallow gas hydrate and actively venting methane plumes into the overlying ocean (Hustoft et al., 2009; Petersen et al., 2010; Bünz et al., 2012; Smith et al., 2014; Plaza-Faverola et al., 2015)., which has persisted for over a range of timescales (Ambrose et al., 2015 and Plaza-Faverola et al., 2015). MSM57-Leg 2 was predominantly focused on the upper continental margin, where abundant gas flares near the up-dip limit of gas hydrate stability, have been interpreted to result from recent gas hydrate destabilization (Westbrook et al., 2009 and Thatcher et al., 2013). In addition, MSM57-Leg-2 sampling included one MeBo site on Vestnesa Ridge as well as gravity coring and temperature measurements in pockmarks above the gas hydrate system on Svyatogor Ridge (Johnson et al, 2015).

9.2 Methods

9.2.1 Sediment Core Description

Detailed sedimentologic observations and descriptions were recorded manually for each core section on visual core description sheets. A wide variety of features that characterize the sediments were recorded, including lithology, grain size, sedimentary structures, color, diagenetic precipitates, and core disturbance. This information was synthesized for each core in Strater® 5.0.710 software package by Golden Software, LLC, which generates a one-page graphical description of each core (see Appendix 3 Core Descriptions). On the graphical core descriptions the core photos and recovery at each site are shown, as well as the magnetic susceptibility profiles for each core and additional details about the samples taken (see Appendix 3 Core Descriptions). For MSM57-Leg 1 cores, detailed lithologic variations are depicted on the graphical core descriptions via the symbology of the stratigraphic column and accompanying legends, while for MSM57-Leg 2, a simplified lithologic column is shown and the lithologic variations are described in the text of the core description.

Naming of sediments on the graphical core descriptions (e.g. silty clay) were determined using the textural classification of the ODP sediment-classification scheme of Mazzullo et al. (1988) (Fig. 62). Grain size variations of the sediments were determined by visual observation and through poking of the sediments with a needle, which allows for the more subtle differentiation between clay and silty clay, for example. Additional textural and compositional information about the sediments was confirmed through the initial examination of smear slides at sea. The Munsell color designation (hue, value and chroma) of the sediments was determined by visual comparison with the Munsell soil color chart (Munsell Color Co., 1975).

Table 21: MeBo and Gravity Cores collected during MSM57 Legs 1 and 2**.**

GeoB	Instrument	Location	Latitude	Longitude	Date 2016	Water Depth	Maximum Core Depth	Recovery
St. No.	Tool-No.	Name	N	E	(UTC)	m	cm	%
21601-1	GC-1	Lunde Pockmark	79°00.504'	6°54.637'	41122	1211	572	
21604-1	MeBo123	Lunde Pockmark	79°00.503'	6°54.625'	41123	1213	280	38.46
21605-1	GC-2	Lunde Pockmark	79°00.506'	6°54.613'	41123	1214	765	
21606-1	GC-3	Reference Station	78°59.806'	6°57.808'	41123	1200	584	
21608-1	MeBo124	Lunde Pockmark	79°00.502'	6°54.615'	41124	1212	530	31.57
21609-1	GC-4	Lunde Pockmark	79°00.413'	6°54.269'	41124	1212	535	
21609-2	GC-5	Lunde Pockmark	79°00.403'	6°54.253'	41124	1212	60	
21610-1	MeBo125	Lunde Pockmark	79°00.503'	6°54.621'	41124	1212	2280	43.36
21612-1	GC-6	Lunde Pockmark	79°00.4266'	6°54.673'	41125	1213	273	
21613-1	MeBo126	Background	78°59.806'	6°57.808'	41125	1198	6250	41.74
21616-1	MeBo127	Lunde Pockmark	79°00.418'	6°54.245'	41127	1210	1390	26.14
21617-1	GC-7	Lunde Pockmark	79°00.205'	6°55.867'	41128	1212	Bent Core	
21617-2	GC-8	Lunde Pockmark	79°00.201'	6°55.870'	41128	1210	56	
21619-1	GC-9	Lunde Pockmark	79°00.427'	6°54.677'	41129	1213	478	
21620-1	GC-10	at TL02-5 site	79°00.339'	6°55.170'	41129	1207	596	
21621-1	MeBo128	Lunde Pockmark	79°00.430'	6°54.255'	41130	1211	775	59.21
21623-1	GC-11	Lomvi Pockmark	79°00.212'	6°55.950'	41131	1216	165	
21624-1	GC-12	Lomvi Pockmark	79°00.171'	6°55.498'	41131	1217	267	
21626-1	MeBo129-1	Cont.-Margin Site 1	78°33.212'	09°27.070'	41134	404	2290	31.47
21626-2	MeBo129-2	Cont.-Margin Site 1	78°33.212'	09°27.070'	41135	404	2530	12.83
21630-1	GC-13	Cont. -Margin	78°33.241'	09°23.344'	41137	436	198	
21631-1	MeBo130	Cont.-Margin Site 4	78°33.236'	09°27.337'	41137	405	1530	7.11
21631-2	GC-14	Cont.-Margin Site 4	78°33.237'	09°27.336'	41138	405	287	
21631-3	MeBo131	Cont.-Margin Site 4	78°33.236'	09°27.337'	41138	405	1530	31.15
21631-4	MeBo132	Cont.-Margin Site 4	78°33.236'	09°27.337'	41139	405	2030	42.96
21631-5	GC-15	Cont.-Margin Site 4	78°33.236'	09°27.337'	41140	405	126	
21632-1	MeBo133	Cont.-Margin Site 5	78°33.132'	09°29.6527'	41140	391	1025	26.67
21632-2	MeBo134	Cont.-Margin Site 5	78°33.132'	09°29.6527'	41140	391	2530	11.27
21633-1	MeBo135	Cont.-Margin Site 3	78°32.9347'	09°22.7898'	41142	446	1775	24.54
21633-2	GC-16	Cont.-Margin Site 3	78°32.938'	09°22.786'	41143	445	250	
21633-3	MeBo136	Cont.-Margin Site 3	78°32.9347'	09°22.7898'	41143	445	3795	14.88
21634-1	MeBo137	Cont.-Margin Site 6	78°33.5851'	09°32.5283'	41145	340	2160	20.28
21634-2	GC-17	Cont.-Margin Site 6	78°33.589'	09°32.528'	41145	338	111	
21636-1	GC-18	Svyatogor Ridge	78°21.322'	05°42.129'	41146	1625	478	
21637-1	MeBo138	Lunde Pockmark	79°00.426'	06°54.246'	41147	1209	2395	36.86
21638-1	GC-19	Lunde Pockmark	79°00.424'	06°54.678'	41149	1210	250	
21639-1	MeBo139	Cont.-Margin Site 5	78°33.132'	09°29.6527'	41149	391	2615	46.9
21640-1	GC-20	Svyatogor Ridge	78°21.303'	05°42.309'	41151	1623	544	
21641-1	GC-21	Svyatogor Ridge	78°21.659'	05°41.594'	41151	1634	406	
21643-1	MeBo140	Cont.-Margin Site 7	78°35.288'	09°23.963'	41152	402	3330	52.55
21644-1	GC-22	Cont.-Margin Site 5	78°33.132'	09°29.6527'	41153	391	380	

Of particular interest during the MSM57 Expedition were the visual indications of disruption to the sediment caused by the dissociation of gas hydrate in the recovered cores. Massive hydrate was often sampled prior to core description, but some less massive forms that were not sampled on the catwalk dissociated within the core and left distinct textural disturbances. The two primary textures identified as resulting from the dissociation of gas hydrate are soupy and mousse-like as defined during the ODP Leg. 204 expedition at Hydrate Ridge (Tréhu et al., 2003). Soupy sediments are watery, homogeneous, and fluidized. These sediments are often associated with void spaces in the core because they are able to flow from their original position during core recovery and therefore retain no original sedimentary

structures. Wet, watery mousse-like sediment texture is soft and deforms plastically under slight pressure from one finger. Mousse-like texture contains gas vesicles and obscures primary sedimentary structures. Mousse-like and soupy textures related to the dissociation of gas hydrate not sampled prior to description were observed at several sites and noted on the graphical descriptions for each core. Soupy disturbances at the top of each core (top of first section); however, are not necessarily related to gas hydrate presence but rather drilling-related disturbance.

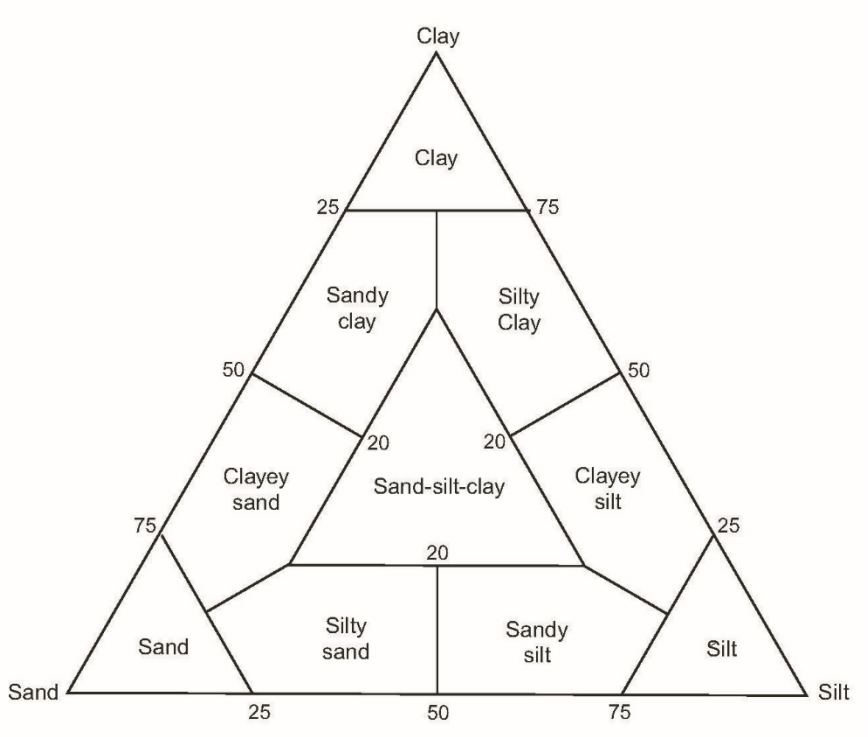

Fig. 62: Ternary diagram for determining sediment names based on texture using the relative proportion of sand, silt, and clay.

9.2.2 Sediment Core Imaging

All core sections were imaged immediately after being split and scraped using the *SmartCIS* 1600LS line scanning system of the MARUM GeoB Core Repository (www.marum.de/en/Infrastructure/GeoB-smartCIS-1600-Line-Scanner.html). It was useful to freshly scrape the cores immediately prior to imaging in order to capture the ephemeral nature of some sedimentary features. This is holds particularly true for iron sulfide precipitates, which become oxidized within minutes after core splitting. All images were acquired at a 500 dpi resolution. In order to retain the relative variability in core color within each hole, we found it more expedient to fix the aperture of the camera at f/8 that would image most cores without the need for further adjustment. Care was taken to ensure that the system was correctly calibrated using the "white tile" procedure prior to scanning each core and that the camera position was correctly set up. A digital ruler was added to the images. Output from the *SmartCIS* includes a jpeg file for each scanned section with a digital ruler on the right side of the image. Red-green-blue (RGB) profiles for all images were also saved.

9.2.3 Preliminary Results

9.2.3.1 MSM57 Leg 1

Vestnesa Ridge Reference Sites

The deposition of sediments on Vestnesa Ridge is mainly controlled by paleoclimatic and paleoceanographic environmental changes. The sediments recovered by MeBo and gravity cores are characterized by silty clay with layers rich in coarse, terrigenous ice-rafted debris (IRD) that were deposited during extensive glaciations of the Svalbard margin. Intercalated layers with relatively low IRD, but abundant planktonic foraminifers (mostly *Neogloboquadrina pachyderma*) in the coarse fraction were deposited during periods of Atlantic Water inflow to the Arctic Ocean during seasonally open waters in a sea ice cover with only few icebergs (Spielhagen et al, 2004).

MeBo126 was taken as a reference core (Fig. 17) and recovery was 41.74%, 2465 cm on a maximum coring depth of 6250 cmbsf. The gravity core recovery from the reference site ranges from 584 cm (GC-3) to 596 cm (GC-10). The sediments here are characterized by facies that consist primarily of gray silty clay to dark gray silty clay with disseminated FeS, that often enhance the visibility of bioturbation. Pebbles of different sizes (up to 5 cm) and coarse lithology can be present and are interpreted as ice-rafted debris (IRD). There is the sporadic presence of mollusc fragments. Biogenic particles are limited to planktonic and benthic foraminifera. Contacts between lithologies are commonly gradational. In the background cores, a brownish layer (ca 30 cm thick) is observed between 300 and 400 cmbsf that is characterized by low magnetic susceptibility, which Jessen et al. (2010) described as “Mass transport deposits”. These sediments are deposited between 24,080 ±150 and 23,550 ±185 cal years BP over large areas of the western Svalbard slope and can be used as a time marker in the regional slope stratigraphy.

Lunde Pockmark

The lithology recovered in cores from the Lunde Pockmark (Fig. 17) is very similar to the reference site. It is mainly characterized by gray silty clay to dark gray silty clay with moderate to common FeS that often enhances the visibility of bioturbation. IRD layers made of subangular grains <1cm and pebbles-interpreted as dropstones of different sizes (up to 5 cm) can occur at different sediment depths and are interpreted as IRD. The difference with the reference site is represented by carbonate cemented layers, and carbonate nodules and rubbles (ca 1—3 cm in diameter) that have been found in the southwest sector of the pockmark where gas flares in the water column and high amplitude anomalies in the seismic data were observed. A 27 cm thick layer of carbonate cemented sub-angular and rounded peddles with whitish aragonite crystals developed in fissures was found at MeBo127 site in the second core. Different layers of carbonate nodules and rubbles were found at varying depths in the gravity cores and are described below.

The MeBo sediment core recovery in this active pockmark ranges from 100—905 cmbsf with a recovery rate ranging between 26.14—59.21%. The maximum coring depth ranges from 280 cmbsf in MeBo123 to 2280 cmbsf in MeBo125. MeBo123, 124 and 125 were nearby in the northeast sector of the Lunde Pockmark. The drilled length has been quite low for MeBo123 (280 cm bsf) and MeBo124 (530 cm bsf), while for MeBo125 has reached a maximum depth of 2280 m bsf. Overall core recovery of MeBo125 sums up to 905 cm.

The two other MeBo sites (MeBo127 and 128) as well as MeBo138, drilled during MSM57 Leg 2, are characterized by clear evidence of present and past seepage activity. MeBo127 overall core recovery was 281 cm (26.14%) with a maximum coring depth of 1390 cm bsf. At ca. 100 cm bsf we found carbonate nodules and gas hydrate, along with several voids due to gas expansion. In core 2 there a 27-cm thick carbonate cemented layer has been found (described above). The typical 'mousse-like texture' was recognized in cores 4 and 5. MeBo128 had the best core recovery rate of the entire leg (59.21%), on a total drilled length of 775 cm bsf and a total core recovery of 447 cm. The sediment is silty clay and in core 3 between 530 and 775 cm bsf there are several cracks due to gas expansion. The lithology changes to gray clay towards the deepest sediment intervals. MeBo138 had a core recovery of 36.86% and contained abundant authigenic carbonates in all recovered cores except core 6. Mousse-like and soupy sediment textures were also observed in the sediment record of MeBo138.

The gravity core recovery from the Lunde Pockmark ranges from 56 cm to 765 cm. The short recovery (56 cm, GC-8) was from one of the pits. Overall, the cores with shorter recovery (< 100 cm) are those containing gas hydrate, although in two cores (GC-6; GC-9) the recovery was longer. Underpinning a non-linear relationship between core recovery and gas hydrate content. The lithology is mainly gray silty clay to dark gray silty clay with moderate to common FeS. The presence of pebbles interpreted as dropstones are consistent with IRD deposition. Particles coarser than silty clay cannot be carried as suspension load and thus are most likely transported and deposited either as bed-load by strong local bottom currents, within mass movements or as IRD. Abundant mollusc shell fragments similar to *Pharengena* s.l. and *Isorroprondon* sp. previously found in Lomvi Pockmark (Ambrose et al., 2015) and dated approximately 17,707 to 16,680 yrs. BP dominate a shell layer recovered by several gravity cores during MSM57 (in GC-1 and GC-2 at ca 300 cm bsf; in GC-6 and GC-9 at 240 and 400 cm bsf respectively; in GC-04 at 350 and 450 cm bsf). In GC-7, and GC-8 the very short recovery (92 and 56 cm respectively) was due to the presence of abundant carbonate rubbles and nodules in the lower part of the cores. In GC-11 isolated carbonate nodules occur at ca 110 cm bsf. In several intervals, we observed the 'mousse-like texture' characteristic of gas charged and previously gas hydrate bearing sediments.

Lomvi Pockmark

The cores in Lomvi (Fig. 17) are characterized by similar lithology as described above; gray silty clay to dark gray silty clay. The recovery for GC-7, and GC-8 was rather low (92 and 56 cm respectively). The presence of abundant carbonate rubbles and nodules in the lower part of the cores suggest that the gravity corer got stuck in these coarse layers. In GC-11 (core recovery: 165cm) carbonate nodules occur between 110 and 130 cm and 'mousse-like texture' characterized the bottom of the core. Likewise the "background cores" from the reference site, Gravity core GC-12 (core recovery: 267 cm) recovered at 140—185 cm bsf the brownish layer characterized by low magnetic susceptibility and previously described as "Mass transport deposits" over large areas of the western Svalbard slope, dated to 24,080 ±150 and 23,550 ±185 cal years BP (Jessen et al., 2010). The bottom 30 cm of the Lomvi cores are characterized by the 'mouss-like texture' and also contain shell fragments, most likely *Pharengena* s.l. and *Isorroprondon* sp.

9.2.3.2 MSM57 Leg 2

Continental Margin Sites

Cores collected from the upper continental margin sites (MeBo129—140 and Gravity cores 13—17 and 22; Fig. 18) were quite variable in their lithology at the core section scale between clay, silty clay, sandy clay, pebbly clay, clayey sand, sand, and pebbly sand, with variable amounts of gravel to pebble sized rocks. The ice rafting and/or glacial debris associated with trough mouth fan deposition, meltwater discharge, and bottom current activity was on the upper slope throughout the Quaternary. Given a maximum seafloor penetration of ~38 m (MeBo136) at these sites, and the high sedimentation rates associated with trough mouth fans, we suspect most of the recovered records represent deposition during the late Pleistocene to recent, however, no biostratographic or other age constraints were determined at sea. Core tops in both the MeBo and gravity cores collected on these upper continental margin sites commonly contained pebbles, which were also observed on seafloor imagery captured by the MeBo. These pebbles and cobbles of variable lithology are likely exposed at the seafloor due to known bottom current activity (Rebesco et al, 2013 and Eiken and Hinz, 1993) that has removed or inhibited deposition of the fine sediment fractions. In one particular case (Site MeBo134) sea floor pebbles, complete with modern encrusting organisms, were trapped in the upper most core at the surface and pushed downward during successive coring, inhibiting recovery for almost 10 meters below the seafloor. Discontinuous stratigraphy due to gaps in recovery in the MeBo cores make correlation of the recovered cores difficult using lithology or magnetic susceptibility. However, gravity cores appear to have recovered similar stratigraphy at sites proximal to each other (i.e. in GC pairs, 13 & 16, 14 & 15, and 17 and 22). Very similar porewater ammonium profiles in both the MeBo and gravity cores suggest nearly uniform organic matter degradation within a common stratigraphy.

Smear slide examination of the fine sediment fraction compositions show that the continental margin sediments at these sites (MeBo Sites 129-140 and Gravity cores 13-17 and 22) are dominated by angular to sub-rounded rock fragments and mineral grains (quartz, quartz rich lithics, heavy minerals and both microcline and plagioclase feldspars) of clay to fine sand size. Dropstone compositions identified during core description included quartzite, biotite schist, sandstone/siltstone, and occasional intrusive igneous and coal pebbles. Many of the dropstones showed evidence of *in situ* chemical weathering, containing weathering rinds that stained the surrounding sediments. Marine biogenic tests and carbonate shell fragments from macro-organisms are largely diluted by the strong lithogenic sediment components at these sites, however some planktonic foraminifera, carbonate shell fragments, and siliceous sponge spicules were occasionally observed in smear slide and macroscopically on the split core surface. Because smear slides exclude the larger grains in a sediment fraction, coarse fraction (>63 µm) sediment examination may reveal a more accurate estimate of the biogenic fraction. It is notable that visible foraminifera were observed during core splitting in some clay dominated intervals. Macroscopic bivalve shells (possibly chemosynthetic) were observed both as fragments and larger pieces (>1 cm) during core description and are noted in the descriptions. Black iron sulfide precipitates of both iron monosulfides and pyrite were observed in smear slides, as fine dusty precipitates or cubic crystals in non-framboidal circular clusters, and on the split core surfaces as black patches or darker colored black zones within the sediments. Authigenic carbonates were present in several cores as discolored (usually lighter tones) patches in clays, as nodules (both MeBo140), or fully cemented sediment intervals (MeBo139) and were confirmed through smear slides and instant chemical reaction (calcium carbonate) or delayed reaction (dolomite) with 10% HCl. MeBo sites 139 and 140 contained several authigenic carbonate occurrences. In addition, Site 129-2 may have authigenic carbonate occurrences as well, however, carbonate dropstones should also be

considered; future carbon isotope measurements could resolve this issue. A clast of carbonate cemented sand with pebbles was notable in Core 1 at Site MeBo139 as it may also be a detrital clast as well. Dolomite cemented sediments were observed in cores 5 and 6 at Site MeBo139.

Svyatogor Ridge

Three gravity cores (GC-18, 20, and 21) were collected from two pockmarks along the crest of Svyatogor Ridge (Fig. 19). These pockmarks lie above a well-developed gas and gas hydrate system that lies offset from Vestnesa Ridge along the Molloy transform fault, and could be charged by both biotic and abiotic methane (Johnson et al., 2015). Previous water column flare mapping and gravity coring during CAGE-UiT led expeditions to this region have not documented methane seeps in the water column or sampled neither gas hydrates nor significant gas in cores recovered from these pockmarks. These findings overall suggest that many of the pockmarks, although morphologically distinct, are inactive at present. In agreement with earlier observations, seafloor mapping during MSM57 did not identify any water column methane flares and methane concentrations in gravity cores were low (see Chapter 13, Gas and Gas Hydrates), likewise alkalinity measurements (see Chapter 12, Pore Water) suggest that the SMTZ lies at a greater depth than reached by coring.

Sediments recovered in by cores GC-18, 20 and 21 were composed predominantly of clays and silty clays that varied in color (brown, olive brown, greenish grey, to grey). Smear slide examination revealed, a similar lithogenic sediment composition to the continental margin sites, though, with a higher proportion of foraminifera. Core description revealed only few dropstones in these records and iron monosulfides were present throughout most of the sedimentary sequence. No authigenic carbonate occurrences were observed. Magnetic susceptibility records in GC-18 and 20 were consistent with the background stratigraphy observed in previously collected cores by CAGE, while GC-21 showed depleted values, probably due to AOM related magnetite dissolution in the past (e.g. Novosel et al, 2005).

Vestnesa Ridge

Cores collected from Vestnesa Ridge, Lunde Pockmark during Leg 2 (Fig. 17) included MeBo138, discussed within the context of the Leg 1 cores above, and GC-19 which was collected in a plastic bag liner to promptly harvest shallow seafloor gas hydrates for preservation in liquid nitrogen for post-cruise structural analyses.

10 Infrared Thermal Imaging of Sediment Cores

(C.-W. Hsu)

10.1 Introduction

Gas hydrates are solid crystals consisting of water molecule cages stabilized by methane or other low weight gas molecules. The gas hydrate stability zone (GHSZ) can be found in marine sediment at depths of hundreds of meters below the seafloor, where high pressure and low temperature conditions are present. The presence of gas hydrate in marine sediments is generally inferred from reflection seismic data where a bottom-simulating reflector (BSR) indicates the lower boundary of the gas hydrate bearing sediment (Bünz et al., 2012; Kvenvolden, 1993). During this cruise the aim was to develop a better understanding of the abundance and distribution pattern of gas hydrate in marine sediment below the seafloor of Vestnesa Ridge and West continental margin of Svalbard, with the mobile drilling system MeBo and gravity corer (Figs. 17 and 18). During core recovery, gas hydrate dissociation occurs as soon as it is out of the GHSZ. Intervals in the sediment core where gas hydrate has recently dissociated or is actively dissociating, are relatively cold to the surrounding sediment, because dissociation of gas hydrate is an endothermic reaction. These intervals called “cold spots” can be documented and measured with an infrared (IR) thermal camera by imaging the surface of retrieved core liners. Several previous studies have successfully identified thermal anomalies associated with gas hydrates through infrared thermal imaging (Riedel et al., 2006; Ryu et al., 2013; Tréhu et al., 2004; Wei et al., 2015). During this cruise a ThermaCam SC 640 camera (FLIR Systems) was used to obtain thermal images and measure the surface temperature of sediment cores. Infrared thermal imaging could detect gas hydrate simultaneously while scanning the sediment core, providing valuable information for further sampling strategies for sedimentology, gas and pore water geochemistry.

10.2 Methodology

The core sections of MeBo and gravity cores were imaged using the IR camera as soon as possible after recovery. The IR camera was fixed on a tripod with a focal distance 150 cm between camera and core liner. Each image covered approximately 60 cm depth range of the core, ice cubes which are visible in the monitor while scanning were used as markers of each 50 cm depth range of the core (Fig. 63). The temperature measurements of the IR system ranged from –40°C to 120°C and the precision of the camera was 0.1 °C with the accuracy of ± 2°C.

The raw data were converted and exported as JEPG format using the ThermaCAM™ Researcher Professional software 2.10. All IR images were stitched consecutively, temperature logs were extracted along central axis of the core from IR images (Figs. 64-67). The temperature of core liner containing sediment devoid of gas hydrate were represented as background temperature of each core. The background temperatures indicated that there are no significant variations (less than 1.0°C) within each core. Thus, the specific background temperature was assigned to each core liner individually. The temperature anomalies were characterized by ΔT, which was calculated from the difference between measured and background temperature to interpret the content of the cores. Although it is possible that some IR cold temperature anomalies result from other effects, for example decompression of gas pockets. Previous studies (Bahk et al., 2013; Riedel et al., 2006; Tréhu et al., 2004; Wei et al., 2015) suggest that distinct, strong cold anomalies are a reliable indicator of gas hydrate presence. The observations during ODP Leg 204 reveal that gas expansion pockets generally seem to have equilibrated with the ambient temperature and appear as warm spots (Tréhu et al., 2004).

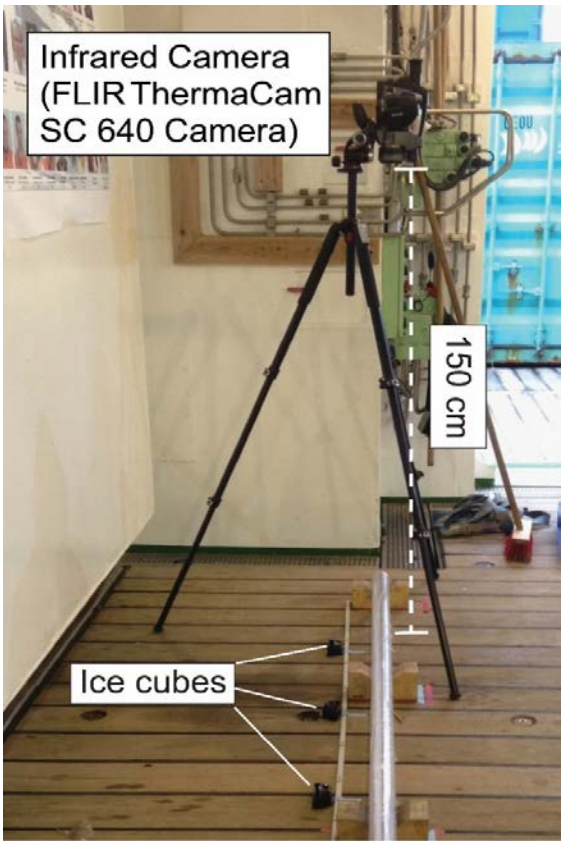

Fig. 63: Left: The infrared camera was fixed on a tripod with a focal distance 150 cm between camera and core liner. Ice cubes were used as reference position for post processing and stitching of the images. **Right:** The monitor of camera shows the temperature anomalies simultaneously while scanning of GC-9. The cold region (dark blue to black) indicated the appearances of gas hydrate, the warm part (red to orange) indicated the voids in the core liner.

Table 22: List of infrared thermal imaging of MeBo and gravity corer during MSM57 and main observation.

Station No.	Location	Core length (cm)	Temp. anomalies	Observation and remark
GC-1	Lunde Pockmark, Vestnesa Ridge	577	No	No obvious temperature anomaly.
MeBo123	Lunde Pockmark, Vestnesa Ridge	100	-	Not applicable, drilling was failed.
GC-2	Lunde Pockmark, Vestnesa Ridge	765	No	No obvious temperature anomaly.
GC-3	Background, Vestnesa Ridge	584	No	No obvious temperature anomaly.
MeBo124	Lunde Pockmark, Vestnesa Ridge	161	-	Not applicable, drilling was failed.
GC-4	Lunde Pockmark, Vestnesa Ridge	ca. 535	-	Sampled with plastic foil, gas hydrate.
GC-5	Lunde Pockmark, Vestnesa Ridge	ca. 60	-	Sampled with plastic foil, gas hydrate pieces were collected.
MeBo125	Lunde Pockmark, Vestnesa Ridge	905	No	No obvious temperature anomaly.
GC-6	Lunde Pockmark, Vestnesa Ridge	273	Yes	Positive anomalies at 197 - 204 cm (voids), negative anomalies ΔT down to -3°C from 232 - 273 cm (gas hydrate).
MeBo126	Background, Vestnesa Ridge	2465	No	No obvious temperature anomaly.
MeBo127	Lunde Pockmark, Vestnesa Ridge	281	Yes	Negative anomalies ΔT down to -2°C in 1P at 89 - 100 cm (gas hydrate).
GC-7	Lomvi Pockmark, Vestnesa Ridge	92	-	Not applicable; core barrel was bent during coring, gas hydrate was found in the core catcher.

GC-8	Lomvi Pockmark, Vestnesa Ridge	56	Yes	Negative anomalies ΔT down to -1.5°C at 12 - 19 cm, possible disseminated gas hydrate at 9 ~ 20 cm.
GC-9	Lunde Pockmark, Vestnesa Ridge	478	Yes	Negative anomalies ΔT down to -2.5°C at 330 - 478 cm, massive gas hydrate.
GC-10	TL02-5 site, Vestnesa Ridge	596	No	No obvious temperature anomaly.
MeBo128	Lunde Pockmark, Vestnesa Ridge	447	Yes	Negative anomalies ΔT down to - 5 °C at 631 - 647 cm (core 3R), gas hydrate.
GC-11	Lomvi Pockmark, Vestnesa Ridge	165	Yes	Negative anomalies ΔT down to - 3°C at 148 - 165 cm, gas hydrate.
GC-12	Lomvi Pockmark, Vestnesa Ridge	267	Yes	Negative anomalies ΔT down to - 3°C at 237 - 259 cm, gas hydrate.
MeBo129-1	Cont.-Margin Site 1	395	No	No obvious temperature anomaly.
MeBo129-2	Cont.-Margin Site 1	254	No	No obvious temperature anomaly.
GC-13	Cont.-Margin	198	No	No obvious temperature anomaly.
MeBo130	Cont.-Margin Site 4	53	No	No obvious temperature anomaly.
GC-14	Cont.-Margin Site 4	287	No	No obvious temperature anomaly.
MeBo131	Cont.-Margin Site 4	116	No	No obvious temperature anomaly.
MeBo132	Cont.-Margin Site 4	81	No	No obvious temperature anomaly.
GC-15	Cont.-Margin Site 4	126	No	No obvious temperature anomaly.
MeBo133	Cont.-Margin Site 5	268	No	No obvious temperature anomaly.
MeBo134	Cont.-Margin Site 5	283	No	No obvious temperature anomaly.
MeBo135	Cont.-Margin Site 3	427	No	No obvious temperature anomaly.
GC-16	Cont.-Margin Site 3	250	No	No obvious temperature anomaly.
MeBo136	Cont.-Margin Site 3	555	No	No obvious temperature anomaly.
MeBo137	Cont.-Margin Site 6	431	-	Not applicable, out of GHSZ.
GC-17	Cont.-Margin Site 6	111	-	Not applicable, out of GHSZ.
GC-18	Svyatogor Ridge	478	No	No obvious temperature anomaly.
MeBo138	Lunde Pockmark	870	Yes	Negative anomalies in core 3P-1, 3P-2, 4P-1, 6P-1 and 7R-1, gas hydrate.
GC-19	Lunde Pockmark	ca.300	-	Sampled with plastic foil, gas hydrate was found as layers or likewise beds and veins.
MeBo139	Cont.-Margin Site 5	1203	No	No obvious temperature anomaly.
GC-20	Svyatogor Ridge	544	No	No obvious temperature anomaly.
GC-21	Svyatogor Ridge	406	No	No obvious temperature anomaly.
MeBo140	Cont.-Margin Site 7	1708	No	No obvious temperature anomaly.
GC-22	Cont.-Margin Site 5	380	No	No obvious temperature anomaly.

10.3 Results

Infrared thermal imaging of sediment cores was documented for most of MeBo drill sites and gravity core sites (Table 22). Few exceptions such as MeBo123, MeBo124, MeBo137, GC-4, GC-5, GC-7, and GC-17 were not applicable for imaging due to delay of core retrieval, out of gas hydrate stability zone, or different sampling strategy (Table 22). The negative temperature anomalies were observed in the

sediment cores at Lunde Pockmark and Vestnesa Pockmark, there was no temperature anomaly or valuable observed from thermal imaging at continental margin sites.

10.3.1 Gas Hydrate in Lunde Pockmark

Gas hydrates were recovered by both MeBo and gravity cores in Lunde Pockmark. GC-6 and GC-9 were located at the south-eastern rim of the pockmark, the IR images indicated the appearance of the shallowest gas hydrate at depth 232 cmbsf and 330 cmbsf of GC-6 and GC-9, respectively (Fig. 64). The temperature logs showed distinct cold anomalies down to -3°C and strong positive anomalies indicated voids in the sediment core due to the gas decompression during the core recovery. The positive spikes in the temperature logs were artifacts from the relatively warm end caps of each liner section.

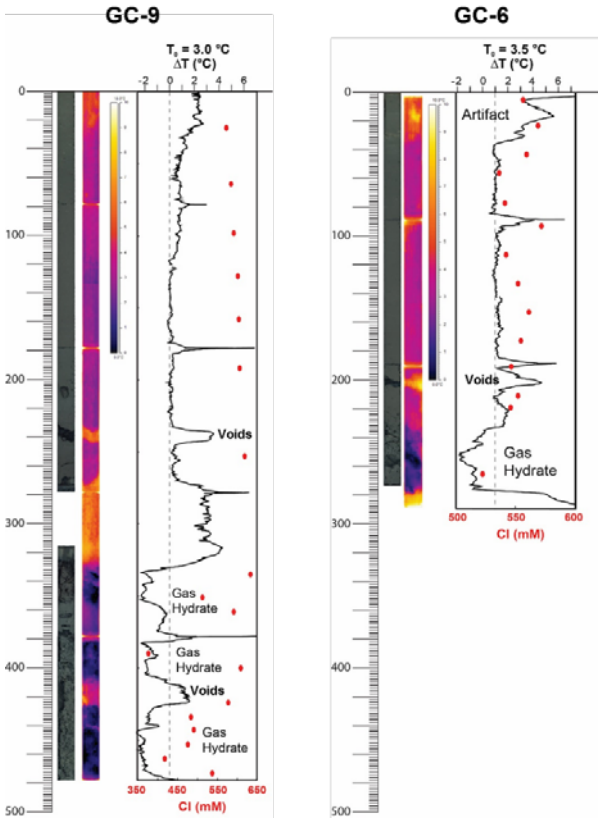

Fig. 64: Core images, IR images, temperature logs and pore water chloride concentration profiles of GC-6 and GC-9. The color bar of the IR images was ranged from 0 to 10°C. Temperature profiles showed the differences between the measured temperature and background temperatures of core liners, expressed as ΔT. Positive ΔT values correlate with voids in the cores and negative ΔT values represent dissociating gas hydrates. The concentrations of chloride (red dot) supported that refreshing signals in the interval of cold spot where soupy textures sediment appeared due to the gas hydrate dissociation.

MeBo127, MeBo128 and MeBo138 were located at the southern rim of Lunde pockmark, the IR images indicated that the appearance of the shallowest gas hydrate at core 1P, core 3R, and core 3P of MeBo127, MeBo128 and MeBo138, respectively (Fig. 65). The core 1P of MeBo127 was drilled at depth from 0 to 575 cmbsf, IR image showed that ΔT values were down to -2°C, with relatively refreshing chloride signal compared to the other core sections, the mousse-like texture was described in the cold spots. The core image of core 1P was taken after smoothing the surface of sediment core, therefore no mousse-like texture was shown in the core image.

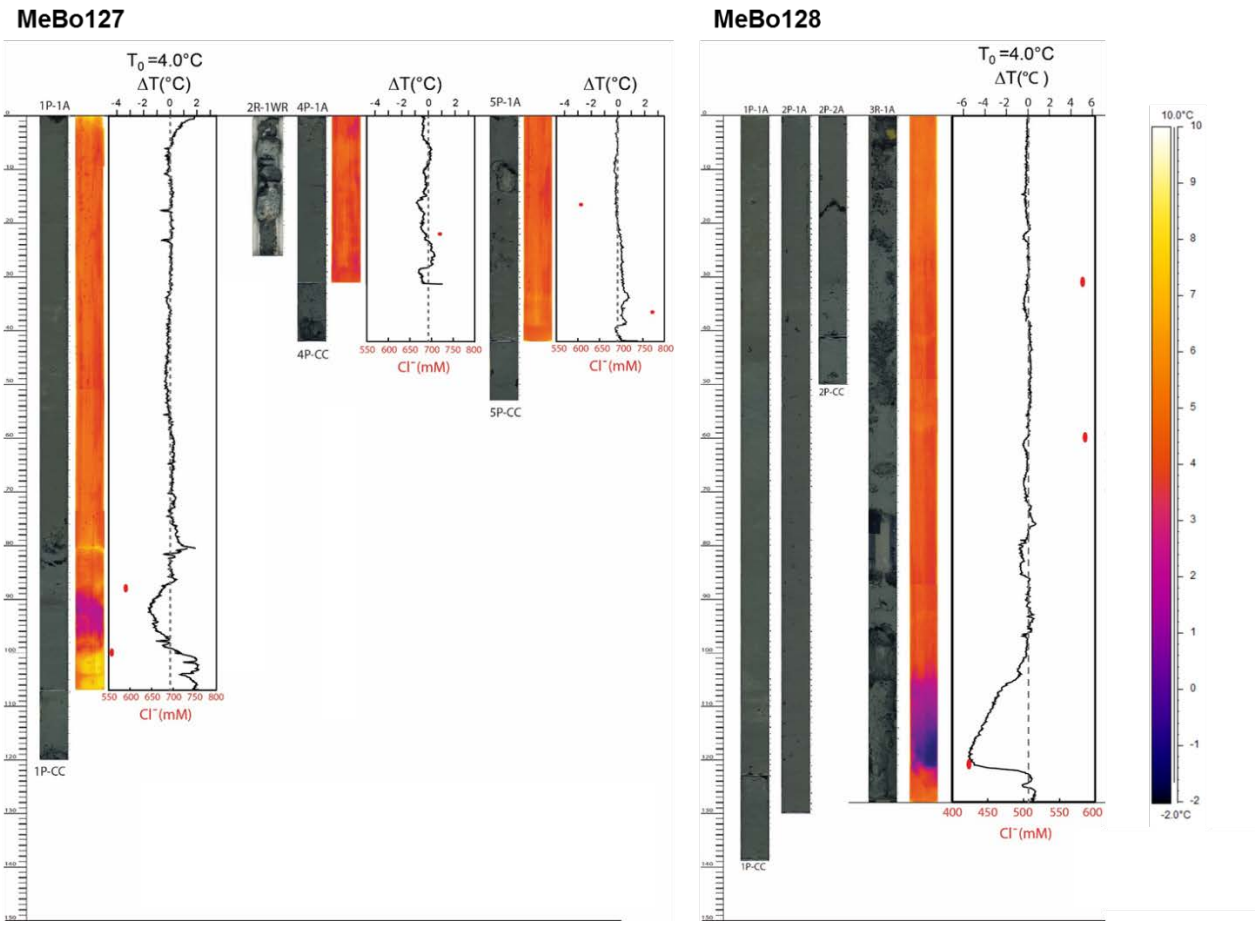

Fig. 65: Core images, IR images, temperature logs and pore water chloride concentration profiles of MeBo127 and MeBo128. The color bar of the IR images was ranged from -2 to 10°C. Temperature profiles showed the differences between the measured temperature and background temperatures of core liners, expressed as ΔT. The concentration of chloride (red dot) supported that refreshing signals in the interval of cold spot where soupy textures sediment appeared due to the gas hydrate dissociation.

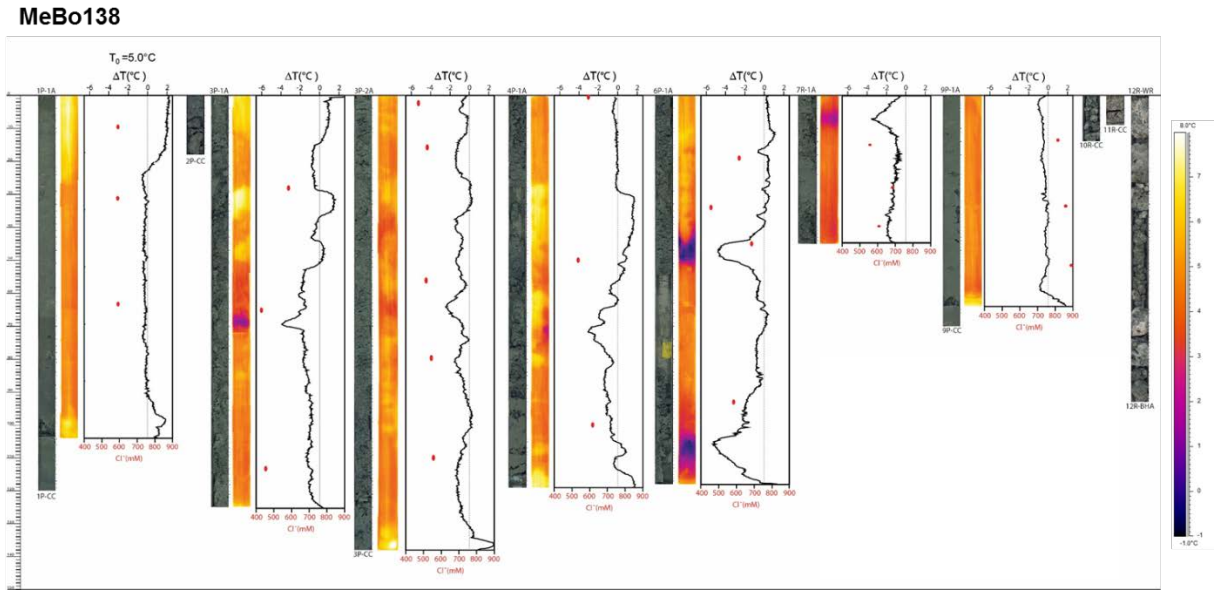

Fig. 66: Core images, IR images, temperature logs and pore water chloride concentration profiles of MeBo138. The colour bar of the IR images was ranged from -1 to 8°C. Temperature profiles showed the differences between the measured temperature and background temperatures of core liners, expressed as ΔT. There were five significant intervals with negative anomalies of temperature in the core 3P, core 4P, core 6P and core 7R.

The core 3R of MeBo128 was taken at depth from 530 to 775 cmbsf, IR image showed that ΔT value was down to -6°C, with strongly refreshing chloride signal at bottom of the core section, the mousse-like textures were document in the core image.

The temperature logs and the IR images of MeBo138 showed that gas hydrates were widely distributed in this sites from 515 to 1220 cmbsf (Fig. 66). There was a technical issue during the MeBo recovery in this site: MeBo was staying 2 hours at 100 m water depth which is out of gas hydrate stability zone. Therefore, intervals with small amount of gas hydrate could be completely dissociated and its temperature might equilibrate with surrounding sediment. However, there were at least five significant negative anomalies of temperature in core 3P, core 4P, core 6P and core 7R which is shown in Fig. 66.

10.3.2 Lomvi Pockmark

Gas hydrates were recovered by gravity cores in Lomvi pockmark. GC-7, GC-8 and GC-11 were located at north-eastern depression of the pockmark, GC-12 was located at the south-western depression of the pockmark. There is no IR-images of GC-7 due to the core barrel bending during the sampling. However, the disseminated gas hydrates were found in the core catcher of GC-7. The IR images indicated that the appearance of the shallowest gas hydrate at depth 15 cmbsf, 150 cmbsf and 235 cmbsf of GC-8, GC-11 and GC-12, respectively (Fig. 67). The temperature logs showed that distinct cold anomalies down to -3.5°C. The positive spikes in the temperature logs were artifacts from the relatively warm end caps of each liner section.

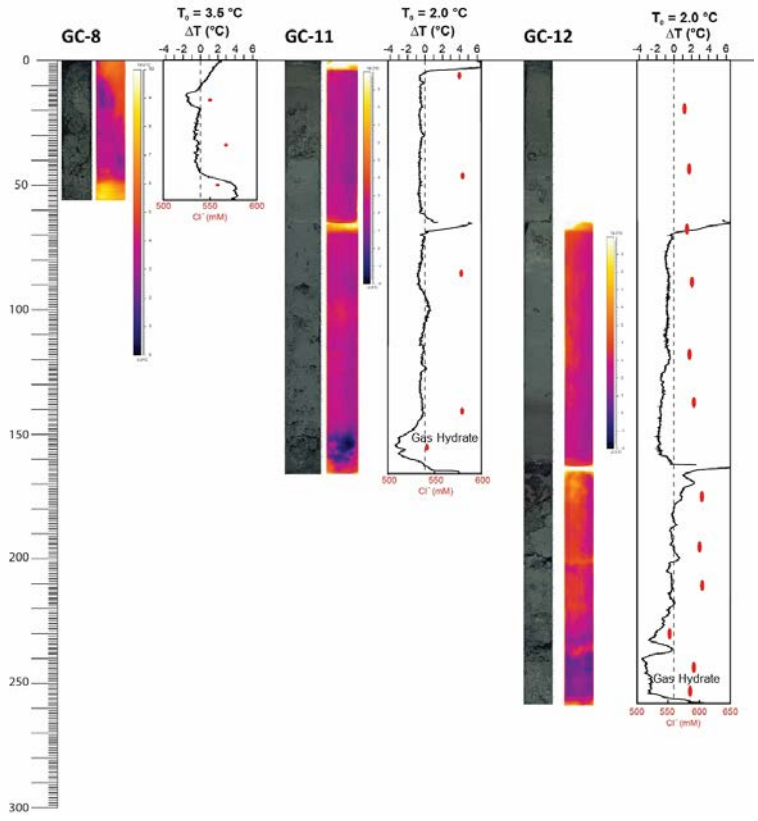

Fig. 67: Core images, IR images, temperature logs and pore water chloride concentration profiles of GC-8, GC-11, and GC-12. The colour bar of the IR images was ranged from 0 to 10°C for GC-8 and from -2 to 10°C for GC-11 and GC-12. Temperature profiles showed the differences between the measured temperature and background temperatures of core liners, expressed as ΔT. The concentrations of chloride (red dot) supported that refreshing signals in the interval of cold spot where soupy textures sediment appeared due to the gas hydrate dissociation.

11 Measurements of Magnetic Susceptibility with a Multi-Sensor Core Logger

(M. Riedel, N. Stange, J. E. Johnson)

11.1 Introduction

During cruise MSM57 we used a multi-sensor core logger (MSCL) from the University of Bremen to measure magnetic susceptibility on the recovered gravity and MeBo cores. Magnetic susceptibility is a useful indicator for stratigraphic correlations between drill/core sites and is widely used during drilling operations, including ODP and IODP expeditions (Blum, 1997; available online at http://www-odp.tamu.edu/publications/tnotes/tn26/TOC.HTM). Also, in case of methane advection, it has been noted previously (e.g. Novosel et al., 2005) that magnetic susceptibility is much reduced in sediments with a record of anaerobic oxidation of methane (AOM).

A bulk of previous gravity coring along the west Svalbard margin has established a magnetic susceptibility reference record (Jessen et al., 2010), to which we can compare and tie our new results from expedition MSM57.

11.2 Methods

11.2.1 The MSCL

A Geotek MSCL was provided by the working group Marine Geophysics by Prof. Dr. Tilo von Dobeneck at the University of Bremen, for onboard core-measurements during expedition MSM57 (Figs. 68, 69). The MSCL was equipped only with a magnetic susceptibility meter and a temperature probe (measuring ambient room temperature). The magnetic susceptibility is measured with a Bartington® meter, controlled through the track-software. Initially, for Leg 1 of MSM57, only a MS2C loop sensor with a diameter of 14 cm was available and utilized both for gravity and MeBo cores. For Leg 2 of MSM57, a MS2C65 sensor with loop-diameter of 6.5 cm was available for the MeBo cores. All gravity cores were still processed using the larger-diameter loop sensor.

11.2.2 Data Acquisition and Processing

Prior to logging of each core, the multi-sensor track software by Geotek is used to establish communication to the sensors and track-motor. After this first check, the susceptibility sensor was zeroed. No extra calibration of the susceptibility meter was performed onboard. Each core section was put on the track and we typically logged each core at an interval of 2 cm using a measurement time of 10 seconds for higher resolution, as we expected overall low ($< 100 \cdot 10^{-5}$ SI) magnetic susceptibility values in the cores off the western margin of Svalbard. Only two cores were measured at 1 cm resolution (GC-18, -20, and 21 from Svyatogor Ridge).

Since GC-9 and GC-12 were split prior to logging, these two gravity cores were logged as half rounds. For processing, there has been a correction of the reduced cross section area. Additionally, the split archive of GC-12 was relogged. The comparison of the magnetic susceptibility measurements on the whole round and half round of GC-12 shows that the used correction factor for reduced cross section area is appropriate.

The cores were not let to equilibrate to room temperature (~16°C, which would have taken ~3 hours) as core-logging had to be done immediately after recovery and prior to any sub-sampling of the material for geochemical proxies of methane advection and gas hydrate occurrence. No temperature correction was therefore performed. We also did not apply any drift-correction to the susceptibility meter. This neglect did not lead to any obvious problems that we could detect onboard.

We sequentially logged each core section including core-catchers where available. However, due to incomplete core recoveries at MeBo drill sites the raw-data are first assigned to an initial depth below seafloor, which is modified to reflect correct depth in situ in a post-measurement analysis step. Each core section is (in case of incomplete recovery per core-stroke) assumed to start at "0cm" below top of intended core-interval.

We processed the raw susceptibility values as outlined below to obtain volume specific susceptibility values that may be comparable to previous records. Due to the different nature of core-diameter of gravity cores (12 cm) and MeBo cores (5.6 cm for push and 6.3 cm for rotary cores) we also need to process the data to account for the difference in loop-diameter.

Volume specific magnetic susceptibility

The data obtained from the magnetic susceptibility system provides uncorrected, volume specific magnetic susceptibility, κ_{uncor} (dimensionless, $*10^{-5}$ SI units). To obtain the corrected Volume Specific Magnetic susceptibility (K) the data must be corrected for the relative effect of size of the core and the size of the loop sensor being used:

$\kappa = \kappa_{uncor} / \kappa_{rel}$ ($*10^{-5}$ SI units), with

$\kappa_{rel} = 4.8566*(dcore/Dloop)^2 - 3.0163*(dcore/Dloop)+0.6448.$

Fig. 68: Logger with large-diameter loop (14 cm) to log gravity cores.

Fig. 69: Logger with smaller-diameter loop (6.5 cm) to log MeBo cores, available for Leg 2 of MSM57 only.

11.3 Results

The individual logs for the cores are shown as part of the stratigraphic and sedimentological descriptions of each core (see sections 8 and 9 for details). Here we show one example of cross-correlation of lithologic units defined from gravity cores taken at MeBo Sites along a transect at the continental margin off Svalbard in water depths of 445 m to 338 m. Magnetic susceptibility shows a characteristic shape within the upper 1.5 mbsf of cores in deeper water allowing to identify the same peaks and troughs (as well as changes in gradient) from core to core (Fig. 70). At the two sites in lower water depths the magnetic susceptibility was generally lower than for sites in deeper water and did not show any patterns useful for correlation. This can be due to a change in the rather heterogeneous sedimentional environment. On the other hand, it is quite possible that there was a consumption of magnetic minerals in connection to AOM, especially since GC-22 is located at an active seep site.

Sediments recovered at these sites reflect a mostly glacially dominated sedimentation pattern, with numerous dropstones mixed within a clay-dominated matrix. Some sand-layers as well as authigenic carbonate was recovered. Pore-water analyses made from these cores included measurements of the total alkalinity (TA), which is a proxy for methane advection. Typically TA is at a local maximum within the sulfate-methane transition zone (SMTZ). However, down-core variations in TA (e.g. gradient in concentration) may also be lithologically controlled (Fig. 71). Further analyses and correlations will be made post-expedition.

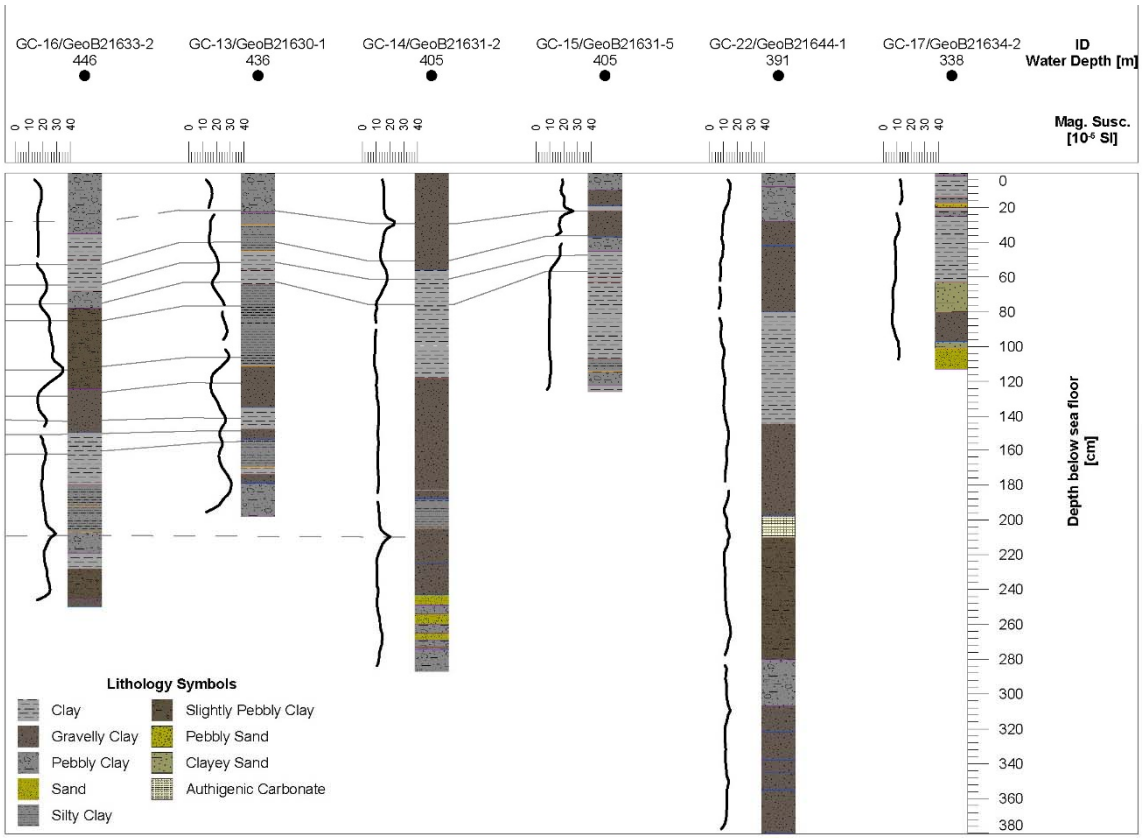

Fig. 70: Correlation of stratigraphic units with magnetic susceptibility for the gravity cores taken at the MeBo Sites at the continental margin off Svalbard.

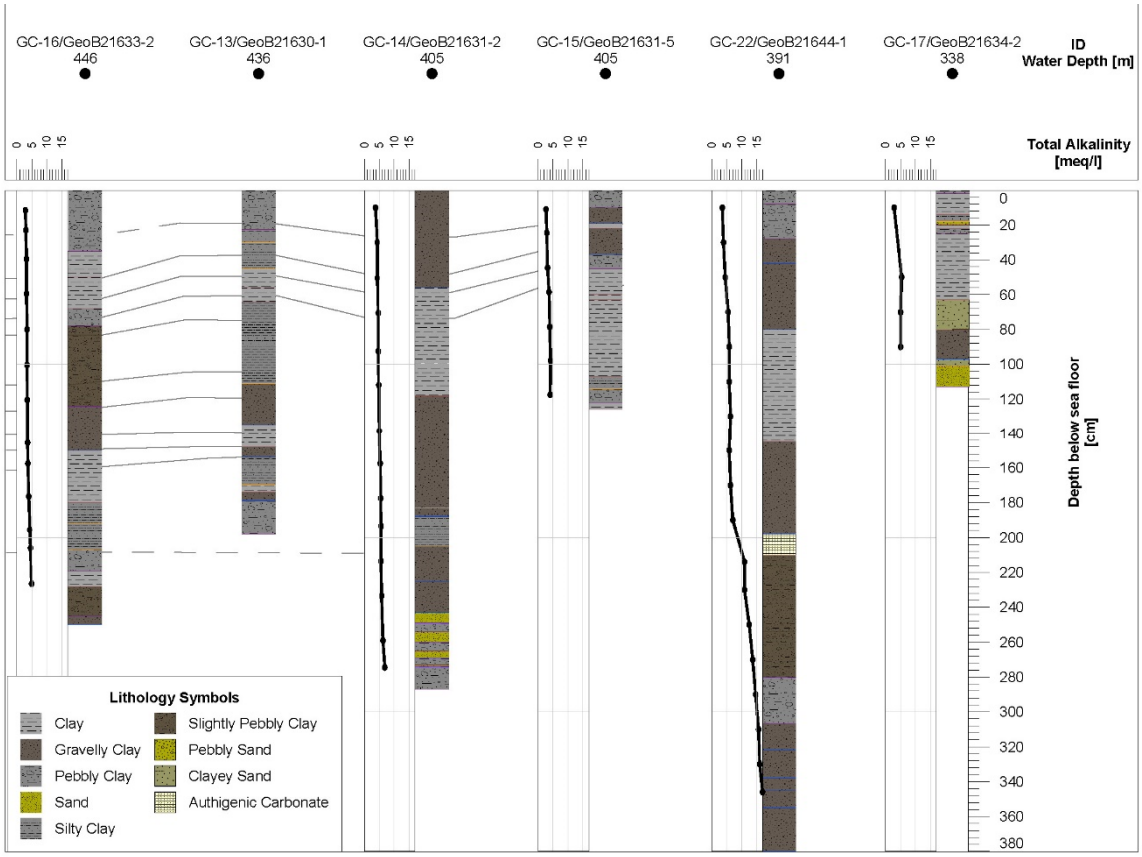

Fig. 71: Correlation of stratigraphic units as shown in Fig. 70 with total alkalinity (TA) measured for the gravity cores taken at the MeBo Sites at the continental margin off Svalbard.

12 Pore Water Geochemistry

(W.-L. Hong, C. Schmidt, H. Yao, K. Hamann, K. Wallmann)

12.1 Introduction

During the first leg of cruise MSM57, MeBo drilling and gravity coring were conducted at two active pockmarks, Lunde and Lomvi, along Vestnesa Ridge to investigate the dynamics of gas hydrates and fluid flow. During the second leg, sediments were recovered on the upper continental slope of Svalbard at the edge of the gas hydrate stability zone where recent bottom water warming may induce gas hydrate dissociation.

Analyses were carried out onboard and augmented by an extensive subsampling program for onshore analyses of key geochemical species (Table 23).

Table 23: Pore water analyses and sub-sampling plan during MSM57

Onboard analysis	**Treatment**	**Institute in charge**
Total alkalinity	Onboard titration	CAGE/GEOMAR
Ammonium	Onboard spectrophotometry	CAGE/GEOMAR
Chloride	Onboard titration	CAGE/GEOMAR
Pore Water sub-sampling		
Anions (IC)	None	GEOMAR
Cations (ICP)	Add 20 µl HNO_3	GEOMAR
Hydrogen sulfide	Add 1.5 ml $Zn(OAc)_2$	CAGE
δ^{13}C-DIC	Add 10 µl $HgCl_2$	CAGE
Sr/B	None	CAGE
δ^{18}O/D	None	CAGE
Sediment sub-sampling from squeezer cakes		
POC, PIC, N, S	None	GEOMAR
Biomarker analysis	Freezer -20°C	CAGE
Pyrite	Vacuum, -20°C	CAGE

For the onboard analyses, we measured concentrations of chloride, ammonium, and total alkalinity. Chloride is a biologically inert chemical species. Its concentration is depleted when freshwater is added to saline pore fluids by a range of different processes including infiltration by meteoric waters, diagenetic transformation of water-rich minerals (e.g. smectite, biogenic opal) into water-poor phases (e.g. illite, opal-CT) and through the dissociation of gas hydrates. Chloride contents higher than in seawater are observed where deep-seated brines ascend to the surface or when fresh water is removed from ambient pore space by the formation of gas hydrates.

The concentrations of total alkalinity and ammonium are useful indicators of key biogeochemical reactions: organic matter degradation and anaerobic oxidation of methane (AOM). During the decomposition of organic matter, macro nutrients such as ammonium and phosphate are released to the pore fluid. High ammonium levels then indicate active organic matter turnover. Total alkalinity (TA) defines the buffer capacity of the fluid, which indicates the concentration of bicarbonate and hydrogen sulfide in the pore fluid. Bicarbonate and hydrogen sulfide are actively produced during the AOM-coupled sulfate reduction, a reaction mediated by a consortium of bacteria and archaea:

$$CH_4 + SO_4^{2-} \longrightarrow HCO_3^- + HS^- + H_2O$$

Besides being indicators of biogeochemical reactions, both ammonium and TA concentrations also reflect the degree of cation exchange and silicate diagenesis, processes happening at greater depth.

12.2 Methods

12.2.1 Sediment and Pore Water Sampling

Sediment samples were taken from gravity cores (GC) and MeBo cores. The sampling was done in the hanger of the ship at ambient temperature of ~10°C. For most of the cores, MSCL scanning was performed before the core was cut into halves. Whole round cores were stored on the deck before MSCL scanning at air temperature of 2 to 4°C. We sampled 2-3 cm thick(?) sediment slices from the working halves of gravity cores and 8-10 cm thick sections from the working halves of MeBo cores. The depth intervals of the sampling were chosen according to core recovery and the distribution of gas hydrates in the core. Sediments both at the splitting surface and in contact with the liner were not sampled to avoid potential contamination from the drilling fluid and seawater. Sediments from the top ca. 10 cm of the MeBo core sections were usually not sampled because they were often wet and appeared to be disturbed by the drilling operation. Sandy sections are also avoided where possible because the seawater that was used as drilling fluid may easily penetrate these high-permeability sediments. Especially for the samples from MeBo core 139, where thick well-sorted sand layers were recovered, samples with sand almost always contained low TA, low ammonium, and seawater-like chloride content, a clear sign for severe seawater contamination. The degree of contamination will be assessed for all samples employing onshore measurements of sulfate as sulfate is expected to be absent below the SMTZ and any sulfate present in the deeper core sections very likely originates from seawater contamination during drilling. Caution is advised when interpreting the raw, uncorrected pore water data from this report. Concentrations may change significantly after the sulfate correction has been applied.

Two GEOMAR argon-gas squeezers were used to extract pore water from the sediments. 14 samples were squeezed simultaneously in each squeezer. On average, it took 30 to 45 minutes to squeeze 5-10 ml of pore water. Squeezing was performed in the vessel's cold room at 4°C. Gas pressure was monitored and seldom exceeded 5 bar during the squeezing. While squeezing, the pore water was filtered through 0.2 µm cellulose Whatman filters and collected in acid-washed 20 or 10 ml bottles. In addition to the squeezing method, some gravity cores were treated with rhizons (purchased from Rhizosphere, The Netherlands) in order to gain pore fluids from undisturbed whole cores.

Alkalinity titrations and sub-sampling for hydrogen sulfide were done immediately after the extraction of pore water. Ammonium was analyzed within 1 to 2 hours after pore water sampling. Chloride titrations and further sub-sampling were conducted after the ammonium analyses were completed. After pore water squeezing, sediment squeeze cakes were subsampled into three aliquotes: one halve for biomarker analyses (CAGE), one sixth for pyrite extraction (CAGE), and the remaining portion for element analyses at GEOMAR. The fraction for biomarker analyses was stored in a -20°C freezer to inhibit organic compound degradation. The fraction for pyrite analysis was vacuumed and stored in the -20°C freezer to avoid oxidation (Table 23).

12.2.2 Onboard Chemical Analyses

Analyses for total alkalinity (TA) were carried out on board using a METROHM titration unit 916- ti touch. TA was determined by titration with 0.02 N HCl using a methyl red indicator. The solution was bubbled with argon to remove CO_2 and H_2S gas released during the titration. Onboard analyses for chloride (Cl) were carried out using a METROHM titration unit SIS665. The Cl concentration was determined with $AgNO_3$ and a K-Chromat and K-Dichromat indicator. IAPSO seawater standard was used for both onboard titration methods to check the reproducibility and accuracy of the chemical analyses. The error (±1 SD) of the Cl and TA analyses amount to ±2 mM (±0.3 %) for Cl and ± 0.05 mEq. dm^{-3} (±2 %) for TA according to replicate analyses of the IAPSO standard. Onboard analyses for ammonium (NH_4^+) were carried out using a Hitachi U2800A spectrophotometer applying a calibration curve with eight standards covering the concentration range between 0 and 332.62 µM. Aliquots for NH_4^+ analyses were diluted with Milli-Q water prior to measurements by factors between 2 and 10 in order to bring the concentration in the calibration range. Replicate onboard analyses of samples and ammonium standards suggest an error of ±5 % for the determination of NH_4 concentrations. The ammonium and chloride determinations are compromised when dissolved sulfide occurs at high concentrations (>1 mM). Hence, sulfide was removed from sulfide-rich samples taken at active seep sites prior to analysis. Sulfide was either removed by bubbling with argon gas (10 min., prior to ammonium analysis) or by acid addition (1:1 dilution with 0.05 N HNO_3 followed by overnight storage in open vials at 4°C in the cold room, prior to Cl determination). Towards the end of the cruise the procedure was updated. Subsamples were first acidified (1:1 dilution with 0.05 N HNO_3), then bubbled with argon gas for 10 minutes, and subsequently used for both, TA and Cl analyses. Samples from MeBo Hole 138 and GC22 were treated in this way. Repeated tests showed that the slope of the NH_4 calibration curve was not affected by acid addition.

12.3 Preliminary Results

12.3.1 Site Statistics and Subsampling

Samples taken and analyzed by the geochemistry group are listed in Table 24. Corresponding locations and core recoveries can be found in the station list. About 500 samples were processed during the cruise. 13 additional water samples were taken with Rhizon in sections containing gas hydrate. These Rhizon samples were taken after gas hydrate was fully dissociated.

Table 24: Number of samples taken and analyzed during MSM57.

Station	Location	TA	NH_4	Cl	IC	ICP	TH_2S	$\delta^{13}C$ -DIC	Sr/B-Iso.	$\delta^{18}O$/ D	Sedi-ment
Leg 1											
GC-1	Lunde, non-seep	28	28	0	26	26	28	28	28	0	28
GC-2	Lunde, non-seep	26	26	0	26	26	26	26	26	0	26
GC-3	Reference	14	14	0	14	14	14	14	14	0	14
MeBo125	Lunde, non-seep	9	8	0	9	9	9	9	9	0	9
GC-6	Lunde, Seep	14	14	0	17	17	14	14	14	11	17
MeBo126	Reference	28	28	28	27	26	28	27	27	24	28
MeBo127	Lunde Pockmark	5	4	0	3	3	5	5	5	3	5
GC-8	Lunde Pockmark	3	0	3	3	3	3	0	3	0	3
GC-9	Lunde, seep	7	8	20*	14	14	8	8	8	18	9
GC-10	Reference	13	13	11	13	13	13	13	13	0	13
MeBo128	Lunde Pockmark	9	9	7	9	9	9	9	8	9	9
GC-11	Lomvi-seep	6	6	6	6	6	6	6	6	6	6
GC-12	Lomvi-seep	11	11	13+	13	13	11	11	11	12	11

Leg 2											
MeBo129-1	CM 1, 404 m	8	7	9	7	7	9	9	5	2	9
MeBo 129-2	CM1, 404 m	5	4	6	5	5	4	2	3	2	6
GC-14	CM4, 405 m	14	14	14	14	14	14	14	12	13	14
MeBo132	CM4, 405 m	5	2	6	3	3	0	0	0	2	6
GC-15	CM4, 405 m	7	7	7	7	7	7	0	0	0	7
MeBo133	CM5, 391 m	9	9	9	9	9	9	9	5	0	9
MeBo134	CM5, 391 m	10	10	10	10	7	6	5	9	9	10
MeBo135	CM3, 446 m	16	16	16	16	15	10	12	11	0	16
GC-16	CM3, 445 m	13	13	13	13	13	13	13	13	0	13
MeBo136	CM3, 445 m	27	27	27	25	25	0	16	15	10	27
MeBo137	CM6, 340 m	16	16	16			12	8	10	7	18
GC-17	CM6, 338 m	4	4	4							0
GC-18	Svyatogor Ridge	20	20	20	20	20	0	0	0	0	20
MeBo138	Lunde Pockmark	25	25	25	25	25	25	23	23	24	25
GC-19	Lunde Pockmark	4	0	0	4	4	4	4	4	4	4
MeBo139	CM5, 391 m	27	27	30	27	26	12	15	20	19	34
GC-20	Svyatogor Ridge	12	12	0	12	12	12	0	0	0	12
GC-21	Svyatogor Ridge	15	15	0	15	15	15	0	0	0	15
MeBo140	CM7, 402 m	58	59	59	59	57	24	35	33	39	60
GC-22	CM5, 391 m	19	19	19	19	19	19	18	0	17	19

* 11 additional samples from Rhizon after gas hydrate completely dissociated and 1 additional squeeze cake taken the next day
+ 2 additional samples from Rhizon after gas hydrate completely dissociated

12.3.2 Preliminary Results

Depths of sulfate-methane-transition-zone and the supply of methane

From the profiles of total alkalinity, we can estimate the depth of sulfate methane transition zone (SMTZ), where both sulfate and methane are exhausted due to AOM, at the horizon where total alkalinity is the highest. Our estimated SMTZ corresponds well to the depth where methane concentration starts to increase at each site (see Chapter 13). The actual SMTZ has to be confirmed by further onshore analyses of sulfate concentration. We observed the shallowest SMTZ (0.5 to 1.5 mbsf) from the pits of the two pockmarks (GC-6, GC-8, GC-9, GC-11, GC-12, MeBo127, MeBo128, and MeBo138; Figs. 72B, C, E) where methane supply is the strongest. Gas hydrates and authigenic carbonates were usually recovered from these cores. For the sites in the pockmark but not directly associated with strong seeping (GC-1, GC-2, and MeBo125), the depths of SMTZ range between three to six meters. No gas hydrates were recovered from these sites. Occasional authigenic carbonate nodules and /or concretions were found. For the sites outside of the pockmark (GC-3, GC-10, MeBo126), SMTZ is usually beyond the recovery of gravity cores (> 5 mbsf). Both gas hydrate and authigenic carbonates were absent from these sites. In the sediments of these sites, a common observation are the black patches, presumably mono-sulfide minerals. These black patches may indicate weak but not absent sulfide production. Organic matter-coupled sulfate turnover might be responsible for such weak sulfide production.

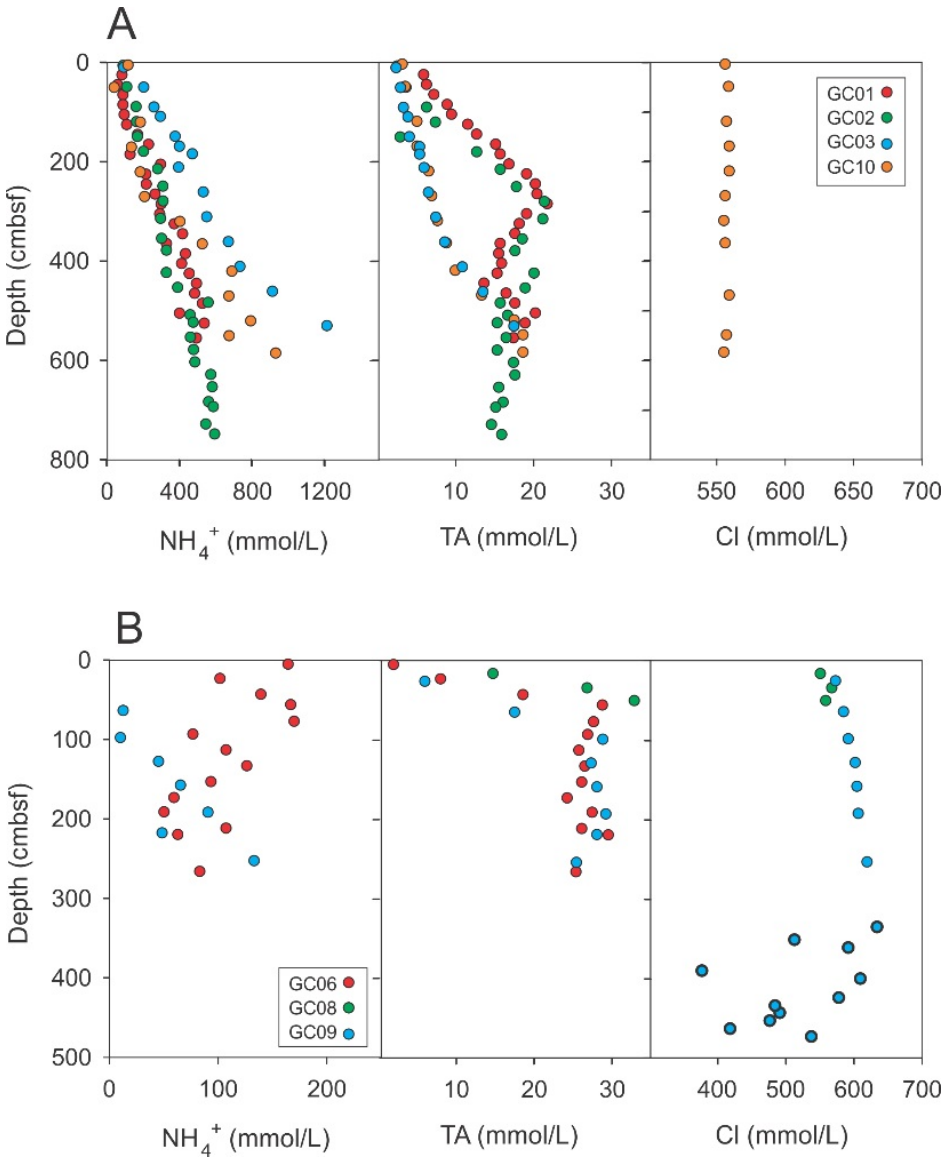

Figs. 72A, B: onboard analyses of ammonium, chloride, and total alkalinity (TA). Symbols with thick outlines represent samples with potential influence from gas hydrate dissociation.

Reduction of total alkalinity below SMTZ and at depth

Below our proposed depths of SMTZ, total alkalinity slightly decreases with depth in most of the sites. From the two MeBo drillings that recovered sediments from greater depth (MeBo125 and MeBo126), we can confirm such reduction continues to greater depth. Precipitation of authigenic carbonates may, to some degree, explain such reduction, especially for the section immediately below SMTZ. Nodules and/or concretions of authigenic carbonates were found often below the depth SMTZ, which supports our interpretation. Further shore-based analyses of cation concentrations and the carbon isotopic signature of dissolved inorganic carbon are planned to further understand the processes that govern the carbon cycles at these sites.

Gas hydrate dynamics inferred from chloride profiles.

Some of the pore water samples were taken specifically to target sections with gas hydrate. After gas hydrates were fully dissociated from either half round or whole round cores, we sampled the pore water mostly via rhizons and a few samples via squeezing. The comparison of the chloride content

from these samples with the IR images suggest very dynamic gas hydrate system in the pockmarks (see Chapter 10). A common observation among different hydrate-containing sites is the dilution of chloride concentration in the sections with hydrate and enrichment in chloride either above and below such hydrate layer. One best example is the profile from GC-9. Pore water samples taken from the core interval showing cold temperatures in the IR images show chloride reduction up to ~250 mM comparing to the samples without hydrate (Fig. 72B).

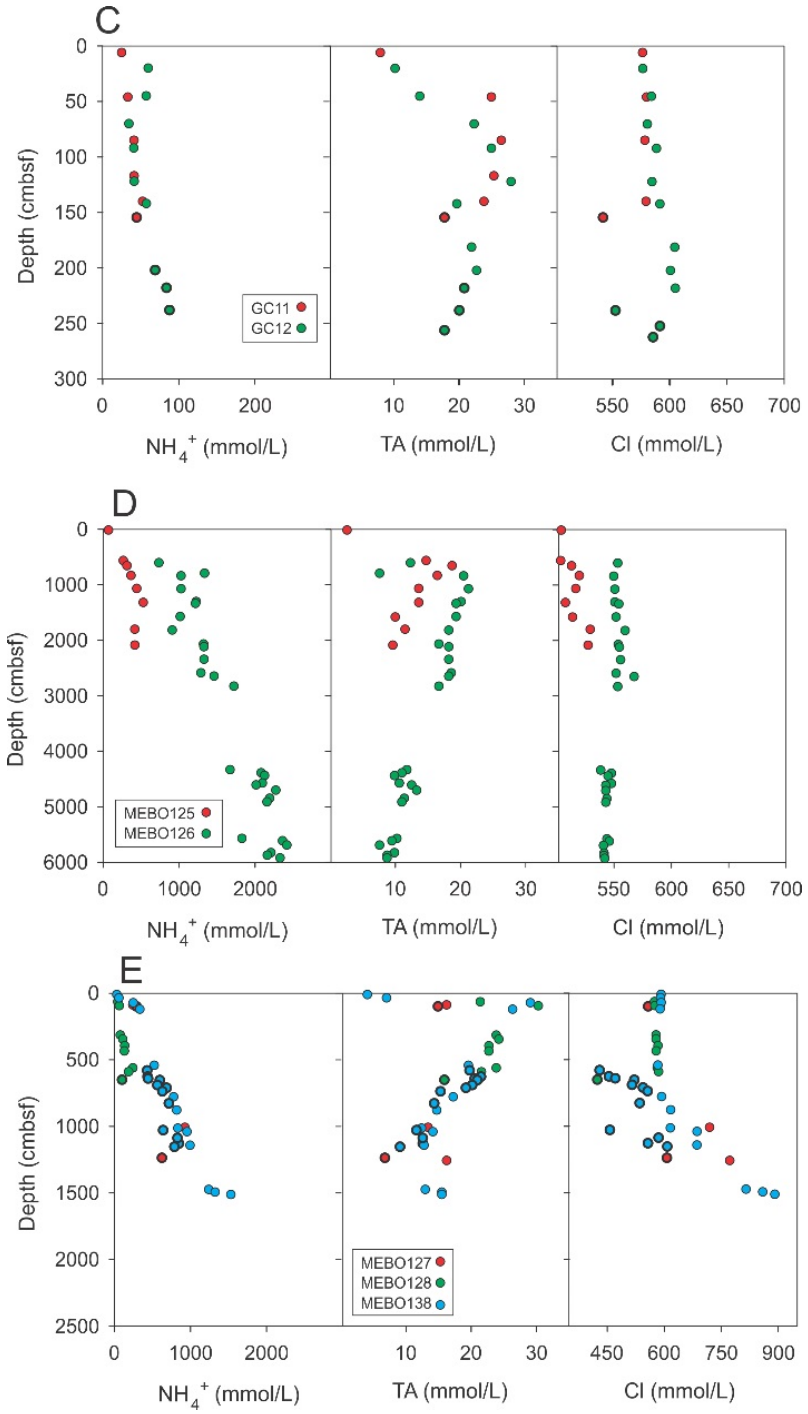

Figs. 72C, D, E: onboard analyses of ammonium, chloride, and total alkalinity (TA). Symbols with thick outlines represent samples with potential influence from gas hydrate dissociation.

Immediately above the gas hydrate bearing interval, chloride content is as high as 633 mM, 78 mM more than the seawater concentration. As the depth decreases, the enrichment of chloride decreases

but is still significantly higher than seawater concentration even in the shallowest sample at 25 cmbsf, whose chloride concentration is 572 mM. The linear diffusional profile above 335 cmbsf suggests that the pore water system is in a quasi-steady state and that methane supply is sufficient to sustain rapid hydrate formation over a period of time. Future modeling work can provide estimation of gas hydrate abundance and the rate of hydrate formation from the two pockmarks.

Such enrichment is further confirmed by the MeBo sites targeting the seismic reflector in Lunde Pockmark: MeBo127, 128, 138 (Fig. 72E). By comparing the chloride profiles from these three sites and the background site outside of the pockmark footprint (MeBo126), we observed a continuous chloride enrichment from the top of the site down to approximately 16 mbsf with the highest chloride concentration of 890 mM (Fig. 73). Interestingly, right below the depth with the highest chloride enrichment (with a 2-meter unrecovered gap), we recovered sections with carbonate-cemented sediments (sections 10–12 with total length of about 1 meter). The role of this carbonate layer with respect to fluid flow and gas hydrate dynamics is of great interest. While the low porosity and permeability of carbonate itself stop any transport of fluid, fractures in the carbonate are great conduits for fluid. The interpretation of such positive anomaly in chloride is difficult as one would need very rapid hydrate formation, much faster than the chloride diffusion, to create such positive anomaly. Either massive hydrate was present in the 2-meter gap that we were not able to recovery, or massive gas hydrate growth happened in the fractures of the carbonate-cemented sediments is still not clear. Lateral transport of fluid is another alternative to explain such enrichment. In this case, the carbonate-cemented sediments clogged the conduits for fluid transport. The source of such hyper-saline fluid might not be directly beneath our drilling sites.

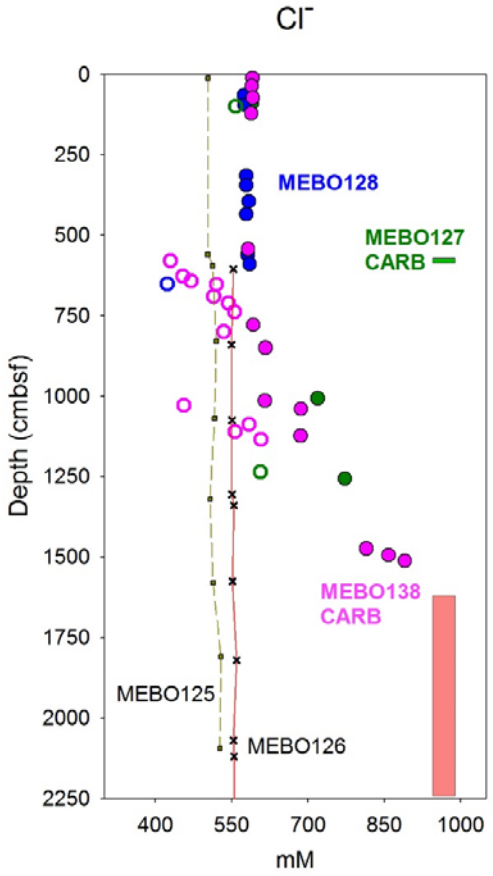

Fig. 73: Comparison of chloride profiles from three seeping sites from Lunde Pockmark (MeBo127, 128, and 138) and two reference sites (MeBo125 and 126). Empty symbols represent samples with potential influence from gas hydrate dissociation. Carbonate-cemented sediments were observed from the bottom of MeBo127 (green column) and MeBo138 (pink column).

We made an estimation of the saturation of gas hydrate from Lunde and Lomvi Pockmarks based on the available chloride profiles (Fig. 74). The baseline profile is from the non-hydrate samples. We

used a first-order regression for the three gravity cores and a four-order polynomial regression for the three MeBo cores. By comparing the baseline with the chloride content in the samples with gas hydrate present, we estimated the gas hydrate saturation assuming a binary mixing. The saturation is between 3–42% of pore space with the highest saturation estimated from GC-09 in Lunde Pockmark. Later refinement of this estimation is needed by including seawater contamination correction and considering porosity.

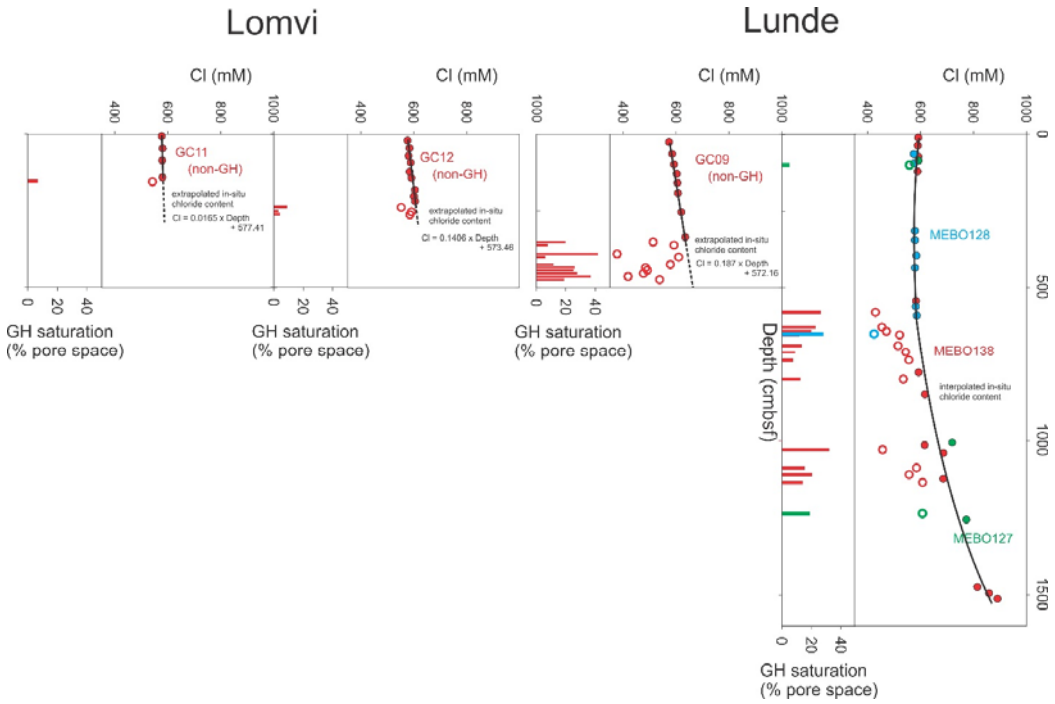

Fig. 74: Estimation of gas hydrate saturation assuming a binary mixing of fresh water from hydrate dissociation and the ambient pore water. Open symbols represent samples influenced by gas hydrate dissociation while the solid symbols are samples without. The in-situ chloride content of the ambient pore water was estimated from the samples not influenced by gas hydrate dissociation. The saturation ranges from several percent to 42 % pore space. The highest saturation was observed from GC-09 in Lunde Pockmark.

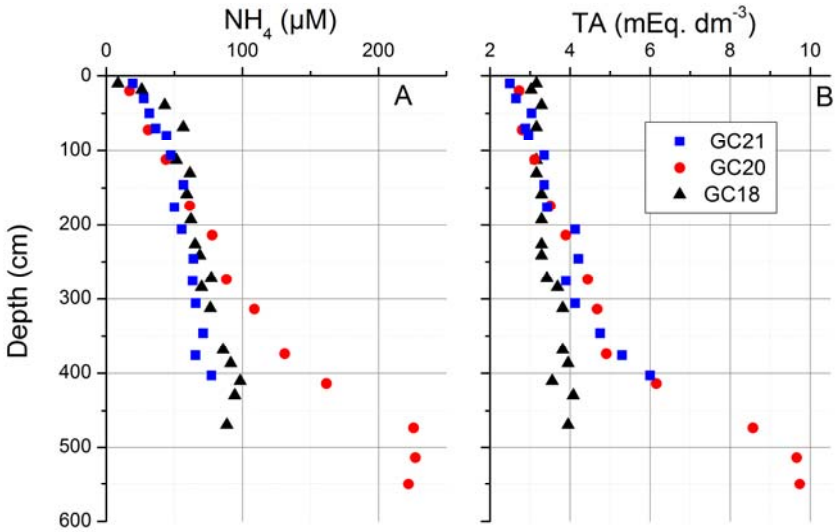

Fig. 75: Dissolved ammonium (NH_4) and total alkalinity (TA) in pore fluids recovered at the Svyatogor Ridge.

Svyatogor Ridge

In contrast to the pockmarks Lunde and Lomvi, pockmarks on the Svyatogor Ridge showed no indication for active gas seepage. The TA pore water profiles confirm that methane does not reach the surface sediments sampled by the gravity corer (Fig. 75). It may be possible to penetrate into the methane-sulfate transition zone and the underlying methane-bearing sediments employing MeBo or other deep-reaching drilling devices.

Upper continental slope off Svalbard

Sediments were taken at the up-dip limit of the gas hydrate stability zone (GHSZ) off Svalbard where intense gas seepage occurs that has been attributed to the destabilization of gas hydrates due to the recent warming in the Arctic for the past 30 years. The modern base of the GHSZ is located at around 400 m water depth considering a mean annual bottom water temperature of 3°C and salinity of 35 PSU. In the past, it was possibly located at larger depths assuming mean bottom water temperatures were lower than today. A subsequent rise in temperature may have induced gas hydrate dissociation (melting) that in turn contributed to the gas seepage observed at the modern seafloor around 400 m water depth. Hydrate dissociation reduces the salinity of ambient pore fluids because fresh water is released into the pore space where hydrates dissociate. The data indeed show strong Cl depletions at around 17–23 m sediment depths in cores taken at the up-dip limit of the modern GHSZ (Fig. 76A). This observation points towards hydrate melting. However, the depth of the Cl depletion and the Cl gradients in the overlying sediment sequence indicate that hydrate melting took place several thousands to hundreds of years ago. The warming that has been observed over the last three decades could only affect hydrates residing at shallower depth and would not produce the gradual decrease in chloride observed over the top 15 m of the sediment column. In contrast, the intriguing Cl changes at 0–4 m sediment depth observed in GC-22 (Fig. 76A) might be related to more recent hydrate dynamics driven by e.g. seasonal changes in bottom water temperature. The deeper station at 445 m water depth also showed a continuous down-core decline in dissolved Cl over the top 15 m that may point towards hydrate melting at larger sediment depths that were, however, not drilled during the MeBo deployment (Fig. 76B). The MeBo core taken at shallow water depths (340 m) above the modern GHSZ features no Cl depletion (Fig. 76B). Pore fluids will be further analyzed at GEOMAR and CAGE to decipher the distribution and origin of Cl depletions. Cl will be reanalyzed using ion chromatography, sulfate will be determined to detect contamination by seawater, and water samples will be analyzed for δD and $\delta^{18}O$ to characterize the freshwater source. Numerical modeling will be conducted at GEOMAR and CAGE to investigate different scenarios (bottom water warming, isostatic rebound, injection of warm fluids, etc.) that may have induced gas hydrate dissociation and caused the observed Cl depletions.

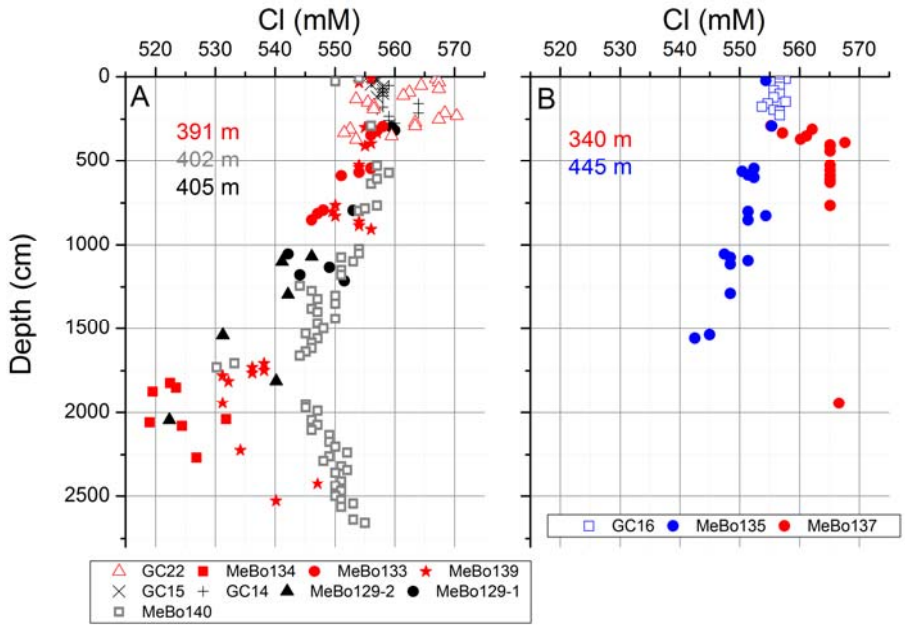

Fig. 76: Dissolved chloride concentrations in pore fluids recovered at the upper continental slope off Svalbard. A. Samples taken at the up-dip limit of the GHSZ. B. Samples taken above and below the up-dip limit of the GHSZ.

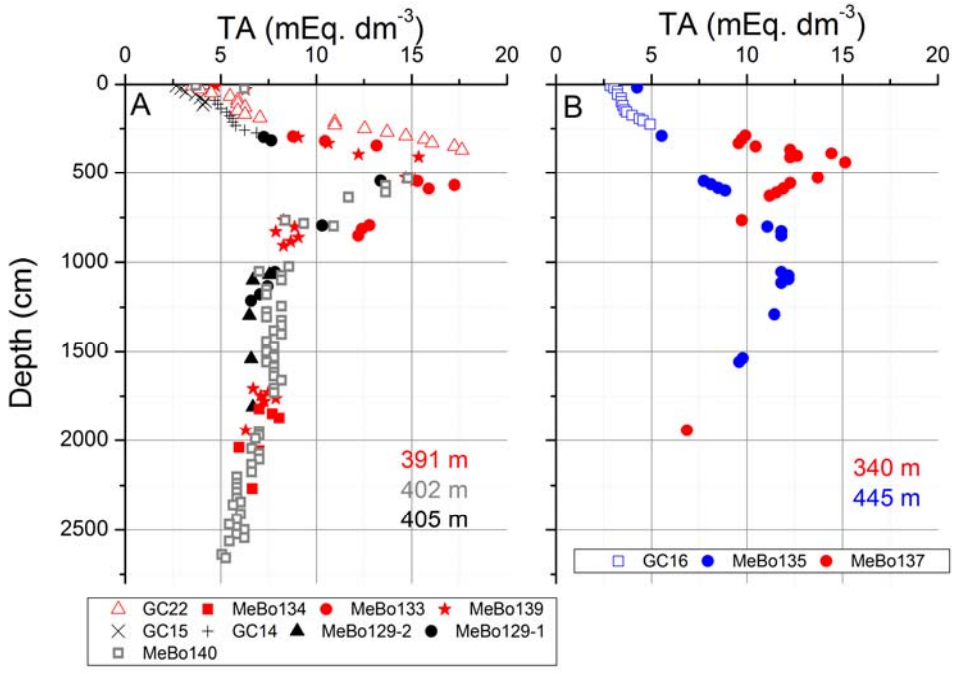

Fig. 77: Total alkalinity (TA) in pore fluids recovered at the upper continental slope off Svalbard. A. Samples taken at the up-dip limit of the GHSZ. B. Samples taken above and below the up-dip limit of the GHSZ.

Dissolved ammonium increased gradually with sediment depth (Fig. 78). The down-hole increase was probably induced by the slow degradation of N-bearing organic matter. NH_4 profiles showed the same pattern between 391 and 445 m water depth. This homogeneity may indicate that similar types and amounts of organic matter accumulate over this depth range. Elevated NH_4 values at the 340 m site may reflect enhanced input of organic matter at shallow water depths (Fig. 78B). The determination of POC and total N contents in sediments and numerical modeling at GEOMAR will shed further light on the organic matter turnover and mean sediment accumulation rates in the study area.

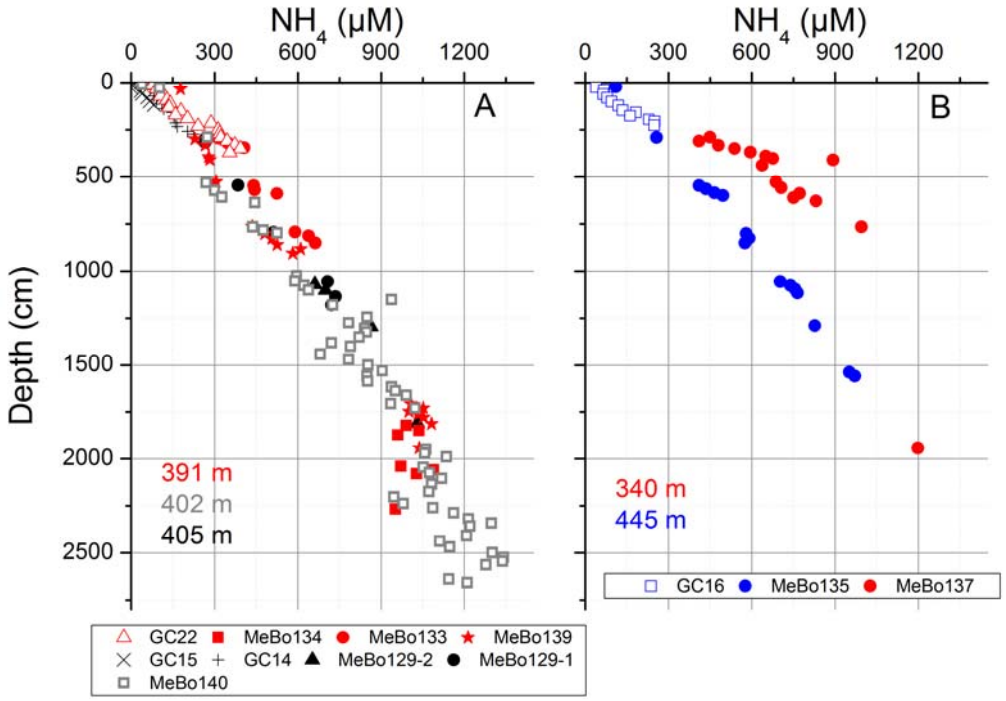

Fig. 78: Dissolved ammonium (NH_4) in pore fluids recovered at the upper continental slope off Svalbard. A. Samples taken at the up-dip limit of the GHSZ. B. Samples taken above and below the up-dip limit of the GHSZ.

13 Gas and Gas Hydrate Analysis

(T. Pape, J. Malnati, M. Lange)

13.1 Introduction

Generation of light hydrocarbons, such as methane, in the deep subsurface followed by upward migration results in methane enrichment in overlying sediments. In case methane concentrations exceed solubility, gas hydrates might form at relatively low temperature and high pressure conditions (Fig. 79 left) in the so-called gas hydrate stability zone (GHSZ).

In sediments overlying gas hydrates methane is consumed via the microbially-mediated sulfate-dependent anaerobic oxidation of methane (e.g., Barnes and Goldberg, 1976; Hoehler et al., 1994; Reeburgh, 1976) in a distinct zone called the sulfate-methane transition (SMTZ, Fig. 79 right). The position of the top of the gas hydrates (ToGH) and that of the SMTZ are controlled by the gas flux intensity and the concentration gradient between the top of the GHSZ and the methane-depleted seawater (Bhatnagar et al., 2008; Borowski et al., 1996).

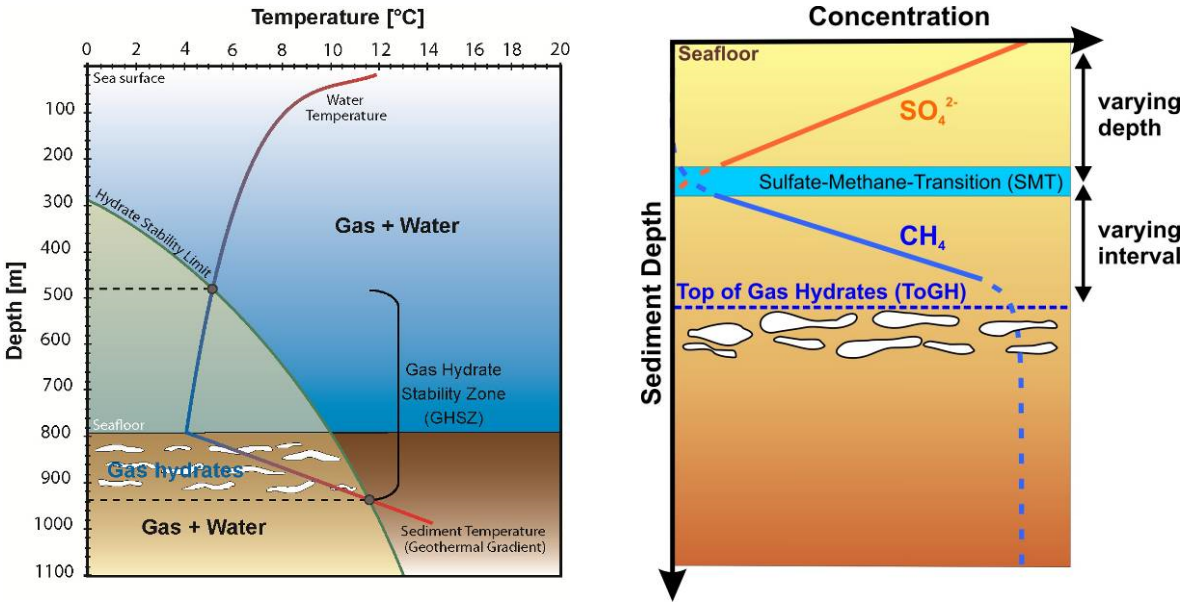

Fig. 79: Left: Typical profiles of water and sediment temperature as well as hydrate phase boundary that jointly define the extent of the Gas Hydrate Stability Zone (GHSZ). Right: General zonation of methane and sulfate in methane-rich marine sediments and relative positions of the sulfate-methane-transition zone (SMTZ) and the top of the gas hydrates.

Although a great portion of dissolved gas is lost during retrieval of the sediment in non-pressure vessels from the seafloor and subsequent sample preparation on deck, determination of *ex-situ* methane profiles enables assessment of both, methane distributions in the subsurface and positions of the SMTZ (and potentially of the ToGH, respectively). However, because of their comparably low abundances, concentrations of non-methane hydrocarbons in unpressurized cores are usually close to detection limits when conventional gas chromatography analysis is used. Pressure core sampling and subsequent controlled degassing is the only means that enables accurate determination of *in-situ* concentrations of light hydrocarbons (see chapter 14).

So far, two hydrate crystal structures (sI and sII) were abundantly found in nature with hydrate sI being the most widespread (e.g., Sloan, 2003). Hydrate crystal structures sII is more stable than sI, i.e.

it can also exist at comparably lower pressure and higher temperature conditions. While volatiles in sI hydrates consist of methane and ethane only, sII hydrates additionally contain propane and isomers of butane in relevant concentrations. Therefore, the crystal structure of a given hydrate piece, its stability and spatial distribution, respectively, can be assessed when molecular compositions of the hydrate-bound volatiles are known. Hydrates are a compact reservoir of light hydrocarbons which facilitate precise determination of their molecular and isotopic compositions at a given site.

Moreover, molecular compositions of light hydrocarbons bear information on the formation processes of light hydrocarbon. While microbial light hydrocarbons formed at relatively shallow depth below seafloor consist of methane (C_1) and much smaller amounts of ethane (C_2) only, thermogenic hydrocarbons generated at greater sediment depth are characterized by significant fractions of C_2 to C_6-hydrocarbons. Therefore, the molecular ratio of methane vs. higher hydrocarbons (C_1/C_{2+}) enables assessment of the predominant source and formation depth, respectively (e.g., Bernard et al., 1976). Even more detailed information on formation processes of light hydrocarbons can be gained from the stable carbon and hydrogen isotopic signatures ($\delta^{13}C$, $\delta^{2}H$; Schoell, 1988; Whiticar, 1999).

Major objectives of the gas analysis works during cruise MSM57 were:

- to analyze molecular compositions of light hydrocarbons contained in gas hydrates and void gas in order to characterize formation processes and depths, hydrate crystal structures, stabilities etc.;
- to determine *ex-situ* concentration profiles of dissolved methane in order to assess methane distributions, positions of SMTZ, and respective methane flux in the working areas;
- to prepare high concentration methane samples for isotopic analysis in the MARUM lab.

13.2 Methods

Sampling and preparation

For analysis of methane dissolved in pore water, a modified headspace technique after Kvenvolden and McDonald (1986) was used. 3 ml of bulk sediment retrieved either with MeBo70 or with a conventional gravity corer were transferred to 20 ml glass vials prefilled with 5 ml NaOH, thereby creating a headspace volume of 12 ml. For all MeBo cores, sediment samples were taken from the lowermost part of each liner immediately after removal of the pilot chuck and the core catcher (2.5 m vertical resolution). Assuming that highest methane concentrations were present in deep sediments, which therefore would be affected most by sediment degassing, sampling of MeBo cores was started with the deepest core barrels. For gravity cores in rigid PVC liners, samples were taken from the segment cuts (1 m vertical resolution). Additional samples were taken with respect to conspicuous lithological changes and/or sampling for pore water extraction. Considering different durations until cores are accessible for sampling, *ex-situ* concentrations obtained for MeBo cores might be generally lower compared to those obtained for gravity cores.

Gas that accumulated in sediment fractures or created voids (‘void gas’) was collected for subsequent analysis of its molecular composition. For this, a butyl rubber septum was placed on the liner and holes of 1 mm in diameter were drilled through the septum into the liner thereby minimizing escape of void gas and/or inflow of air from/to the liner. Gas was gathered by inserting a cannula attached to a plastic syringe through the septum into the core liner. The void gas was transferred into glass serum vials that were prefilled with saturated NaCl solution.

For preparation of hydrate-bound gas, hydrates were transferred into a plastic syringe and left for dissociation. The released gas was transferred into glass serum vials that were prefilled with saturated NaCl solution. Additional gas samples were obtained during controlled degassing of the MeBo pressure vessels (MDP, for methodology see Chapter 14).

In total 398 (GC: 159, MeBo: 239) headspace gas samples, 158 samples of hydrate-bound gas, 25 void gas samples, and 16 gas samples retrieved from pressures cores (MDP, for method see Chapter 14) were prepared and analyzed during MSM57.

Onboard analysis of concentrations of methane and molecular gas compositions

The gas samples were analyzed onboard for their molecular compositions and methane concentrations with a two-channel 6890N (Agilent Technologies) gas chromatograph (GC; Pape et al., 2010). Light hydrocarbons (C_1 to C_6) were separated, detected, and quantified with a capillary column connected to a Flame Ionization Detector, while permanent gases (O_2, N_2, CO_2) as well as C_1 and C_2 hydrocarbons were determined using a stainless steel column packed with mole sieve and coupled to a Thermal Conductivity Detector. Calibrations and performance checks of the analytical system were conducted regularly using commercial pure gas standards and gas mixtures. The coefficient of variation determined for the analytical procedure is lower than 2%.

Stable carbon and hydrogen isotopic compositions of methane ($\delta^{13}C\text{-}CH_4$, $\delta^{2}H\text{-}CH_4$) will be investigated at the MARUM for a detailed source assignment on samples characterized by elevated (> ca. 0.2 mM) methane concentrations.

13.3 Preliminary Results

13.3.1 Working Area Vestnesa Ridge

13.3.1.1 Ex situ Concentrations of Dissolved Methane

Reference sites

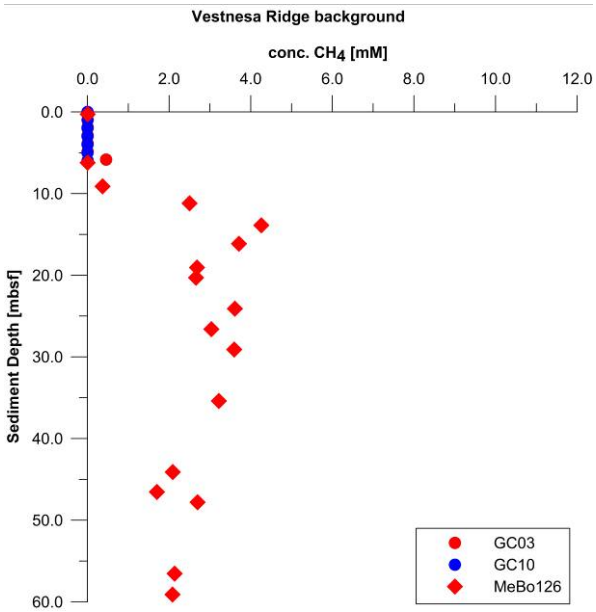

Fig. 80: *Ex-situ* concentration profiles of dissolved methane at reference sites distant to pockmarks.

At Vestnesa Ridge two reference sites distant to pockmarks were investigated for distributions of dissolved methane during MSM57. Gas hydrates were absent in cores recovered from both sites. At reference site GC-10 located between Lunde and Lomvi Pockmark methane was virtually absent in the uppermost six meters of sediment (Fig. 80), i.e. this gravity core did not penetrate the SMTZ. At reference site GC-3/MeBo126 located ca. 3.4 km SE of Lomvi Pockmark dissolved methane was present in sediments deeper than 5.84 mbsf. MeBo126 revealed a strong increase in concentrations of dissolved methane between 6.22 mbsf and 13.88 mbsf (4.3 mM) and below that interval slightly decreasing concentrations with increasing depth down to the deepest sample at 59.10 mbsf (2.1 mM). Corresponding shapes of profiles for dissolved methane and total alkalinity (Chapter 12) established for sedimentary sequences of GC-3 and MeBo126 suggest that the SMTZ at this site was positioned at about 8 mbsf.

Lunde Pockmark

Lunde Pockmark 'northeast' (non-hydrate-bearing)

Two gravity cores and cores from a MeBo hole established at the north-eastern edge of Lunde Pockmark were sampled for gas analysis. Gas hydrates were not observed in these cores. Both gravity cores, GC-1 and GC-2, showed methane enrichments below ca. 2.7 mbsf with maximum concentrations of ca. 11 mM in GC-1 at about 580 cmbsf (Fig. 81). In the accompanying core MeBo125 highest methane concentrations up to about 4.9 mM were found in the uppermost 8.8 meters of sediment. Below that depth methane concentrations varied between ca. 2.6 and 3.6 mM. Higher *ex-situ* concentrations of dissolved methane in samples collected with gravity cores compared to those prepared from MeBo cores might result from relatively faster accessibility to gravity cores and, thus, faster preservation of samples in general.

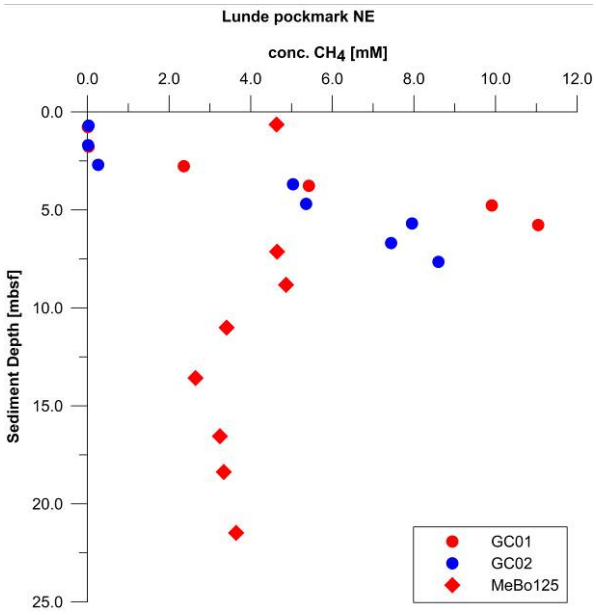

Fig. 81: *Ex-situ* concentration profiles of dissolved methane at the north-eastern edge of Lunde Pockmark.

Lunde Pockmark 'southeast' (hydrate-bearing)

Two gravity cores, GC-6 and GC-9, recovered from the south-eastern edge of Lunde Pockmark were sampled for gas analysis. Gas hydrates were found below ca. 260 cmbsf in GC-6 and below ca. 450 cmbsf in GC-9.

Both gravity cores showed an increase in methane concentrations up to about 9.8 mM (Fig. 82) between ca. 50 and 140 cmbsf and 70 cmbsf and 180 cmbsf, respectively. A local methane depletion was observed in the interval between about 190/210 cmbsf and 270/290 cmbsf, which in the case of GC-6 also comprised occurrences of gas hydrates. In GC-9, a significant enrichment in dissolved methane (up to ca. 20 mM) at 377 cmbsf was measured. Corresponding shapes of profiles for dissolved methane and total alkalinity (Chapter 12) established for cores GC-6 and GC-9 suggest that the SMTZ at this site was positioned at about 0.5 mbsf.

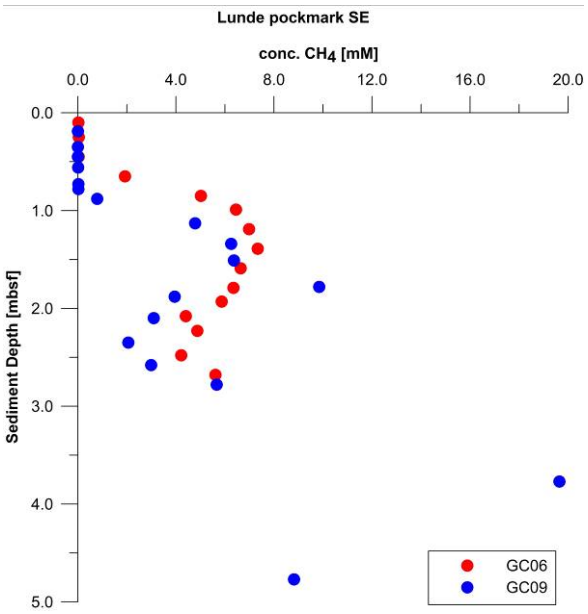

Fig. 82: *Ex-situ* concentration profiles of dissolved methane at pockmarks at the SE edge of Lunde Pockmark.

Lunde Pockmark 'southwest' (hydrocarbon seepage site, hydrate-bearing)

Cores/Sedimentary sequences from three MeBo holes, MeBo127, -128, -138 drilled at the south-western edge of Lunde Pockmark, where seafloor hydrocarbon discharge was observed, were sampled for gas analysis. At this site Gas hydrates were found at about 50 cmbsf (GC05), 80 cmbsf (MeBo127), and 650 cmbsf (MeBo128).

Due to poor core recovery with from holes MeBo127 and MeBo128 an *ex-situ* methane concentration profile in high resolution was only obtained for cores from hole MeBo138 (Fig. 83). Methane concentrations in these sediments varied strongly between 0.6 mM and 7.4 mM with several local concentration maxima and minima. Highest methane concentrations measured at 1.04 mbsf suggest a very shallow SMTZ at this site, which is also inferred from total alkalinity profiles (Chapter 12).

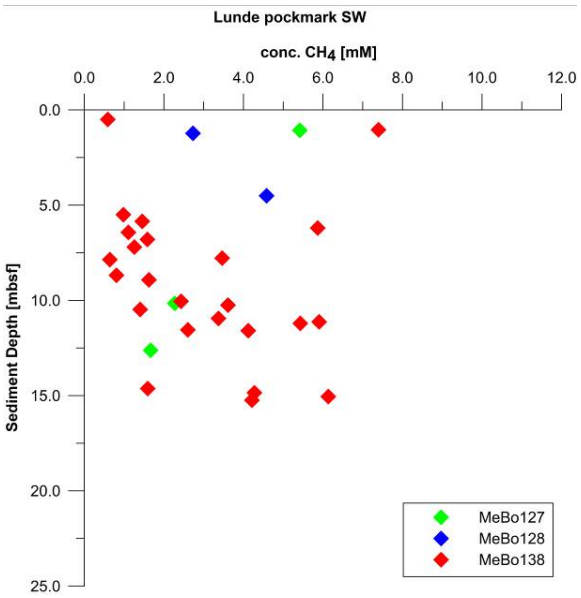

Fig. 83: *Ex-situ* concentration profiles of dissolved methane of MeBo holes drilled at the south-western edge of Lunde Pockmark.

Lomvi Pockmark

Three gravity cores from Lomvi Pockmark (GC-8, GC-11, GC-12) were sampled for methane concentrations. Gas hydrates were found at depths below ca. 150 cmbsf in GC-11 and ca. 240 cmbsf in GC-12.

In GC-11 from the north-eastern edge of Lomvi Pockmark concentrations of dissolved methane strongly increased from 0.03 mM at 50 cmbsf to 5.9 mM at 73 cmbsf (Fig. 84). Methane concentrations decreased with increasing depth down to ca. 130 cmbsf, while maximum concentrations of ca. 16 mM were measured close to the base of the gravity core (165 cmbsf), where hydrates were present. For core GC-12 recovered from a pit in the western sector of the pockmark, increasing methane concentrations with increasing sediment depth were observed between about 80 and 160 cmbsf (ca. 4 mM). A single peak with concentrations up to 14 mM was found at 170 cmbsf. Below that depth relatively uniform concentrations were observed, except for the deepest sample

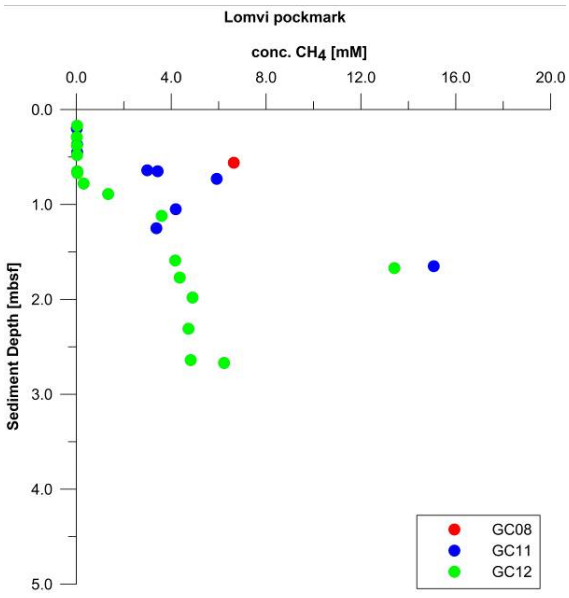

Fig. 84: *Ex-situ* concentration profiles of dissolved methane in gravity cores collected at Lomvi Pockmark.

13.3.1.2 Molecular Composition of Light Hydrocarbons at Vestnesa Ridge

Molecular compositions of light hydrocarbons at Vestnesa Ridge could be determined for several sites of investigation that are characterized by different intensities of gas flux from below, including sites of gas seepage and non-seepage sites considered as reference (Fig. 85). The sample set comprised different high-purity gas types including hydrate-bound gas, void gas and gas prepared from the MeBo pressure vessels (MDP).

The deepest gas sample from the reference site (MeBo126) that was collected at the base of the borehole with the MDP was characterized by a comparably low C_1/C_{2+} ratio suggesting prevalence of a thermogenic source. Remarkably, void gas samples from overlying sediments showed an increase in C_1/C_{2+} with decreasing depth between ca. 59.1 mbsf (C_1/C_{2+} ca. 480) and 48.2 mbsf (C_1/C_{2+} ca. 2.730), i.e. relative enrichments of methane compared to non-methane hydrocarbons. This data suggests microbial methane production in respectively shallow sediments at this site.

Void gas samples collected during MeBo125 from the northeastern edge of Lunde Pockmark, where neither seafloor gas seepage nor the presence of shallow hydrates were recorded, showed a similar trend in C_1/C_{2+} ratios in the interval between 18.1 and 15.7 mbsf, with higher relative proportions of methane in shallower sediments.

Gas prepared from hydrates present in shallow sediments at the southwestern and southeastern edges of Lunde Pockmark and at Lomvi Pockmark was characterized by low C_1/C_{2+} ratios (< 425) as well. The similarity in molecular hydrocarbon composition of gas in deep sediments at the reference site and that bound in shallow hydrates suggests that pockmark-associated hydrates are fuelled by thermogenic hydrocarbons from greater depth. Considering the abundant presence of non-methane hydrocarbons it might be assumed that hydrate structure sII is the dominant hydrate crystal structure at Lunde and Lomvi Pockmark.

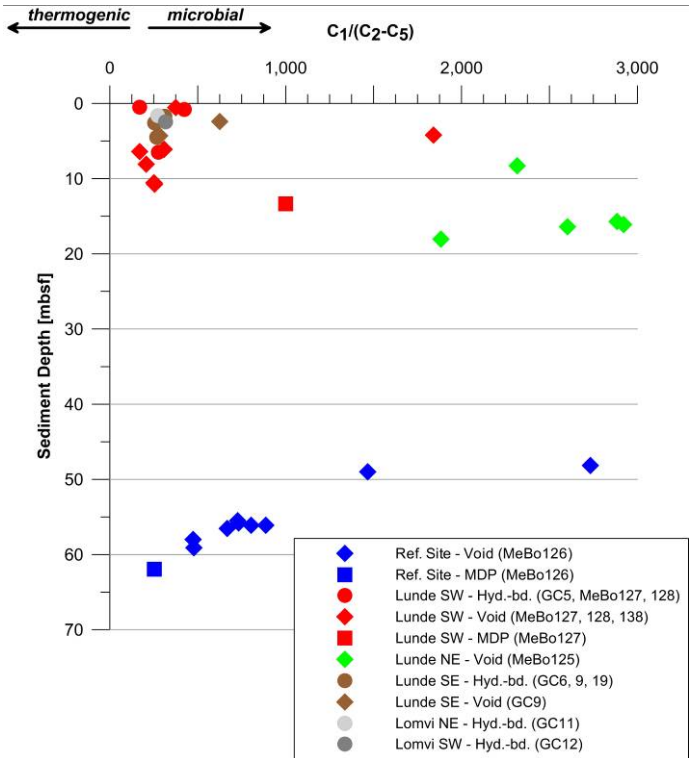

Fig. 85: Molecular hydrocarbon composition of the different gas types collected at the Vestnesa Ridge. Void = void gas; MDP = gas released during degassing of the MeBo pressure vessel; Hyd.-bd. = hydrate-bound gas.

13.3.2 Working Area Svyatogor Ridge

13.3.2.1 Ex situ Concentrations of Dissolved Methane

Vertical methane concentration profiles are available for three gravity cores collected at the Svyatogor Ridge (Fig. 86). While GC-18 and GC-21 that penetrated the uppermost 478 cm and 406 cm of sediment, respectively, did not show significant methane concentrations, slight methane enrichments were detected below approximately 240 cmbsf in GC-20 approaching 0.3 mM at 544 cmbsf.

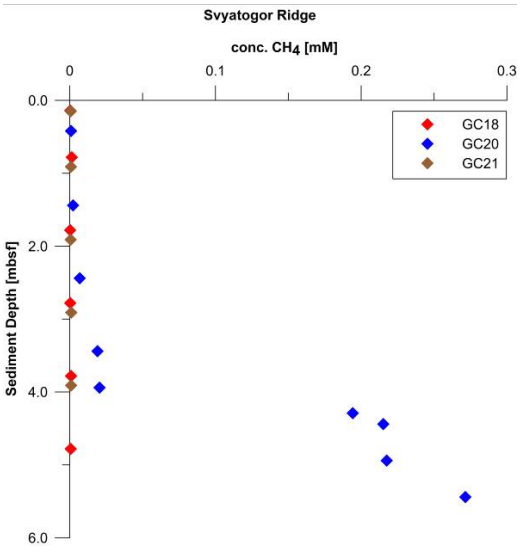

Fig. 86: *Ex-situ* concentration profiles of dissolved methane in gravity cores recovered from Svyatogor Ridge.

Due to only low-concentrated headspace samples from that region, precise molecular gas compositions could not be determined.

13.3.3 Working Area Upper Continental Slope off Svalbard

13.3.3.1 Ex situ Concentrations of Dissolved Methane

Reference site (436 m water depth)

The only core recovered from the reference site ('CM') at the continental margin off Svalbard, GC-13, showed negligible amounts of dissolved methane in the uppermost 200 cm (Fig. 87).

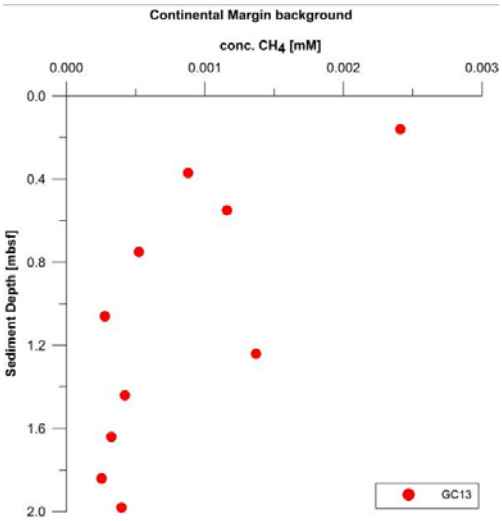

Fig. 87: *Ex-situ* concentration profiles of dissolved methane in GC13 recovered from the reference site off Svalbard.

Within the up-dip area of the GHSZ

Continental Margin Site 1 (404 m water depth)

The composite record of MeBo129-1and 129-2 showed a strong increase in *ex-situ* concentrations of dissolved methane between about 330 mbsf and 790 cmbsf (Fig. 88). In deeper sediments methane concentrations varied between 1.0 and 5.8 mM, with maximum concentrations detected at 11.3 mbsf. Because of the relatively dense sampling, several depth levels, where methane enrichments and depletions occurred could be documented.

Corresponding shapes of profiles for dissolved methane and total alkalinity (Chapter 12) established for MeBo129-1 and -2 suggest that the SMTZ at this site was positioned between about 3.0 and 5.5 mbsf.

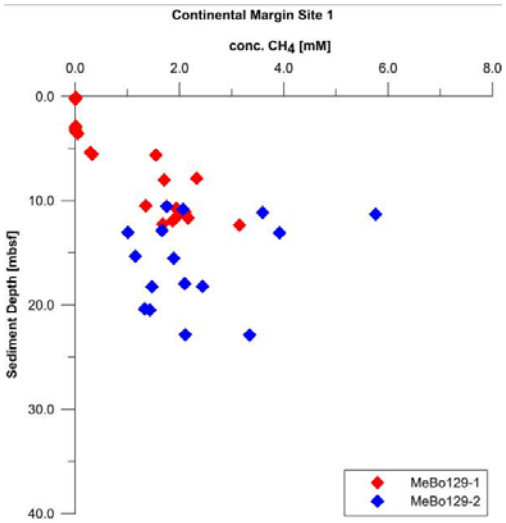

Fig. 88: *Ex-situ* concentration profiles of dissolved methane at MeBo sites from Continental Margin Site 1 off Svalbard.

Continental Margin Site 4 (405 m water depth)

Two gravity cores and two MeBo sites were sampled for gas analysis from Continental Margin Site 4 located only a few hundred meters NE of Continental Margin Site 1. Similar to observations at the latter site, methane was nearly absent in GC-14 and GC-15 that penetrated the uppermost 2.87 m and 1.26 m, respectively, as well as in the shallowest sample from MeBo130 (Fig. 89). Enrichments in dissolved methane between 3.1 and 3.7 mM were found at 12.96 mbsf at MeBo130 and at 20.30 mbsf and, remarkably, at 0.96 mbsf at MeBo132 .

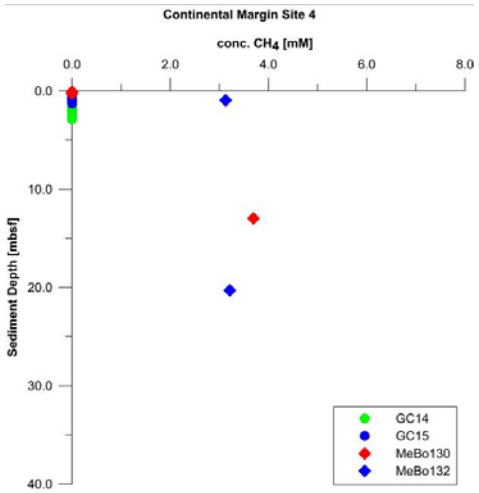

Fig. 89: *Ex-situ* concentration profiles of dissolved methane of sediments recovered from Continental Margin Site 4 off Svalbard.

Continental Margin Site 7 (402 m water depth)

A single MeBo hole, MeBo140, was recovered from Continental Margin Site 7, positioned in an area characterized by gas seepage in the NW sector of the working area. Elevated methane concentrations (> 0.7 mM) were measured throughout the hole from 2.9 to 26.5 mbsf (Fig. 90). Between 5.5 mbsf and ca. 20 mbsf concentrations scattered between 1.4 and 6.4 mM with peaks e.g. at 7.6 mbsf and 19.6 mbsf. Below that interval concentrations showed only slight variations around 2 mM.

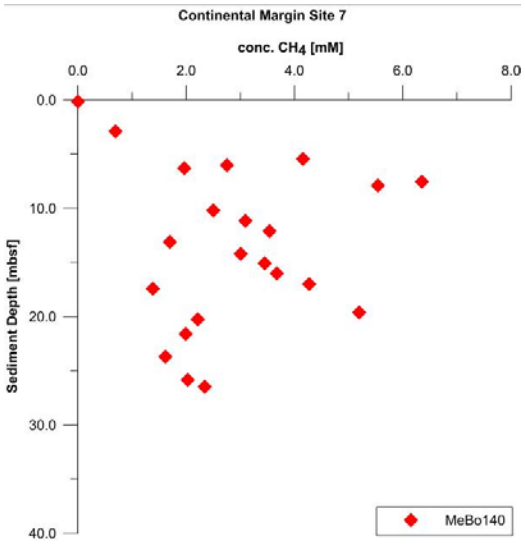

Fig. 90: *Ex-situ* concentration profiles of dissolved methane from Continental Margin Site 7 off Svalbard.

Continental Margin Site 5 (391 m water depth)

At continental Margin Site 5, located in an area characterized by strong seafloor gas seepage, one gravity core and three MeBo holes were sampled for gas analysis. GC-22, MeBo133 and 139 showed that the uppermost ca. 3.8 meters of sediment were nearly devoid of dissolved methane (Fig. 91). MeBo133 and MeBo139 additionally showed a steep methane concentration gradient between about 5.6 mbsf and 8.6 mbsf. Below that interval a trend of decreasing concentration with increasing depth becomes apparent although concentrations scattered remarkably. At several depths local enrichments of methane were observed (e.g., MeBo134: 12 mbsf, 21 mbsf; MeBo139: 18 to 19.5 mbsf).

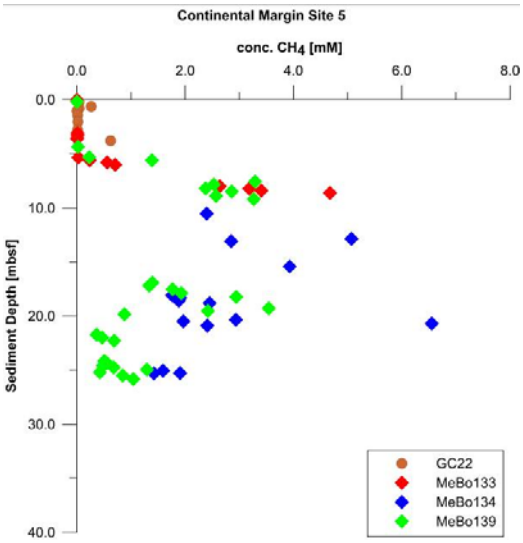

Fig. 91: *Ex-situ* concentration profiles of dissolved methane recovered from Continental Margin Site 5 off Svalbard.

Considering profiles of *ex-situ* methane concentrations and total alkalinity (Chapter 12) it might be assumed that the SMTZ at Continental Margin Site 5 is positioned at about 5 mbsf.

Above and below the up-dip limit of the GHSZ

Continental Margin Site 3 (445 m water depth)

At Continental Margin Site 3, located below the up-dip limit of the GHSZ, one gravity core and two MeBo holes were analyzed for distributions of methane (Fig. 92). While all three records indicated the virtual absence of methane in the uppermost ca. 10 meters of sediment, a steep increase in methane concentrations between about 10.5 mbsf and 15.4 mbsf was measured at MeBo135 and -136. Highest methane concentrations of about 6.5 mM were found at the base of MeBo136 at ca. 37 mbsf. At two specific depth levels, at about 23.3 and 25.9 mbsf, local methane enrichments separated by a conspicuous methane concentration minimum at ca. 25.8 mbsf were observed.

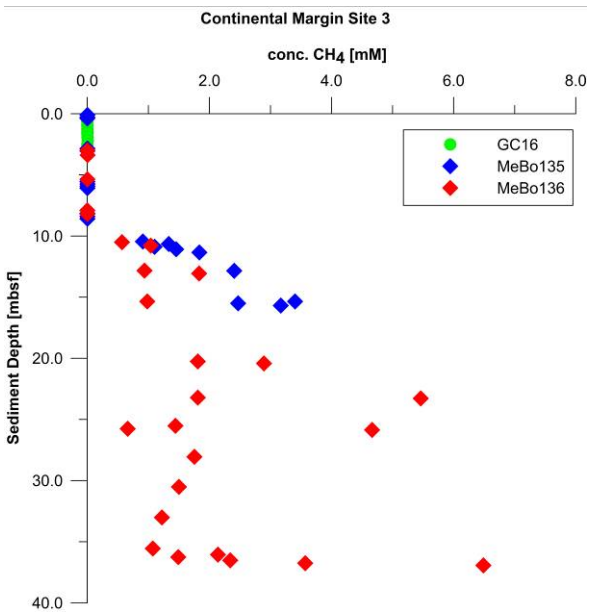

Fig. 92: *Ex-situ* concentration profiles of dissolved methane from Continental Margin Site 3 positioned below the up-dip limit of the GHSZ off Svalbard.

Profiles of methane concentrations and total alkalinity (Chapter 12) established for MeBo135 suggest that the SMTZ at Continental Margin Site 3 is positioned between about 8 and 10 mbsf.

Continental Margin Site 6 (340 m water depth)

One gravity core and a corresponding MeBo hole recovered from Continental Margin Site 6, that is located above the up-dip limit of the GHSZ, were analyzed for methane concentrations (Fig. 93). Methane was absent in the uppermost ca. 4 meters of sediment but approached a local concentration maximum at ca. 6.0 mbsf. A position of the SMTZ at about 4.0—4.5 mbsf at this site could also be inferred from the total alkalinity profile (Chapter 12). A second level of methane enrichment was found close to the base of MeBo137 at ca. 19.3 mbsf. However, due to poor core recovery methane distributions between 9 mbsf and 19 mbsf could not be determined.

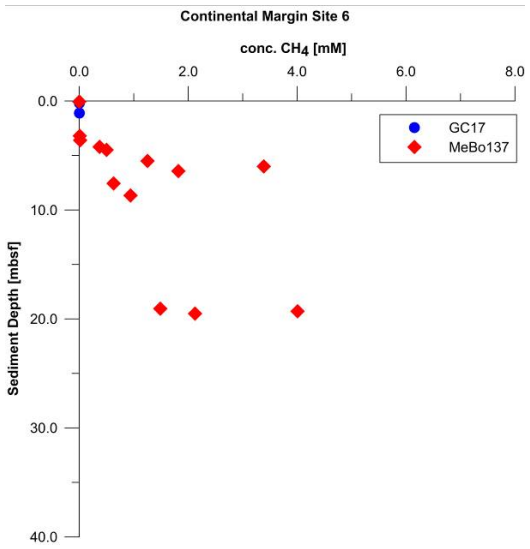

Fig. 93: *Ex-situ* concentration profiles of dissolved methane from Continental Margin Site 6 situated above the up-dip limit of the GHSZ off Svalbard.

13.3.3.2 Molecular Composition of Light Hydrocarbons at the Upper Continental Slope off Svalbard

At the continental slope off Svalbard only void gas samples from 1 and 7 were available for analysis of molecular hydrocarbon compositions (Fig. 94). While Site 1 is located in a non-seepage area, Site 7 is situated in an area where seafloor seepage was documented from several sites

C_1/C_{2+} ratios exceeding 4,000 at both Continental Margin Sites suggest the prevalence of microbial hydrocarbons. For samples from Site 7 a comparably great variability in C_1/C_{2+} ratios (4.400 to 13.500) was observed (see also Fig. 85).

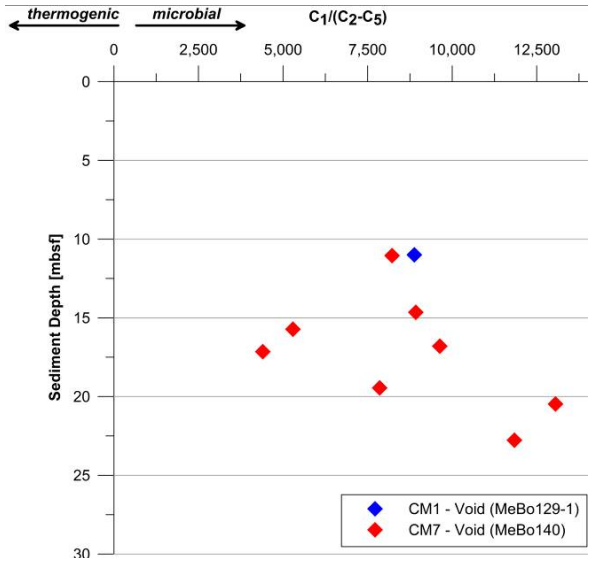

Fig. 94: Molecular hydrocarbon composition of void gas collected during MeBo stations 129-1 and 140 at Continental Margin Sites 1 and 7 at the upper continental slope off Svalbard.

14 MeBo Pressure Coring System – Design, Deployment and Initial Results

(D. Wunsch, T. Pape and MeBo-Team)

A pressure coring system has been developed for the recovery of pressure sediment cores with the sea floor drill rigs MeBo70 and MeBo200 within the German joint BMWi/BMBF-Project SUGAR. The so-called MDP (MeBo Druckkern Probennehmer) core barrel is deployed like a wire-line inner core barrel when quantitative sampling of gas from the sediments cored is required. The actual version of the MDP was tested for the first time during Cruise SO247 off New Zealand with MeBo200 in spring 2016 and technically improved then.

The main goal of the MDP deployments during MSM57-1 was to recover sediment cores under ambient pressure for subsequent determination of *in-situ* gas volumes through controlled gas release/pressure reduction. This information is typically lost when a core is recovered by conventional means.

14.1 Technical Description

The pressure core barrel consists of (a) a cutting shoe or drill bit cutting the sediment core with the required core diameter; (b) a piston using hydrostatic pressure to force the penetration of the core into the core barrel; (c) a pressure housing and a valve that closes after the coring process in order to maintain the *in-situ* pressure within the core barrel; (d) a core catcher that inhibits loss of sediment before the valve is closed; and (e) a latching device that ensures the correct position of the pressure core barrel within the MeBo drill string and activates closing of the valve when the core barrel is recovered by means of an overshot using the wireline method.

Compared to conventional MeBo core barrels the MDP comprises a number of activation and lifting mechanism required to achieve gas-tight sealing of the core inside the pressure vessel. This results in a comparably smaller length and diameter of the core (Table 25).

Table 25: Specifications of MDP when deployed on MeBo70 platform.

Specification	Unit
Outer Diameter	73 mm
Length	3.4 m
Core Diameter	45 mm
Liner Length (theoretical max. core length)	1.3 m
Operating Pressure	200 bar

The piston system supports core penetration into the liner and, thus, allows cutting a relatively small core compared to the borehole diameter. Its functionality is based on the pressure gradient between the pressure enclosed in the core barrel housing and the ambient pressure. This pressure gradient controls movement of the piston that forces the sediment core into the liner at the same rate as the core barrel is pushed into the sediment. Prior to the coring procedure the piston is locked mechanically until a touch sensor gets into contact with the sediment at the bottom of the drilled hole during the start of the coring process. Throughout the coring process the piston works like a syringe driven by the hydrostatic pressure at the depth of the borehole. A damping system positioned above the piston regulates the speed of the piston and also that of the incoming core.

After the core has been cut, the overshot is lowered into the drill string as in the case of a conventional MeBo core barrel. After the overshot has latched onto the MDP locking mechanism the wire-line is pulled. Before unlocking the MDP - and therefore enabling the recovery of the tool - the sealing mechanisms are activated by an additional axial lift in the upper part of the tool. Valves above and below the core are closed and the core is recovered under near in-situ conditions (Fig. 95).

Fig. 95: Sealed bottom valve of MDPs deployed at station GeoB21613-1 (cores 29P and 30P)**.**

14.2 MDP Deployments

Four MDPs have been prepared for deployment during leg MSM57-1. Two MDPs were deployed at station GeoB21613-1 (MeBo126) and one at station GeoB21616-1 (MeBo127). Due to operational reasons in relation to the drilling program, it has been decided at short notice to cancel a fourth MDP deployment. When recovered on deck all three pressure core barrels were found to be sealed pressure-tight, i.e. maintaining near *in-situ* pressure (Table 26). However, while GeoB21613-1 (core 30P) and GeoB21616-1 (core 6P) contained sediments, GeoB21613-1 (core 29P) only recovered pressurized fluids. The lack of sediments after the first coring run (GeoB21613-1, core 29P) was most likely due to a technical malfunction of the piston system, which could have been caused by repeatedly changing pressure regimes in the course of MeBo deployments at stations GeoB201604-1, GeoB201608-1 and GeoB21610-1 when usage of the MDP was eventually cancelled.

Table 26: MDP deployments during MSM57-1 and specifications of cored sections.

Station (core barrel)	Water Depth	Coring Depth	Recovery Pressure	Sediment recovery rate
	[m]	[mbsf]	[bar]	[%]
GeoB21613-1 (29P)	1200	60.3	113.8	0
GeoB21613-1 (30P)	1200	61.4	120.0	54
GeoB21616-1 (6P)	1210	12.8	107.1	49

The average sediment recovery rate of the three MDP deployments was 34.3%. This recovery rate refers to the actually recoverable sediment core that enters the liner when the core is drilled.

14.3 Initial Results from Core Degassing

In order to perform the core degassing procedure an assembly of gas-tight valves and ports (modified after Dickens et al., 2003; Paull et al., 1996) and a pressure sensor for continuous monitoring of the internal pressure were connected to the MDP pressure chamber. During Cruise MSM57-1 pressurized fluid (gas and water) was released incrementally from the pressure chamber into a gas-tight, scaled syringe for gas sub-sampling and determination of fluid volumes. Repeatedly, after release of a certain gas aliquot, gas sub-samples were taken and transferred into glass serum vials for analysis of molecular compositions.

Both sediment pressure cores obtained during MSM57-1 were degassed quantitatively while the evolution of pressure inside the MDP pressure chamber was recorded (Fig. 96; Table 27).

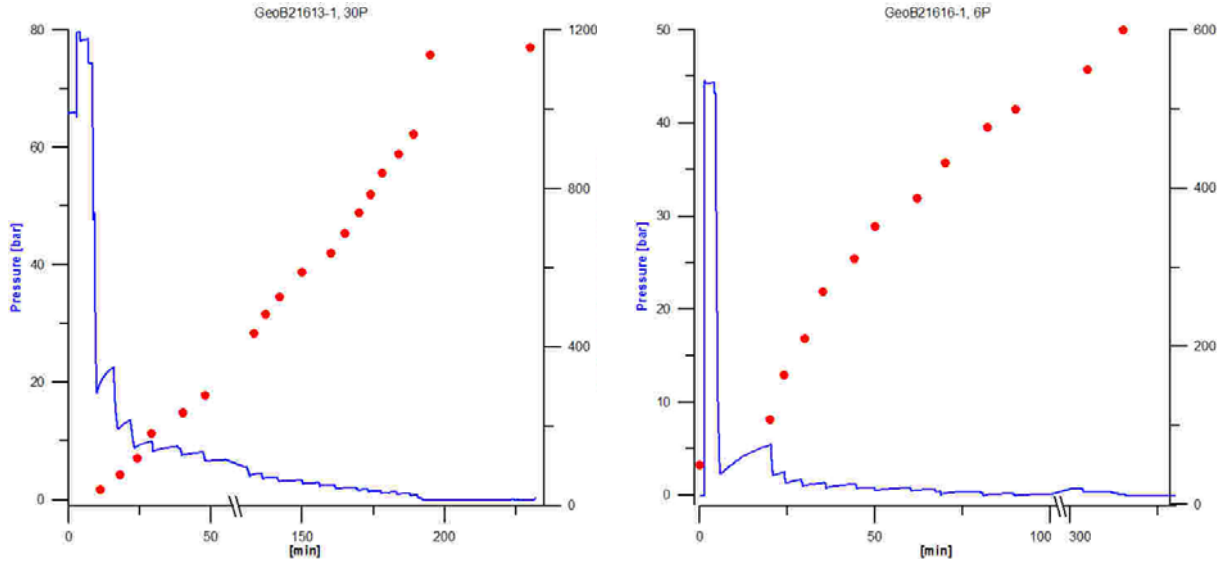

Fig. 96: Degassing characteristics of two pressurized sediment cores collected with MeBo70 during cruise MSM57-1. Left: Pressure and cumulative fluid volume released vs. time during degassing of core 30P from GeoB21613-1. Right: Pressure and cumulative fluid volume released vs. time during degassing of core 6P from GeoB21616-1.

During degassing of both sediment cores a slight saw tooth-like shape of the pressure-time profile was observed at the initial stage of incremental gas removal (time span ca. 5— 40 min). In earlier studies this pattern was referred to the presence of gas hydrates (e.g., Dickens et al., 2003). However, volumetric fluid to sediment ratios of ca. 1.3 and 1.0 (Table 27), respectively, are comparably low (e.g., Pape et al., 2011) and do not support the presence of hydrates in these cores. Instead, temporal small-scale pressure increases during core degassing may be attributed to sudden formation of migration pathways.

Table 27: Degassing characteristics of pressure cores (Total fluid volume = Total water volume + Total gas volume).

GeoB Station	Core no.	Core length [mm]	Core volume [L]	Total water volume released [L]	Total gas volume released [L]	Total fluid volume released [L]	Volumetric fluid – sediment ratio [L L^{-1}]
21613-1	30P	550	0.8747	0.646	0.511	1.157	1.323
21616-1	6P	390	0.6203	0.249	0.351	0.600	0.967

n.d. = not determined

Analysis of molecular composition demonstrated that gas released from core 30P nearly exclusively consisted of light hydrocarbons, which predominantly originate from thermocatalysis of organic matter in the deep subsurface (C_1/C_2+C_3 = 253; Whiticar, 1999; Table 28).

Table 28: Average molecular composition of gas released from pressure cores during MSM57-1 (100 mol-% = all volatiles stated).

GeoB Station	Core no.	CH_4	C_2H_6	C_3H_8	C_1/C_2+C_3	N_2	O_2/Ar
21613-1	30P	79.88	0.31	0.01	253.0	16.58	3.23
21616-1	6P	43.92	0.04	b.d.l	1,000.0	46.59	9.45

b.d.l. = below detection limit (< 0.005 mol-%)

In contrast, nitrogen, oxygen and argon were found in relatively high portions in the gas released from core 6P, GeoB21616-1. The presence of these components in the released gas was most likely due to atmospheric air that is generally required for the functionality of the MDP piston system and might be partially trapped inside the pressure chamber. Air is meant to be quantitatively released prior to the sealing of the pressure vessel but residual amounts may still remain inside. Nevertheless, molecular compositions clearly showed that microbial hydrocarbons ($C_1/(C_2+C_3)$ = 1,000) were prevailing at that depth. Void gas prepared from shallower sediments recovered with conventional MeBo barrels at both sites showed very similar molecular hydrocarbon compositions (see Chapter 13), thus, demonstrating the high quality of the gas obtained with the MDP. Preliminary calculations considering fluid volumes released during degassing, methane percentage in the fluid, and assumed sediment pore volume in the core suggest that the released methane exclusively resulted from exsolution caused by pressure reduction.

14.4 Post-Degassing Processing

Subsequent to degassing, i.e. when pressure inside the pressure chamber has dropped to atmospheric pressure, the core liner containing the depressurized sediment core was removed from the pressure chamber through the lower valve. A piston system was used to continuously push the core from the MDP liner into an external liner in a sliding motion. Finally, the core was processed like a conventional core (e.g. splitting, lithological description, line scan imaging, and storage).

14.5 Conclusions

During MSM57-1 the MDP pressure core barrel worked in the planned manner. Technical modifications made after an intensive assessment subsequent to Cruise SO247 have increased reliability and performance of the MDP significantly. Numerous processes have been prepared and implemented in order to simplify communication between MeBo operators and MDP engineer. Consistent and standardized documentation of coring runs during SO247 and MSM57-1 improved knowledge about the MDP functionality and increased the chances of establishing MDP as a reliable tool for advanced formation evaluation.

15 Data and Sample Storage and Availability

Metadata of the cruise as well as the station list will be submitted to PANGAEA immediately after the cruise. Sediment cores are stored at the MARUM GeoB Core Repository. Samples, data and other information of the cruise are available upon request to the chief scientist Gerhard Bohrmann. In addition, data (raw and processed) will be submitted to PANGAEA along with the scientific publication.

16 Acknowledgements

R/V MARIA S. MERIAN cruise MSM57 to Vestnesa Ridge and the upper continental margin off Svalbard was planned, coordinated, and carried out by MARUM "Center for Marine Environmental Sciences" at the University of Bremen in cooperation with CAGE, the excellence cluster and "Centre for Arctic Gas Hydrate, Environment and Climate" of the University of Tromsø and the GEOMAR, Helmholtz-Zentrum für Ozeanforschung, Kiel. The cruise was financed by the German Research Foundation (DFG) and funds from CAGE and Statoil. The shipping operator Reederei Briese Schiffahrts GmbH & Co KG provided technical support on the vessel. We would like to specially acknowledge the master of the vessel, Björn Maaß and his crew for their continued contribution to a pleasant and professional atmosphere aboard R/V MARIA S. MERIAN. Many thanks are going to the staff of the Control Station German Research Vessels. We also thank our logistic department at MARUM, specifically Götz Ruhland and Marcon Klann, the MARUM administration department and Angelika Rinkel and Greta Ohling for their help in preparing the cruise and support during the post-processing.

17 References

Ambrose, W.G., Panieri, G., Schneider, A., Plaza-Faverola, A., Carroll, M.L., Åström, E.K.L., Locke, W.L., Carroll, J., 2015. Bivalve shell horizons in seafloor pockmarks of the last glacial-interglacial transition: a thousand years of methane emissions in the Arctic Ocean. Geochemistry, Geophysics, Geosystems 16, 4108-4129.

Andreassen, K., Ødegaard, C.M., Rafaelsen, B., 2007b. Imprints of former ice streams, imaged and interpreted using industry three-dimensional seismic data from the south-western Barents Sea. In: Davies, R. J., Posamentier, H. W., Wood, L. J. & Cartwright, J. A. (eds) Seismic Geomorphology: Applications to Hydrocarbon Exploration and Production. Geological Society, London, Special Publications 277, 151–169.

Bahk, J.J., Kim, G.Y., Chun, J.H., Kim, J.H., Lee, J.Y., Ryu, B.J., Lee, J.H., Son, B.K., Collett, T.S., 2013. Characterization of gas hydrate reservoirs by integration of core and log data in the Ulleung Basin, East Sea. Mar Petrol Geol 47, 30-42.

Barnes, R.O. and Goldberg, E.D., 1976. Methane production and consumption in anaerobic marine sediments. Geology, 4(5): 297-300.

Bernard, B.B., Brooks, J.M. and Sackett, W.M., 1976. Natural gas seepage in the Gulf of Mexico. Earth and Planetary Science Letters, 31(1): 48-54.

Berndt, C., Feseker, T., Treude, T., Krastel, S., Liebetrau, V., Niemann, H., Bertics, V.J. Dumke, I., Dünnbier, K., Ferré, B., Graves, C., Gross, F. Hissmann, K., Hühnerbach, V., Krause, V., Lieser, K., Schauer, J., Steinle, L., 2014. Temporal constraints on hydrate-controlled methane seepage off Svalbard, Science, 343(6168), 284–287.

Bhatnagar, G., Chapman, W.G., Dickens, G.R., Dugan, B. and Hirasaki, G.J., 2008. Sulfate-methane transition as a proxy for average methane hydrate saturation in marine sediments. Geophysical Research Letters, 35: L03611.

Blum, P., 1997. Physical properties handbook: a guide to the shipboard measurement of physical properties of deep-sea cores. ODP Tech. Note, 26. Available online at: http://www-odp.tamu.edu/publications/tnotes/tn26/INDEX.HTM.

Borowski, W.S., Paull, C.K. and Ussler III, W., 1996. Marine pore-water sulfate profiles indicate in situ methane flux from underlying gas hydrate. Geology, 24(7): 655-658.

Bünz, S. 2013. R/V Helmer Hanssen Cruise No. 2013007 - Part I, University of Tromsø cruise report, Tromsø – Longyearbyen, 08-07-13 to 21-07-13 Institutt for Geologi, Univ. i Tromsø, Tromsø, 33 pp. DOI 10.3289/CR_ECO2_24445.

Bünz, S., Polyanov, S., Vadakkepuliyambatta, S., Consolaro, C., and Mienert, J., 2012. Active gas venting through hydrate-bearing sediments on the Vestnesa Ridge, offshore W-Svalbard: Marine Geology, 332, p. 189-197.

Caress D.W., Chayes D.N., 1995. Current Status of MB-System, Version 4.2, February 28, 1995. LamontDoherty Earth Observatory of Columbia University. (http://www.ldeo.columbia.edu/res/pi/MB-System/)

Chabert, A., Minshull, T.A., Westbrook, G.K., Berndt, Ch., Thatcher, K.E., Sarkar, S., 2011. Characterization of a stratigraphically constrained gas hydrate system along the western continental margin of Svalbard from ocean bottom seismometer data. J. Geophys. Res., 116, B12102.

Crane, K., Sundvor, E., Buck, R., Martinez, F., 1991. Rifting in the Northern Norwegian-Greenland Sea: Thermal tests if asymmetric sreading, J. of Geophys. Res., 96, B9, 14529-14550.

Davis, E.E., Villinger, H.W., 2006. Transient formation fluid pressures and temperatures in the Costa Rica forearc prism and subducting oceanic basement: CORK monitoring at ODP Sites 1253 and 1255. Earth and Planetary Science Letters, 245, 232-244.

Dickens, G.R., Schroeder, D., Hinrichs, K.-U., and the Leg 201 scientific party, 2003. The pressure core sampler (PCS) on ODP Leg 201: General operations and gas release, in: Proceedings of the Ocean Drilling Program, Initial Reports Volume 201, edited by: D'Hondt, S.L., Jørgensen, B.B., Miller, D.J., et al.

Eiken, O., and Hinz, K., 1993, Contourites in the Fram Strait: Sedimentary Geology, 82, p. 15-32.

Eldholm, O., Thiede, J., and Taylor, E., 1987. Evolution of the Norwegian continental margin: background and objectives. In Eldholm, O., Thiede, J., Taylor, E., et al., Proc. ODP, Init. Repts., 104: College Station, TX (Ocean Drilling Program), 5–25.

Engen, O., Faleide, J.I., Dyreng, T.K., 2008. Opening of the Fram Strait gateway: A review of plate tectonic constraints. Tectonophysics 450, 51-69.

Feseker, T., Foucher, J.P., Harmegnies, F., 2008. Fluid flow or mud eruptions? Sediment temperature distributions on Håkon Mosby mud volcano, SW Barents Sea slope. Marine Geology 247, 194-207.

Fisher, R.E., Sriskantharajah, S., Lowry, D., Lanoisellé, M., Fowler, C.M.R., James, R.H., Hermansen, O., Lund Myhre, C., Stohl, A., Greinert, J., Nisbet-Jones, P.B.R., Mienert, J., Nisbet, E.G., 2011. Arctic methane sources: Isotopic evidence for atmospheric inputs. Geophysical Research Letters 38, L21803.

Fohrmann, H., Backhaus, J.0., Blaume, F., Haupt, B.J., Kampf, J., Michels, K. ,Mienert, J., Posewang, J., Ritzrau, W., Rumohr, J., Weber, M., Woodgate, R., 2001. Modern ocean current-controlled sediment transport in the Greenland —Iceland—Norwegian (GIN) seas. In: Schafer, P., Ritzrau, W., Schlüter, M., Thiede, J. (Eds), The Northern North Atlantic: A Changing Environment. Springer-Verlag, Berlin, pp. 135-154.

Freudenthal, T. and Wefer, G., 2013. Drilling cores on the sea floor with the remote-controlled sea floor drilling rig MeBo. Geoscientific Instrumentation, Methods and Data Systems, 2(2). 329-337.

Harland, W.B., Geddes, I., Doubleday, P.A., 1997. Central western Spitsbergen. In: Harland, W.B., Anderson, L.M., Manasrah, D. (Eds), The Geology of Svalbard. Memoirs of the Geological Society of London, pp. 154-178.

Hoehler, T.M., Alperin, M.J., Albert, D.B. and Martens, C.S., 1994. Field and laboratory studies of methane oxidation in an anoxic marine sediment: Evidence for a methanogen-sulfate reducer consortium. Global Biogeochemical Cycles, 8(4): 451-463.

Hong, W.-L., Sauer, S., Panieri, G., Ambrose, W.G., James, R.H., Plaza-Faverola, A., Schneider, A., 2016. Removal of methane through hydrological, microbial, and geochemical processes in the shallow sediments of pockmarks along eastern Vestnesa Ridge (Svalbard). Limnology and Oceanography, n/a-n/a.

Howe, J.A., Shimmield, T.M., Harland, R.E.X., Eyles, N., 2008. Late Quaternary contourites and glaciomarine sedimentation in the Fram Strait. Sedimentology 55, 179-200.

Hustoft, S., Bünz, S., Mienert, J., Chand, S., 2009. Gas hydrate reservoir and active methane-venting province in sediments on < 20 Ma young oceanic crust in the Fram Strait, offshore NW-Svalbard. Earth and Planetary Science Letters 284, 12-24.

Hyndman, R.D., Davis, E.E., and Wright, J.A., 1979. The measurement of marine geothermal heat flow by a multi-penetration probe with digital acoustic telemetry and in situ thermal conductivity, Mar. Geophys. Res., 4, 181–205.

Jessen, S.P., Rasmussen, T.L., Nielsen, T., Solheim, A., 2010. A new Late Weichselian and Holocene marine chronology for the western Svalbard slope 30,000–0 cal years BP. Quaternary Science Reviews 29, 1301-1312.

Johnson, J.E., Mienert, J., Plaza-Faverola, A., Vadakkepuliyambatta, S., Knies, J., Bünz, S., Andreassen, K., and Ferré, B., 2015. Abiotic methane from ultraslow-spreading ridges can charge Arctic gas hydrates. Geology, v. 43, no.5, p. 371-374.

Jokat, W., Geissler, W., Voss, M., 2008. Basement structure of the north–western Yermak Plateau. Geophys. Res. Lett. 35.

Ker, S., Le Gonidec, Y., Marsset, B., Westbrook, G.K., Gibert, D., Minshull, T.A., 2014. Fine-scale gas distribution in marine sediments assessed from deep-towed seismic data. Geophysical Journal International, 196, 1466-1470.

Knies, J., Matthiessen, J., Vogt, Ch., Laberg, J.S., Hjelstuen, B.O., Smelror, M., Larsen, E., Andreassen, K., Eidvin, T., Vorren, T.O., 2009. The Plio-Pleistocene glaciation of the Barents Sea–Svalbard region: a new model based on revised chronostratigraphy. Quaternary Science Reviews, 28, 812-829.

Knies, J., Mattingsdal, R., Fabian, K., Grøsfjeld, K., Baranwal, S., Husum, K., De Schepper, S., Vogt, C., Andersen, N., Matthiessen, J., 2014. Effect of early Pliocene uplift on late Pliocene cooling in the Arctic-Atlantic gateway, Earth Planet. Sci. Lett., 387, 132–144.

KONGSBERG, 2016. EM1002 Maintenance Manual
https://www.km.kongsberg.com/ks/web/nokbg0397.nsf/AllWeb/BAE46B078F70A48AC1257F5B0036DCAE/$file/164894-EM1002-Complete-Maintenance-Manual.pdf?OpenElement

KONGSBERG EM122, 2013. Data Sheet
https://www.km.kongsberg.com/ks/web/nokbg0397.nsf/AllWeb/E016DF00EBFC2964C12571B1003F9DDA/$file/306105_em122_product_specification.pdf?OpenElement

Kopf, A.J., Freudenthal, T., Ratmeyer, V., Bergenthal, M., Lange, M., Fleischmann, T., Hammerschmidt, S., Seiter, C. and Wefer, G. (2015) Simple, affordable, and sustainable borehole observatories for complex monitoring objectives. Geoscientific Instrumentation, Methods and Data Systems, 4(1). 99-109.

Kopf, A.J., Belke-Brea, M., Ferentinos, G., Fleischmann, T., Geraga, M., Kufner, S., Schlenzek, S., Steiner, A., Tryon, M. Wiemer, G. 2012. Report and preliminary results of RV POSEIDON Cruise P429. MEDFLUIDS: Slope Stability, Mud volcanism, Faulting and Fluid Flow in the Eastern Mediterranean Sea (Cretan Sea, Mediterranean Ridge) and Ligurian Margin (Nice slope), Heraklion / Greece, 22.03.2012 - La Seyne sur Mer / France, 06.04.2012. Berichte, Fachbereich Geowissenschaften, Universität Bremen. urn:nbn:de:gbv:46-00103965-10.

Kopf, A., Hammerschmidt, S., Saffer, D.M., Lauer, R., Davis, E.E., LaBonte, A., Meldrum, R., Heesemann, M., Macdonald, R., Toczko, S., Wheat, C.G., Jannasch, H., Edwards, K., Haddad, A., Orcutt, B., Villinger, H., Araki, E., Kitada, K., Kimura, T., Kido, Y., 2011. The SmartPlug and GeniusPlug: Simple retrievable observatory systems for NanTroSEIZE borehole monitoring. Proc. IODP, vol 332, (21pp.).

Kowalik, Z., Marchenko, A., Brashnikov, D., Marchenko, N. 2015. Tidal currents in the western Svalbard Fjords, Oceanologia, 57, 318-327.

Kvenvolden, K.A., 1993. Gas Hydrates - Geological Perspective and Global Change. Rev Geophys 31, 173-187.

Kvenvolden, K.A. and McDonald, T.J., 1986. Organic geochemistry on the Joides Resolution: An Assay, Tech. Note. Ocean Drill. Prog., Texas A&M Univ, College Station, Tex., pp. 147 pp.

Landvik, J.Y., Ingólfsson, Ó., Mienert, J., Lehman, S.J., Solheim, A., Elverhøi, A., Ottesen, D.A.G., 2005. Rethinking Late Weichselian ice-sheet dynamics in coastal NW Svalbard. Boreas, 34, 7-24.

Landvik, J.Y., Bondevik, S., Elverhøi, A., Fjeldskaar, W., Mangerud, J., Salvigsen, O., Siegert, M.J., Svendsen, J.I., Vorren, T.O., 1998. The last glacial maximum of Svalbard and the Barents Sea area: ice sheet extent and configuration. Quat. Sci. Rev., 17, 43–75.

Lister, C.R.B., 1979. The pulse-probe method of conductivity measurement, Geophys. J. R. Astr. Soc., 57, 451–461.

Mattingsdal, R., Knies, J., Andreassen, K., Fabian, K., Husum, K., Grøsfjeld, K., de Schepper, S., 2014. A new 6 Myr stratigraphic framework for the Atlantic–Arctic gateway. Quaternary Science Reviews, 92, 170-178.

Mazzullo, J.M., Meyer, A., and Kidd, R.B., 1988. New sediment classification scheme for the Ocean Drilling Program. In Mazzullo, J., and Graham, A.G. (Eds.), Handbook for Shipboard Sedimentologists. ODP Tech. Note, 8:45-67.

Munsell Color Company, Inc., 1975. Munsell Soil Color Charts: Baltimore, MD (Munsell).

Novosel, I., Spence, G.D., Hyndman, R.D., 2005. Reduced Magnetization Produced by Increased Methane Flux at a Gas Hydrate Vent. Marine Geology, 216(4), 265–274.

Panieri, G., James, R.H., Camerlenghi, A., Westbrook, G.K., Consolaro, C., Cacho, I., Cesari, V., Cervera, C.S., 2014. Record of methane emissions from the West Svalbard continental margin during the last 23.500 yrs revealed by δ13C of benthic foraminifera. Global and Planetary Change 122, 151-160.

Pape, T., Bahr, A., Klapp, S.A., Abegg, F., Bohrmann, G., 2011. High-intensity gas seepage causes rafting of shallow gas hydrates in the southeastern Black Sea, Earth. Planet. Sci. Lett., 307, 35-46.

Pape, T., Bahr, A., Rethemeyer, J., Kessler, J.D., Sahling, H., Hinrichs, K.U., Klapp, S.A., Reeburgh, W.S. and Bohrmann, G., 2010. Molecular and isotopic partitioning of low-molecular weight hydrocarbons during migration and gas hydrate precipitation in deposits of a high-flux seepage site. Chemical Geology, 269(3-4): 350-363.

Paull, C.K., Matsumoto, R., Wallace, P.J., et al., 1996. Proceedings of the Ocean Drilling Program, Initial Reports: Explanatory Notes, Vol. 164. 2, pp. 13–41.

Petersen, C.J., Bünz, S., Hustoft, S., Mienert, J., Klaeschen, D., 2010. High-resolution P-Cable 3D seismic imaging of gas chimney structures in gas hydrated sediments of an Arctic sediment drift. Marine and Petroleum Geology 27, 1981-1994.

Plaza-Faverola, A., Bünz, S., Johnson, J.E., Chand, S., Knies, J., Mienert, J., Franek, P., 2015. Role of tectonic stress in seepage evolution along the gas hydrate charged Vestnesa Ridge, Fram Strait. Geophysical Research Letters, 42(3), 733–742.

Plaza-Faverola, A., Westbrook, G.K., Ker, S., Exley, R.J.K., Gailler, A., Minshull, T.A., Broto, K., 2010. Evidence from three-dimensional seismic tomography for a substantial accumulation of gas hydrate in a fluid-escape chimney in the Nyegga pockmark field, offshore Norway. Journal of Geophysical Research 115, B08104.

Posewang, J., Mienert, J., 1999. High-resolution seismic studies of gas hydrates west of Svalbard. Geo-Marine Letters 19, 150-156.

Rajan, A., Mienert, J., Bünz, S., 2012. Acoustic evidence for a gas migration and release system in Arctic glaciated continental margins offshore NW-Svalbard. Marine and Petroleum Geology, 32, 36-49.

Rebesco,M., Wåhlin, A., Laberg, J.S., Schauer, U., Beszczynska-Möller, A., Lucchi, R.G., Noormets, R., Accettella, D., Zarayskaya, Y., Diviacco, P., 2013. Quaternary contourite drifts of the Western Spitsbergen margin, Deep Sea Research Part I: Oceanographic Research Papers, 79, 156-168.

Reeburgh, W.S., 1976. Methane consumption in Cariaco Trench waters and sediments. Earth and Planetary Science Letters, 28(3): 337-344.

Riedel, M., Long, P.E., Collett, T.S., 2006. Estimates of in situ gas hydrate concentration from resistivity monitoring of gas hydrate bearing sediments during temperature equilibration. Mar Geol 227, 215-225.

Ritzmann, O., Jokat, W., 2003. Crustal structure of northwestern Svalbard and the adjacent Yermak Plateau: evidence for Oligocene detatchment tectonics and non-volcanic breakup. Geophysical Journal International 152, 139-159.

Ryu, B.J., Collett, T.S., Riedel, M., Kim, G.Y., Chun, J.H., Bahk, J.J., Lee, J.Y., Kim, J.H., Yoo, D.G., 2013. Scientific results of the Second Gas Hydrate Drilling Expedition in the Ulleung Basin (UBGH2). Mar Petrol Geol 47, 1-20.

Sahling, H., Römer, M., Pape, T., Bergès, B., dos Santos Fereirra, C., Boelmann, J., Geprägs, P., Tomczyk, M., Nowald, N., Dimmler, W., Schroedter, L., Glockzin, M., Bohrmann, G. 2014. Gas emissions at the continental margin west of Svalbard: mapping, sampling, and quantification. Biogeosciences 11, 6029-6046.

Sarkar, S., Berndt, Ch., Minshull, T.A., Westbrook, G.K., Klaeschen, D., Masson, D.G., Chabert, A., Thatcher, K.E., 2012. Seismic evidence for shallow gas-escape features associated with a retreating gas hydrate zone offshore west Svalbard. Journal of Geophysical Research: Solid Earth, 117, B09102.

Schauer, U. and Beszczynska-Möller, A. 2009. Problems with estimation and interpretation of oceanic heat transport conceptual remarks for the case of Fram Strait in the Arctic Ocean, Ocean Science 5, pp. 487-494.

Schoell, M., 1988. Multiple origins of methane in the earth. Chemical Geology, 71(1-3): 1-10.

Sloan, E.D., 2003. Fundamental principles and applications of natural gas hydrates. Nature, 426: 353-359.

Smith, A.J., Mienert, J., Bünz, S., Greinert, J., 2014. Thermogenic methane injection via bubble transport into the upper Arctic Ocean from the hydrate-charged Vestnesa Ridge, Svalbard. Geochemistry, Geophysics, Geosystems 15, 1945-1959.

Solheim, A., Faleide, J.I., Andersen, E.S., Elverhøi, A., Forsberg, C.F., Vanneste, K., Uenzelmann-Neben, G., Channell, J.E.T., 1998. Late Cenozoic Seismic Stratigraphy and Glacial Geological Development of the East Greenland and Svalbard–Barents Sea Continental Margins. Quaternary Science Reviews, 17, 155-184.

Spielhagen, R.F., Baumann, K.H., Erlenkeuser, H., Nowaczyk, N.R., Norgaard-Pedersen, N., Vogt, C., Weiel, D., 2004. Arctic Ocean deep-sea record of northern Eurasian ice sheet history. Quat. Sci. Rev., 23, 1455–1483.

Thatcher, K.E., Westbrook, G.K., Sarkar, S., Minshull, T.A., 2013. Methane release from warming-induced hydrate dissociation in the West Svalbard continental margin. Journal of Geophysical Research B, Solid Earth 118 (1), 22-38.

Thiede, J. & Myhre, A.M. 1996. Introduction to the North Atlantic-Arctic Gateway: plate tectonic-paleoceanographic history and significance. In: Thiede, J., Myhre, A.M., Firth, J.V., Johnson, G.L. & Ruddiman, W. (eds.), Proceedings of Ocean Drilling Program, Scientific Results 151: College Station, Tx (Ocean Drilling Program), 3-23.

Tréhu, A.M., Bohrmann, G., Rack, F.R., Torres, M.E., et al., 2003. Proc. ODP, Init. Repts., 204: College Station, TX (Ocean Drilling Program).

Tréhu, A.M., Long, P.E., Torres, M.E., Bohrmann, G., Rack, F.R., Collett, T.S., Goldberg, D.S., Milkov, A.V., Riedel, M., Schultheiss, P., 2004. Three-dimensional distribution of gas hydrate beneath

southern Hydrate Ridge: constraints from ODP Leg 204. Earth and Planetary Science Letters 222, 845-862.

Vanneste, M., Guidard, S., Mienert, J., 2005. Bottom-simulating reflections and geothermal gradients across the western Svalbard margin. Terra Nova 17, 510-516.

Vogt, P.R., Gardner, L., Crane, K. 1999. The Norwegian-Barents-Svalbard (NBS) continental margin: Introducing a natural laboratory of mass wasting, hydrates, and ascent of sediment, pore water, and methane. Geo Marine Letters 19, 2-21.

Vogt, P.R., Crane, K., Sundvor, E., Max, M.D., Pfirman, S.L., 1994. Methane-generated (Questionable) pockmarks on young, thickly sedimented oceanic-crust in the Arctic - Vestnesa-Ridge, Fram Strait. Geology 22, 255-258.

Vorren, T.O., Laberg, J.S., 1997. Trough mouth fans — Palaeoclimate and ice-sheet monitors. Quaternary Science Reviews 16, 865—881.

Vorren, T.O., Laberg, J.S., Blaume, F., Dowdeswell, J.A., Kenyon, N.H., Mienert, J., Rumohr, J., Werner, E, 1998. The Norwegian Greenland Sea continental margins: morphology and late Quaternary sedimentary processes and environment. Quaternary Science Reviews 17, 273—302.

Wei, J.G., Pape, T., Sultan, N., Colliat, J.L., Himmler, T., Ruffine, L., de Prunele, A., Dennielou, B., Garziglia, S., Marsset, T., Peters, C.A., Rabiu, A., Bohrmann, G., 2015. Gas hydrate distributions in sediments of pockmarks from the Nigerian margin - Results and interpretation from shallow drilling. Mar Petrol Geol 59, 359-370.

Westbrook, G.K., Thatcher, K.E., Rohling, E.J., Piotrowski, A.M., Pälike, H., Osborne, A.H.,Nisbet, E.G., Minshull, T.A., Lanoisellé, M., James, R.H., Hühnerbach, V., Green, D., Fisher, R.E., Crocker, A.J., Chabert, A., Bolton, C., Beszczynska-Möller, A., Berndt, C., Aquilina, A., 2009. Escape of methane gas from the seabed along the West Spitsbergen continental margin. Geophys. Res. Lett., 36, L15608.

Westbrook, G., Chand, S., Rossi, G., Long, C., Bunz, S., Camerlenghi, A., Carcione, J., Dean, S., Foucher, J.-P., Flueh, E., Gei, D., Haacke, R., Madrussani, G., Mienert, J., Minshull, T., Nouze, H., Peacock, S., Reston, T., Vanneste, M., Zillmer, M. 2008. Estimation of gas hydrate concentration from multi-component seismic data at sites on the continental margins of NW Svalbard and the Storegga region of Norway. Marine and Petroleum Geology 25, 744-758.

Whiticar, M.J., 1999. Carbon and hydrogen isotope systematics of bacterial formation and oxidation of methane. Chemical Geology, 161: 291-314.

18.1 Appendix 1: Station List

MSM57 Station List

						Time (UTC)						
Date 2016	MSM57	Instrument	GeoB	Location	Begin	on	off	End	Latitude	Longitude	Water depth	Remarks
(UTC)	St. No.		St. No.		(UTC)	seafloor	seafloor	(UTC)	N	E	(m)	
02.08.2016	613-1	GC-1	21601-1	Lunde Pockmark	16:25:00	16:54:00	16:54:00	17:18:59	79°00.504'	6°54.637'	1211	577 cm recov.
02.08.2016	614-1	TL01/SVP1	21602-1	outside Pockm.	17:47:00	18:16:00	18:36:40	19:04:00	79°01.036'	6°53.737'	1217	HeatFlow-Test station incl. SV-Probe
02.08.2016	615-1	TL02-1	21603-1	outside Pockm.	20:35:00	21:08:36	21:26:46	-	79°00.577'	6°53.936'	1210	Posidonia position
02.08.2016	615-2	TL02-2	21603-2	outside Pockm.	-	21:52:28	22:02:40	-	79°00.528'	6°54.151'	1213	Posidonia position
02.08.2016	615-3	TL02-3	21603-3	Lunde Pockmark	-	22:39:18	22:58:48	-	79°00.502'	6°54.614'	1212	Posidonia position
02.08.2016	615-4	TL02-4	21603-4	outside Pockm.	-	23:40:48	23:49:42	-	79°00.397'	6°54.864'	1208	Posidonia failed *
03.08.2016	615-5	TL02-5	21603-5	outside Pockm.	-	00:17:55	00:34:50	-	79°00.339'	6°55.170'	1207	Posidonia failed *
03.08.2016	615-6	TL02-6	21603-6	Lomvi Pockmark	-	01:01:40	01:12:05	-	79°00.277'	6°55.538'	1210	Posidonia failed *
03.08.2016	615-7	TL02-7	21603-7	Lomvi Pockmark	-	01:39:35	01:58:02	-	79°00.219'	6°55.610'	1211	Posidonia failed *
03.08.2016	615-8	TL02-8	21603-8	Lomvi Pockmark	-	02:21:48	02:39:11	03:06:59	79°00.180'	6°55.778'	1210	Posidonia failed *
03.08.2016	616-1	MeBo123	21604-1	Lunde Pockmark	04:15:00	06:06:00	09:32:00	11:15:59	79°00.503'	6°54.625'	1213	drill.depth = 2.80 mbsf; recov = 1.0 m
03.08.2016	617-1	GC-2	21605-1	Lunde Pockmark	11:44:00	12:11:00	12:12:00	12:45:59	79°00.506'	6°54.613'	1214	765 cm recov., Posidonia
03.08.2016	618-1	GC-3	21606-1	Reference Station	14:14:00	14:30:20	14:39:00	15:08:59	78°59.806'	6°57.808'	1200	584 cm recov., Posidonia
03.08.2016	619-1	TL03-1	21607-1	outside Pockm.	20:52:00	21:29:50	21:40:50	-	79°00.014'	6°56.901'	1210	Posidonia failed *
03.08.2016	619-2	TL03-2	21607-2	outside Pockm.	-	22:05:45	22:14:34	-	79°00.070'	6°56.562'	1210	Posidonia failed *
03.08.2016	619-3	TL03-3	21607-3	outside Pockm.	-	22:49:20	22:58:15	-	78°59.993'	6°55.651'	1214	Posidonia failed *
03.08.2016	619-4	TL03-4	21607-4	Lomvi Pockmark	-	23:32:33	23:49:19	-	79°00.114'	6°55.674'	1219	Posidonia failed *
04.08.2016	619-5	TL03-5	21607-5	Lomvi Pockmark	-	00:20:39	00:37:36	-	79°00.148'	6°56.008'	1222	Posidonia failed *
04.08.2016	619-6	TL03-6	21607-6	outside Pockm.	-	01:03:40	01:20:55	-	79°00.216'	6°56.146'	1226	Posidonia failed *
04.08.2016	619-7	TL03-7	21607-7	outside Pockm.	-	01:53:30	02:04:00	-	79°00.311'	6°56.895'	1227	Posidonia failed *
04.08.2016	619-8	TL03-8	21607-8	outside Pockm.	-	02:22:00	02:31:50	02:56:59	79°00.372'	6°57.138'	1232	Posidonia failed * new position
04.08.2016	620-1	MeBo124	21608-1	Lunde Pockmark	04:11:00	06:00:00	09:38:00	10:46:00	79°00.502'	6°54.615'	1212	drill. depth = 1.83 mbsf; recov.= 0.97m
04.08.2016	621-1	GC-4	21609-1	Lunde Pockmark	12:48:00	13:22:00	13:23:00	13:48:59	79°00.413'	6°54.269'	1212	Posidonia, reocv. 535 cm, plastic bag
04.08.2016	621-2	GC-5	21609-2	Lunde Pockmark	14:28:00	14:50:00	14:51:00	15:16:59	79°00.403'	6°54.253'	1212	Posidonia, GH, recov. 60 cm, plastic foil
04.08.2016	622-1	MeBo125	21610-1	Lunde Pockmark	15:36:00	17:23:00	04:27:00	05:36:59	79°00.503'	6°54.621'	1212	recov. = 9.06 m
05.08.2016	623-1	TL04-1	21611-1	Lunde Pockmark	06:10:23	06:41:00	06:57:55	-	79°00.570'	6°55.025'	1221	Posidonia Position; Heat Pulse
05.08.2016	623-2	TL04-2	21611-2	outside Pockm.	-	07:32:30	07:49:42	-	79°00.497'	6°54.433'	1213	Posidonia Position; Heat Pulse
05.08.2016	623-3	TL04-3	21611-3	Lunde Pockmark	-	08:05:53	08:15:12	-	79°00.474'	6°54.590'	1213	Posidonia Position
05.08.2016	623-4	TL04-4	21611-4	Lunde Pockmark	-	08:30:33	08:41:35	-	79°00.445'	6°54.607'	1213	Posidonia Position
05.08.2016	623-5	TL04-5	21611-5	Lunde Pockmark	-	09:05:00	09:23:00	-	79°00.446'	6°54.280'	1210	Posidonia Position; Heat Pulse
05.08.2016	623-6	TL04-6	21611-6	Lunde Pockmark	-	09:44:30	10:01:35	-	79°00.424'	6°53.896'	1208	Posidonia Position; Heat Pulse
05.08.2016	623-7	TL04-7	21611-7	outside Pockm.	-	10:22:53	10:31:55	-	79°00.442'	6°53.645'	1206	Posidonia Position
05.08.2016	623-8	TL04-8	21611-8	Lunde Pockmark	-	10:57:08	11:06:00	-	79°00.493'	6°53.929'	1207	Posidonia Position
05.08.2016	623-9	TL04-9	21611-9	Lunde Pockmark	-	11:29:16	11:38:20	-	79°00.483'	6°53.306'	1212	Posidonia Position
05.08.2016	623-10	TL04-10	21611-10	Lunde Pockmark	-	12:13:55	12:30:15	13:10:00	79°00.380'	6°54.602'	1210	Posidonia Position; Heat Pulse
05.08.2016	624-1	GC-6	21612-1	Lunde Pockmark	13:38:00	13:53:00	13:55:00	14:25:00	79°00.4266'	6°54.673'	1213	Posidonia pos.; pit pos.; GH, 273 cm recov.
05.08.2016	625-1	MeBo126	21613-1	Background	14:49:00	17:09:00	06:44:00	08:01:59	78°59.806'	6°57.808'	1198	drill. depth = 62.50 mbsf; recov. 26.42 m
07.08.2016	626-1	TL05-1	21614-1	MeBo126 site	09:15:00	09:41:48	13:25:56	10:39:59	78°59.806'	6°57.808'	1207	without Posidonia
07.08.2016	627-1	TL06-1	21615-1	NW Vestnesa Ridge	12:28:00	13:08:28	14:23:47	-	79°06.966'	6°08.728'	1233	Posidonia Position; Heat Pulse

Appendix 1: Station List continued

MSM57 Station List												
					Time (UTC)							
Date 2016 (UTC)	MSM57 St. No.	Instrument	GeoB St. No.	Location	Begin (UTC)	on seafloor	off seafloor	End (UTC)	Latitude N	Longitude E	Water depth (m)	Remarks
07.08.2016	627-2	TL06-2	21615-2	NW Vestnesa Ridge	-	14:13:36	15:21:10	-	79°06.933'	6°09.690'	1235	Posidonia Position
07.08.2016	627-3	TL06-3	21615-3	NW Vestnesa Ridge	-	15:03:36	16:21:10	-	79°06.895'	6°10.720'	1248	Posidonia Position; Heat Pulse
07.08.2016	627-4	TL06-4	21615-4	NW Vestnesa Ridge	-	16:04:55	16:20:48	-	79°06.854'	6°11.847'	1228	Posidonia Position; Heat Pulse
07.08.2016	627-5	TL06-5	21615-5	NW Vestnesa Ridge	-	16:55:05	17:05:20	17:36:59	79°06.806'	6°12.832'	1230	without Posidonia
07.08.2016	628-1	MeBo127	21616-1	Lunde Pockmark	21:16:00	01:17:00	17:32:00	18:53:00	79°00.418'	6°54.245'	1210	drill depth = 13.90m; recov. = 13.90 m, CORK
08.08.2016	629-1	GC-7	21617-1	Lunde Pockmark	19:38:00	19:59:00	20:28:00		79°00.205'	6°55.867'	1212	Recovery 92cm, core bent, Posidonia pos. GH
08.08.2016	629-2	GC-8	21617-2	Lunde Pockmark	21:02:00	21:22:00	21:49:00		79°00.201'	6°55.870'	1210	Posidonia Position,recov. = 56cm
08.08.2016	630-1	TL07-1	21618-1	Lunde & NoName Pockma	22:35:00	23:06:02	23:23:22	-	79°00.421'	6°54.245'	1214	Posidonia Position, HP
08.08.2016	630-2	TL07-2	21618-2	Lunde & NoName Pockma	-	23:39:54	23:57:08	-	79°00.416'	6°54.248'	1214	Posidonia Position, HP
09.08.2016	630-3	TL07-3	21618-3	Lunde & NoName Pockma	-	00:11:09	00:27:40	-	79°00.407'	6°54.231'	1217	Posidonia Position, HP
09.08.2016	630-4	TL07-4	21618-4	Lunde & NoName Pockma	-	00:42:52	00:59:40	-	79°00.393'	6°54.191'	1215	Posidonia Position, HP
09.08.2016	630-5	TL07-5	21618-5	Lunde & NoName Pockma	-	01:16:10	01:21:55	-	79'00.379'	6°54.158'	1212	Posidonia, HP; tilt of 55° prob. no penetration
09.08.2016	630-6	TL07-6	21618-6	Lunde & NoName Pockma	-	02:32:30	02:43:50	-	79°00.346'	6°54.094'	1210	Posidonia Position, HP
09.08.2016	630-7	TL07-7	21618-7	Lunde & NoName Pockma	-	03:03:50	03:12:40	-	79°00.316'	6°54.074'	1210	Posidonia Position, HP
09.08.2016	630-8	TL07-8	21618-8	Lunde & NoName Pockma	-	03:48:28	04:05:16	-	79°00.277'	6°54.725'	1208	Posidonia Position, HP
09.08.2016	630-9	TL07-9	21618-9	Lunde & NoName Pockma	-	04:23:37	04:40:05	-	79°00.344'	6°54.666'	1210	Posidonia Position, HP
09.08.2016	630-10	TL07-10	21618-10	Lunde & NoName Pockma	-	05:00:28	05:18:40	-	79°00.361'	6°54.574'	1211	Posidonia Position, HP
09.08.2016	630-11	TL07-11	21618-11	Lunde & NoName Pockma	-	05:39:17	05:57:00	-	79°00.407'	6°54.593'	1217	Posidonia Position, HP
09.08.2016	630-12	TL07-12	21618-12	Lunde & NoName Pockma	-	06:16:10	06:35:15	-	79°00.435'	6°54.532'	1214	Posidonia Position, HP
09.08.2016	630-13	TL07-13	21618-13	Lunde & NoName Pockma	-	06:50:39	07:00:00	-	79°00.475'	6°54.524'	1216	Posidonia Position
09.08.2016	630-14	TL07-14	21618-14	Lunde & NoName Pockma	-	07:17:13	07:27:00	-	79°00.496'	6°54.351'	1216	Posidonia Position
09.08.2016	630-15	TL07-15	21618-15	Lunde & NoName Pockma	-	07:54:56	08:10:20	-	79°00.610'	6°53.736'	1212	Posidonia Position, HP
09.08.2016	630-16	TL07-16	21618-16	Lunde & NoName Pockma	-	08:35:45	08:51:48	09:24:00	79°00.674'	6°53.356'	1212	Posidonia Position, HP
09.08.2016	631-1	GC-9	21619-1	Lunde Pockmark	09:56:00	10:21:00	10:22:00	10:52:04	79°00.427'	6°54.677'	1213	Posidonia, like GC-6, GH, recov. = 478 cm
09.08.2016	632-1	GC-10	21620-1	at TL02-5 site	12:09:00	12:32:00	12:33:00	13:06:00	79°00.339'	6°55.170'	1207	no Posidonia,recov. = 596cm
10.08.2016	633-1	MeBo128	21621-1	Lunde Pockmark	12:50:00	14:49:00	20:09:00	21:20:59	79°00.430'	6°54.255'	1211	drill depth = 7.75m, recov = 4.47m
10.08.2016	634-1	TL08-1	21622-1	NoName Pockmark	22:49:00	23:24:14	23.41.20	-	79°01.087'	6°49.855'	1208	Posidonia Position, HP
11.08.2016	634-2	TL08-2	21622-2	NoName Pockmark	-	00:10:12	00.27.08	-	79°01.155'	6°50.041'	1208	Posidonia Position, HP
11.08.2016	634-3	TL08-3	21622-3	NoName Pockmark	-	00:53:30	01.09.18	-	79°01.098'	6°50.481'	1217	Posidonia Position, HP
11.08.2016	634-4	TL08-4	21622-4	NoName Pockmark	-	01:27:58	01.44.30	-	79°01.074'	6°50.637'	1218	Posidonia Position, HP
11.08.2016	634-5	TL08-5	21622-5	NoName Pockmark	-	02:03:36	02.19.45	-	79°01.059'	6°50.949'	1214	Posidonia Position, HP
11.08.2016	634-6	TL08-6	21622-6	NoName Pockmark	-	02:33:34	02.42.25	-	79°01.038'	6°51.129'	1215	Posidonia Position
11.08.2016	634-7	TL08-7	21622-7	NoName Pockmark	-	03:01:20	03.17.55	-	79°00.985'	6°51.258'	1216	Posidonia Position, HP
11.08.2016	634-8	TL08-8	21622-8	NoName Pockmark	-	03:33:28	03.50.05	-	79°00.944'	6°51.492'	1214	Posidonia Position, HP
11.08.2016	634-9	TL08-9	21622-9	NoName Pockmark	-	04:06:55	04.23.10	-	79°00.875'	6°51.533'	1215	Posidonia Position, HP
11.08.2016	634-10	TL08-10	21622-10	NoName Pockmark	-	04:36:20	04.45.30	-	79°00.855'	6°51.802'	1212	Posidonia Position
11.08.2016	634-11	TL08-11	21622-11	NoName Pockmark	-	05:04:58	05.21.12	-	79°00.828'	6°52.223'	1210	Posidonia Position, HP
11.08.2016	634-12	TL08-12	21622-12	NoName Pockmark	-	05:51:50	06.07.55	-	79°00.744'	6°53.085'	1212	Posidonia Position, HP
11.08.2016	634-13	TL08-13	21622-13	NoName Pockmark	-	06:22:11	06.32.06	-	79°00.696'	6°53.176'	122	Posidonia Position

Appendix 1: Station List continued

MSM57 Station List												
						Time (UTC)						
Date 2016	MSM57	Instrument	GeoB	Location	Begin	on	off	End	Latitude	Longitude	Water depth	Remarks
(UTC)	St. No.		St. No.		(UTC)	seafloor	seafloor	(UTC)	N	E	(m)	
11.08.2016	634-14	TL08-14	21622-14	NoName Pockmark	-	07:12:08	07.31.20	-	79°00.592'	6°54.294'	1225	Posidonia Position, HP
11.08.2016	634-15	TL08-15	21622-15	NoName Pockmark	-	07:50:22	08.00.27	-	79°00.599'	6°54.700'	1222	Posidonia Position
11.08.2016	634-16	TL08-16	21622-16	NoName Pockmark	-	08:18:39	08.36.45	09:05:59	79°00.558'	6°54.821'	1220	Posidonia Position, HP
11.08.2016	635-1	GC-11	21623-1	Lomvi Pockmark	09:31:00	09:56:00	09:57:00	10:26:59	79°00.212'	6°55.950'	1216	Posidonia Position, GH,recov.= 165 cm
11.08.2016	636-1	GC-12	21624-1	Lomvi Pockmark	11:08:00	11:31:00	11:32:00	12:03:59	79°00.171'	6°55.498'	1217	Posidonia Position, GH, recov.= 267 cm
11.08.2016	637-1	S-CORK	21625-1	Lunde Pockmark	12:31:00	13:18:00	-	13:48:59	79°00.380'	6°54.297'	1211	Posidonia Position
14.08.2016	638-1	MeBo129-1	21626-1	Cont.-Margin Site 1	16:23:00	18:15:00	11:20:00	-	78°33.212'	09°27.070'	404	drill depth = 22.9 m, recov.= 3.95 m
15.08.2016	638-2	MeBo129-2	21626-2	Cont.-Margin Site 1	-	16:16:00	06:38:00	07:25:59	78°33.212'	09°27.070'	404	drill depth = 2.53 m, recov.= 2.54 m
16.08.2016	639-1	SVP-1	21627-1	Cont. Margin	07:59:00	08:08:00	-	08:19:59	78°33.620'	09°20.270'	460	AML-Probe released with the rope
16.08.2016	640-1	SVP-2	21628-1	North of Svyatogor Ridge	13:27:00	14:03:00	-	14:46:59	78°38.060'	05°41.920'	2221	AML-Probe released with the rope
16.08.2016	641-1	TL09-1	21629-1	Svyatogor Ridge	20:35:00	21:08:00	21:26:50	-	78°21.206'	05°40.542'	1640	Posidonia Position, HP
16.08.2016	641-2	TL09-2	21629-2	Svyatogor Ridge	-	21:59:47	22:17:15	-	78°21.258'	05°41.440'	1619	Posidonia Position, HP?
16.08.2016	641-3	TL09-3	21629-3	Svyatogor Ridge	-	22:52:18	23:08:40	-	78°21.324'	05°42.134'	1630	Posidonia Position, HP?
16.08.2016	641-4	TL09-4	21629-4	Svyatogor Ridge	-	23:28:00	23:44:28	-	78°21.337'	05°42.479'	1628	Posidonia Position, HP
17.08.2016	641-5	TL09-5	21629-5	Svyatogor Ridge	-	00:18:15	00:34:50	-	78°21.372'	05°43.434'	1615	Posidonia Position, HP
17.08.2016	641-6	TL09-6	21629-6	Svyatogor Ridge	-	01:03:48	01:20:40	-	78°21.439'	05°44.178'	1654	Posidonia Position, HP
17.08.2016	641-7	TL09-7	21629-7	Svyatogor Ridge	-	02:05:55	02:14:30	-	78°21.120'	05°44.916'	1651	Posidonia Position
17.08.2016	641-8	TL09-8	21629-8	Svyatogor Ridge	-	03:02:48	03:18:04	-	78°20.813'	05°45.382'	1647	Posidonia Position, HP
17.08.2016	641-9	TL09-9	21629-9	Svyatogor Ridge	-	03:57:53	04:13:55	-	78°20.709'	05°44.346'	1606	Posidonia Position, HP
17.08.2016	641-10	TL09-10	21629-10	Svyatogor Ridge	-	04:48:57	05:05:12	-	78°20.600'	05°43.473'	1618	Posidonia Position, HP
17.08.2016	641-11	TL09-11	21629-11	Svyatogor Ridge	-	05:48:50	06:05:40	-	78°20.473'	05°42.270'	1611	Posidonia Position, HP
17.08.2016	641-12	TL09-12	21629-12	Svyatogor Ridge	-	06:38:40	06:55:10	-	78°20.318'	05°42.559'	1607	Posidonia Position, HP
17.08.2016	641-13	TL09-13	21629-13	Svyatogor Ridge	-	07:33:40	07:20:21	-	78°20.039'	05°42.882'	1630	Posidonia Position, HP
17.08.2016	641-14	TL09-14	21629-14	Svyatogor Ridge	-	08:25:03	08:42:02	-	78°20.130'	05°43.649'	1611	Posidonia Position, HP
17.08.2016	641-15	TL09-15	21629-15	Svyatogor Ridge	-	09:15:48	09:31:51	-	78°20.249'	05°44.380'	1607	Posidonia Position, HP
17.08.2016	641-16	TL09-16	21629-16	Svyatogor Ridge	-	10:05:49	10:20:19	11:00:59	78°20.387'	05°45.147'	1607	Posidonia Position, HP
17.08.2016	642-1	GC-13	21630-1	Cont. -Margin	16:21:00	16:39:00	16:49:00	17:00:00	78°33.241'	09°23.344'	436	Posidonia Position, recov. = 198 cm
17.08.2016	643-1	MeBo130	21631-1	Cont.-Margin Site 4	17:44:00	19:00:00	03:59:00	04:47:59	78°33.236'	09°27.337'	405	drill depth = 15.3 m, recov.= 0.53 m
18.08.2016	643-2	GC-14	21631-2	Cont.-Margin Site 4	08:39:00	08:53:00	-	09:13:00	78°33.237'	09°27.336'	405	Posidonia Position, recov. = 287 cm
18.08.2016	643-3	MeBo131	21631-3	Cont.-Margin Site 4	10:14:00	12:13:00	19:30:00	20:14:59	78°33.236'	09°27.337'	405	drilled depth = 20.3 m, recov. = 1.16 m
19.08.2016	643-4	MeBo132	21631-4	Cont.-Margin Site 4	06:30:00	07:45:00	18:59:00	19:49:59	78°33.236'	09°27.337'	405	drilled depth = 15.3 m, recov. = 0.81 m
20.08.2016	643-5	GC-15	21631-5	Cont.-Margin Site 4	05:14:00	05:29:00	05:29:01	05:47:59	78°33.236'	09°27.337'	405	without Posidonia, recov. = 126 cm
20.08.2016	644-1	MeBo133	21632-1	Cont.-Margin Site 5	06:49:00	07:46:00	15:55:00	16:39:00	78°33.132'	09°29.6527'	391	drill depth = 10.25 m, recov.= 2.68 m
20.08.2016	644-2	MeBo134	21632-2	Cont.-Margin Site 5	19:15:00	20:35:00	17:43:00	18:25:59	78°33.132'	09°29.6527'	391	drill depth = 25.3 m, recov.= 2.83 m
22.08.2016	645-1	MeBo135	21633-1	Cont.-Margin Site 3	06:29:00	07:23:00	17:10:00	17:52:59	78°32.9347'	09°22.7898'	446	drill depth = 25.3 m, recov.= 4.27 m
23.08.2016	645-2	GC-16	21633-2	Cont.-Margin Site 3	05:08:00	05:23:00	05:28:00	05:40:00	78°32.938'	09°22.786'	445	Posidonia Position, recov. = 250 cm
23.08.2016	645-3	MeBo136	21633-3	Cont.-Margin Site 3	06:37:00	07:37:00	07:37:00	08:23:59	78°32.9347'	09°22.7898'	445	drill depth = 37.95 m, recov.= 5.55 m
25.08.2016	646-1	MeBo137	21634-1	Cont.-Margin Site 6	16:14:00	17:00:00	06:26:00	07:00:59	78°33.5851'	09°32.5283'	340	drill depth = 21.6 m, recov.= 4.31 m
25.08.2016	646-2	GC-17	21634-2	Cont.-Margin Site 6	07:42:00	08:03:00	-	08:22:59	78°33.589'	09°32.528'	338	Posidonia Position, recov. = 111 cm

Appendix 1: Station List continued

MSM57 Station List												
					Time (UTC)							Remarks
Date 2016 (UTC)	MSM57 St. No.	Instrument	GeoB St. No.	Location	Begin (UTC)	on seafloor	off seafloor	End (UTC)	Latitude N	Longitude E	Water depth (m)	
26.08.2016	647-1	TL10-1	21635-1	Svyatogor Ridge	04:15:00	04:58:10	05:18:30	-	78°30.243'	05°42.676'	1716	Posidonia Position, HP
26.08.2016	647-2	TL10-2	21635-2	Svyatogor Ridge	-	06:11:10	06:28:00	-	78°29.871'	05°43.316'	1694	Posidonia Position, HP
26.08.2016	647-3	TL10-3	21635-3	Svyatogor Ridge	-	07:09:17	07:25:05	-	78°29.553'	05°43.603'	1691	Posidonia Position, HP
26.08.2016	647-4	TL10-4	21635-4	Svyatogor Ridge	-	07:57:36	08:12:46	-	78°29.438'	05°42.955'	1690	Posidonia Position, HP
26.08.2016	647-5	TL10-5	21635-5	Svyatogor Ridge	-	08:38:10	08:54:00	-	78°29.343'	05°43.442'	1695	Posidonia Position, HP
26.08.2016	647-6	TL10-6	21635-6	Svyatogor Ridge	-	09:18:13	09:34:30	-	78°29.271'	05°43.086'	1689	Posidonia Position, HP
26.08.2016	647-7	TL10-7	21635-7	Svyatogor Ridge	-	10:09:10	10:20:09	-	78°29.150'	05°43.669'	1685	Posidonia Position, HP
26.08.2016	647-8	TL10-8	21635-8	Svyatogor Ridge	-	11:01:10	11:17:01	-	78°29.051'	05°42.085'	1676	Posidonia Position, HP
26.08.2016	647-9	TL10-9	21635-9	Svyatogor Ridge	-	11:53:00	02:08:53	-	78°28.863'	05°41.432'	1680	Posidonia Position, HP
26.08.2016	647-10	TL10-10	21635-10	Svyatogor Ridge	-	12:34:20	12:50:04	-	78°28.810'	05°41.771'	1676	Posidonia Position, HP
26.08.2016	647-11	TL10-11	21635-11	Svyatogor Ridge	-	13:22:30	13:38:39	-	78°28.658'	05°41.900'	1670	Posidonia Position, HP
26.08.2016	647-12	TL10-12	21635-12	Svyatogor Ridge	-	14:16:03	14:32:30	-	78°28.510'	05°41.949'	1671	Posidonia Position, HP
26.08.2016	647-13	TL10-13	21635-13	Svyatogor Ridge	-	15:18:05	15:35:20	16:19:59	78°28.406'	05°40.368'	1686	Posidonia Position, HP
26.08.2016	648-1	GC-18	21636-1	Svyatogor Ridge	17:37:00	18:11:00	18:11:01	18:47:59	78°21.322'	05°42.129'	1625	Posidonia Position, recov. = 478 cm
27.08.2016	649-1	MeBo138	21637-1	Lunde Pockmark	04:46:00	07:54:00	04:13:00	07:06:00	79°00.426'	06°54.246'	1209	drill depth = 23.95 m, recov.= 8.7 m
29.08.2016	650-1	GC-19	21638-1	Lunde Pockmark	04:18:00	04:39:00	04:20:00	05:07:00	79°00.424'	06°54.678'	1210	Posidonia, GH, recov. ~200 cm, plastic foil
29.08.2016	651-1	MeBo139	21639-1	Cont.-Margin Site 5	16:16:00	17:08:00	17:49:00	18:30:00	78°33.132'	09°29.6527'	391	drill depth = 26.15 m, recov.= 12.03 m
31.08.2016	652-1	GC-20	21640-1	Svyatogor Ridge	10:44:00	11:18:00	11:23:00	11:49:00	78°21.303'	05°42.309'	1623	Posidonia Position, recov. = 544 cm
31.08.2016	653-1	GC-21	21641-1	Svyatogor Ridge	12:47:00	13:30:00	13:35:00	14:04:00	78°21.659'	05°41.594'	1634	Posidonia Position, recov. = 406 cm
31.08.2016	654-1	TL11-1	21642-1	Svyatogor Ridge	14:44:00	15:25:20	15:40:56	-	78°23.515'	05°37.316'	1686	Posidonia Position, HP
31.08.2016	654-2	TL11-2	21642-2	Svyatogor Ridge	-	16:16:28	16:24:40	-	78°23.509'	05°38.699'	1652	Posidonia Position
31.08.2016	654-3	TL11-3	21642-3	Svyatogor Ridge	-	16:46:50	17:03:00	-	78°23.514'	05°39.323'	1637	Posidonia Position, HP
31.08.2016	654-4	TL11-4	21642-4	Svyatogor Ridge	-	18:17:30	18:33:10	-	78°23.514'	05°40.459'	1645	Posidonia Position, HP
31.08.2016	654-5	TL11-5	21642-5	Svyatogor Ridge	-	19:03:47	19:18:50	-	78°23.506'	05°41.844'	1641	Posidonia Position, HP
31.08.2016	654-6	TL11-6	21642-6	Svyatogor Ridge	-	19:56:24	20:12:00	-	78°23.720'	05°41.546'	1649	Posidonia Position, HP
31.08.2016	654-7	TL11-7	21642-7	Svyatogor Ridge	-	20:48:30	20:57:26	-	78°23.951'	05°41.285'	1648	Posidonia Position
31.08.2016	654-8	TL11-8	21642-8	Svyatogor Ridge	-	21:34:50	21:43:15	-	78°24.191'	05°41.185'	1640	Posidonia Position
31.08.2016	654-9	TL11-9	21642-9	Svyatogor Ridge	-	22:30:05	22:46:00	23:15:00	78°24.415'	05°41.041'	1656	Posidonia Position, HP
01.09.2016	655-1	MeBo140	21643-1	Cont.-Margin Site 7	06:35:00	07:25:00	04:39:00	05:12:59	78°35.288'	09°23.963'	402	drill depth = 33.3 m, recov.= 17.08 m
02.09.2016	656-1	GC-22	21644-1	Cont.-Margin Site 5	07:00:00	07:11:00	07:11:01	07:30:59	78°33.132'	09°29.6527'	391	without Posidonia, recov. = 380 cm

GC: Gravity corer
TL: Temperature lance
HP: Heat pulse
* = Posidonia did not work correctly and the target location was taken
MeBo: Seafloor drill rig (Meeresbodenbohrgerät)
SVP: Sound velocity probe

18.2 Appendix 2: Heat Flow Values

Table A1: Calibration at Vestnesa Ridge.

614-GeoB21602-TL01-	**Calibration site**								**Date: 02/08/2016**
Penetration	Latitude (target position)	Longitude (target position)	Water Depth [m]	HP	Time in [hh:mm:ss]	Time out [hh:mm:ss]	Clear SF [hh:mm:ss]	Wire out [m]	Remarks
TL01-01	79°01.036'	6°53.741'	1216.5	No	17:57			52	Mounting of SVP probe
	79°01.036'	6°53.737'	1216.8	No	18:16:10			1100	At target depth
	79°01.036'	6°53.739'	1217.8	No	18:36:40			1100	End of calibration time

General Comments: Posidonia not used;
HP: Heat-Pulse to measure in situ thermal conductivity
SF: Seafloor
all Times are reported in UTC (local ship time – 2 hrs)

Table A2: Vestnesa Ridge, Lunde and Lomvi Pockmark.

615-GeoB21603-TL02-									**Date: 02/08/2016**
Penetration	Latitude (target position)	Longitude (target position)	Water Depth [m]	HP	Time in [hh:mm:ss]	Time out [hh:mm:ss]	Clear SF [hh:mm:ss]	Wire out [m]	Remarks
TL02-01	79°00.577'	6°53.936'	1210	Yes	21:08:36	21.25.15	21:26:46	1216	Probe to 1140 m for transit
TL02-02	79°00.528'	6°54.151'	1212.6	No	21:52:28	22:00:30	22:02:40	1224	Probe to 1096 m for transit
TL02-03	79°00.502'	6°54.614'	1216.3	Yes	22:39:18	22:56:56	22:58:48	1223	Probe to 1150 m for transit
TL02-04	79°00.397'	6°54.864'	1208	No	23:40:48	23:48:10	23:49:42	1221	Probe to 10600 m for transit
TL02-05	79°00.339'	6°55.170'	1207	Yes	00:17:55	00:33:18	00:34:50	1217	Probe to 1149 m for transit
TL02-06	79°00.277'	6°55.538'	1210	No	01:01:40	01:10:33	01:12:05	1221	Probe to 1080 m for transit
TL02-07	79°00.219'	6°55.610'	1211.5	Yes	01:39:35	01:56:06	01:58:02	1225	Probe to 1080 m for transit
TL02-08	79°00.180'	6°55.778'	1210	Yes	02:21:48	02:36:58	02:39:11	1224	

General Comments: Posidonia did not function for stations TL02-04 to TL02-08; Battery-power was too weak after three stations;
HP: Heat-Pulse to measure in situ thermal conductivity
SF: Seafloor
kN: kilo-Newton (pull out force)
all Times are reported in UTC (local ship time – 2 hrs)

Table A3: Vestnesa Ridge, Lomvi Pockmark.

619-GeoB21607-TL03-									**Date: 03/08/2016**
Penetration	Latitude (target position)	Longitude (target position)	Water Depth [m]	HP	Time in [hh:mm:ss]	Time out [hh:mm:ss]	Clear SF [hh:mm:ss]	Wire out [m]	Remarks
TL03-01	79°00.014'	6°56.901'	1200	Yes	21:24:50	21:40:28	21:40:50	1210	42 kN pullout; Probe to 1130m for transit
TL03-02	79°00.070'	6°56.562'	1201	No	22:05:45	22:14:18	22:14:34	1210	44 kN pullout Probe to 1130 m for transit

TL03-03	78°59.993'	6°55.651'	1202	No	22:49:20	22:58:03	22:58:15	1214	40.5 kN pullout Probe to 1060 m for transit
TL03-04	79°00.114'	6°55.674'	1210	Yes	23:32:33	23:49:03	23:49:19	1219	43 kN pullout Probe to 1060 m for transit
TL03-05	79°00.148'	6°56.008'	1208	Yes	00:20:39	00:37:11	00:37:36	1222	43.3 kN pullout Probe to 1060 m for transit
TL03-06	79°00.216'	6°56.146'	1210	Yes	01:03:40	01:20:30	01:20:55	1226	43.2 kN pullout Probe to 1130 m for transit
TL03-07	79°00.311'	6°56.895'	1212	No	01:53:30	02:03:26	02:04:00	1227	42 kN pullout Probe to 1130 m for transit
TL03-08	79°00.372'	6°57.138'	1216	No	02:22:00	02:31:26	02:31:50	1232	43 kN pullout

General Comments: Posidonia did not function; Setup was not correct (switch was not on fully on 'F2');
HP: Heat-Pulse to measure in situ thermal conductivity
SF: Seafloor
kN: kilo-Newton (pull out force)
all Times are reported in UTC (local ship time – 2 hrs)

Table A4: Vestnesa Ridge. Lunde Pockmark

623-GeoB21611-TL04-									**Date: 05/08/2016**
Penetration	Latitude (target position)	Longitude	Water Depth [m]	HP	Time in [hh:mm:ss]	Time out [hh:mm:ss]	Clear SF [hh:mm:ss]	Wire out [m]	Remarks
TL04-01	79°00.570'	6°55.025'	1221	Yes	06:40:23	06:57:36	06:57:55	1221	42.8 kN pullout; Probe to 1060 m for transit
TL04-02	79°00.497'	6°54.433'	1213	Yes	07:32:30	07:49:35	07:49:42	1224	43.7 kN pullout; Probe to 1130 m for transit
TL04-03	79°00.474'	6°54.590'	1213	No	08:05:53	08:15:00	:08:15:12	1221	42.3 kN pullout; Probe to 1130 m for transit
TL04-04	79°00.445'	6°54.607'	1213	No	08:30:33	08:41:25	08:41:35	1222	43.6 kN pullout; Probe to 1060 m for transit
TL04-05	79°00.446'	6°54.280'	1210	Yes	09:05:00	09:22:30	09:23:00	1220	37 kN pullout; Probe to 1060 m for transit Probe not fully penetrated
TL04-06	79°00.424'	6°53.896'	1208	Yes	09:44:30	10:01:20	10:01:35	1213	31.5 kN pullout; Probe to 1130 m for transit Probe not fully penetrated
TL04-07	79°00.442'	6°53.645'	1206	No	10:22:53	10:31:45	10:31:55	1212	41.5 kN pullout; Probe to 1130 m for transit
TL04-08	79°00.493'	6°53.929'	1207	No	10:57:08	11:05:45	11:03:00	1214	42 kN pullout; Probe to 1130 m for transit
TL04-09	79°00.483'	6°53.306'	1212	No	11:29:16	11:38:14	11:38:20	1219	41.4 kN pullout; Probe to 1060 m for transit
TL04-10	79°00.380'	6°54.602'	1210	Yes	12:13:55	12:30:03	12:30:15	1217	44 kN pullout;

General Comments: Posidonia did not function for stations TL02-04 to TL02-08; Battery-power was too weak after three stations;
HP: Heat-Pulse to measure in situ thermal conductivity
SF: Seafloor
kN: kilo-Newton (pull out force)
all Times are reported in UTC (local ship time – 2 hrs)

Table A5: Vestnesa Ridge, reference site.

626-GeoB21614-TL05-	**Reference Core site**								**Date: 07/08/2016**
Penetration	Latitude (target position)	Longitude	Water Depth [m]	HP	Time in [hh:mm:ss]	Time out [hh:mm:ss]	Clear SF [hh:mm:ss]	Wire out [m]	Remarks
TL05-01	78°59.806'	6°57.808'	1199	Yes	09:41:48	09:59:58	10:00:08	1207	43.8 kN pullout;

Position intended for MeBo126
HP: Heat-Pulse to measure in situ thermal conductivity
SF: Seafloor
kN: kilo-Newton (pull out force)
all Times are reported in UTC (local ship time – 2 hrs)

Table A6: Vestnesa Ridge, northern bend in ridge axis.

623-GeoB21611-TL06-	**Across faults at bend in ridge**								**Date: 07/08/2016**
Penetration	Latitude (target position)	Longitude (target position)	Water Depth [m]	HP	Time in [hh:mm:ss]	Time out [hh:mm:ss]	Clear SF [hh:mm:ss]	Wire out [m]	Remarks
TL06-01	79°06.966′	6°08.728′	1233	Yes	13:08:28	13:25:49	13:25:56	1241	41.5 kN pullout; Probe to 1160 m for transit
TL06-02	79°06.933′	6°09.690′	1235	No	14:13:36	14:23:35	14:23:47	1241	41.5 kN pullout; Probe to 1080 m for transit
TL06-03	79°06.895′	6°10.720′	1248	Yes	15:03:36	15:20:40	15:21:00	1256	48.3 kN pullout; Probe to 1080 m for transit
TL06-04	79°06.854′	6°11.847′	1228	Yes	16:04:55	16:20:48	16:21:10	1237	41.9 kN pullout; Probe to 1160 m for transit
TL06-05	79°06.806′	6°12.832′	1230	No	16:55:05	17:04:25	17:05:20	1238	40.5 kN pullout

HP: Heat-Pulse to measure in situ thermal conductivity
SF: Seafloor
kN: kilo-Newton (pull out force)
all Times are reported in UTC (local ship time – 2 hrs)

Table A7: Vestnesa Ridge, Lunde Pockmark.

630-GeoB21618-TL07-									**Date: 08/08/2016**
Penetration	Latitude (target position)	Longitude (target position)	Water Depth [m]	HP	Time in [hh:mm:ss]	Time out [hh:mm:ss]	Clear SF [hh:mm:ss]	Wire out [m]	Remarks
TL07-01	79°00.421′	6°54.245′	1210	Yes	23:06:02	23:23:15	23:23:22	1214	36.4 kN pullout; MeBo Site 128 Probe to 1060 m for transit
TL07-02	79°00.416′	6°54.248′	1210	Yes	23:39:54	23:56:59	23:57:08	1214	43.8 kN pullout; Probe to 1060 m for transit
TL07-03	79°00.407′	6°54.231′	1210	Yes	00:11:04	00:27:26	00:27:40	1217	44.4 kN pullout; Probe to 1060 m for transit
TL07-04	79°00.393′	6°54.191′	1212	Yes	00:42:52	00:59:27	00:59:40	1215	31.4 kN pullout; Probe to 1060 m for transit
TL07-05	79°00.379′	6°54.158′	1212	Yes	01:16:10	01:21:55	n/a	1212	Probe bounced; back to surface for checkup → continue
TL07-06	79°00.346′	6°54.094′	1210	Yes	02:32:30	02:48:35	02:48:50	1210	42.4 kN pullout; Probe to 1150m for transit
TL07-07	79°00.316′	6°54.074′	1208	No	03:03:30	03:12:26	03:12:40	1210	42.8 kN pullout; Probe to 1060 m for transit
TL07-08	79°00.277′	6°54.725′	1206	Yes	03:48:28	04:05:03	04:05:16	1208	41.4 kN pullout; Probe to 1060 m for transit
TL07-09	79°00.344′	6°54.666′	1208	Yes	04:23:37	04:39:45	04:40:05	1210	41.8 kN pullout; Probe to 1060 m for transit
TL07-10	79°00.361′	6°54.574′	1209	Yes	12:13:55	12:30:03	12:30:15	1211	39.6 kN pullout; Probe to 1060 m for transit
TL07-11	79°00.407′	6°54.543′	1212	Yes	05:39:17	05:56:46	05:57:00	1217	42.3 kN pullout; Probe to 1060 m for transit
TL07-12	79°00.435′	6°54.532′	1214	Yes	06:16:10	06:34:57	06:35:15	1214	30.1 kN pullout; Probe to 1150 m for transit
TL07-13	79°00.475′	6°54.524′	1214	No	06:50:39	06:59:41	07:00:00	1216	41.5 kN pullout; Probe to 1150 m for transit
TL07-14	79°00.496′	6°54.351′	1213	No	07:17:13	07:26:47	07:27:00	1216	42.6 kN pullout; Probe to 1060 m for transit

TL07-15	79°00.610′	6°54.736′	1209	Yes	07:54:56	08:10:06	08:10:20	1212	42.4 kN pullout; Probe to 1060 m for transit
TL07-16	79°00.674′	6°54.356′	1210	Yes	08:35:45	08:51:38	08:51:48	1212	41.4 kN pullout

HP: Heat-Pulse to measure in situ thermal conductivity
SF: Seafloor
kN: kilo-Newton (pull out force)
all Times are reported in UTC (local ship time – 2 hrs)

Table A8: Vestnesa Ridge Lunde and inactive pockmarks.

634-GeoB21622-TL08-									**Date: 10/08/2016**
Penetration	Latitude (target position)	Longitude	Water Depth [m]	HP	Time in [hh:mm:ss]	Time out [hh:mm:ss]	Clear SF [hh:mm:ss]	Wire out [m]	Remarks
TL08-01	79°01.087′	6°49.855′	1207	Yes	23:24:14	23:41:07	23:41:20	1208	39.8 kN pullout; Probe to 1060 m for transit Position of GC211 from CAGE
TL08-02	79°01.155′	6°50.041′	1210	Yes	00:10:12	00:26:50	00:27:08	1208	43.3 kN pullout; Probe to 1060 m for transit
TL08-03	79°01.098′	6°50.481′	1215	Yes	00:53:30	01:09:02	01:09:18	1217	37.2 kN pullout; Probe to 1060 m for transit
TL08-04	79°01.074′	6°50.637′	1215	Yes	01:27:58	01:44:20	01:44:30	1218	45 kN pullout; Probe to 1060 m for transit
TL08-05	79°01.059′	6°50.949′	1213	Yes	02:03:36	02:19:27	02:19:45	1214	43 kN Probe to 1150 m for transit
TL08-06	79°01.038′	6°51.129′	1213	No	02:33:34	02:42:13	02:42:25	1215	42.8 kN pullout; Probe to 1150 m for transit
TL08-07	79°00.985′	6°51.285′	1214	Yes	03:01:20	03:17:45	03:17:55	1216	42.4 kN pullout; Probe to 1060 m for transit
TL08-08	79°00.944′	6°51.492′	1216	Yes	03:33:28	03:49:55	03:50:05	1214	42.2 kN pullout; Probe to 1060 m for transit
TL08-09	79°00.875′	6°51.533′	1214	Yes	04:06:55	04:22:52	04:23:10	1215	43 kN pullout; Probe to 1060 m for transit
TL08-10	79°00.855′	6°51.802′	1213	No	04:36:20	04:45:10	04:45:30	1212	42.5 kN pullout; Probe to 1060 m for transit
TL08-11	79°00.828′	6°52.223′	1208	Yes	05:04:58	05:20:54	05:21:12	1210	44.6 kN pullout; Probe to 1060 m for transit
TL08-12	79°00.744′	6°53.085′	1210	Yes	05:51:50	06:07:38	06:07:55	1212	44.4 kN pullout; Probe to 1150 m for transit
TL08-13	79°00.696′	6°53.176′	1212	No	06:22:11	06:30:45	06:31:06	1220	46.3 kN pullout; Probe to 1150 m for transit
TL08-14	79°00.592′	6°54.296′	1212	Yes	07:12:08	07:29:12	07:31:20	1225	43 kN pullout; Probe to 1060 m for transit
TL08-15	79°00.599′	6°54.700′	1213	No	07:50:22	07:58:35	08:00:27	1222	42 kN pullout; Probe to 1060 m for transit
TL08-16	79°00.558′	6°54.821′	1215	Yes	08:18:39	08:34:38	08:36:45	1220	43.4 kN pullout

HP: Heat-Pulse to measure in situ thermal conductivity
SF: Seafloor
kN: kilo-Newton (pull out force)
all Times are reported in UTC (local ship time – 2 hrs)

Table A9: Svyatogor Ridge South.

641-GeoB21629-TL09-									**Date: 16/08/2016**
Penetration	Latitude (target position)	Longitude	Water Depth [m]	HP	Time in [hh:mm:ss]	Time out [hh:mm:ss]	Clear SF [hh:mm:ss]	Wire out [m]	Remarks
TL09-01	78°21.206′	5°40.542′	1634	Yes	21:08:00	21:26:32	21:26:50	1640	48.2 kN pullout; Probe to 1520 m for transit

TL09-02	78°21.258′	5°41.440′	1610	Yes	21:59:47	22:16:47	22:17:15	1619	47.4 kN pullout; Probe to 1520 m for transit
TL09-03	78°21.324′	5°42.134′	1623	No	22:52:8	23:18:21	23:08:40	1630	49.2 kN pullout; Probe to 1520 m for transit (HP not triggered)
TL09-04	78°21.337′	5°42.479′	1618	No	23:28:00	23:44:07	23:44:28	1628	47.9 kN pullout; Probe to 1500 m for transit (HP not triggered)
TL09-05	78°21.372′	5°43.434′	1612	Yes	00:18:15	00:34:26	00:34:50	1615	48.1 kN pullout Probe to 1500 m for transit
TL09-06	78°21.439′	5°44.178′	1650	Yes	01:03:48	01:20:20	01:20:40	1654	49.2 kN pullout; Probe to 1550 m for transit
TL09-07	78°20.120′	5°44.916′	1650	No	02:05:55	02:14:30	02:14:55	1651	49.3 kN pullout; Probe to 1520 m for transit
TL09-08	78°20.813′	5°45.382′	1648	Yes	03:02:48	03:18:04	03:18:22	1647	49.1 kN pullout; Probe to 1500 m for transit
TL09-09	78°20.709′	5°44.346′	1605	Yes	03:57:53	04:13:55	04:14:18	1606	48.1 kN pullout; Probe to 1460 m for transit
TL09-10	78°20.600′	5°43.473′	1610	No	04:48:57	05:05:12	05:05:35	1618	47.3 kN pullout; Probe to 1460 m for transit
TL09-11	78°20.473′	5°42.270′	1602	Yes	05:48:50	06:05:40	06:05:55	1611	46.3 kN pullout; Probe to 1460 m for transit
TL09-12	78°20.318′	5°42.559′	1600	Yes	06:38:40	06:55:10	06:55:30	1607	47.3 kN pullout; Probe to 1460 m for transit
TL09-13	78°20.039′	5°42.882′	1609	No	07:33:40	07:20:21	07:51:45	1630	47.7 kN pullout; Probe to 1460 m for transit
TL09-14	78°20.130′	5°43.649′	1602	Yes	08:25:03	08:42:02	08:43:00	1611	47.6 kN pullout; Probe to 1460 m for transit
TL09-15	78°20.249′	5°44.380′	1604	Yes	09:15:48	09:31:51	09:32:00	1607	48.9 kN pullout; Probe to 1460 m for transit
TL09-16	78°20.387′	5°45.147′	1606	Yes	10:05:19	10:20:19	10:20:59	1607	47.7 kN pullout

HP: Heat-Pulse to measure in situ thermal conductivity
SF: Seafloor
kN: kilo-Newton (pull out force)
all Times are reported in UTC (local ship time – 2 hrs)

Table A10: Svyatogor Ridge North.

647-GeoB21635-TL10-									**Date: 26/08/2016**
Penetration	Latitude (target position)	Longitude	Water Depth [m]	HP	Time in [hh:mm:ss]	Time out [hh:mm:ss]	Clear SF [hh:mm:ss]	Wire out [m]	Remarks
01	78° 30.243	05° 42.676	1720	Yes	04:58:00	05:18:06	05:18:30	1716	51.4 kN pullout Probe to 1570 m for transit
02	78° 29.871	05° 43.396	1692	Yes	06:11:00	06:27:48	06:28:00	1694	53.3 kN pullout Probe to 1570 m for transit
03	78° 29.553	05° 43.603	1691	Yes	07:09:15	07:24:44	07:25:05	1691	51.6 kN pullout Probe to 1550 m for transit
04	78° 29.438	05° 42.955	1692	Yes	07:57:36	08:12:26	08:12:46	1690	52.4 kN pullout Probe to 1550 m for transit
05	78° 29.343	05° 43.442	1692	No	08:38:10	08:53:45	08:54:00	1695	35 kN pullout Probe to 1550 m for transit
06	78° 29.271	05° 43.086	1686	Yes	09:18:13	09:34:04	09:34:30	1689	52 kN pullout Probe to 1500 m for transit
07	78° 29.450	05° 43.669	1688	Yes	10:04:10	10:19:42	10:20:09	1689	53.4 kN pullout Probe to 1500 m for transit
08	78° 29.051	05° 42.085	1682	Yes	11:01:10	11:16:42	11:17:01	1676	51.4 kN pullout Probe to 1500 m for transit
09	78° 28.863	05° 41.432	1681	Yes	11:53:00	12:08:38	12:08:53	1680	50.1 kN pullout Probe to 1500 m for transit
10	78° 28.810	05° 41.771	1683	Yes	12:334:20	12:49:42	12:50:04	n.a.	51.7 kN pullout Probe to 1500 m for transit
11	78° 28.658	05° 41.900	1672	Yes	13:22:30	13:38:17	13:38:39	1670	52.4 kN pullout Probe to 1500 m for transit

12	78° 28.510	05° 41.949	1670	Yes	14:16:05	14:32:07	14:32:30	n.a.	50.8 kN pullout Probe to 1500 m for transit
13	78° 28.406	05° 40.368	1687	Yes	15:18:05	15:34:56	15:35:20	1686	51.6 kN pullout Probe to 1500 m for transit

HP: Heat-Pulse to measure in situ thermal conductivity
SF: Seafloor
kN: kilo-Newton (pull out force)
n.a.: not available
all Times are reported in UTC (local ship time – 2 hrs)

Table A11: Svyatogor Ridge Central.

654-GeoB21642-TL11-	**Central portion of Ridge**								**Date: 31/08/2016**
Penetration	Latitude (target position)	Longitude	Water Depth [m]	HP	Time in [hh:mm:ss]	Time out [hh:mm:ss]	Clear SF [hh:mm:ss]	Wire out [m]	Remarks
01	78° 23.515	05° 37.316	1689	Yes	15:25:20	15:40:40	15:40:56	1689	48.4 kN pullout Probe to 1580 m for transit
02	78° 23.509	05° 38.699	1660	No	16:16:28	16:24:10	16:24:40	1652	48.5 kN pullout Probe to 1500 m for transit
03	78° 23.514	05° 39.323	1640	No	16:46:50	17:01:50	17:03:00	1637	probe did not penetrate into sediments
04	78° 23.514	05° 40.459	1652	Yes	18:17:30	18:32:45	18:33:10	1645	50.6 kN pullout Probe to 1500 m for transit
05	78° 23.506	05° 41.844	1641	Yes	19:03:47	19:18:24	19:18:50	1641	48.8 kN pullout Probe to 1500 m for transit
06	78° 23.720	05° 41.546	1646	Yes	19:56:24	20:11:40	20:12:00	1649	50.1 kN pullout Probe to 1580 m for transit
07	78° 23.951	05° 41.285	1647	No	20:48:30	20:56:56	20:57:26	1648	48.7 kN pullout Probe to 1580 m for transit
08	78° 24.191	05° 41.185	1644	No	21:34:50	21:42:52	21:43:15	1640	48.5 kN pullout Probe to 1500 m for transit
09	78° 24.415	05° 41.041	1660	Yes	22:30:05	22:45:15	22:45:35	1656	51.4 kN pullout

HP: Heat-Pulse to measure in situ thermal conductivity
SF: Seafloor; kN: kilo-Newton (pull out force)
all Times are reported in UTC (local ship time – 2 hrs)

18.3 Appendix 3: Core Descriptions Gravity Cores

MSM57-1
GeoB21601-1
GC-1

Core Length: 577 cm

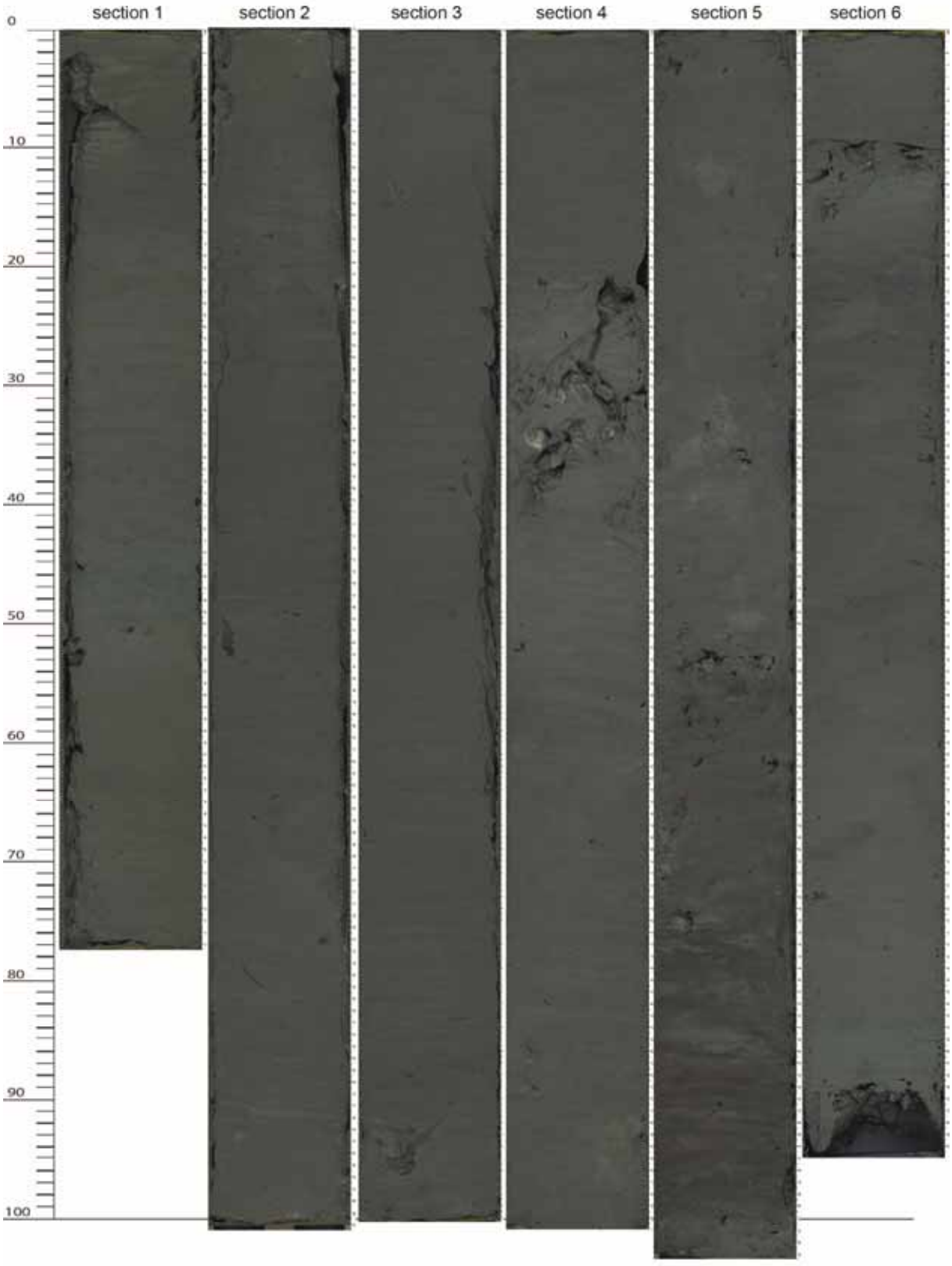

Appendix 3: Core Descriptions Gravity Cores continued

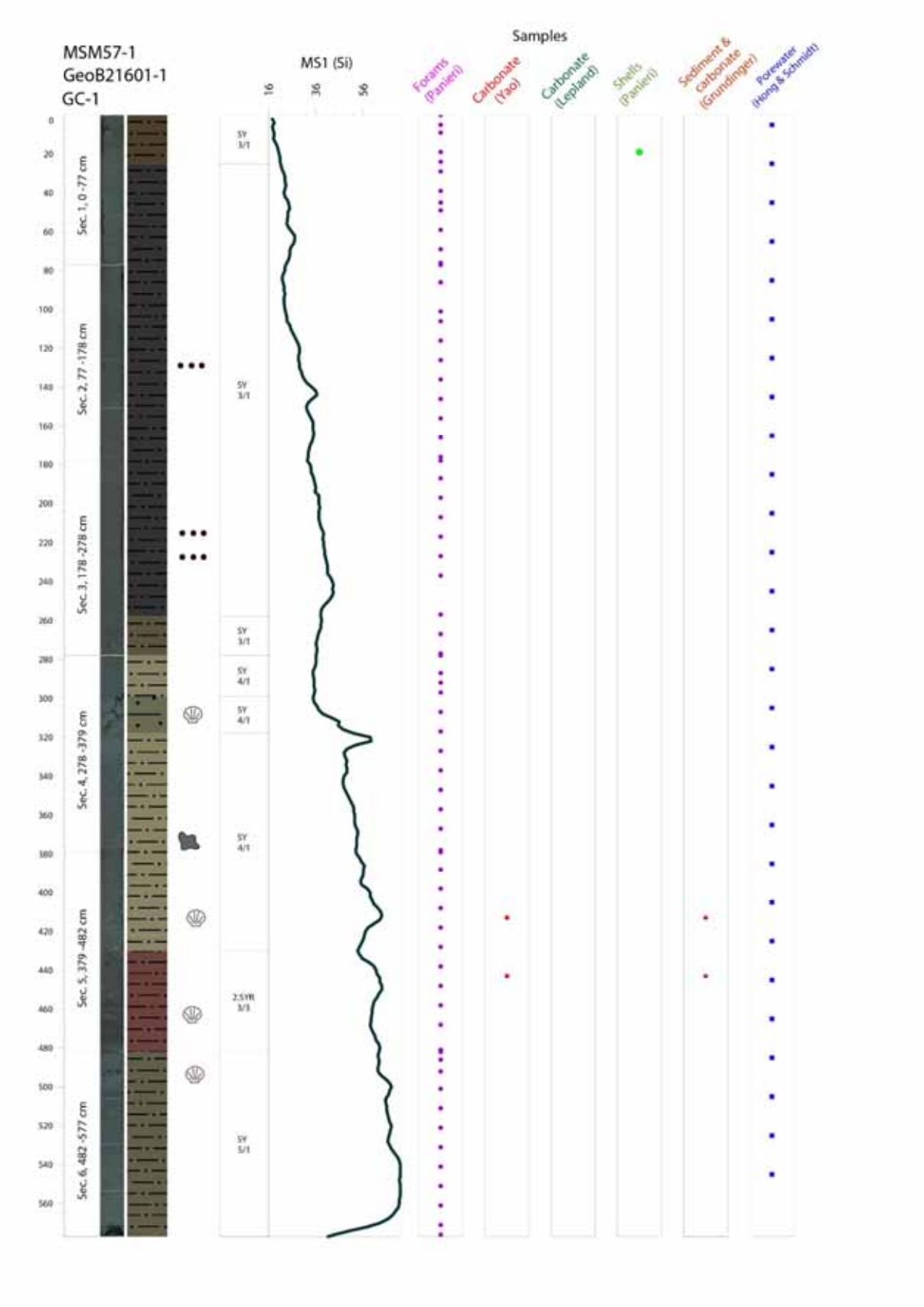

Appendix 3: Core Descriptions Gravity Cores continued

MSM57-1
GeoB21605-1
GC-2

Core Length: 765 cm

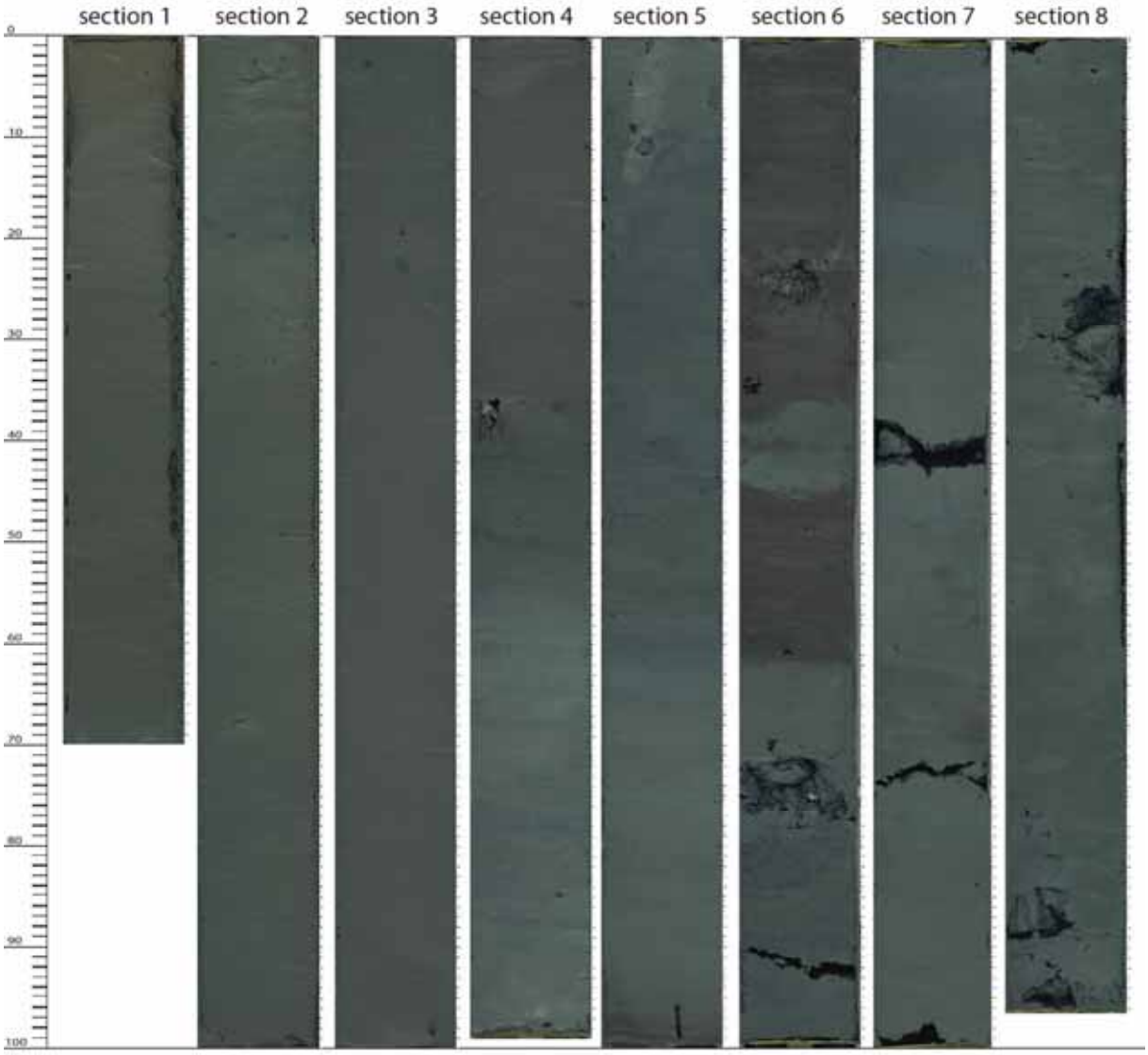

Section No.	Section length (cm)	Top depth (cm)	Bottom depth (cm)	remark
1	70	0	70	
2	100	70	170	
3	100	170	270	
4	99	270	369	
5	100	369	469	
6	100	469	569	
7	100	569	669	
8	96	669	765	

Appendix 3: Core Descriptions Gravity Cores continued

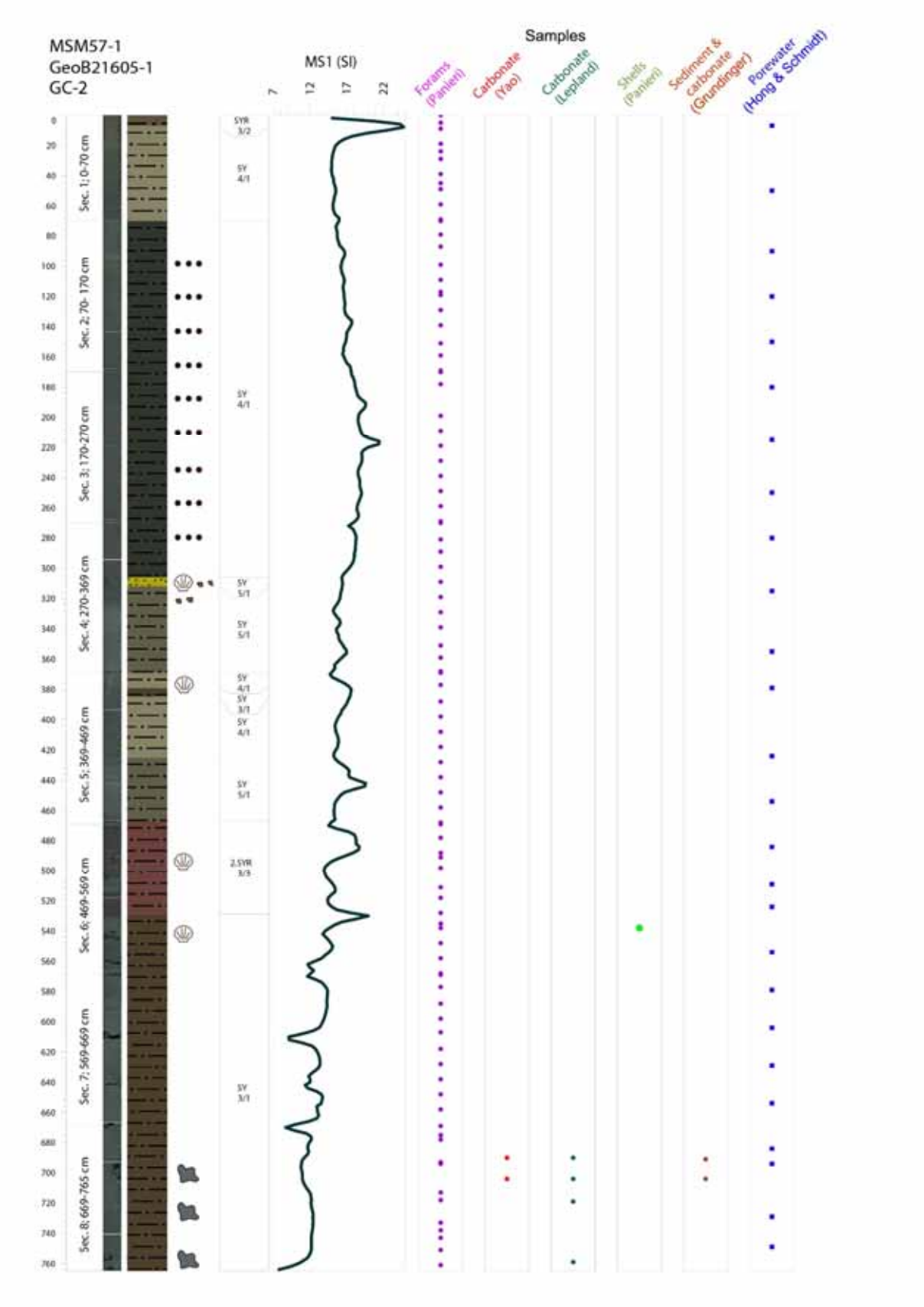

Appendix 3: Core Descriptions Gravity Cores continued

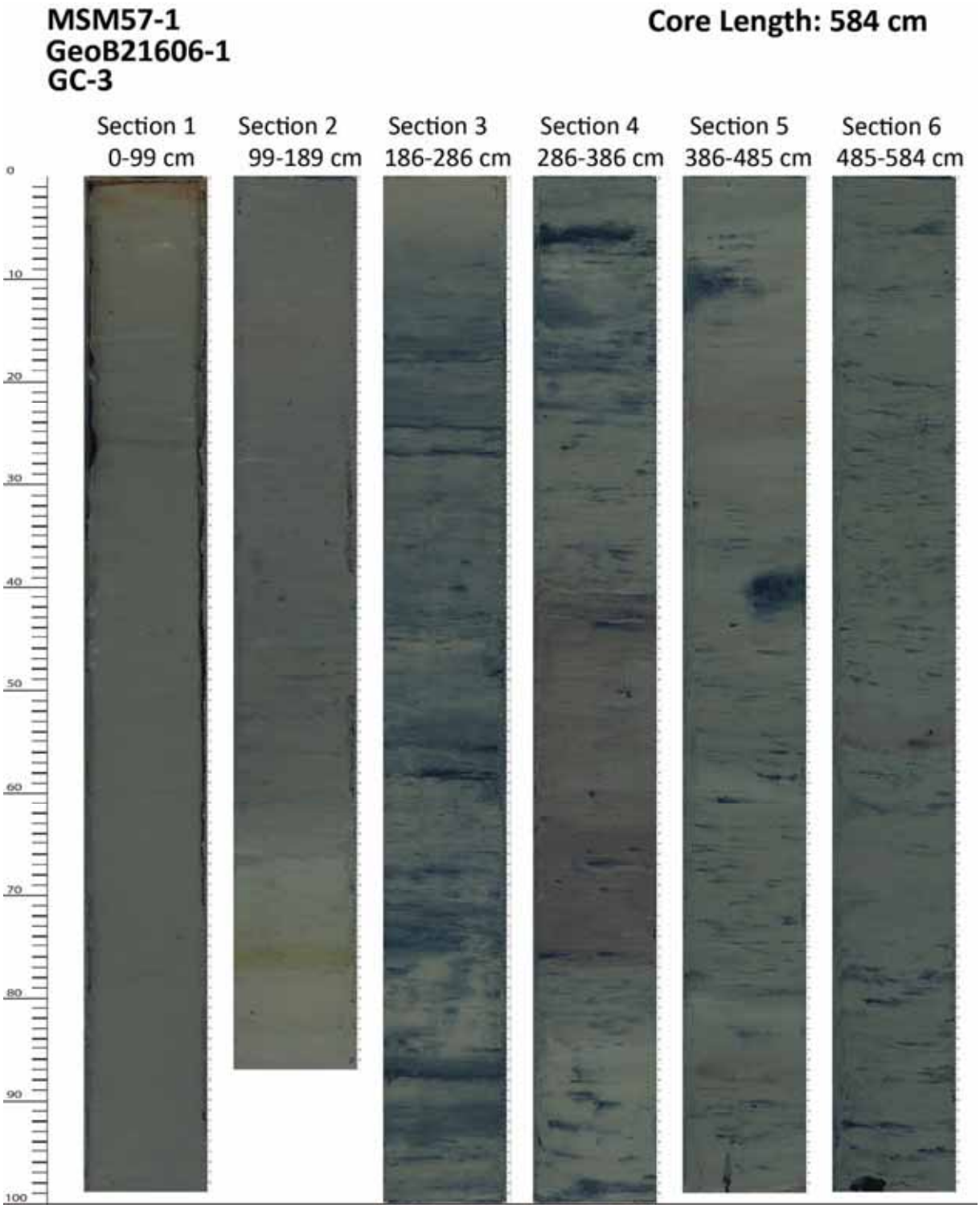

Appendix 3: Core Descriptions Gravity Cores continued

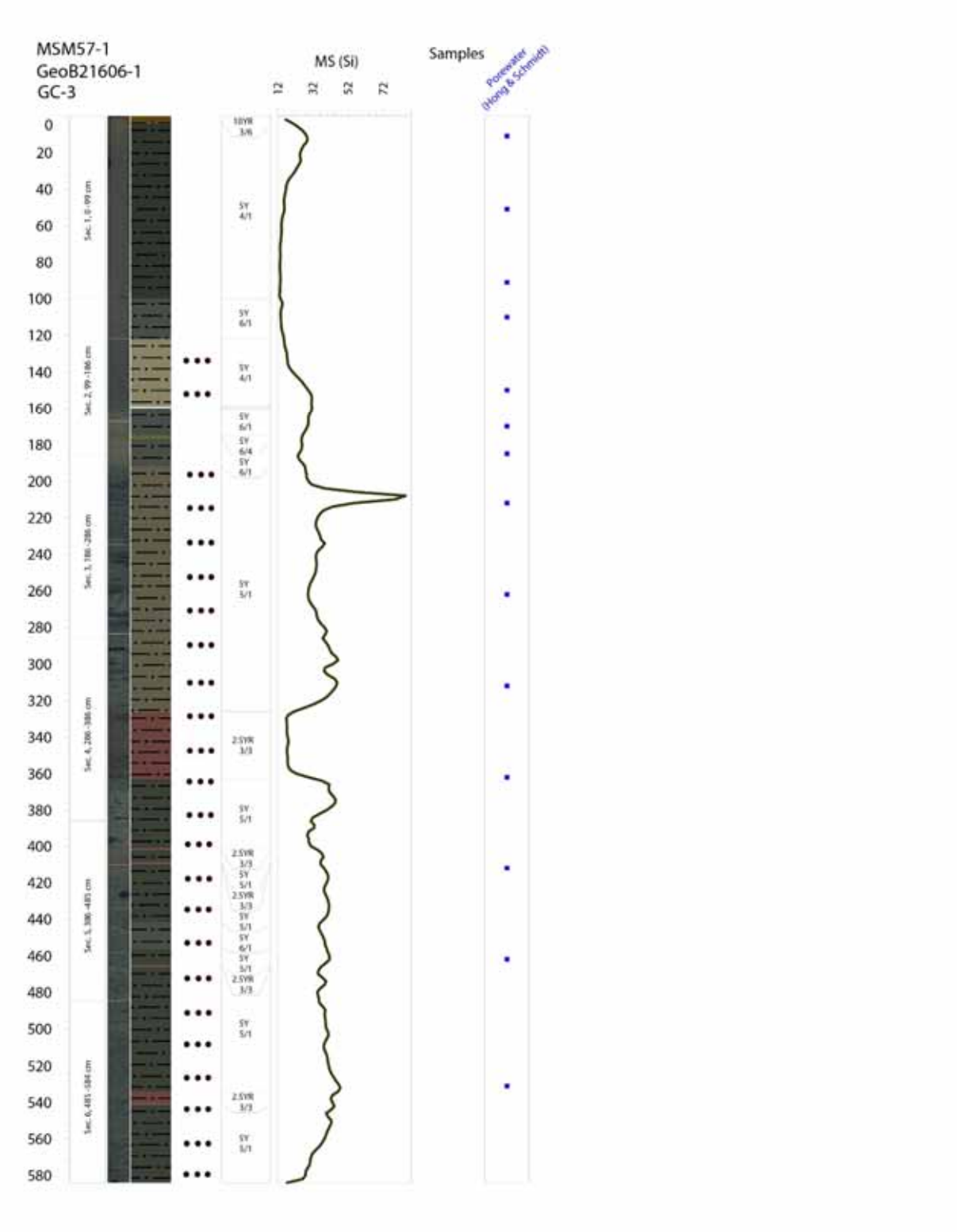

Appendix 3: Core Descriptions Gravity Cores continued

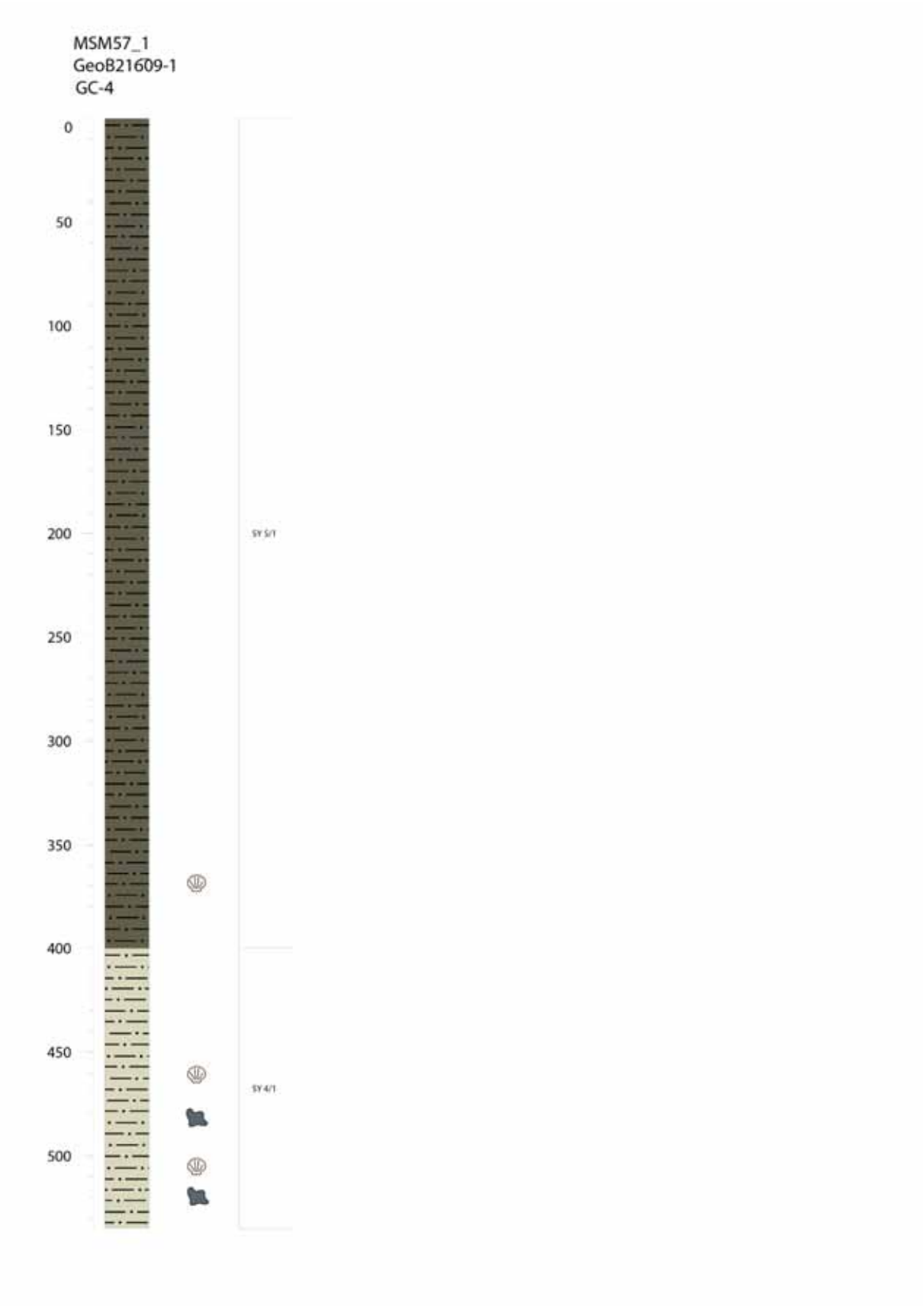

Appendix 3: Core Descriptions Gravity Cores continued

Appendix 3: Core Descriptions Gravity Cores continued

MSM57-1
GeoB21612-1
GC-6

Core Length: 273 cm

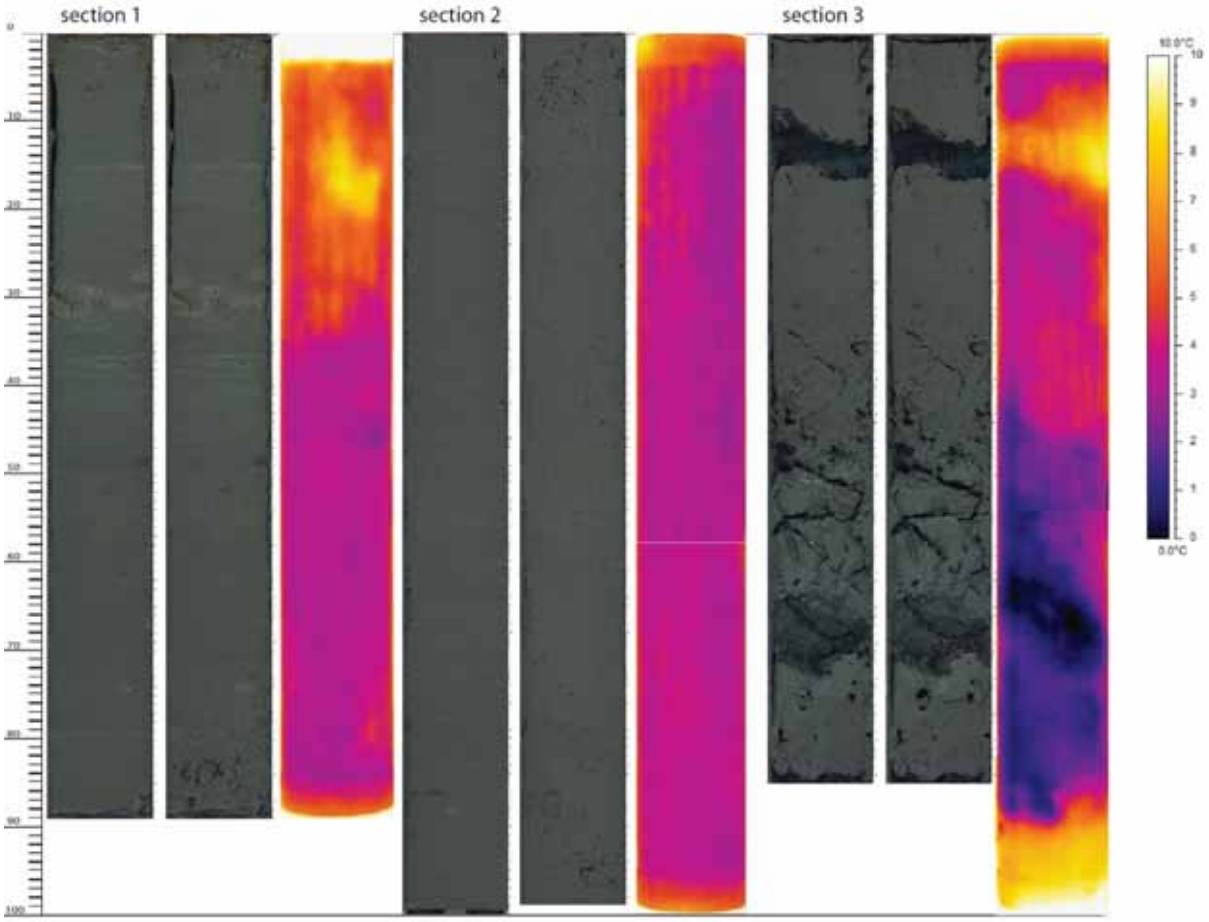

Section No.	Section length (cm)	Top depth (cm)	Bottom depth (cm)	remark
1	89	0	89	
2	99	89	188	
3	85	188	273	Gas Hydrate

Appendix 3: Core Descriptions Gravity Cores continued

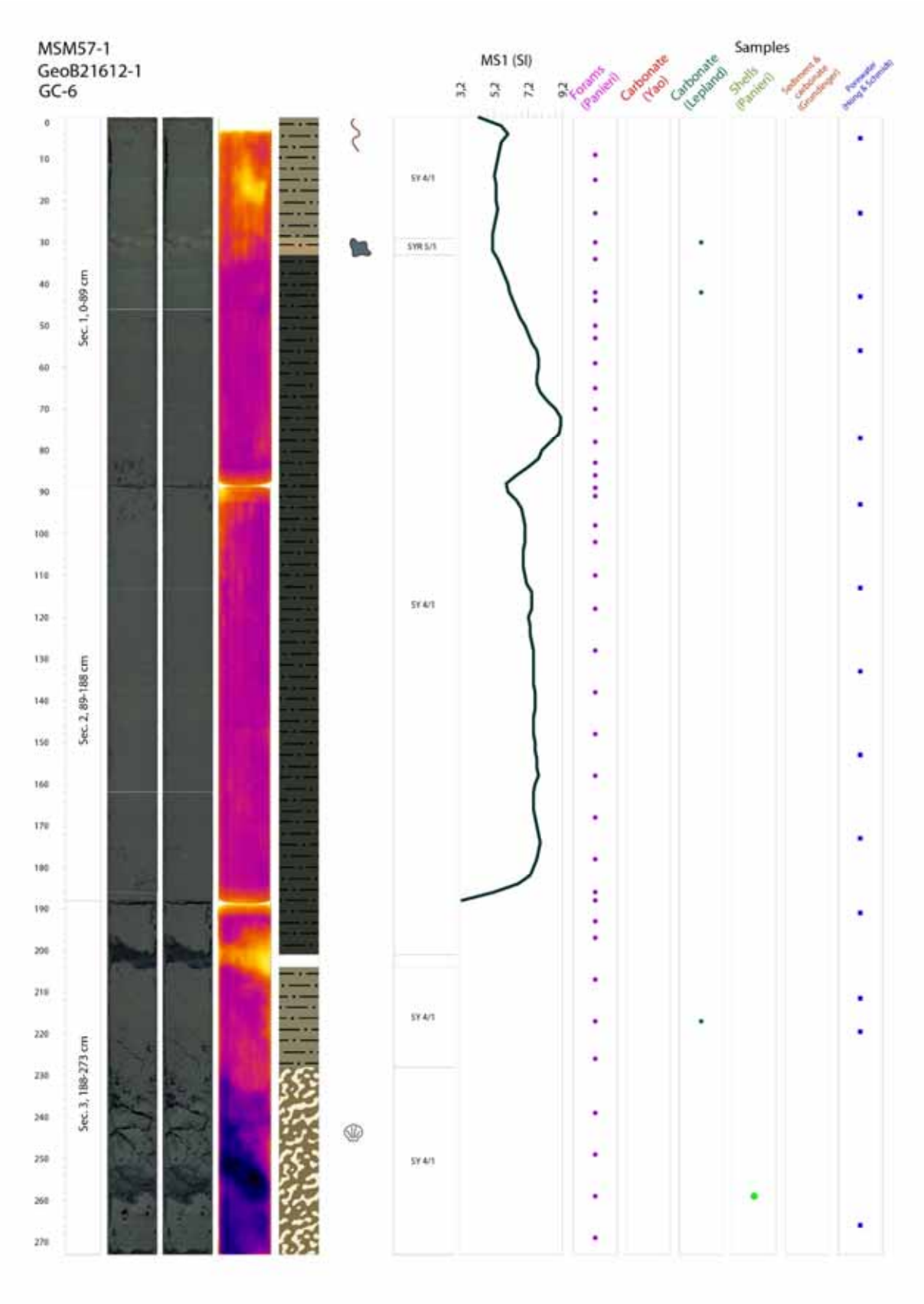

Appendix 3: Core Descriptions Gravity Cores continued

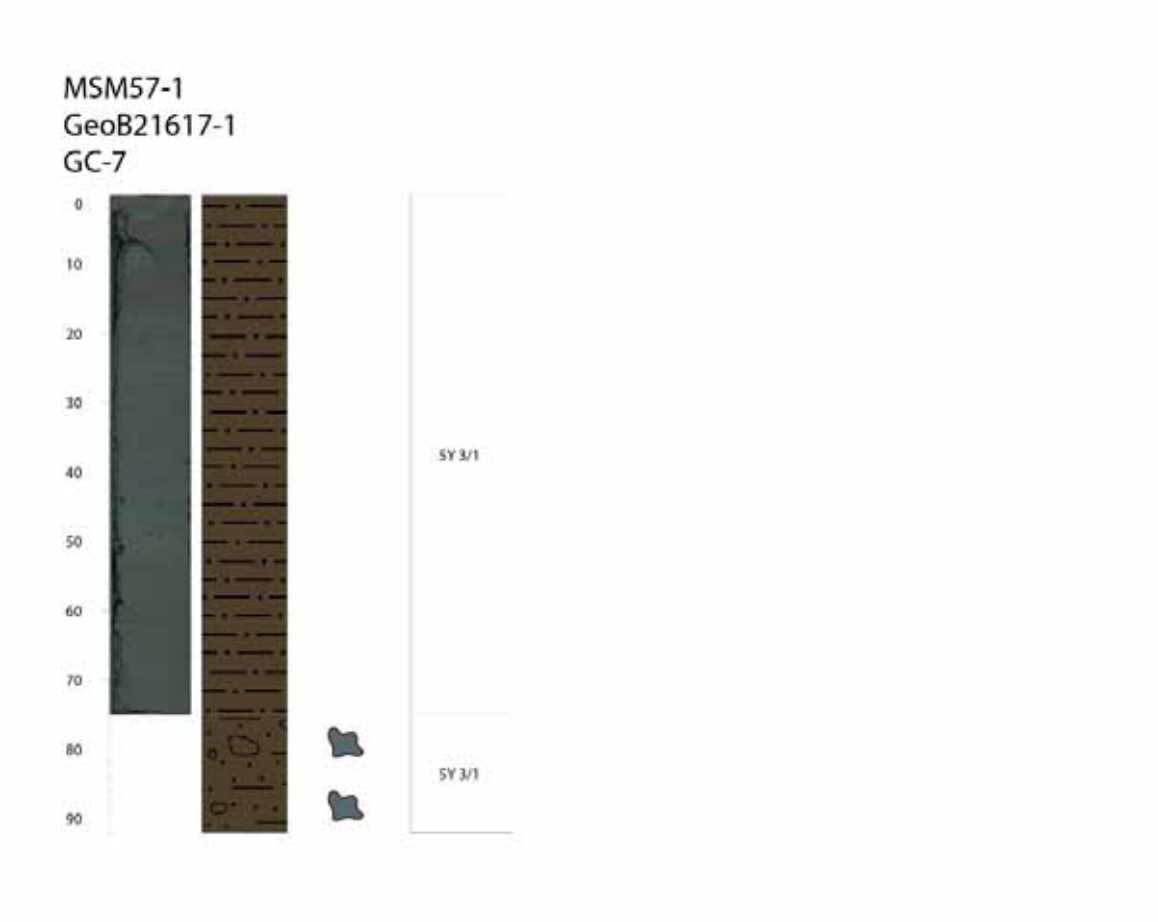

Appendix 3: Core Descriptions Gravity Cores continued

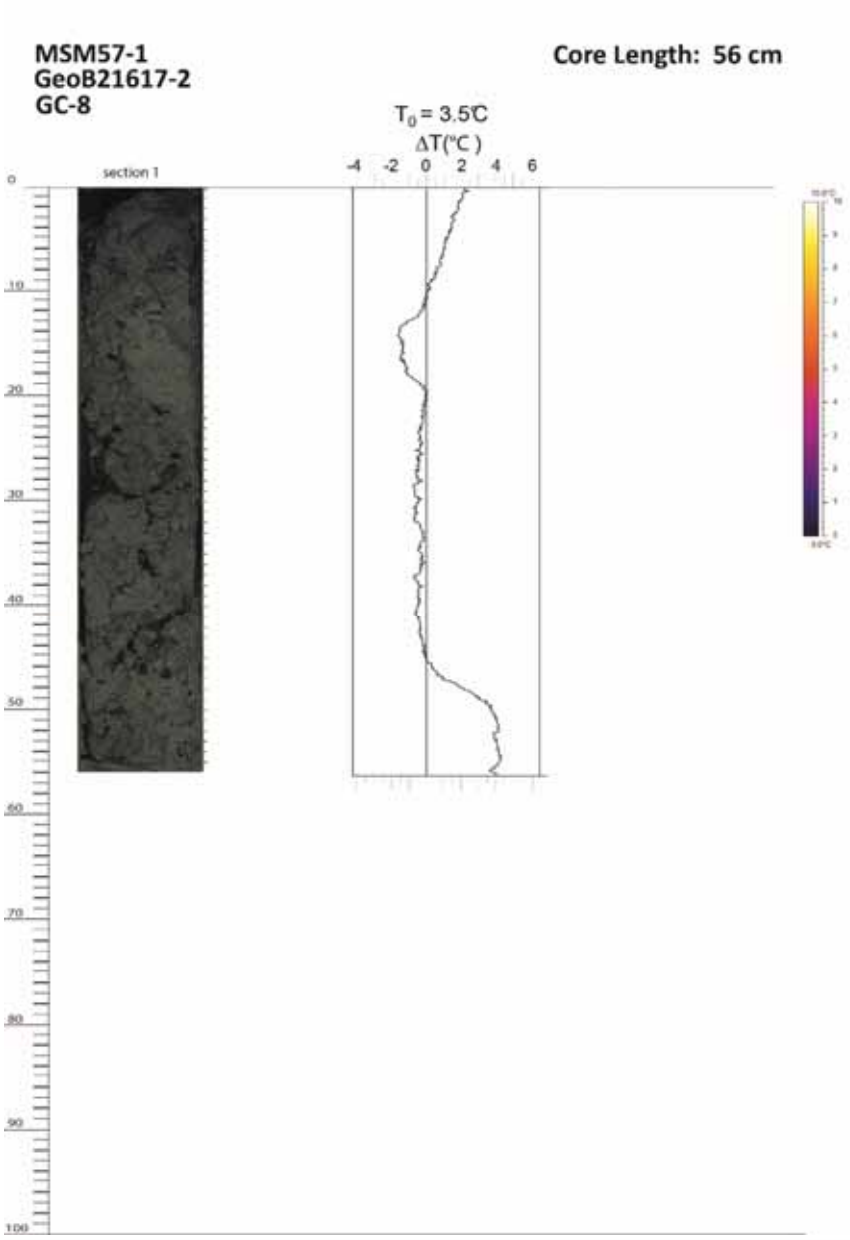

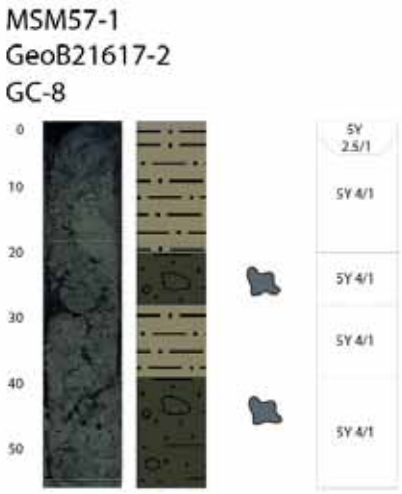

Appendix 3: Core Descriptions Gravity Cores continued

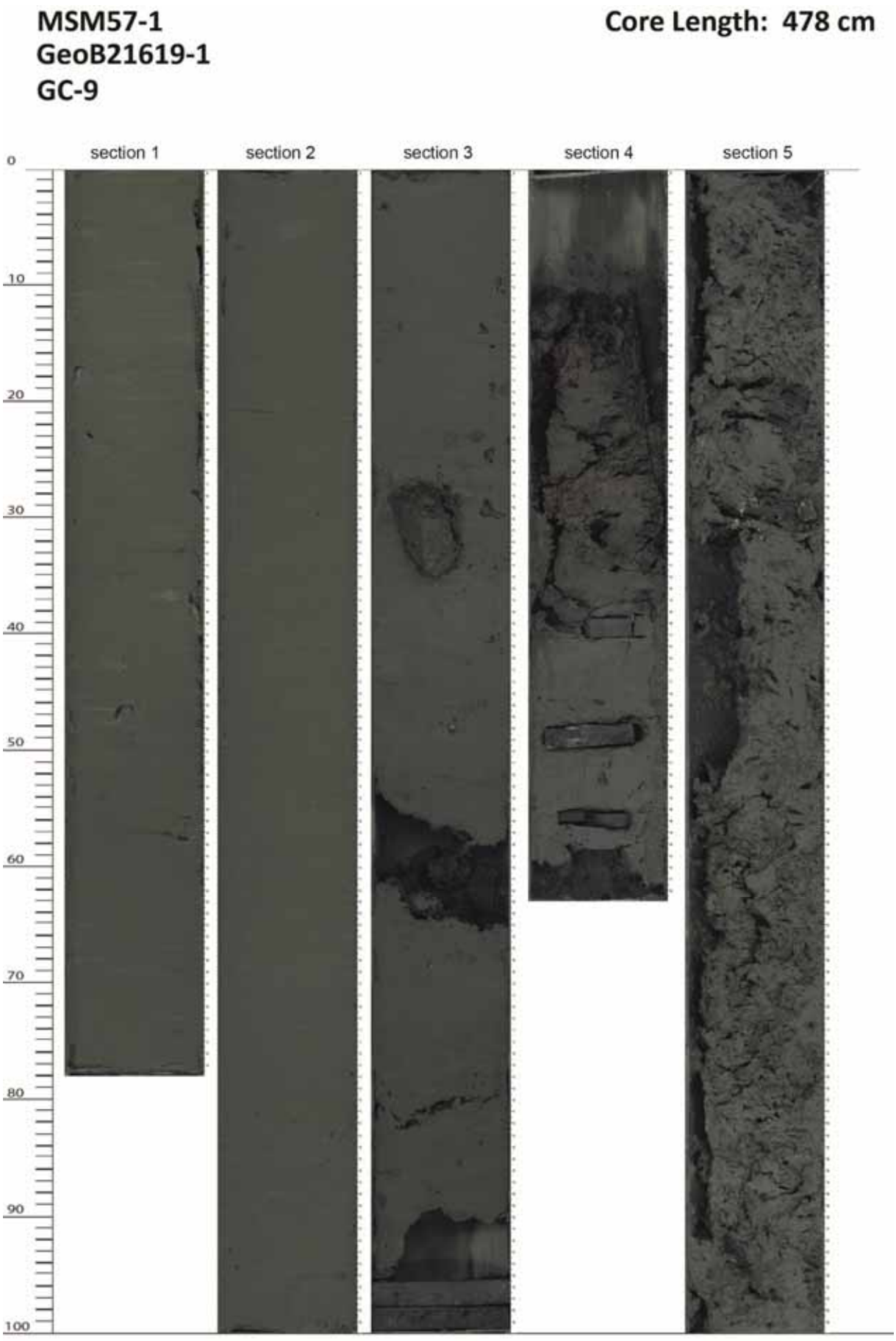

Appendix 3: Core Descriptions Gravity Cores continued

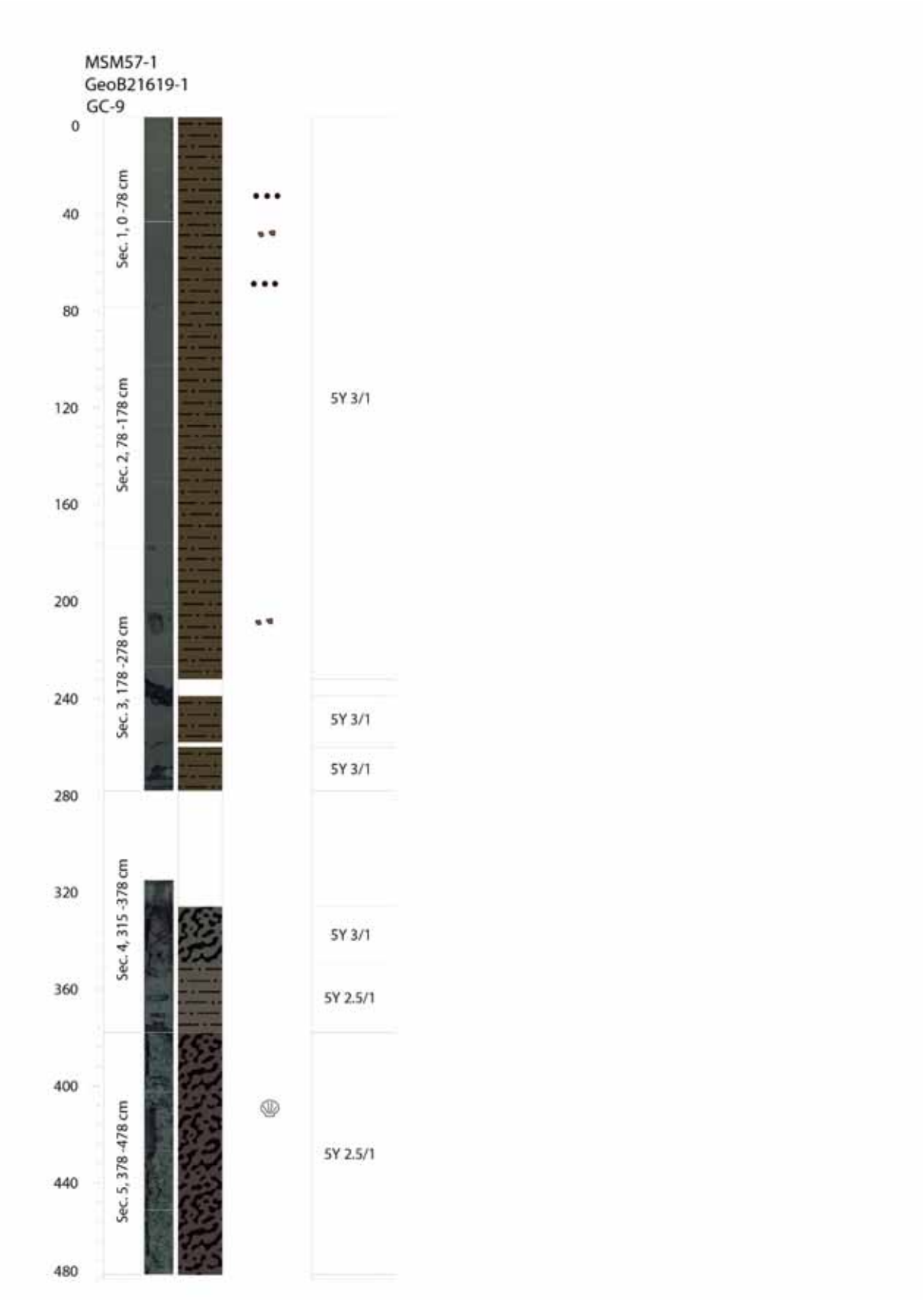

Appendix 3: Core Descriptions Gravity Cores continued

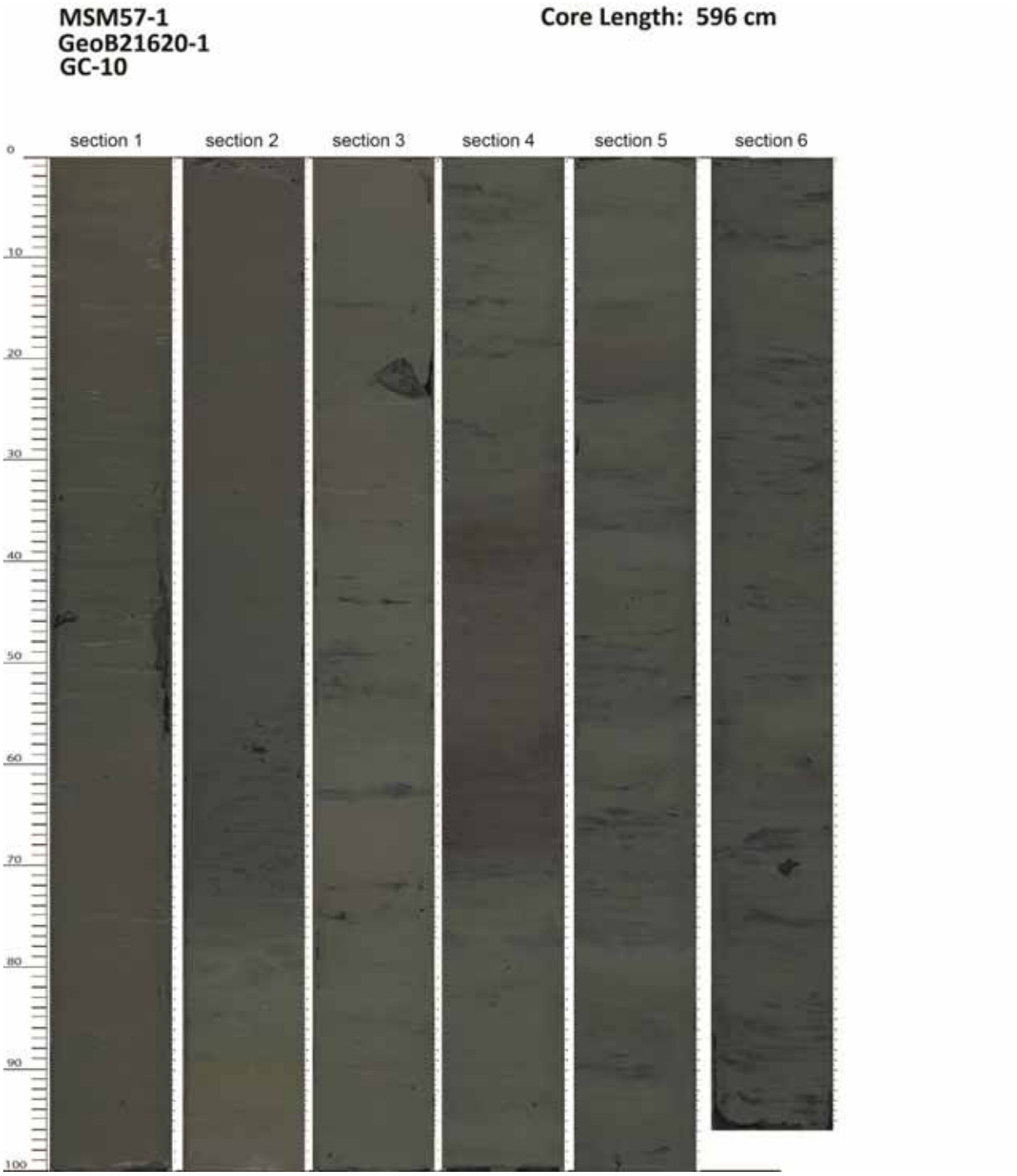

Appendix 3: Core Descriptions Gravity Cores continued

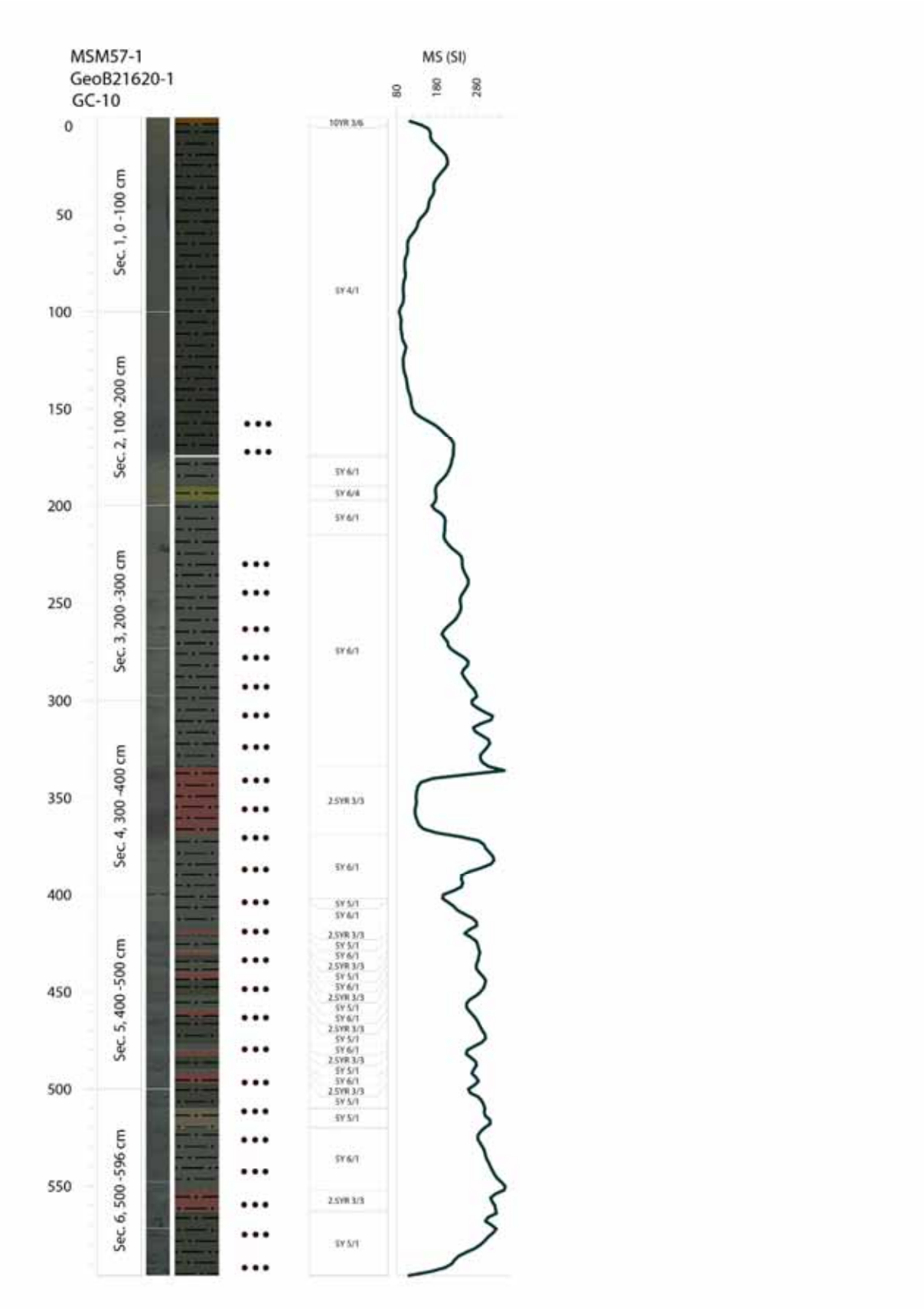

Appendix 3: Core Descriptions Gravity Cores continued

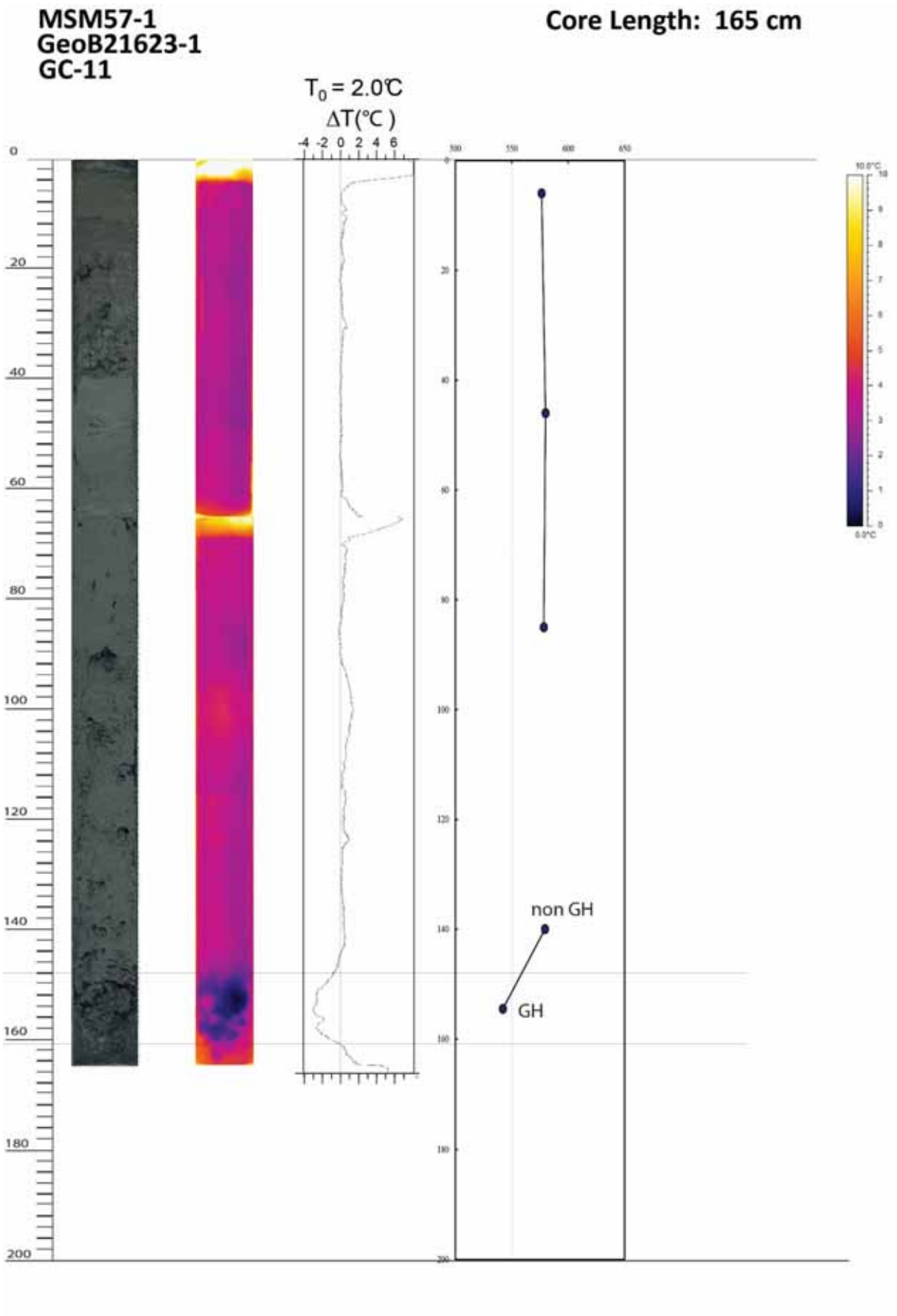

Appendix 3: Core Descriptions Gravity Cores continued

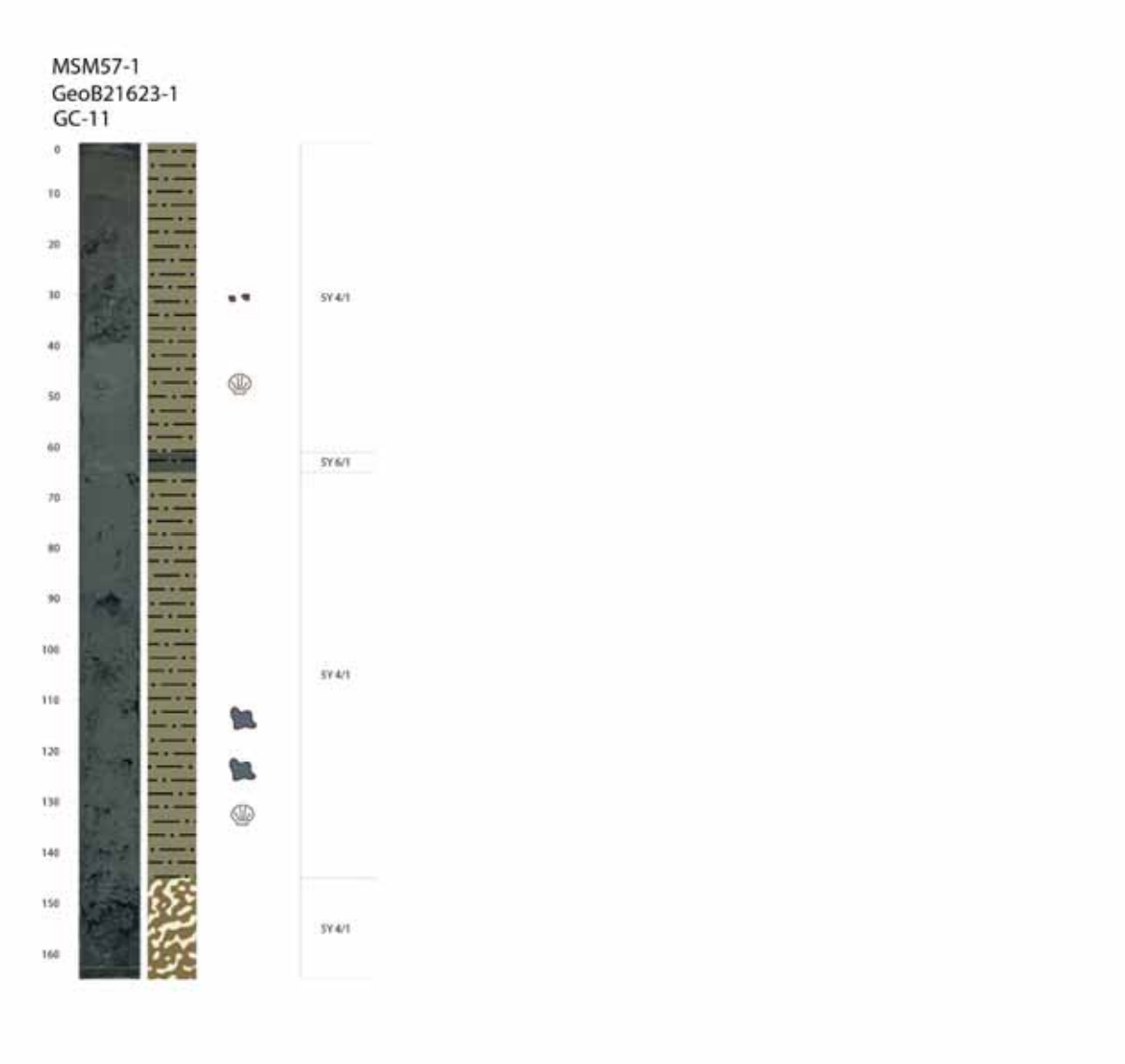

Appendix 3: Core Descriptions Gravity Cores continued

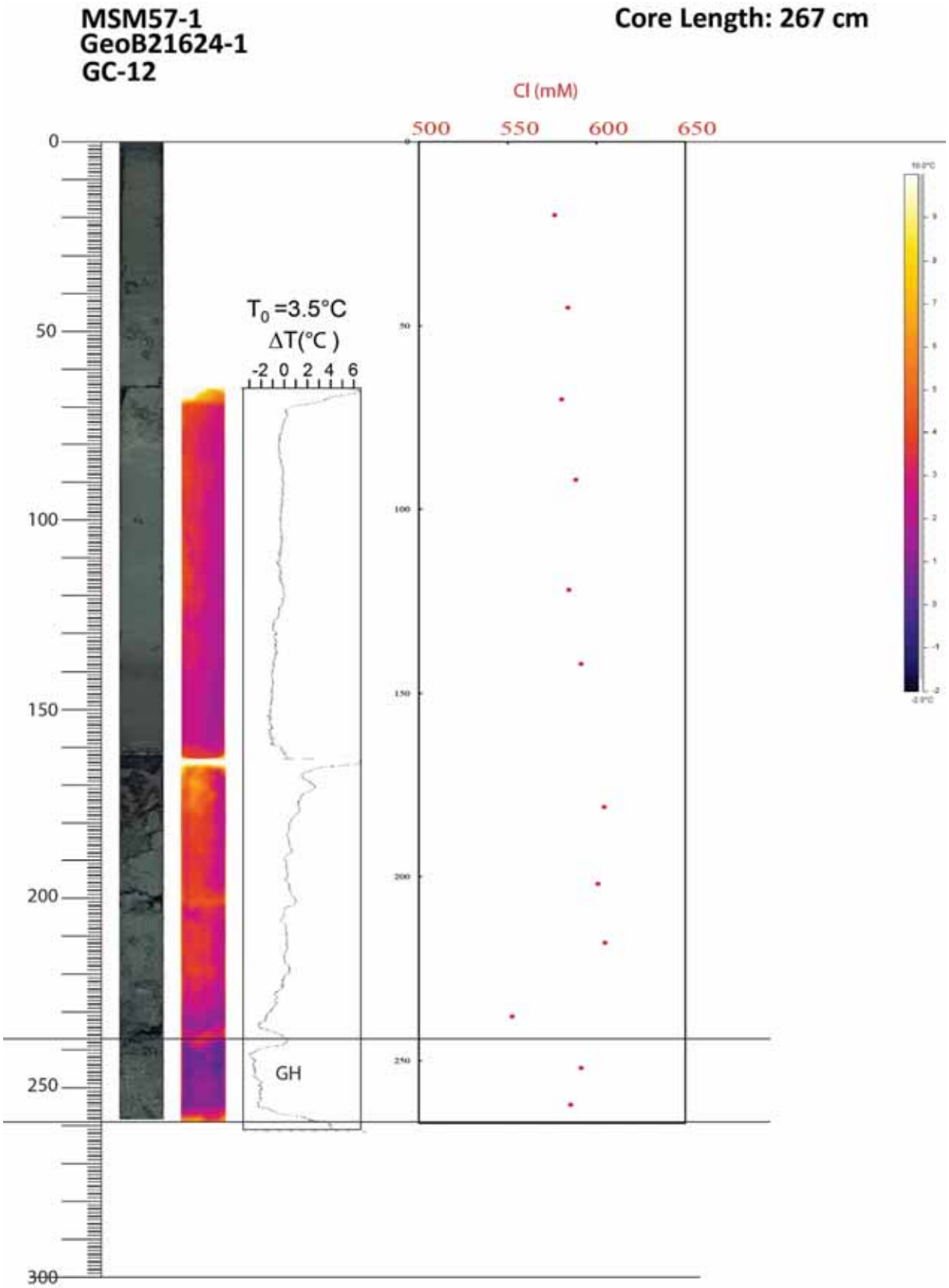

Appendix 3: Core Descriptions Gravity Cores continued

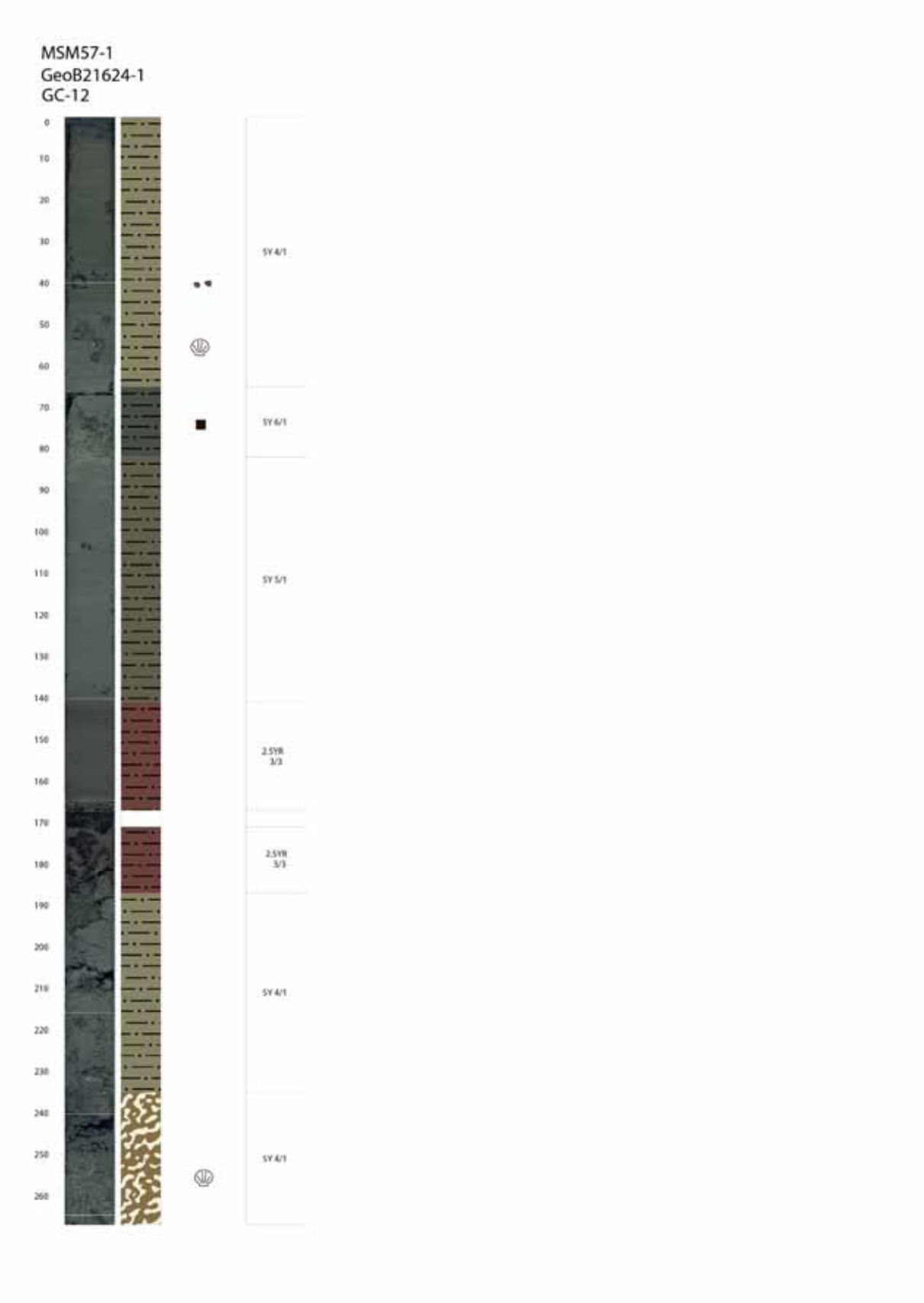

Appendix 3: Core Descriptions Gravity Cores continued

MSM57-2
GeoB21630-1
GC-13

Core Length: 198 cm

Appendix 3: Core Descriptions Gravity Cores continued

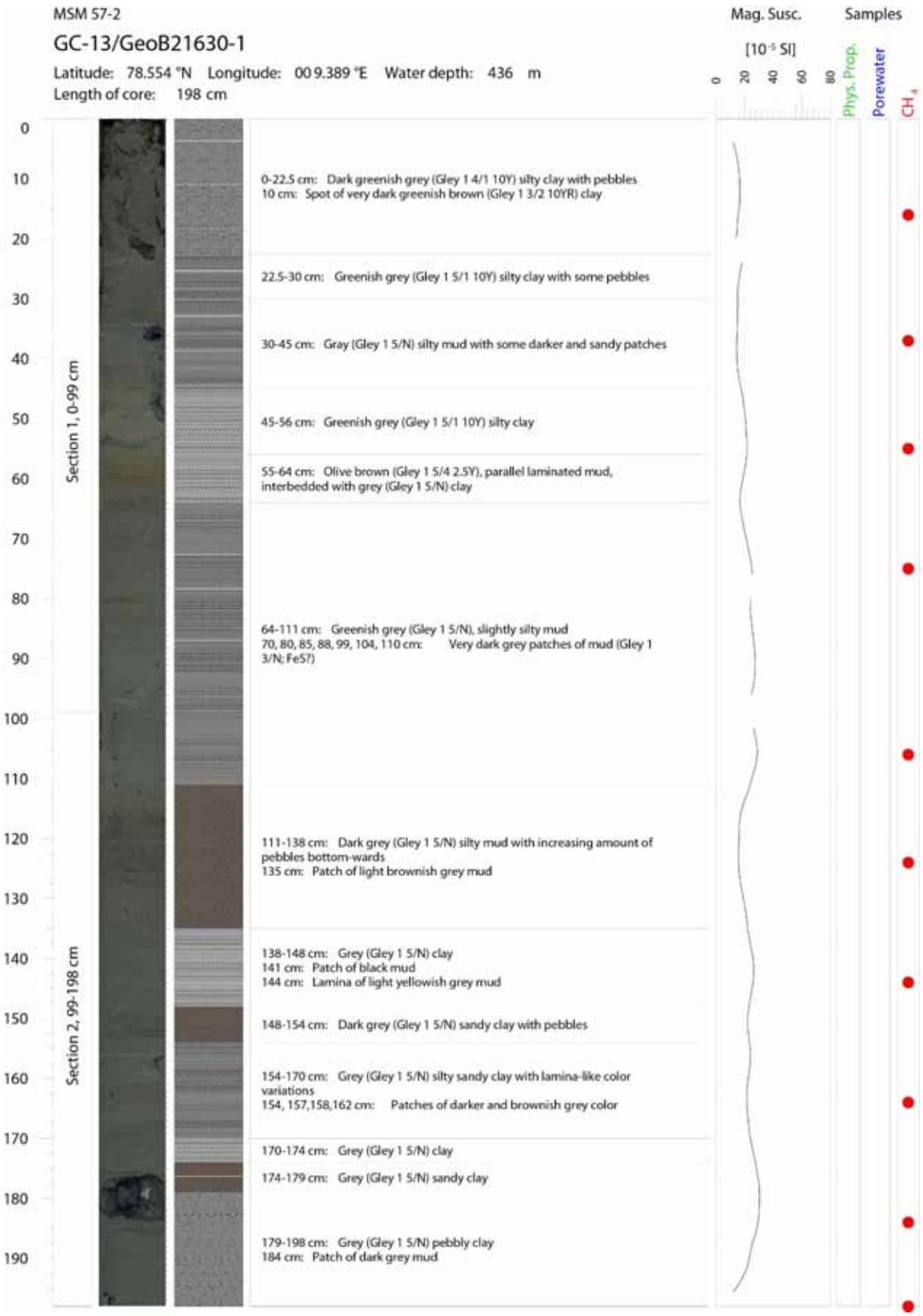

Appendix 3: Core Descriptions Gravity Cores continued

Appendix 3: Core Descriptions Gravity Cores continued

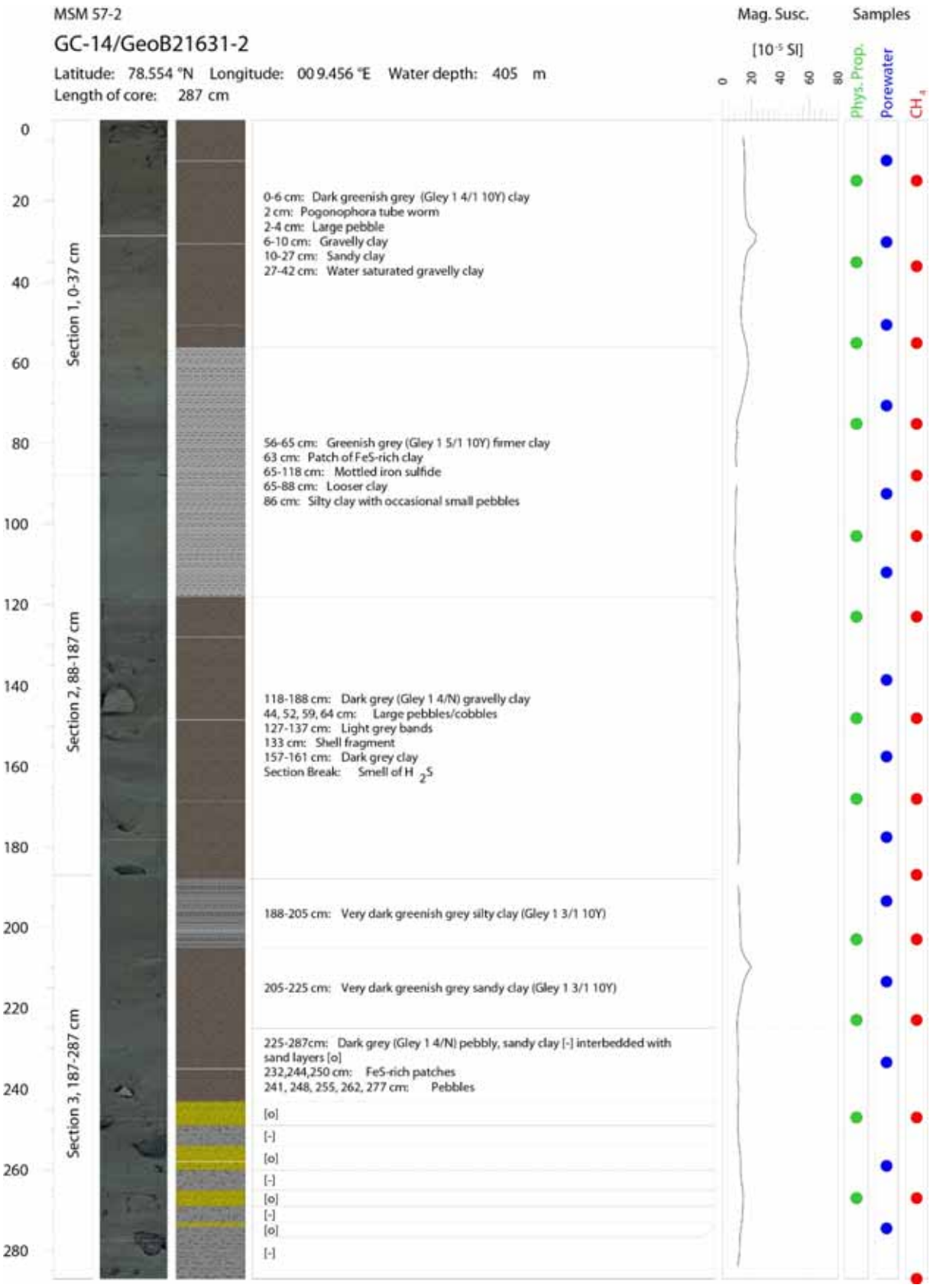

Appendix 3: Core Descriptions Gravity Cores continued

Appendix 3: Core Descriptions Gravity Cores continued

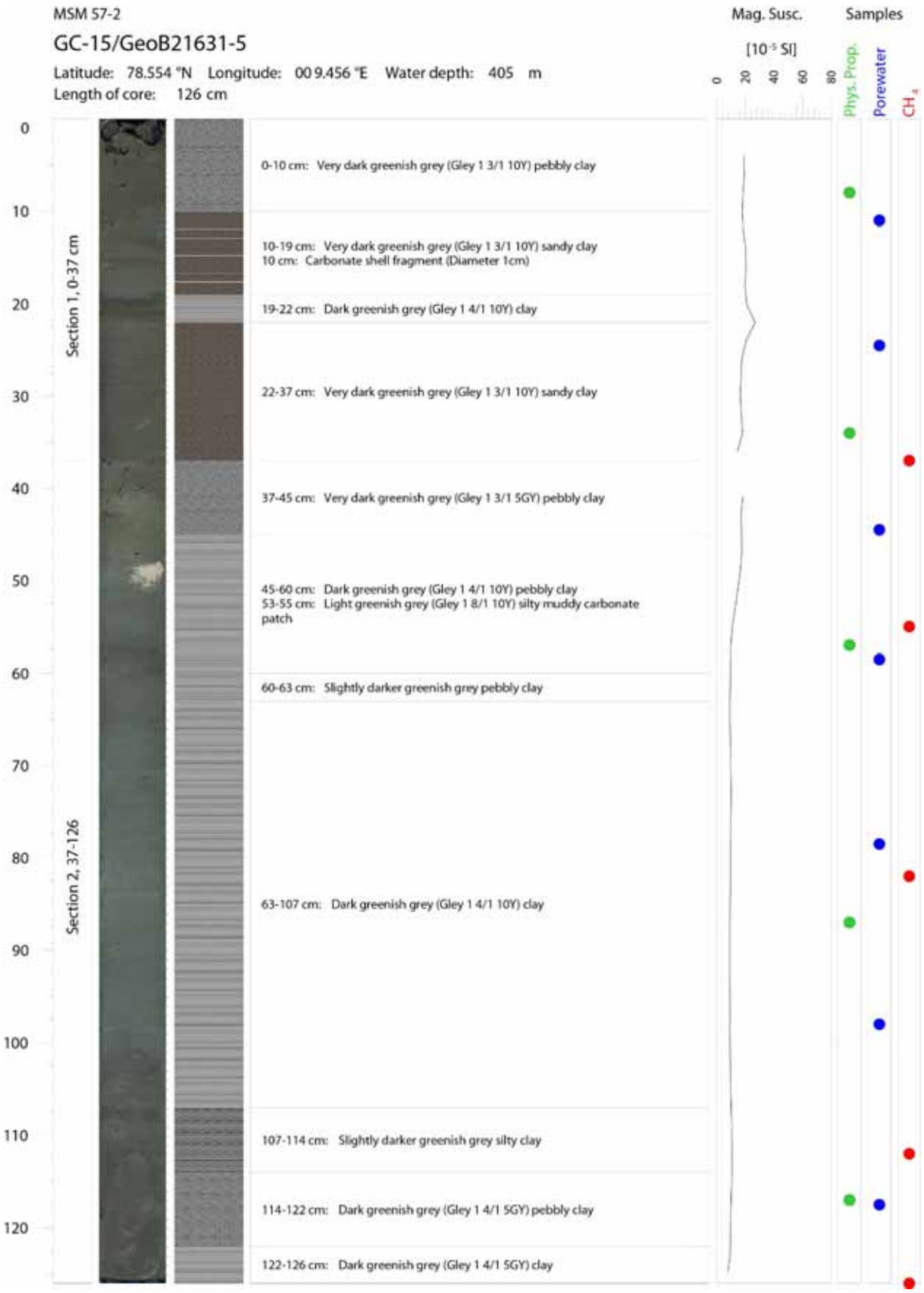

Appendix 3: Core Descriptions Gravity Cores continued

MSM57-2
GeoB21633-2
GC-16

Core Length: 250 cm

Appendix 3: Core Descriptions Gravity Cores continued

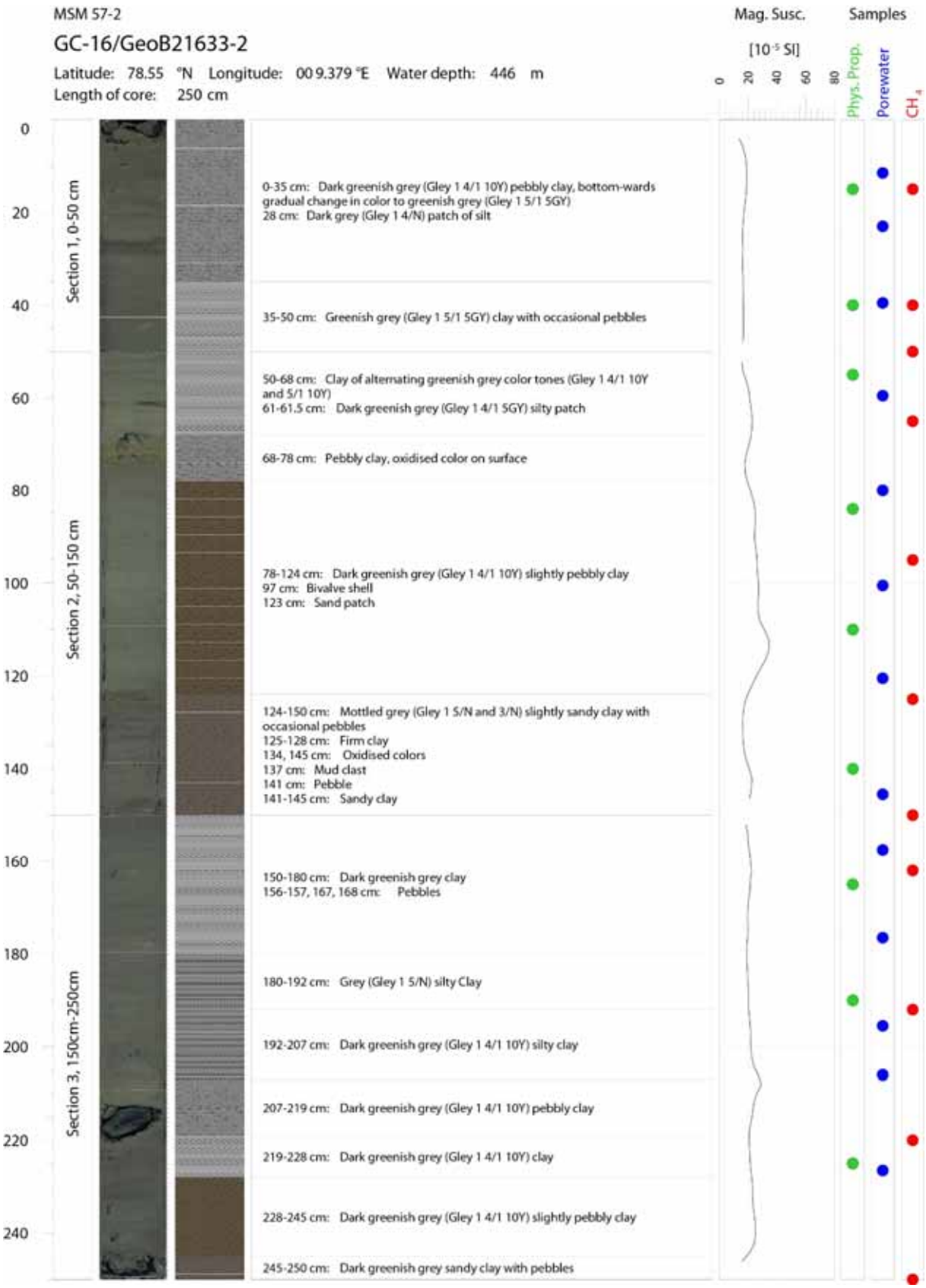

Appendix 3: Core Descriptions Gravity Cores continued

Appendix 3: Core Descriptions Gravity Cores continued

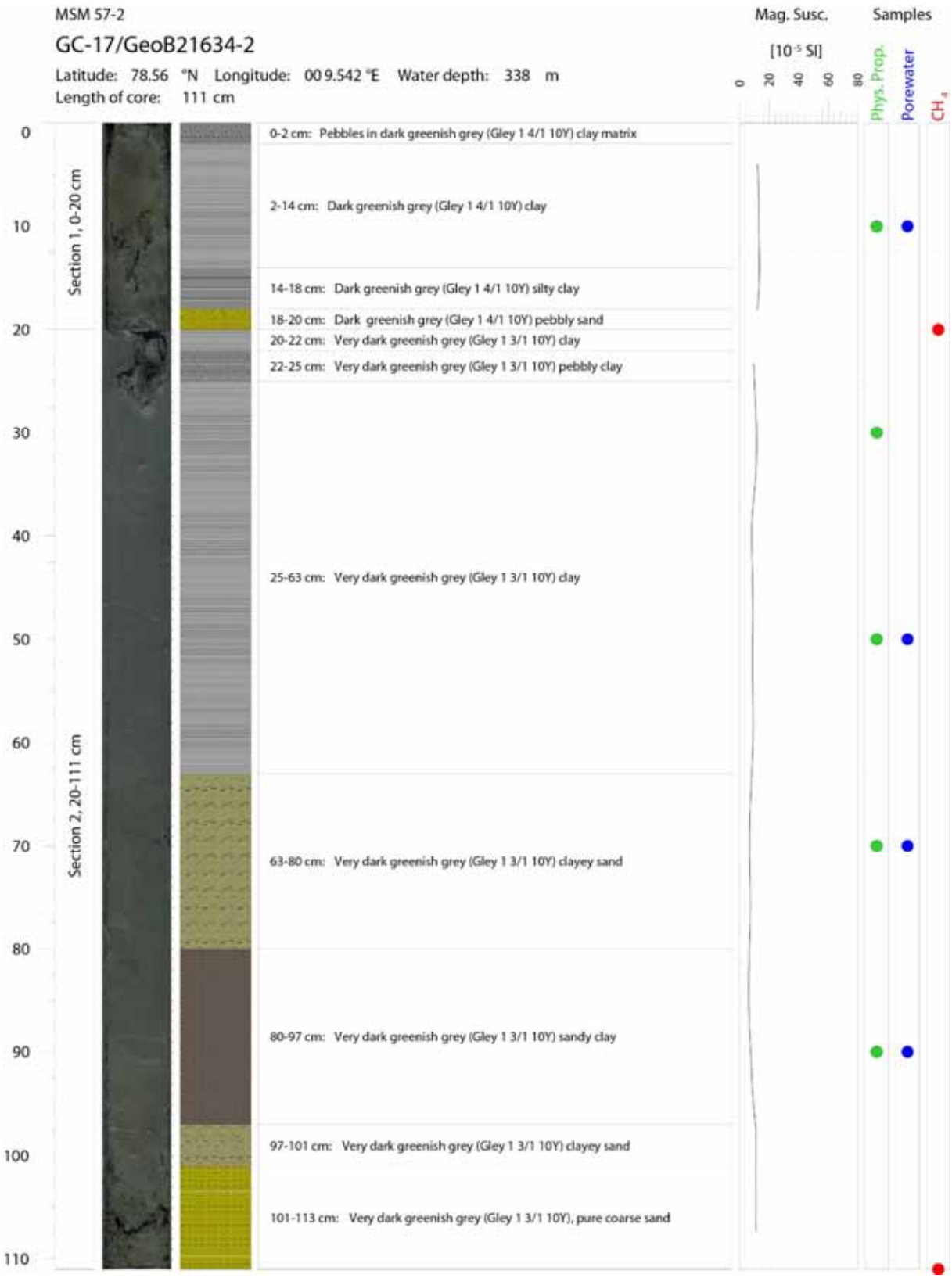

Appendix 3: Core Descriptions Gravity Cores continued

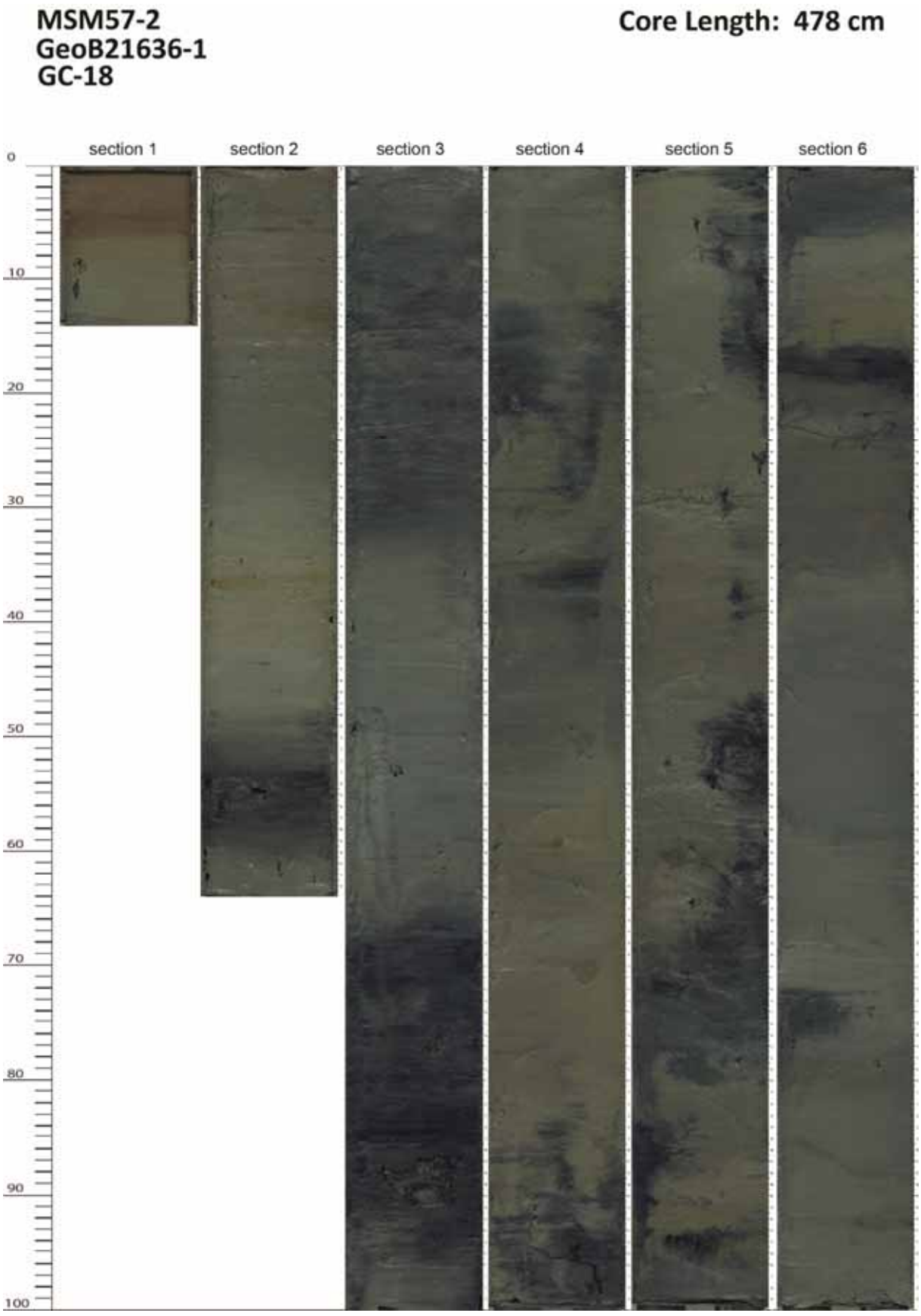

Appendix 3: Core Descriptions Gravity Cores continued

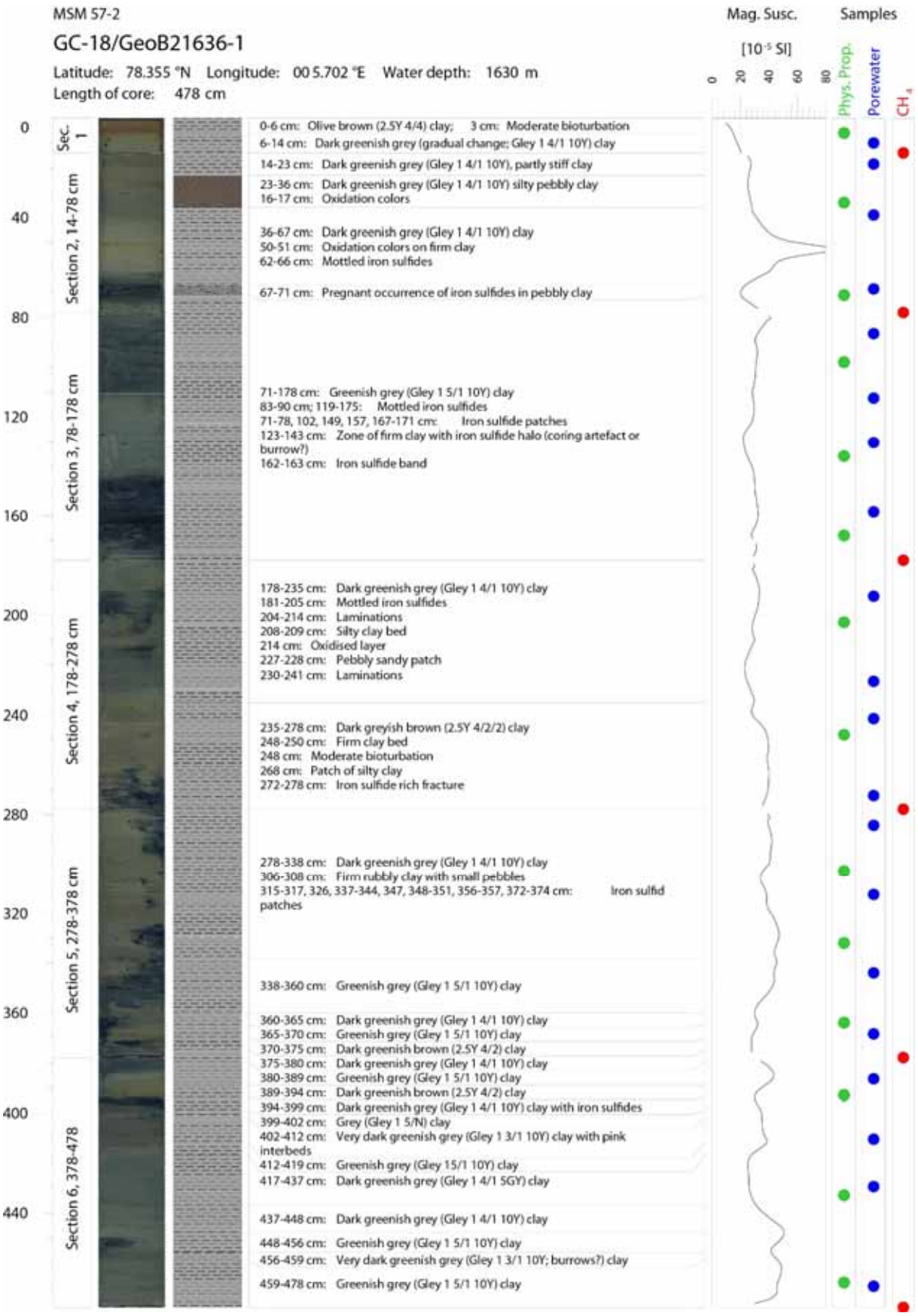

Appendix 3: Core Descriptions Gravity Cores continued

MSM 57-2

Samples

GC-19/GeoB21638-1

Latitude: 79.007°N **Longitude:** 006.911°E **Water depth:** 1212 m
Length of core: 250 cm

Hydrate

0
20
40
60
80
100
120
140
160
180
200
220
240

GeoB21638-1 (0-250cm): Core taken without a hard plastic liner in a plastic bag and split on deck

The gravity core GC-19/GeoB21638-1 was taken in a plastic bag liner.

Abundant gas hydrates were found as layers or likewise beds and veins.
Clayey homogenous sediments with very rare dropstones, one single dropstone was found at the bottom.

The core recovery was about 250 cm.

Images by Christopher Schmidt and Chieh Wei Hsu.

Multiple hydrate samples were taken and stored in a container cooled by liquid nitrogen.

Appendix 3: Core Descriptions Gravity Cores continued

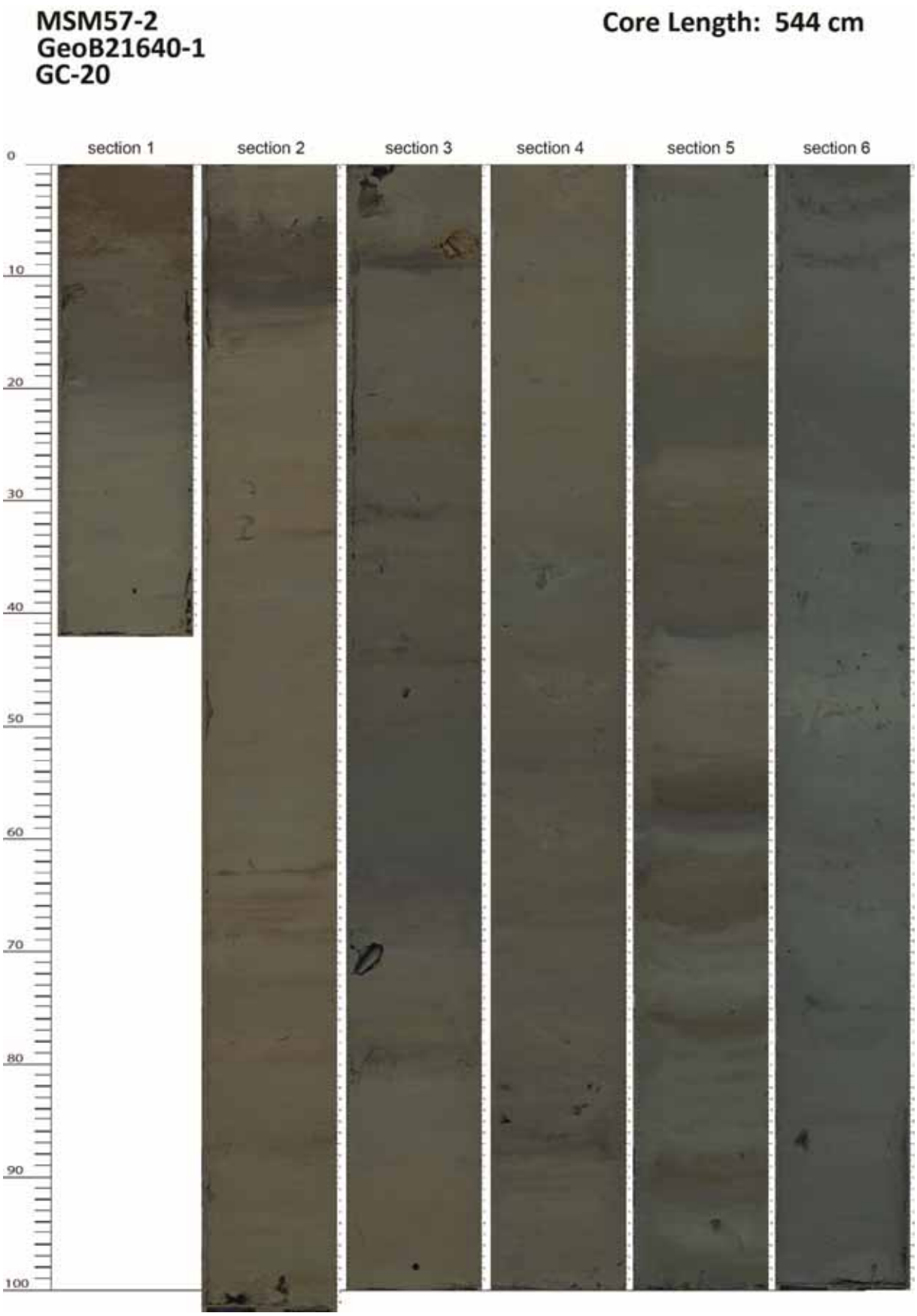

Appendix 3: Core Descriptions Gravity Cores continued

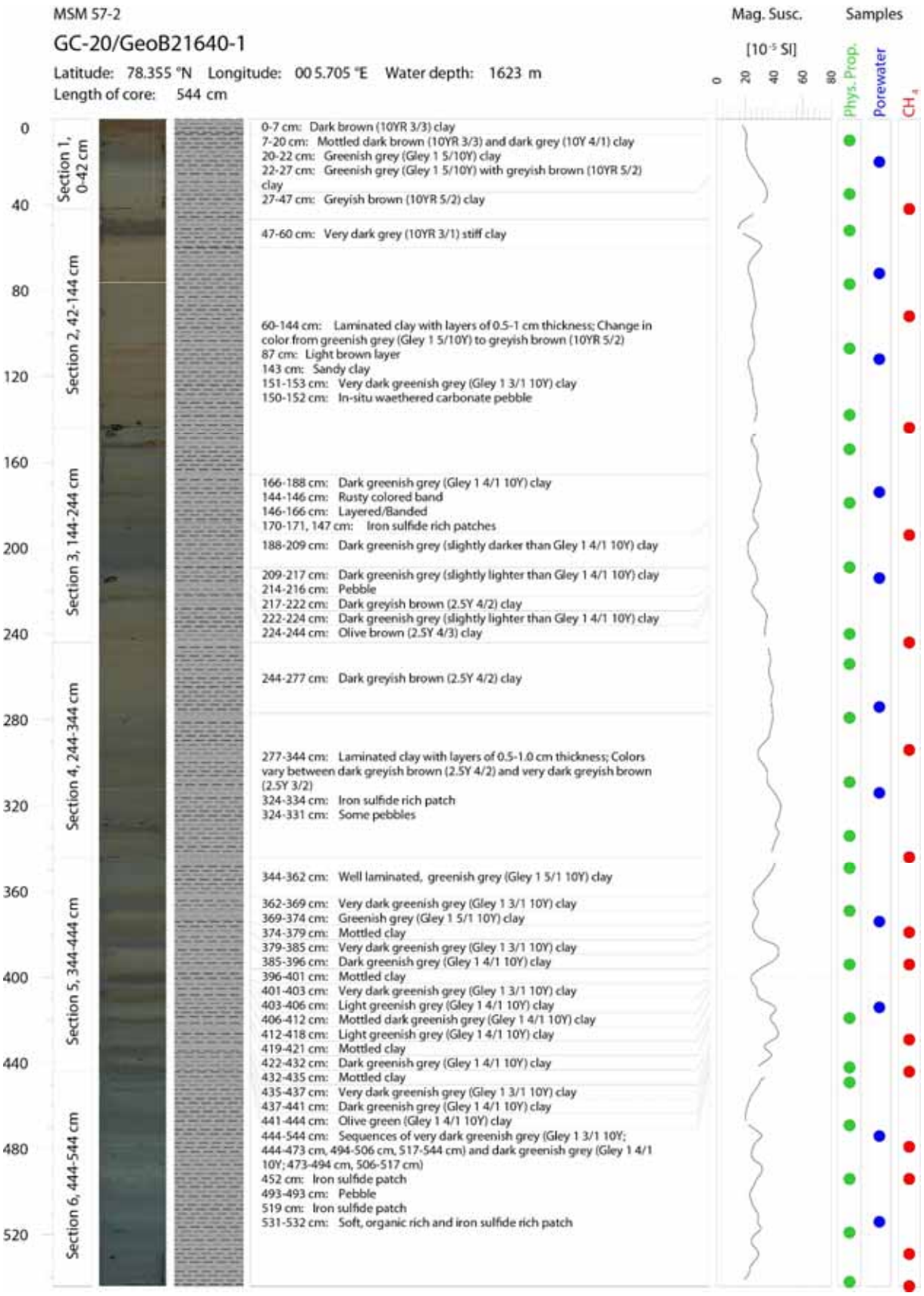

Appendix 3: Core Descriptions Gravity Cores continued

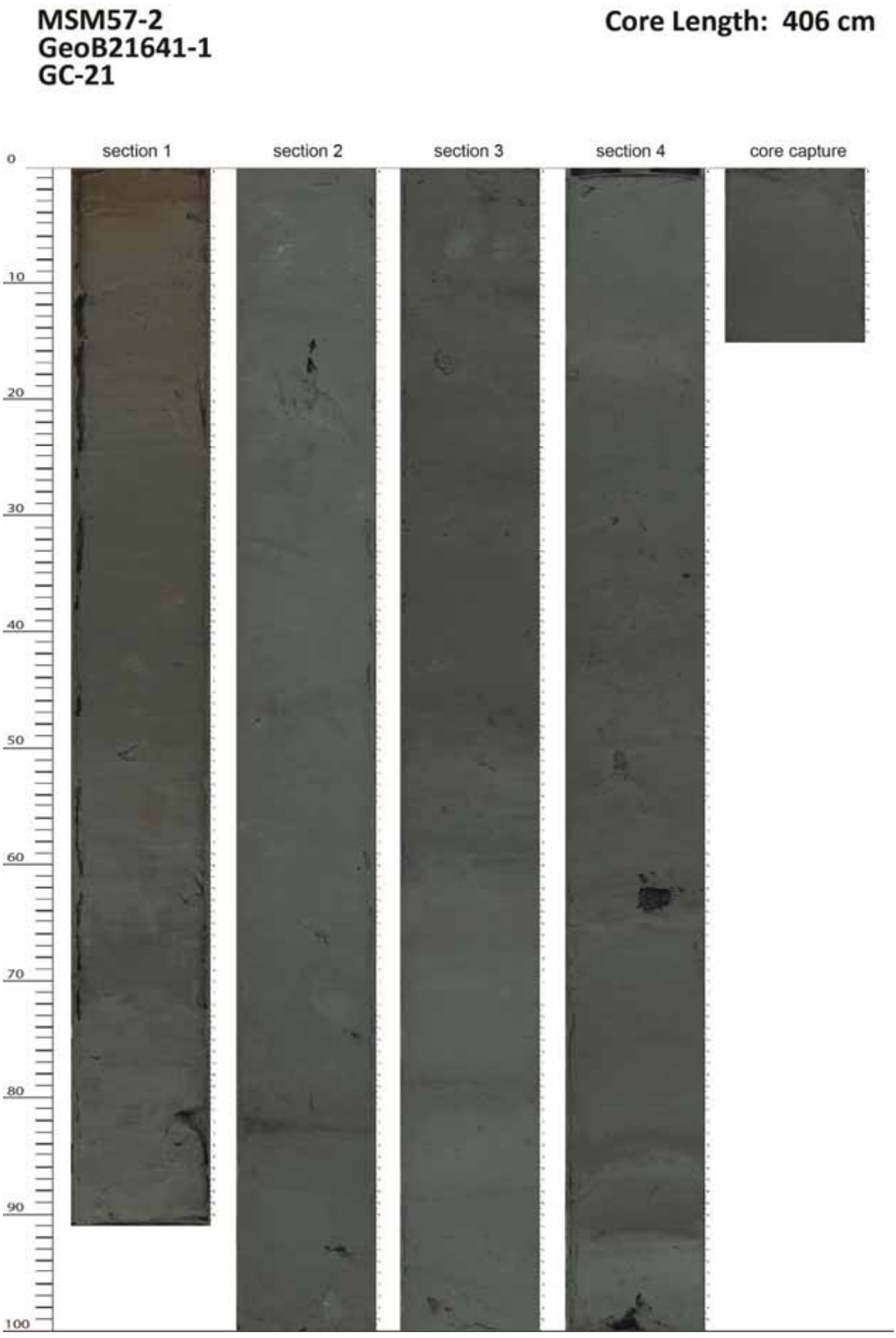

Appendix 3: Core Descriptions Gravity Cores continued

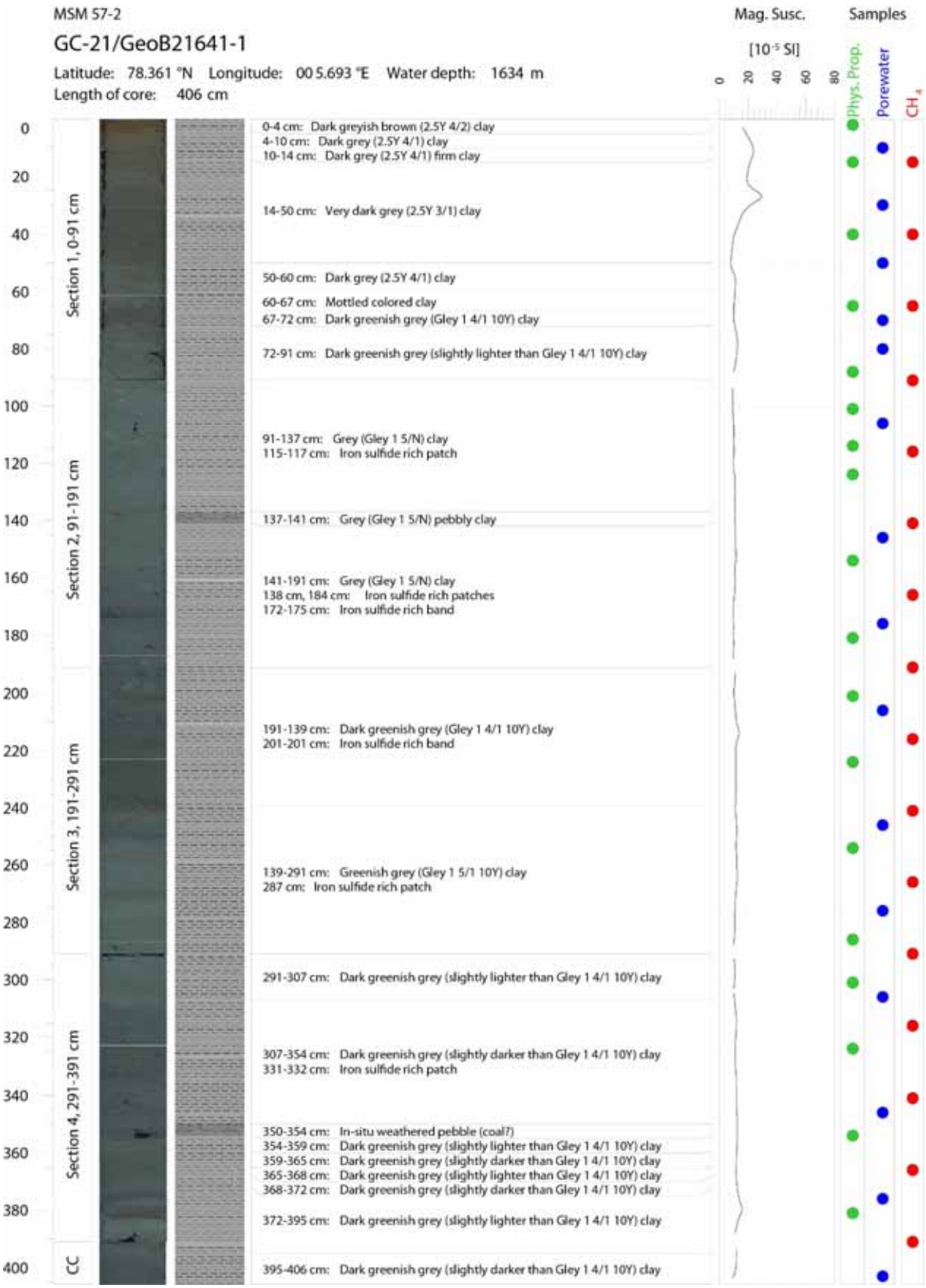

Appendix 3: Core Descriptions Gravity Cores continued

Appendix 3: Core Descriptions Gravity Cores continued

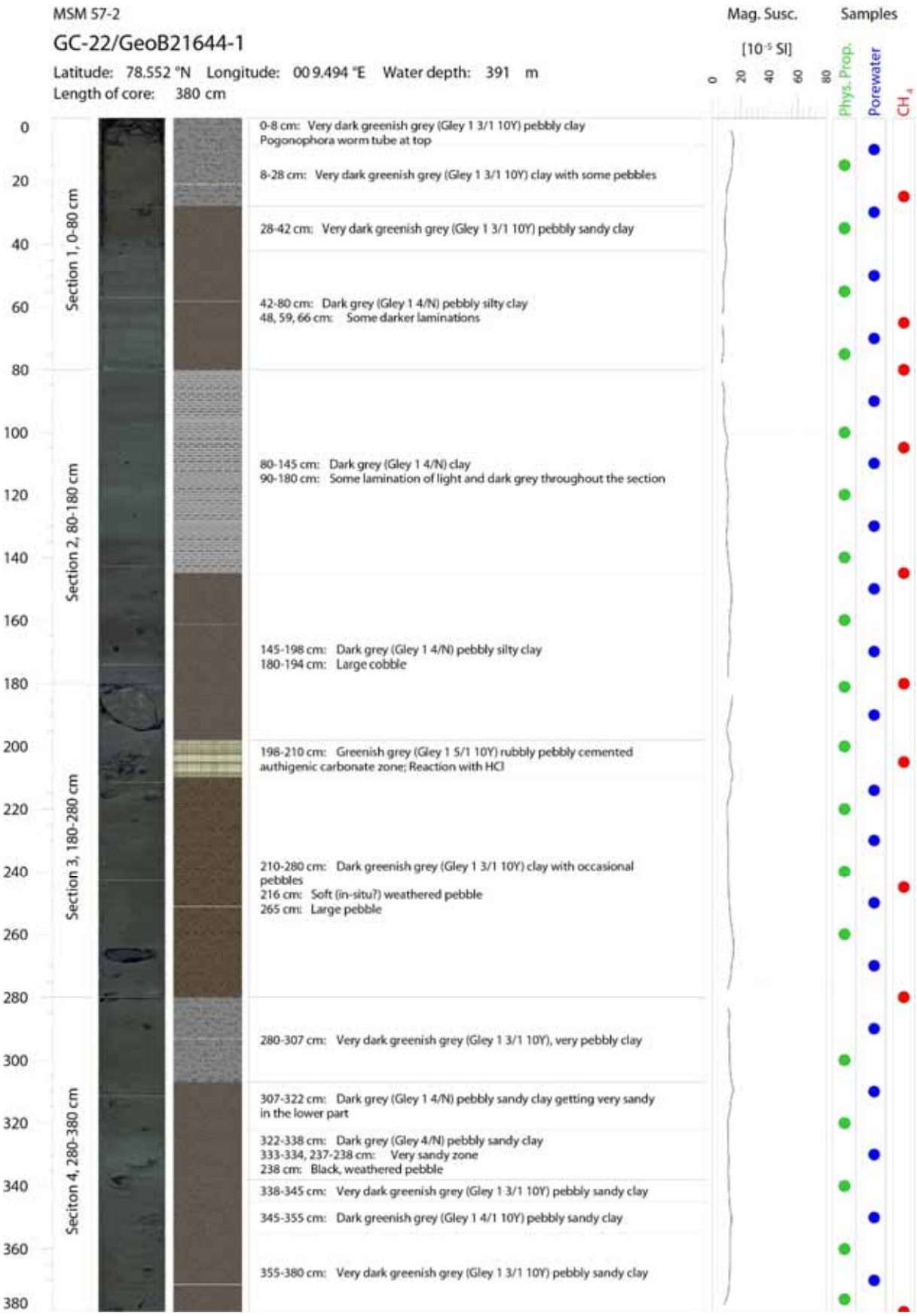

Appendix 3: Core Descriptions Gravity Cores continued

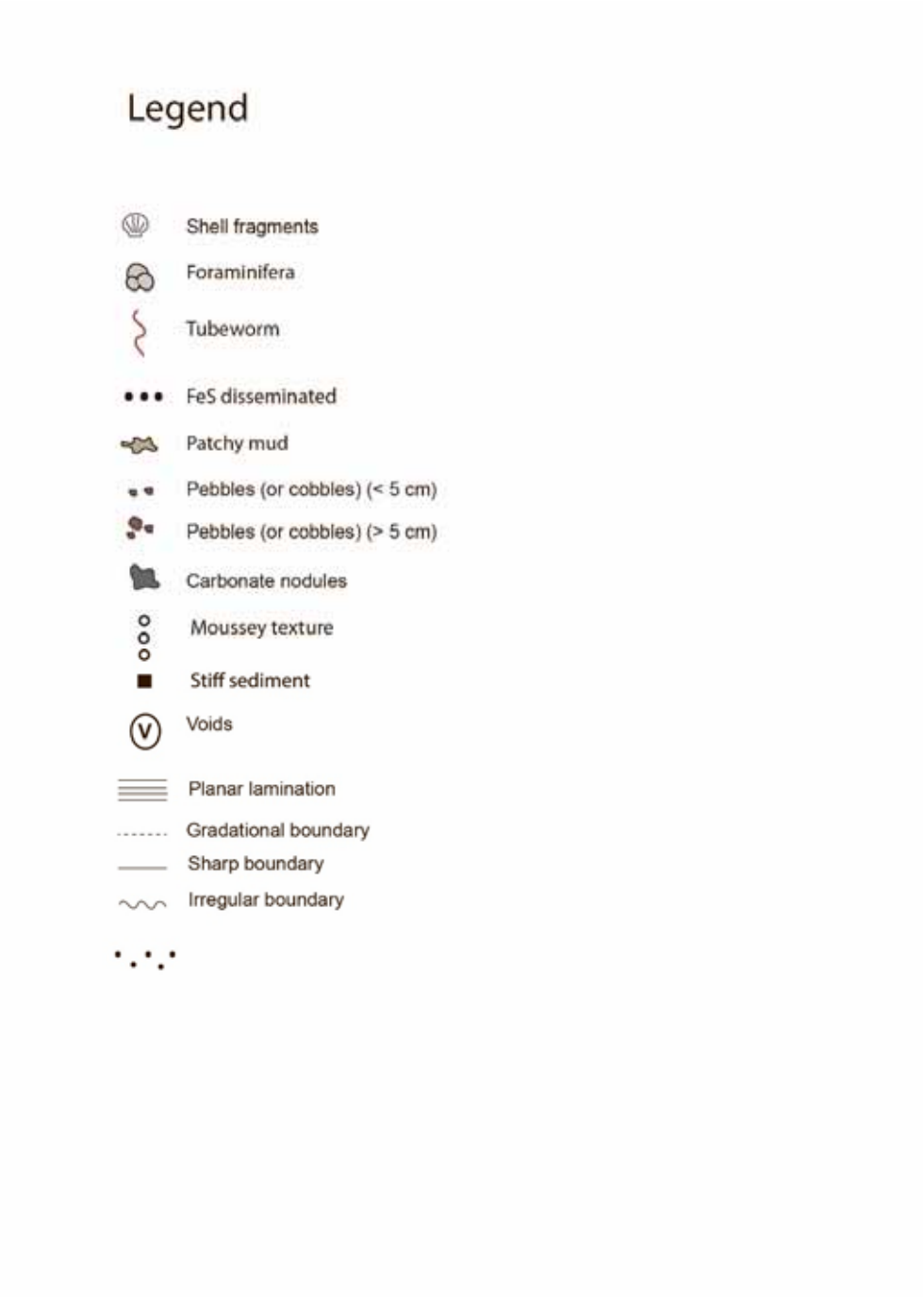

18.4 Appendix 4: Core Descriptions MeBo

MSM57-1
GeoB21604-1
MeBo123

Total Drilled Length: 280 cm
Total Cored Length: 100 cm

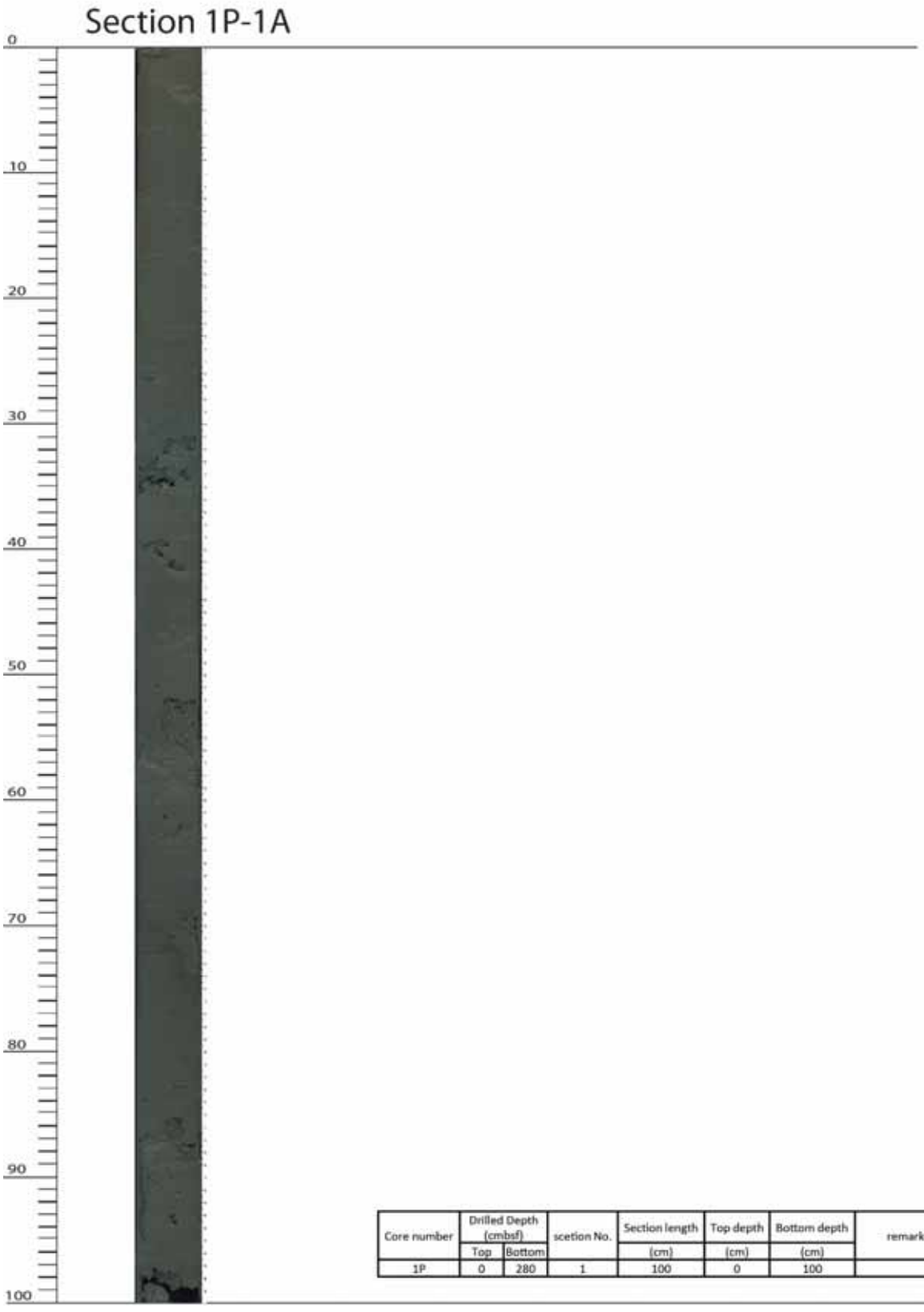

Core number	Drilled Depth (cmbsf)		scetion No.	Section length	Top depth	Bottom depth	remark
	Top	Bottom		(cm)	(cm)	(cm)	
1P	0	280	1	100	0	100	

Appendix 4: Core Descriptions MeBo continued

MSM57-1
GeoB21608-1
MeBo124

Total Drilled Length: 530 cm
Cored Recovery: 161 cm

Core number	Drilled Depth (cmbsf)		scetion No.	Section length	Top depth	Bottom depth	remark
	Top	Bottom		(cm)	(cm)	(cm)	
1P	0	280	1	67	0	67	
2P	280	530	1	94	280	374	

Appendix 4: Core Descriptions MeBo continued

MSM57-1
GeoB21610-1
MeBo125

Total Drilled Length: 2280 cm
Total Cored Length: 905 cm

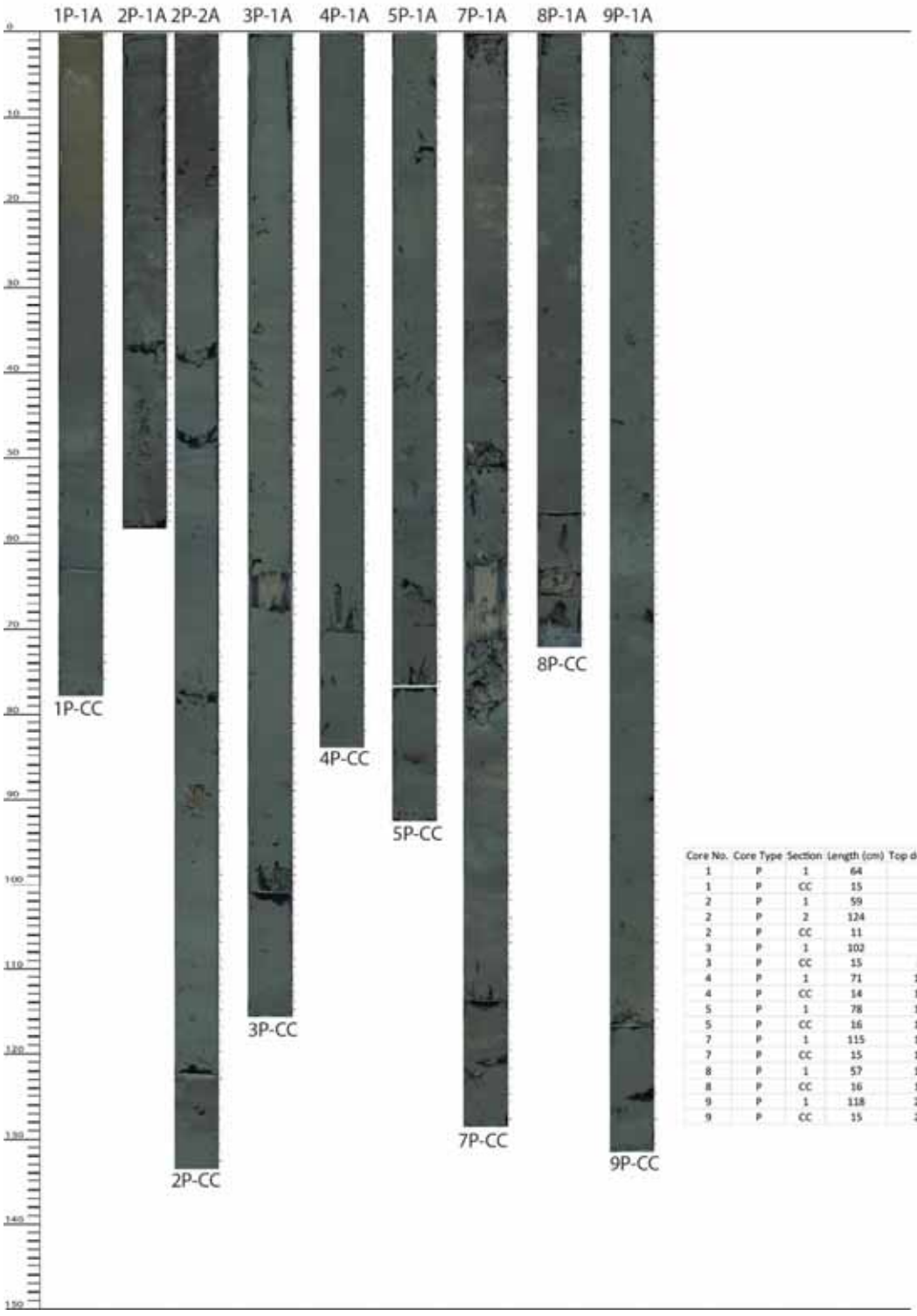

Core No.	Core Type	Section	Length (cm)	Top depth(cm)	bottom depth(cm)
1	P	1	64	0	64
1	P	CC	15	64	79
2	P	1	59	530	589
2	P	2	124	589	713
2	P	CC	11	713	724
3	P	1	102	780	882
3	P	CC	15	882	897
4	P	1	71	1030	1101
4	P	CC	14	1101	1115
5	P	1	78	1280	1358
5	P	CC	16	1358	1374
7	P	1	115	1540	1655
7	P	CC	15	1655	1670
8	P	1	57	1780	1837
8	P	CC	16	1837	1853
9	P	1	118	2030	2148
9	P	CC	15	2148	2163

Appendix 4: Core Descriptions MeBo continued

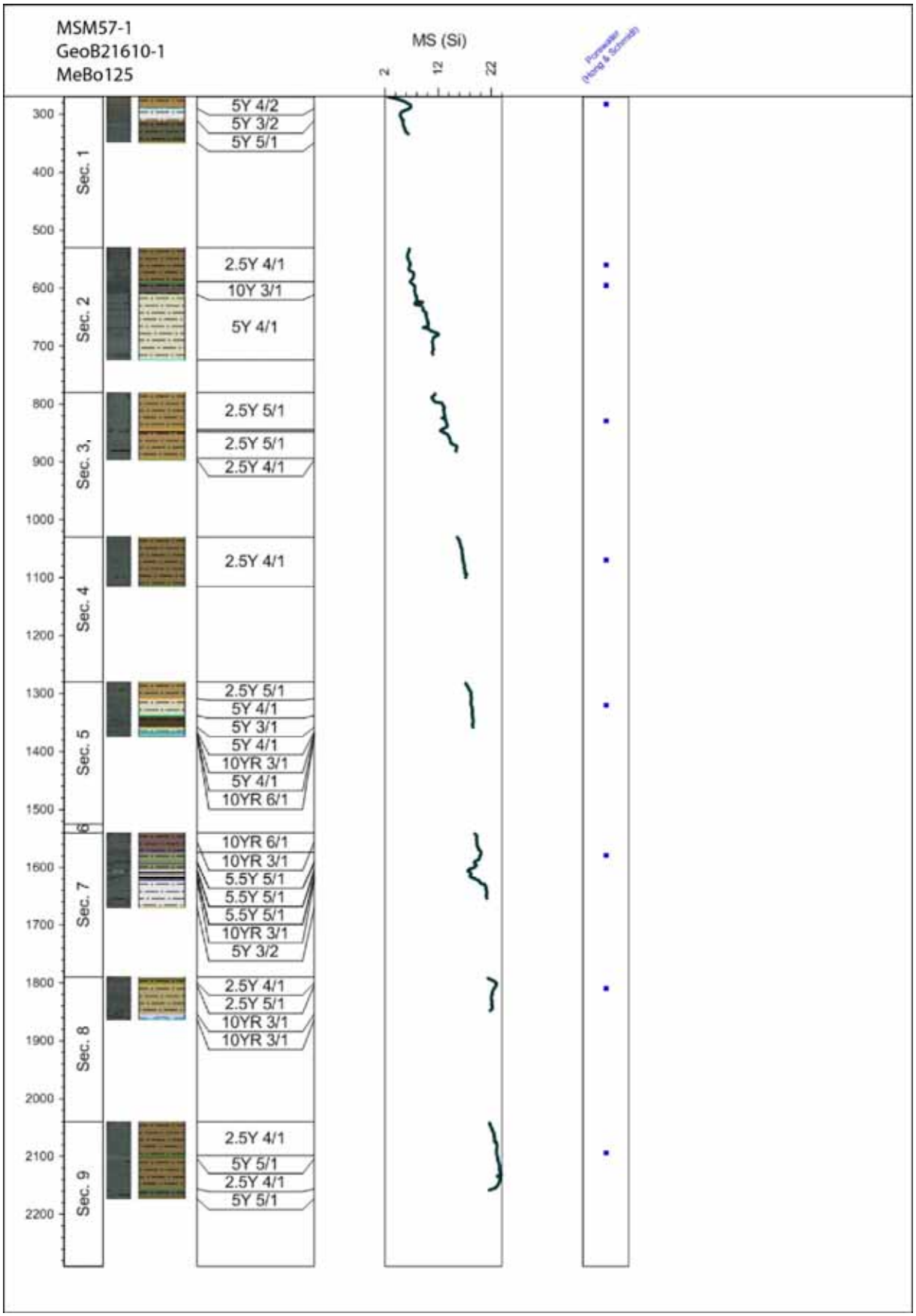

Appendix 4: Core Descriptions MeBo continued

MSM57-1
GeoB21613-1
MeBo126

Total Drilled Length: 6250 cm
Total Cored Length: 2465 cm

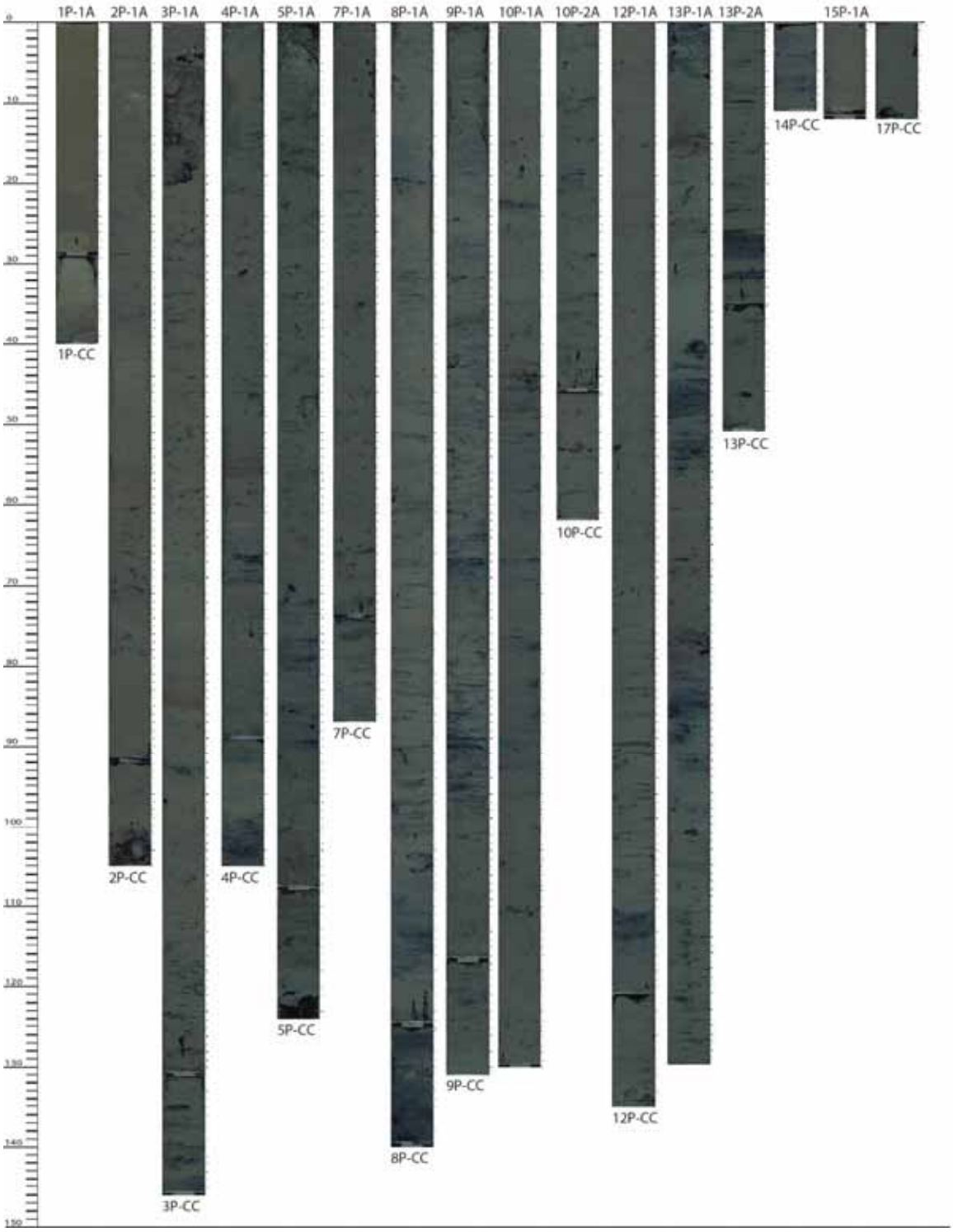

Appendix 4: Core Descriptions MeBo continued

MSM57-1

GeoB21613-1

MeBo126

Total Drilled Length: 6250 cm

Total Cored Length: 2465 cm

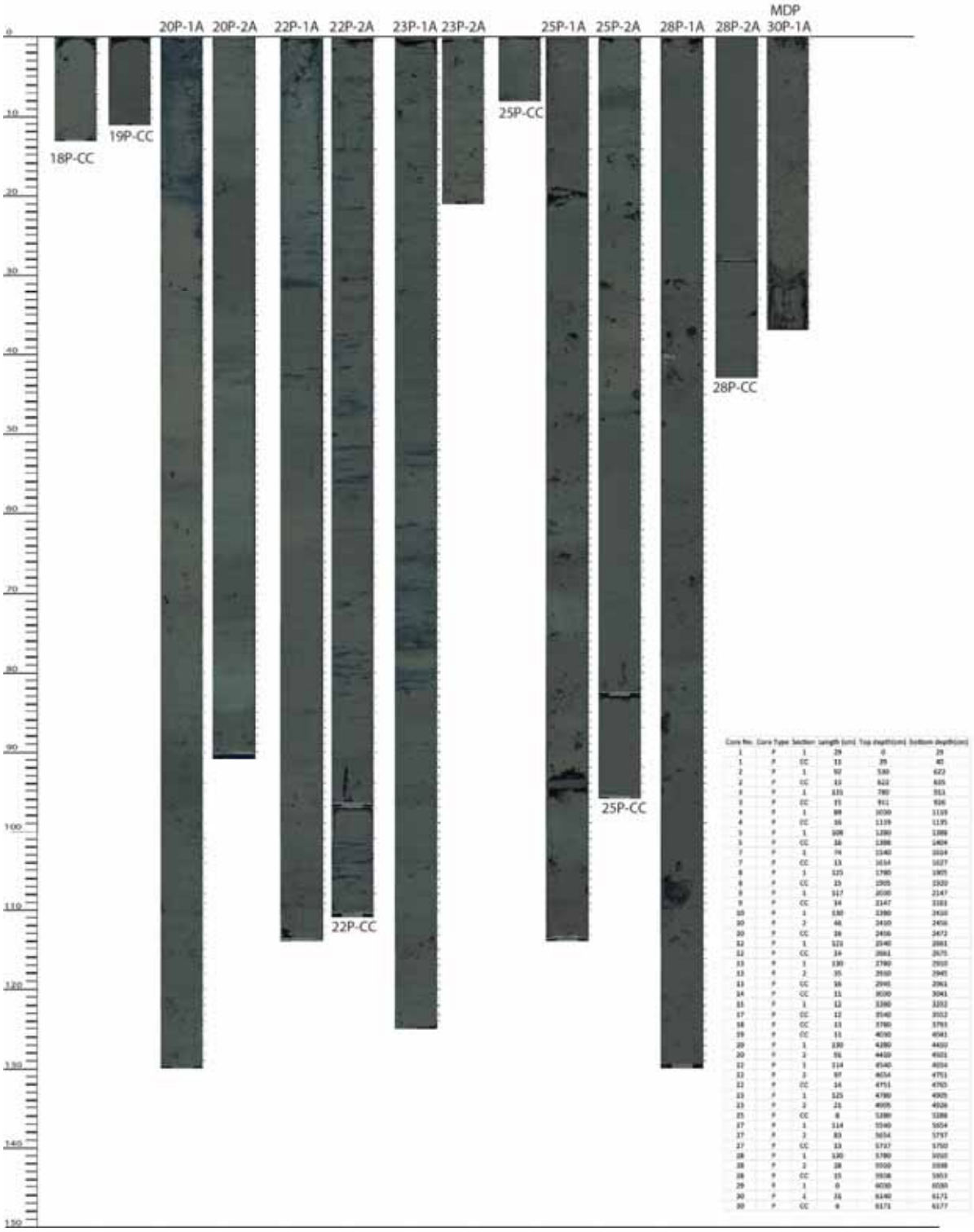

Appendix 4: Core Descriptions MeBo continued

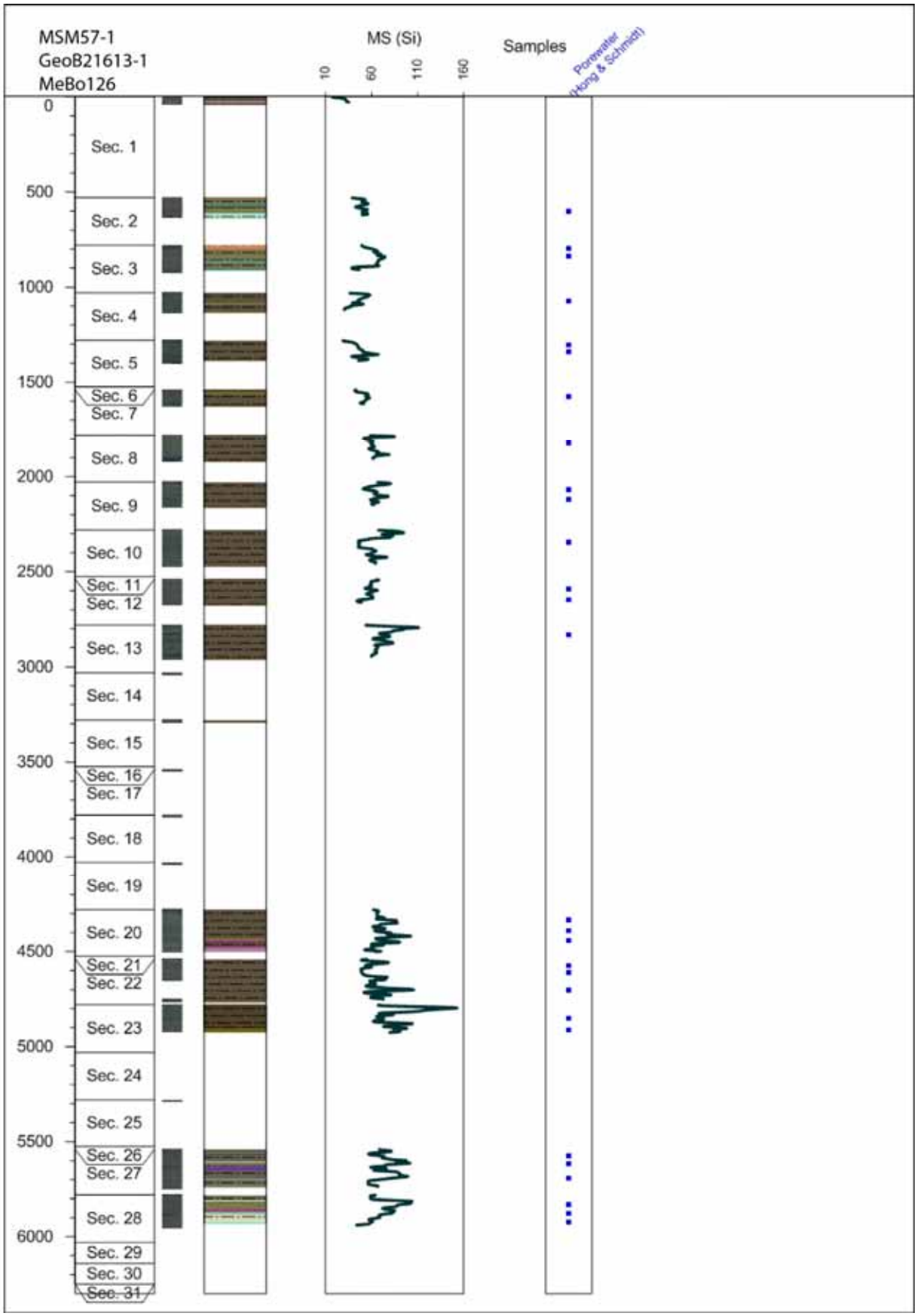

Appendix 4: Core Descriptions MeBo continued

MSM57-1
GeoB21616-1
MeBo127

Core no. :1, 2, 4, 5
Total core Length: 352 cm
Drilled depth: 0-1390 cm

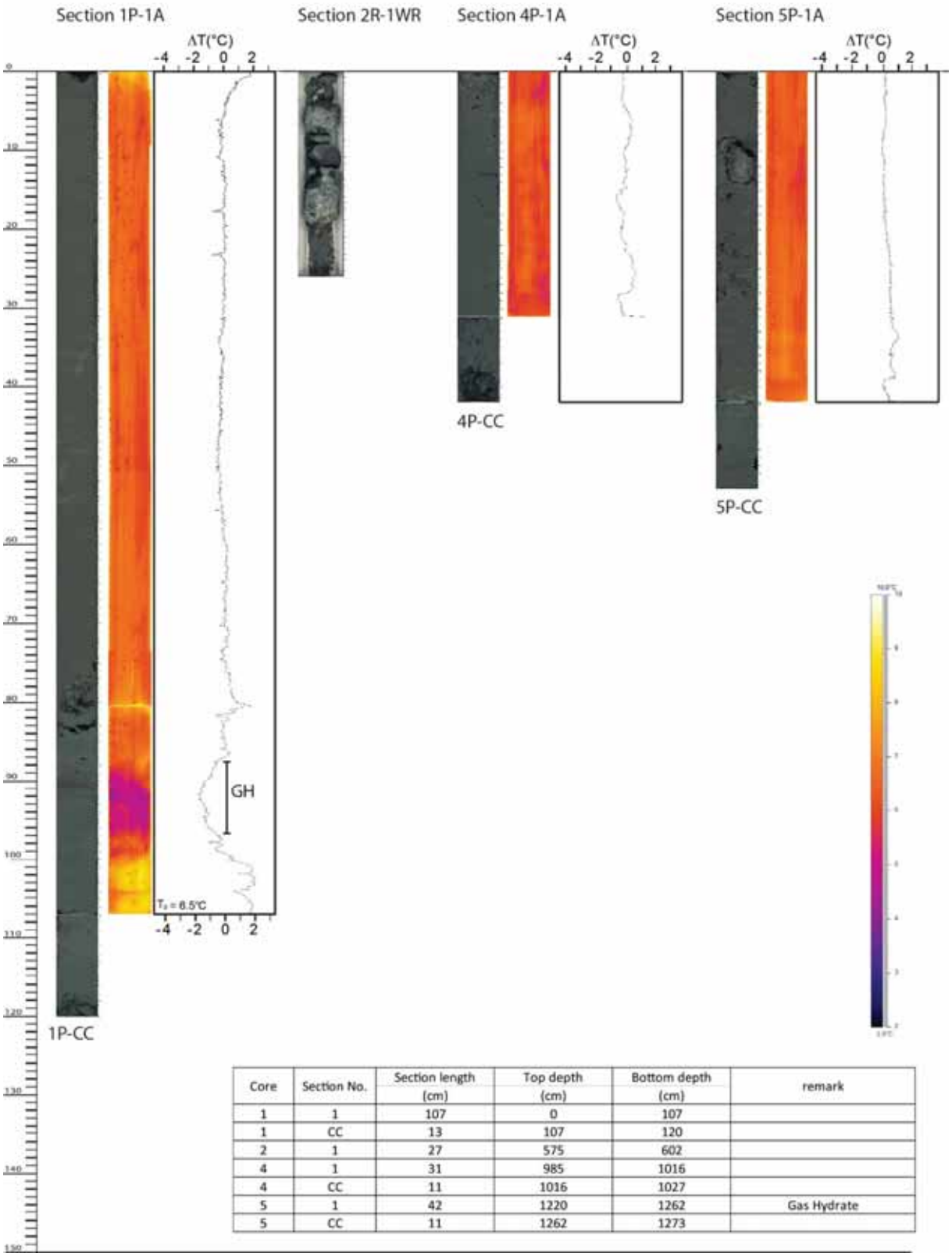

Core	Section No.	Section length (cm)	Top depth (cm)	Bottom depth (cm)	remark
1	1	107	0	107	
1	CC	13	107	120	
2	1	27	575	602	
4	1	31	985	1016	
4	CC	11	1016	1027	
5	1	42	1220	1262	Gas Hydrate
5	CC	11	1262	1273	

Appendix 4: Core Descriptions MeBo continued

MSM57-1
GeoB21621-1
MeBo128

Total Drilled Length: 755 cm
Total Cored Length: 447 cm

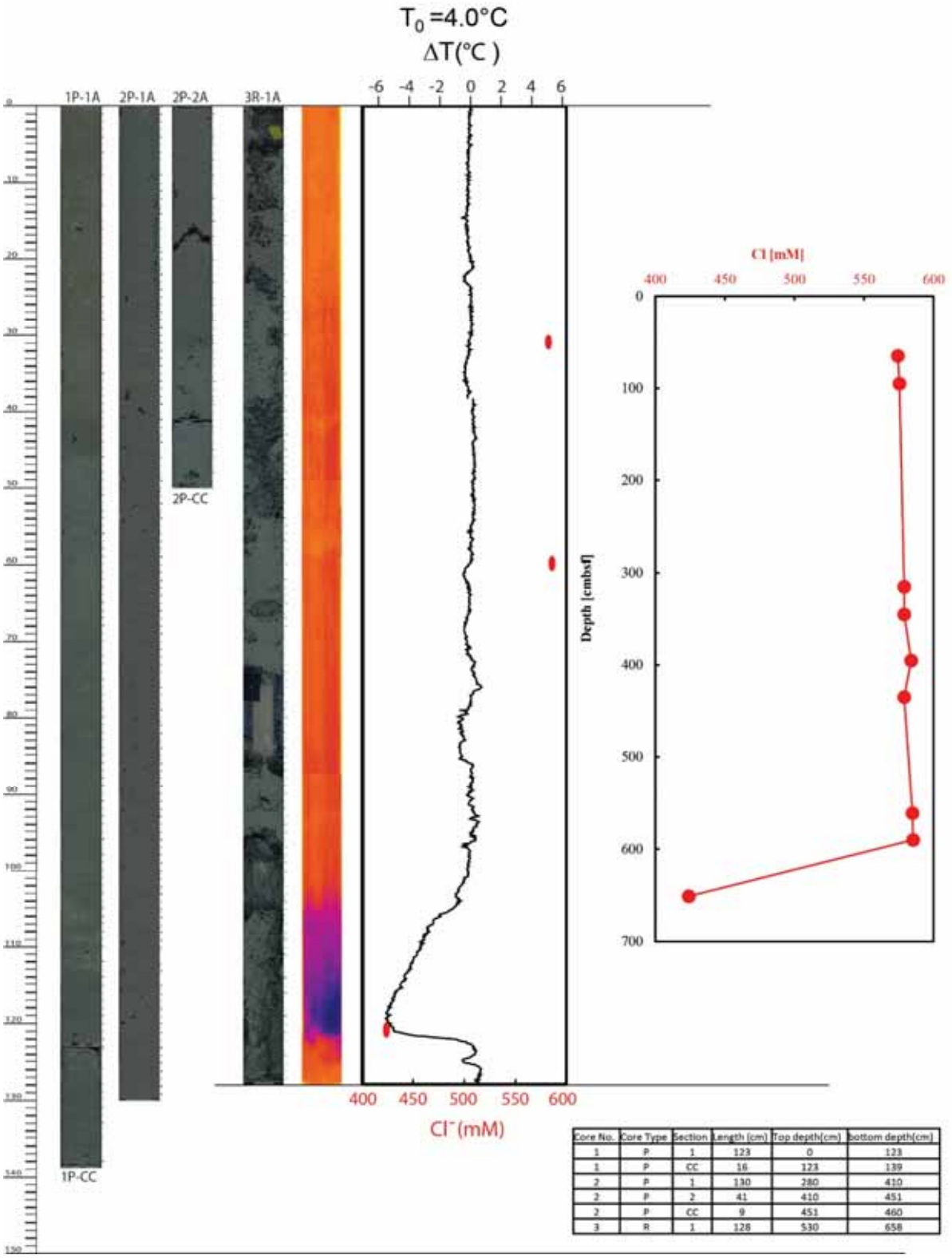

Core No.	Core Type	Section	Length (cm)	Top depth(cm)	Bottom depth(cm)
1	P	1	123	0	123
1	P	CC	16	123	139
2	P	1	130	280	410
2	P	2	41	410	451
2	P	CC	9	451	460
3	R	1	128	530	658

Appendix 4: Core Descriptions MeBo continued

MSM57-2
GeoB21626-1
MeBo129-1

Total Drilled Length: 2290 cm
Total Cored Length: 395 cm

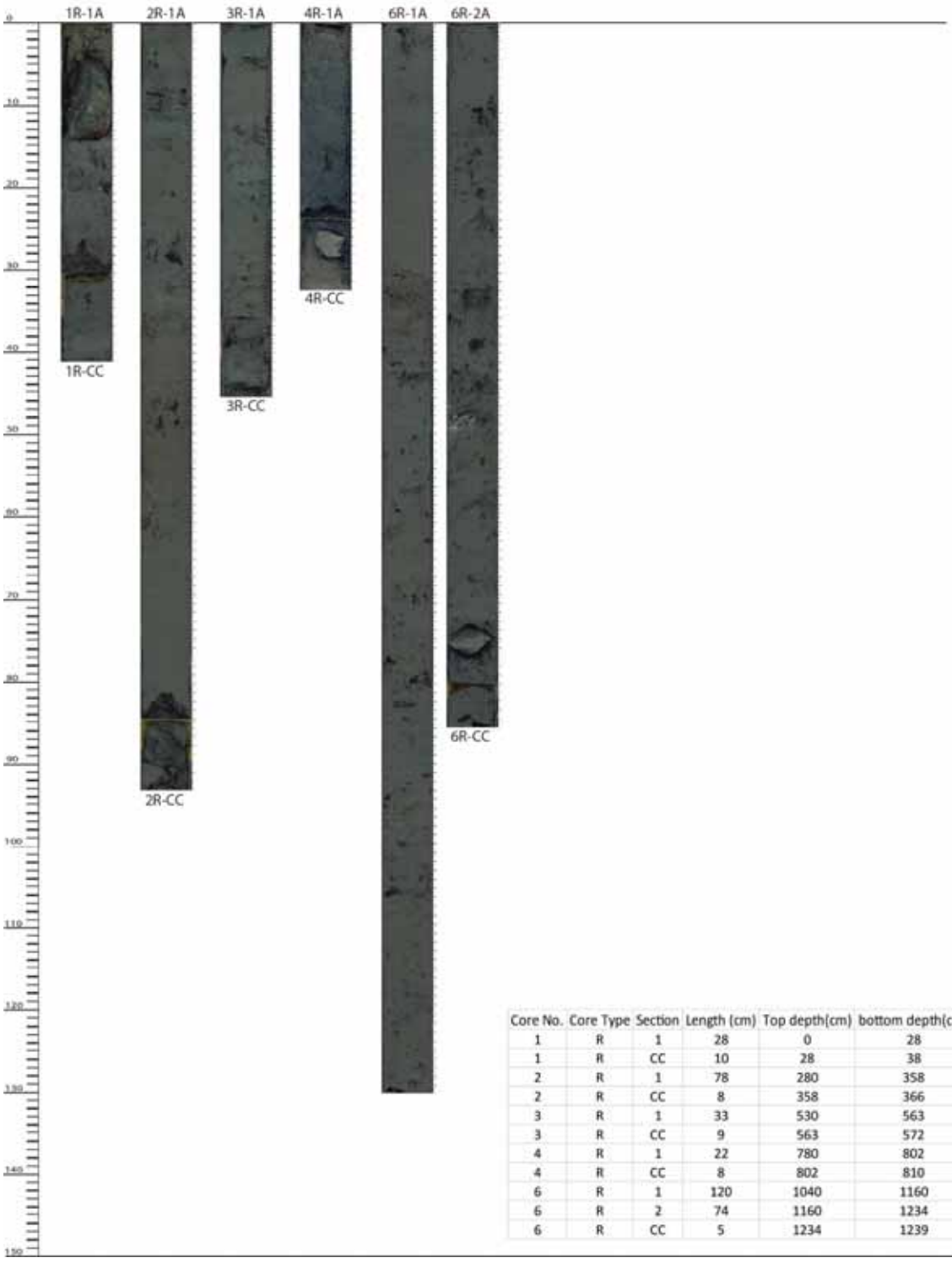

Core No.	Core Type	Section	Length (cm)	Top depth(cm)	bottom depth(cm)
1	R	1	28	0	28
1	R	CC	10	28	38
2	R	1	78	280	358
2	R	CC	8	358	366
3	R	1	33	530	563
3	R	CC	9	563	572
4	R	1	22	780	802
4	R	CC	8	802	810
6	R	1	120	1040	1160
6	R	2	74	1160	1234
6	R	CC	5	1234	1239

Appendix 4: Core Descriptions MeBo continued

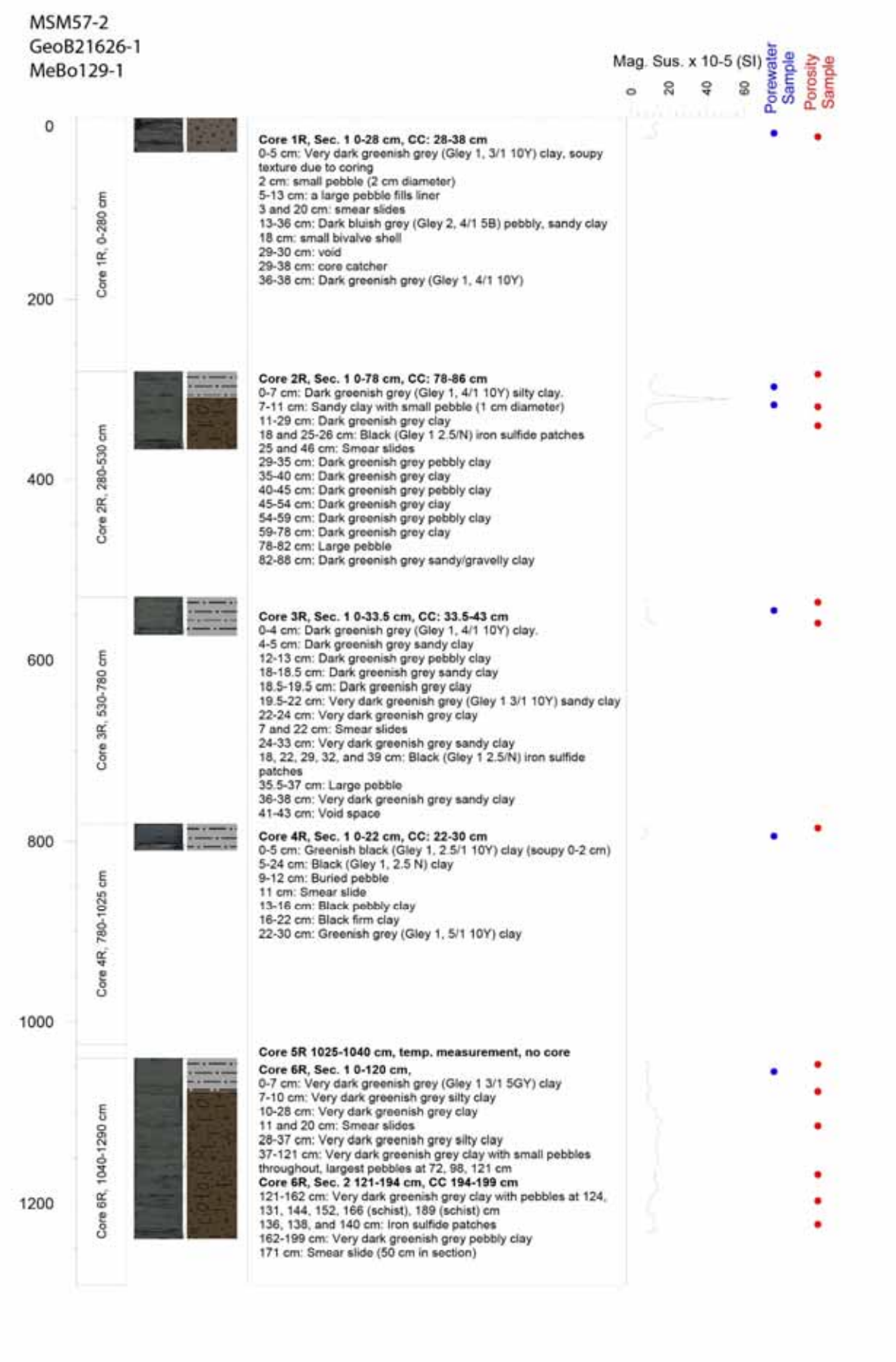

Appendix 4: Core Descriptions MeBo continued

MSM57-2
GeoB21626-2
MeBo129-2

Total Drilled Length: 2530 cm
Total Cored Length: 254 cm

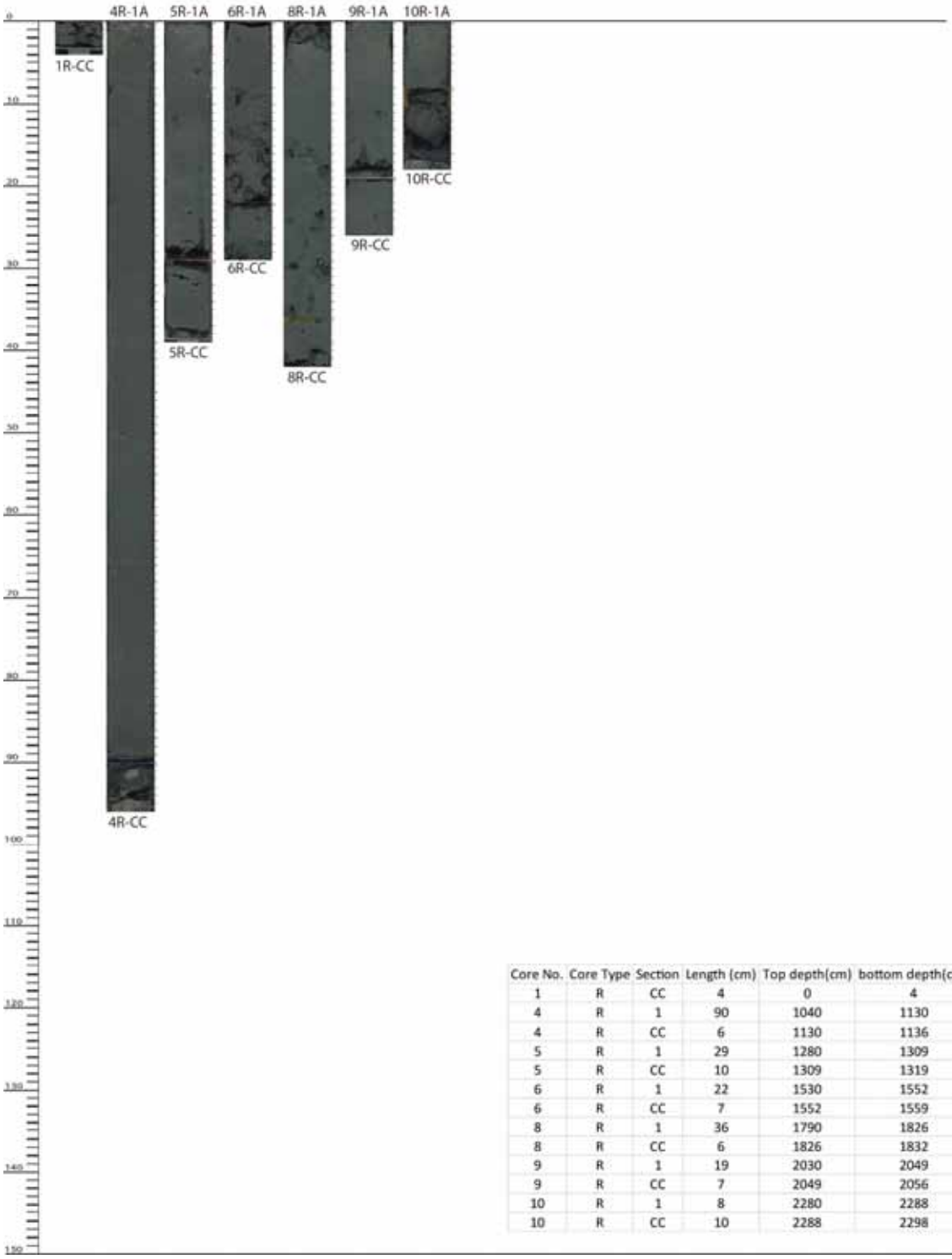

Core No.	Core Type	Section	Length (cm)	Top depth(cm)	bottom depth(cm)
1	R	CC	4	0	4
4	R	1	90	1040	1130
4	R	CC	6	1130	1136
5	R	1	29	1280	1309
5	R	CC	10	1309	1319
6	R	1	22	1530	1552
6	R	CC	7	1552	1559
8	R	1	36	1790	1826
8	R	CC	6	1826	1832
9	R	1	19	2030	2049
9	R	CC	7	2049	2056
10	R	1	8	2280	2288
10	R	CC	10	2288	2298

Appendix 4: Core Descriptions MeBo continued

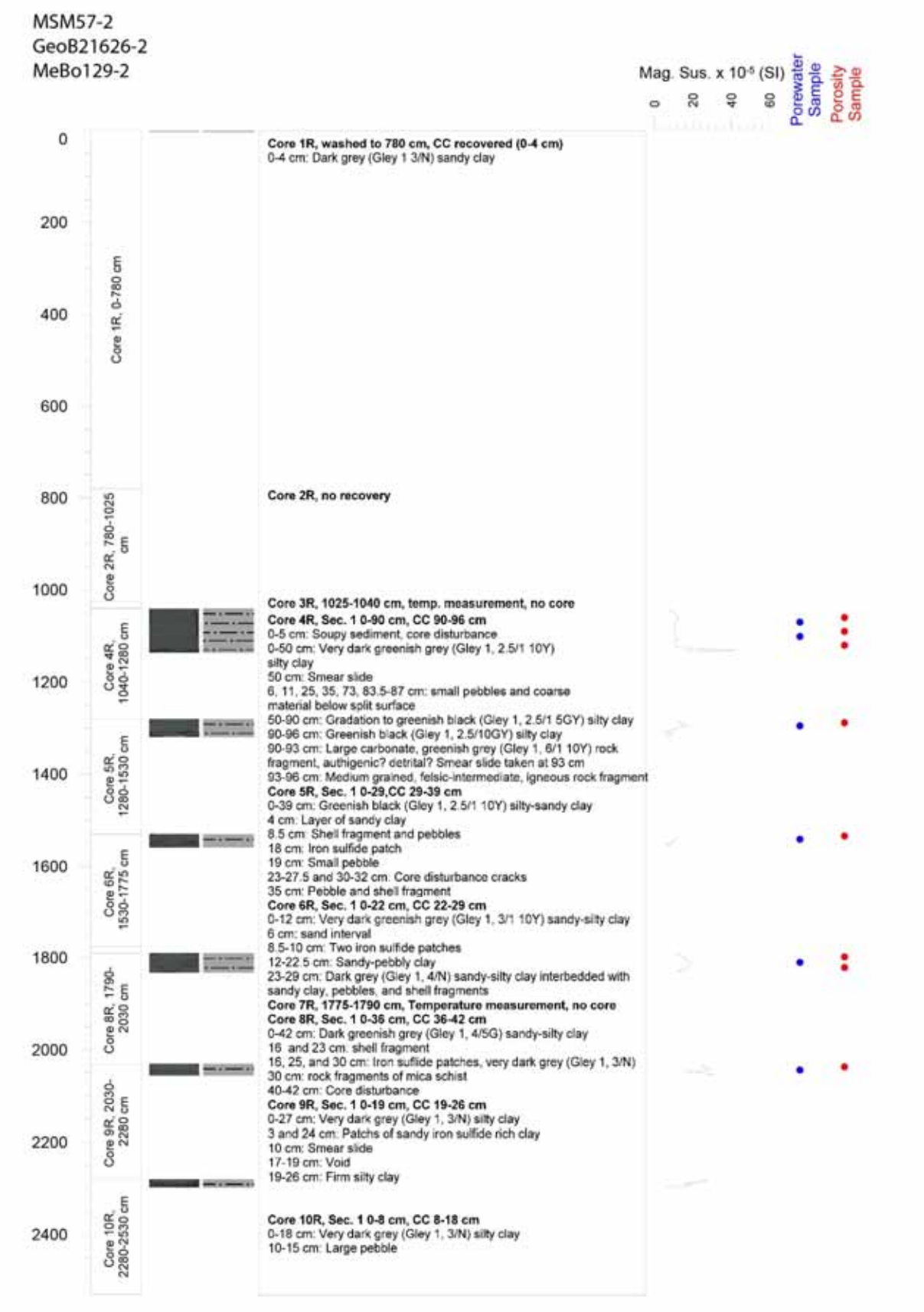

Appendix 4: Core Descriptions MeBo continued

MSM57-2
GeoB21631-1
MeBo130

Total Drilled Length: 1530 cm
Total Cored Length: 53 cm

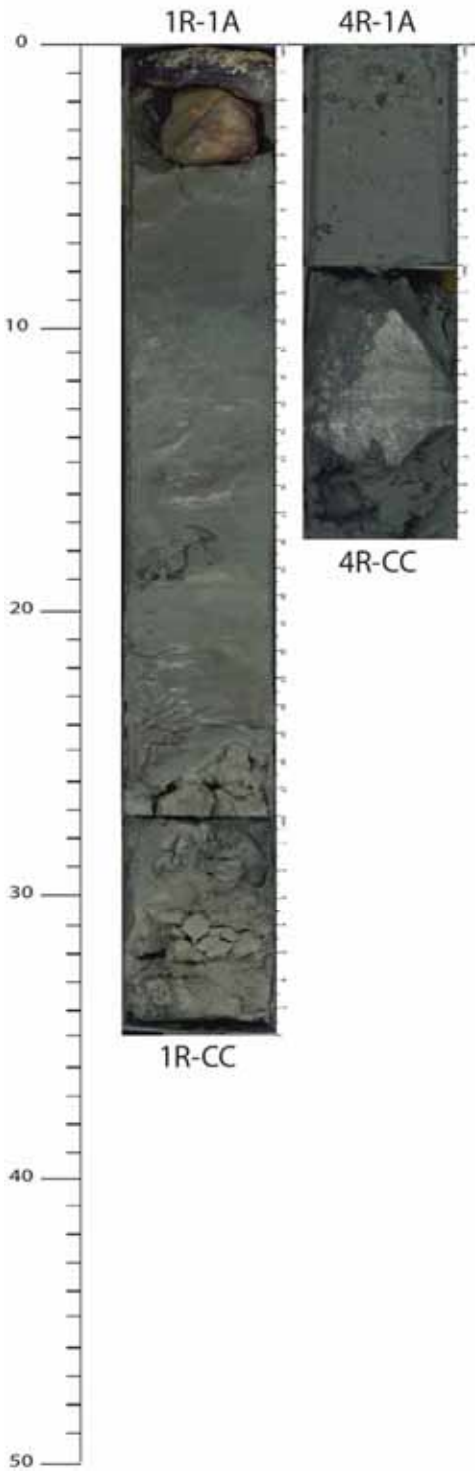

Core No.	Core Type	Section	Length (cm)	Top depth(cm)	bottom depth(cm)
1	R	1	28	0	28
1	R	CC	7	28	35
4	R	1	8	1290	1298
4	R	CC	10	1298	1308

Appendix 4: Core Descriptions MeBo continued

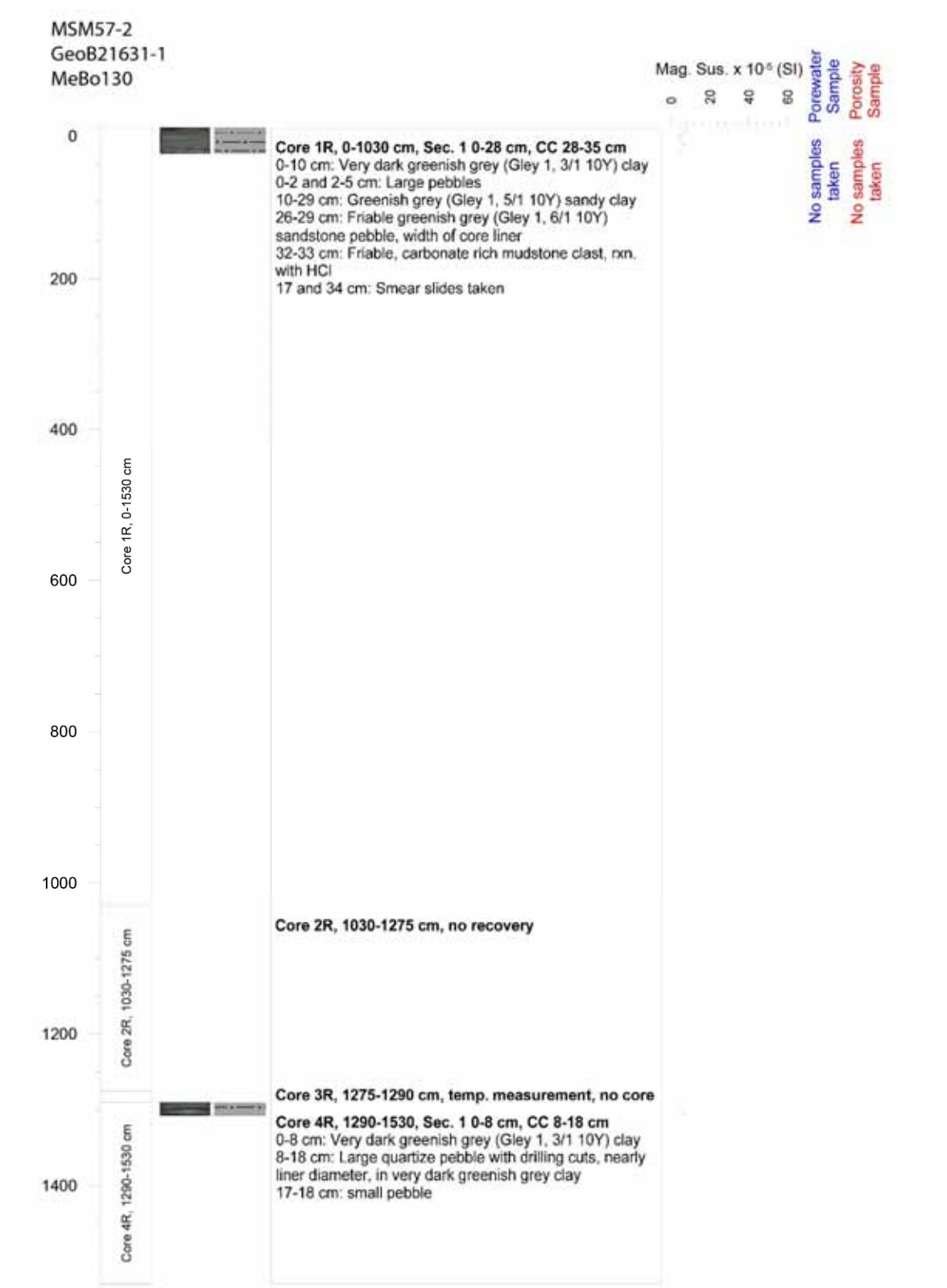

Appendix 4: Core Descriptions MeBo continued

MSM57-2

GeoB21631-3 **Total Drilled Length: 1530 cm**

MeBo131 **Total Cored Length: 81 cm**

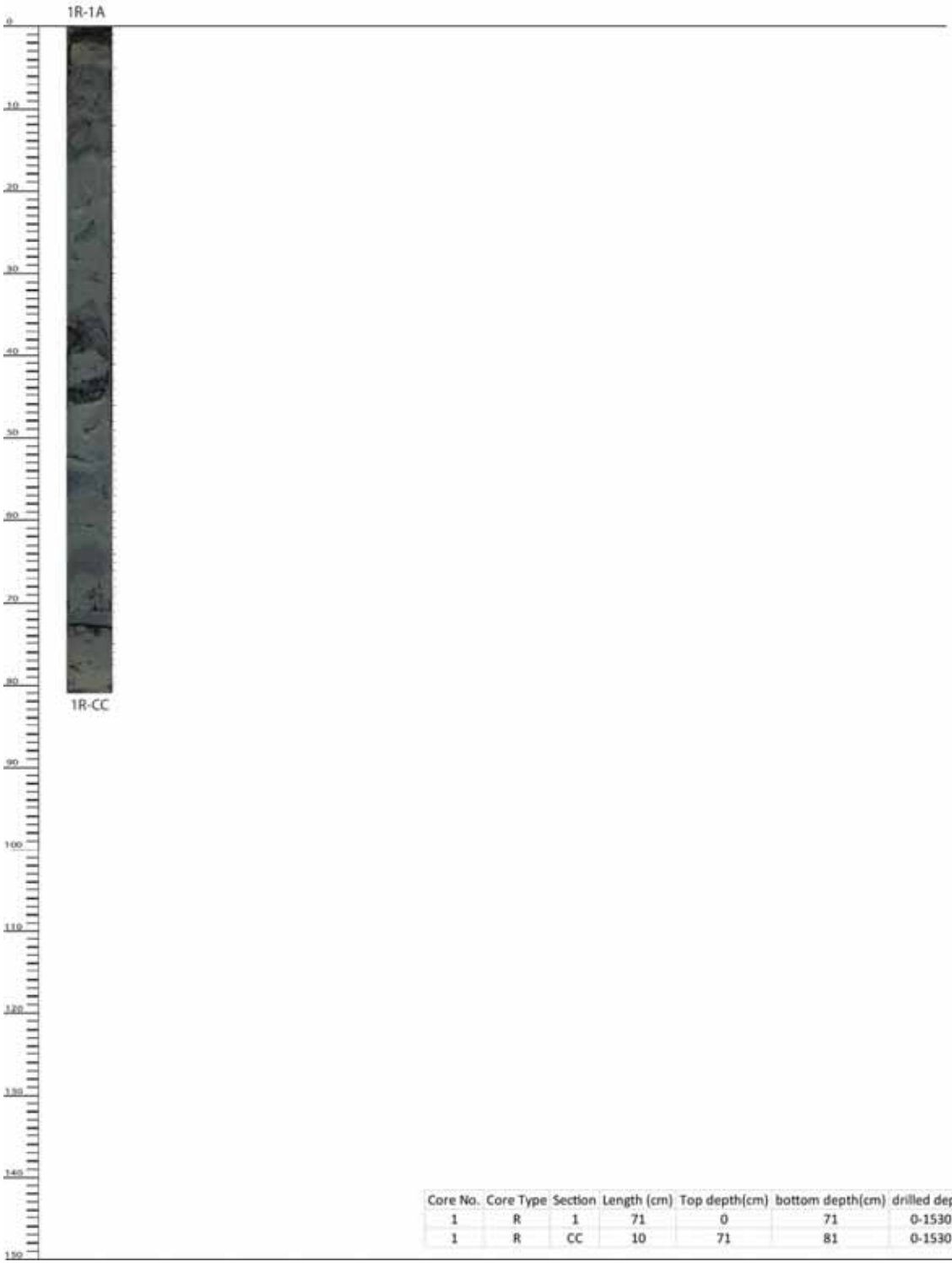

Core No.	Core Type	Section	Length (cm)	Top depth(cm)	bottom depth(cm)	drilled depth
1	R	1	71	0	71	0-1530
1	R	CC	10	71	81	0-1530

Appendix 4: Core Descriptions MeBo continued

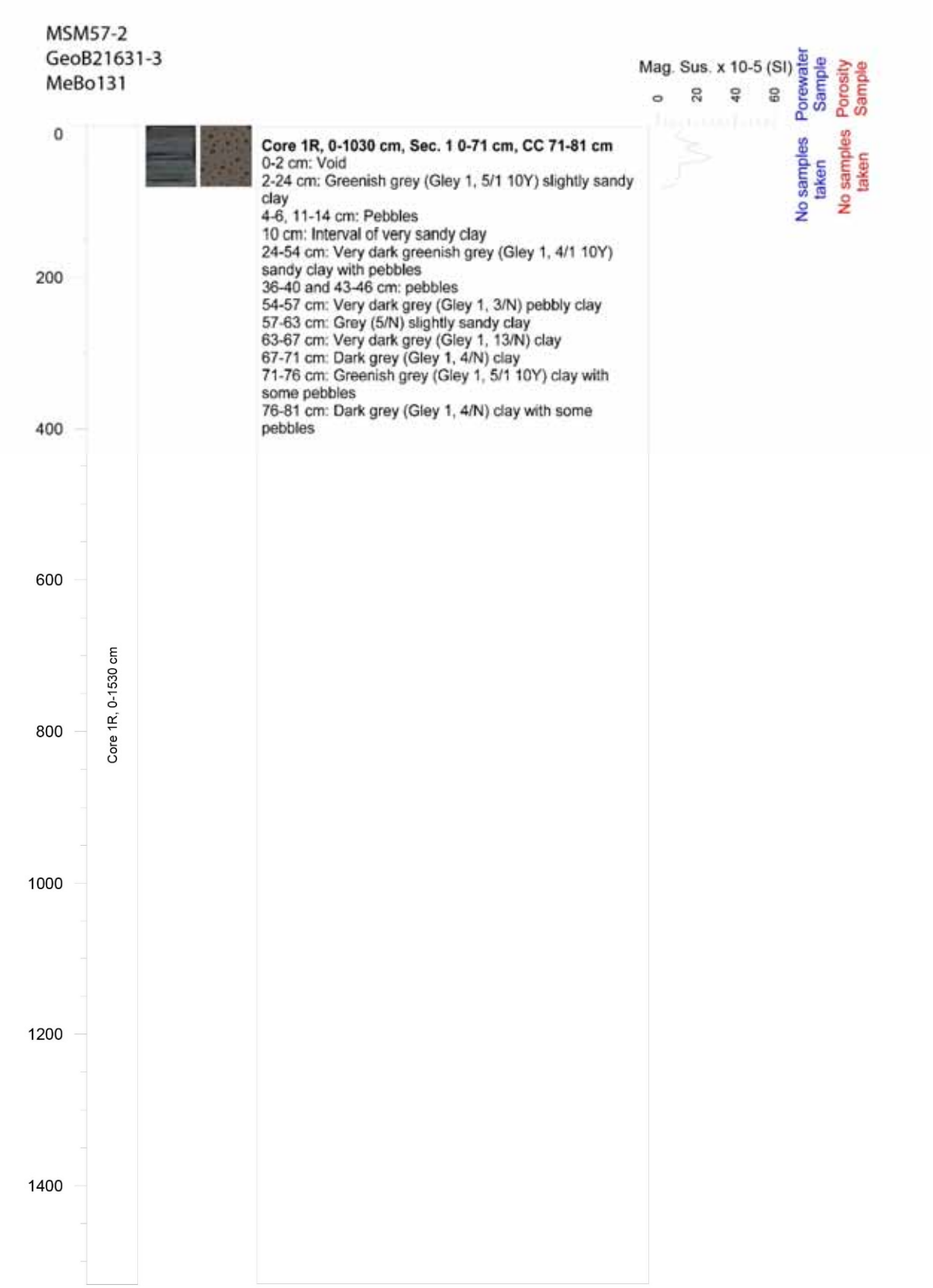

Appendix 4: Core Descriptions MeBo continued

MSM57-2
GeoB21631-4
MeBo132

Total Drilled Length: 2030 cm
Total Cored Length: 116 cm

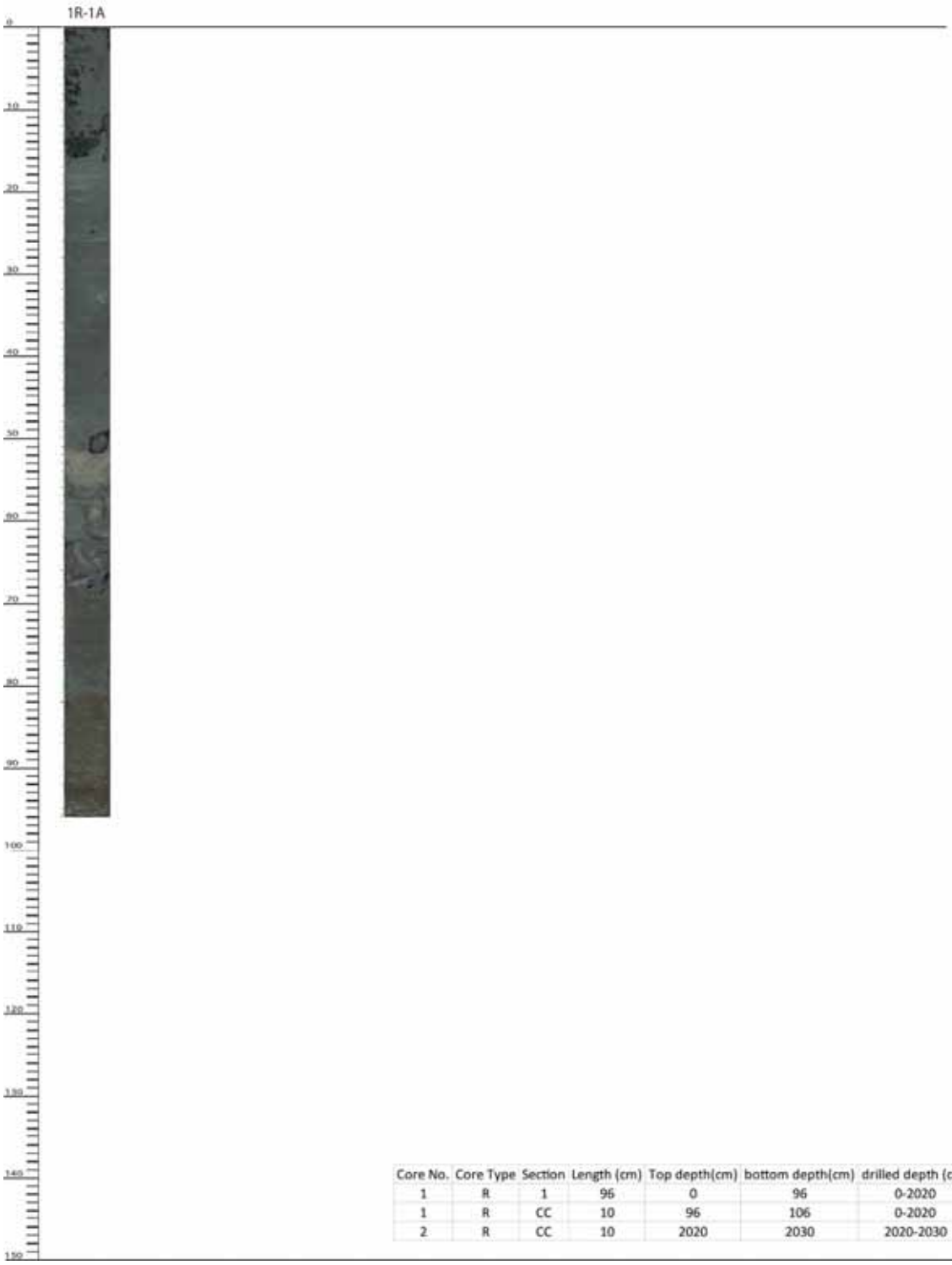

Core No.	Core Type	Section	Length (cm)	Top depth(cm)	bottom depth(cm)	drilled depth (cm)
1	R	1	96	0	96	0-2020
1	R	CC	10	96	106	0-2020
2	R	CC	10	2020	2030	2020-2030

Appendix 4: Core Descriptions MeBo continued

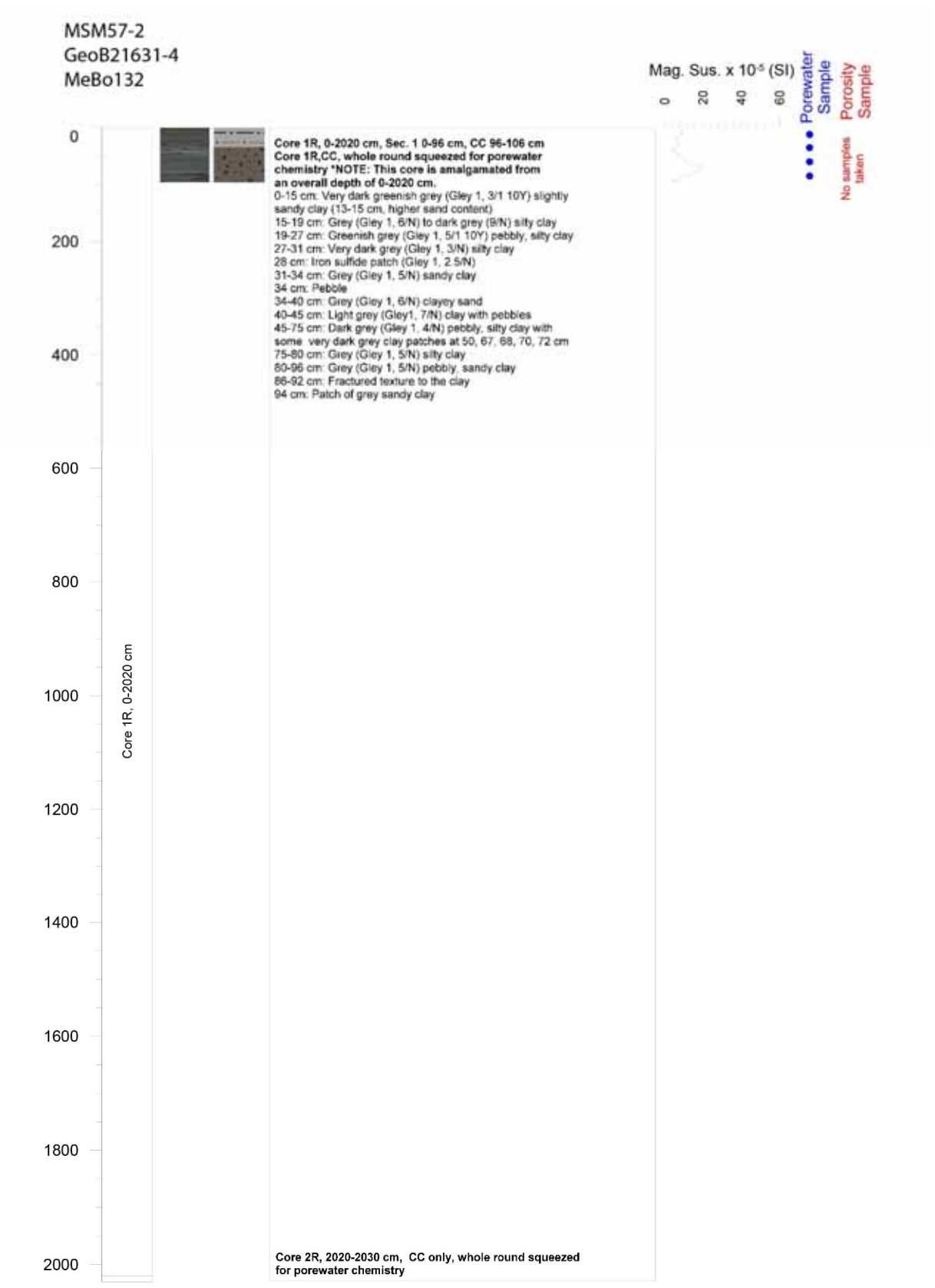

Appendix 4: Core Descriptions MeBo continued

MSM57-2
GeoB21632-1
MeBo133

Total Drilled Length: 1025 cm
Total Cored Length: 268 cm

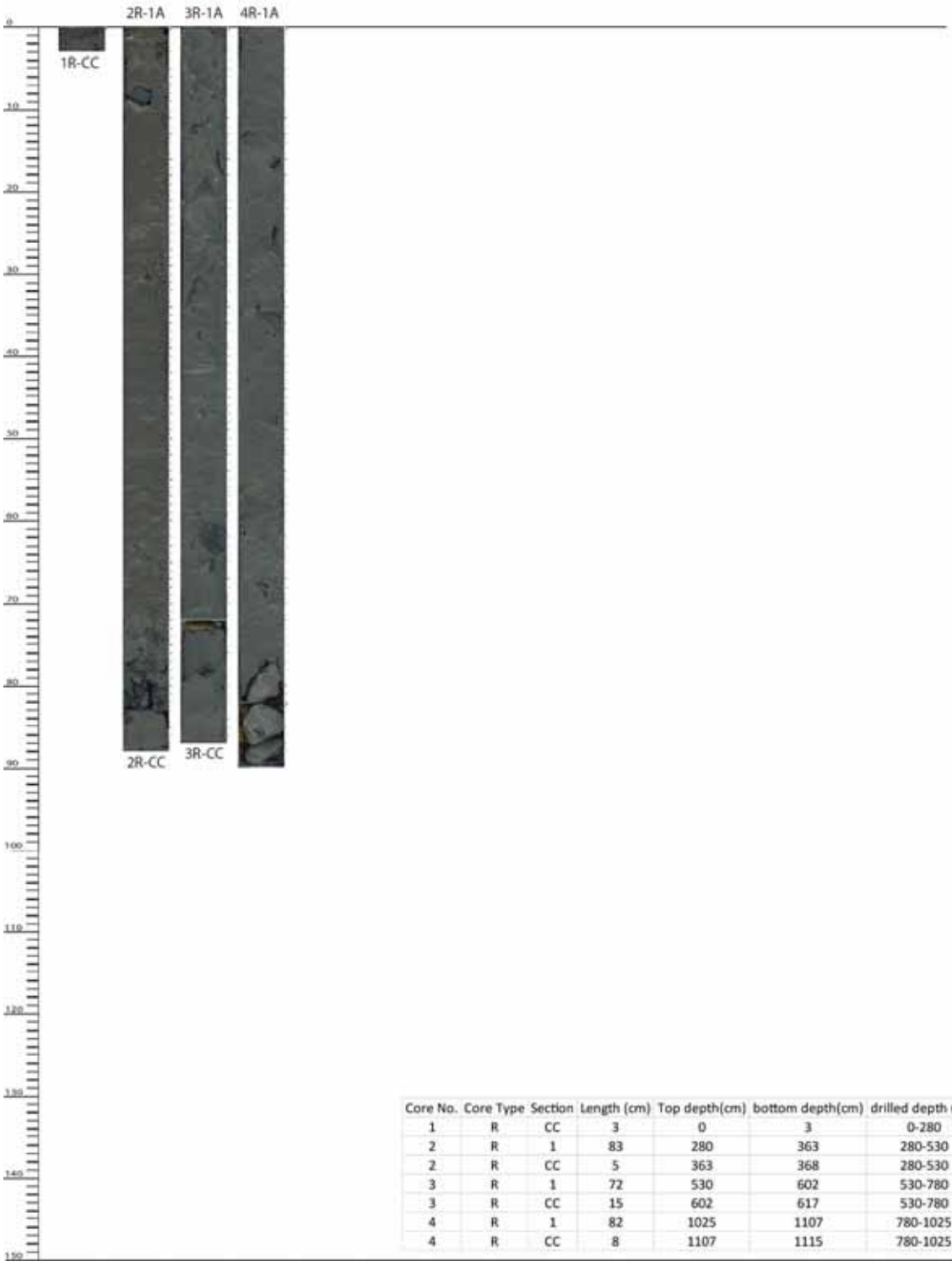

Core No.	Core Type	Section	Length (cm)	Top depth(cm)	bottom depth(cm)	drilled depth (cm)
1	R	CC	3	0	3	0-280
2	R	1	83	280	363	280-530
2	R	CC	5	363	368	280-530
3	R	1	72	530	602	530-780
3	R	CC	15	602	617	530-780
4	R	1	82	1025	1107	780-1025
4	R	CC	8	1107	1115	780-1025

Appendix 4: Core Descriptions MeBo continued

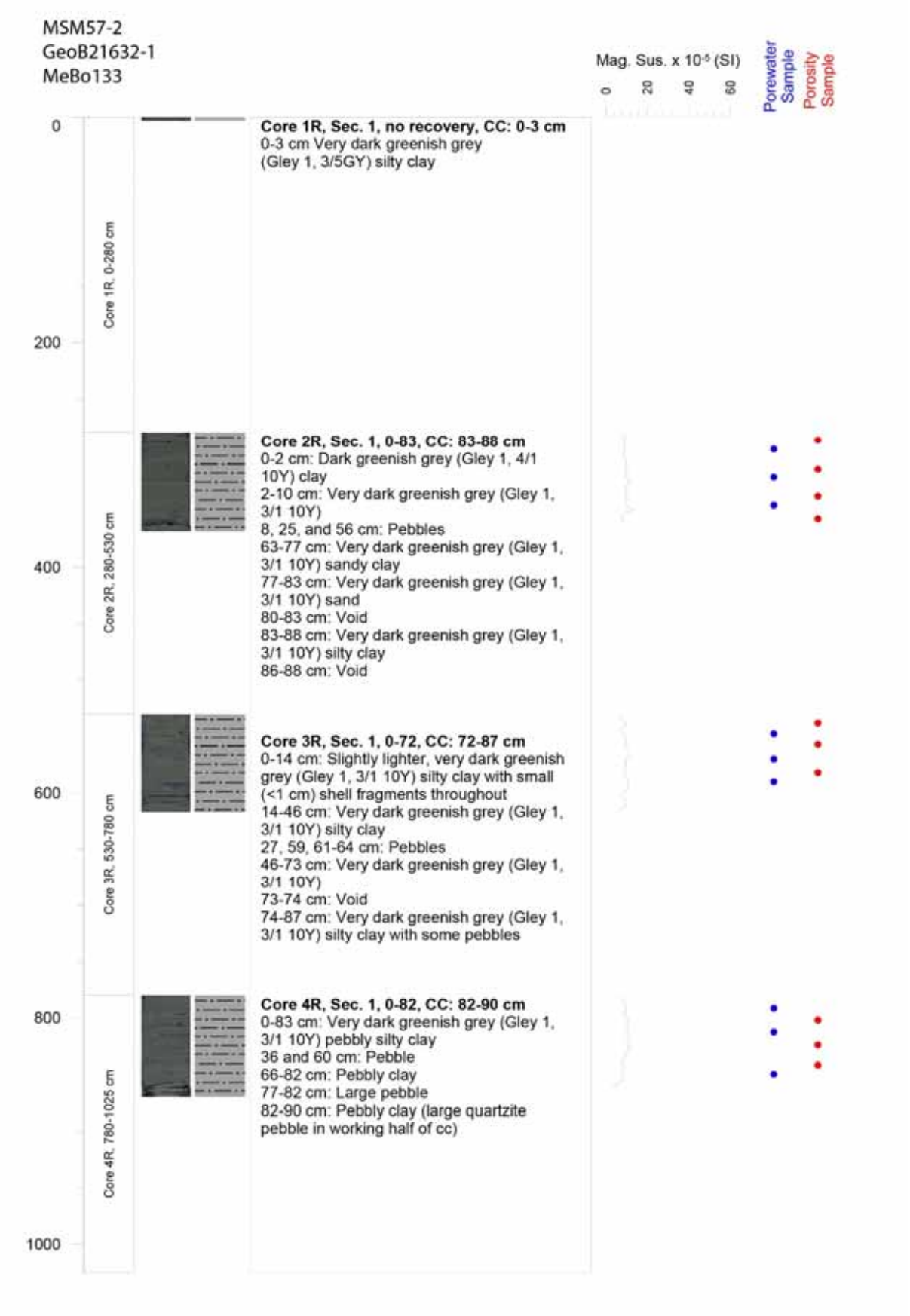

Appendix 4: Core Descriptions MeBo continued

MSM57-2
GeoB21632-2
MeBo134

Total Drilled Length: 2530 cm
Total Cored Length: 283 cm

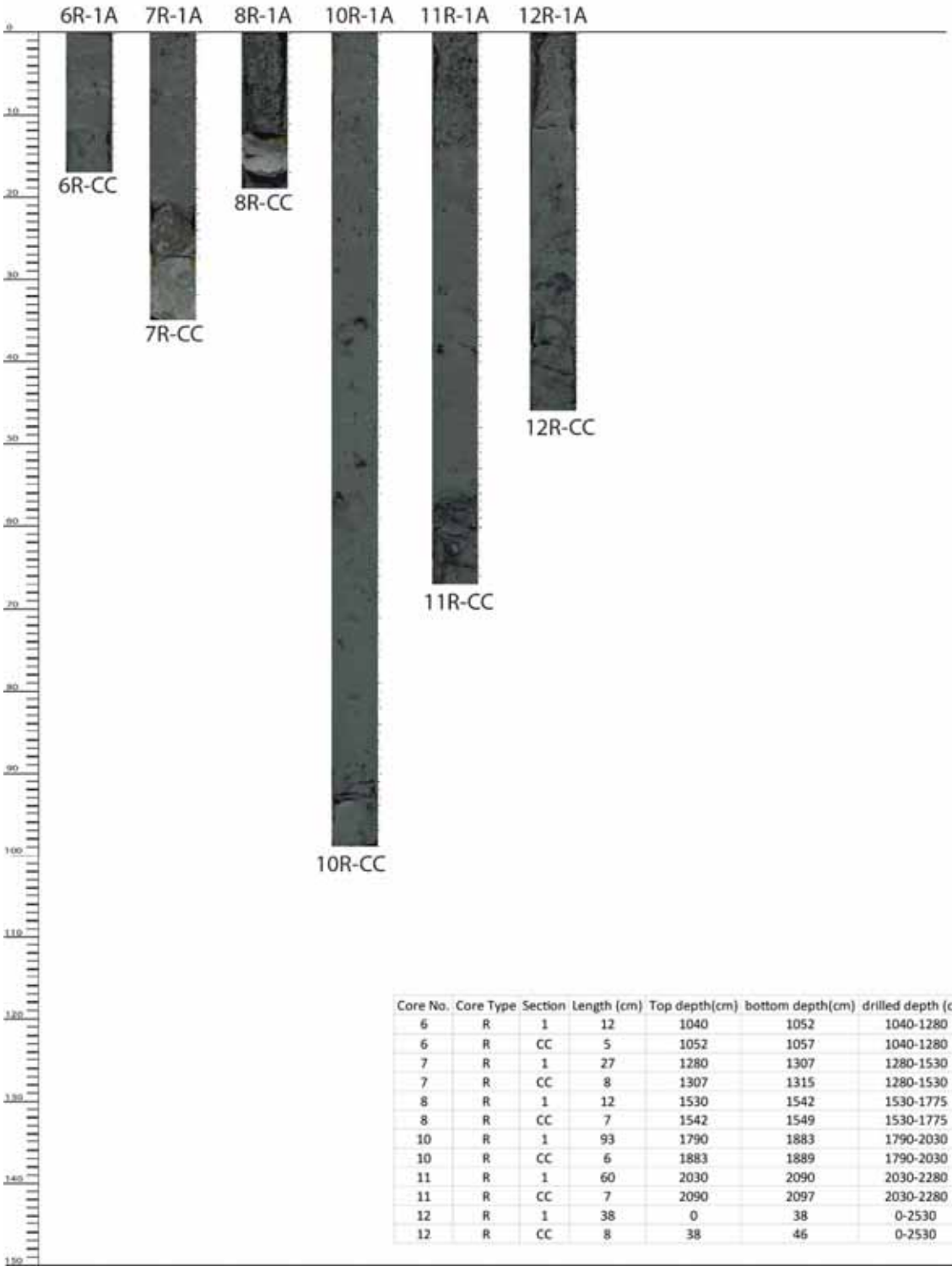

Core No.	Core Type	Section	Length (cm)	Top depth(cm)	bottom depth(cm)	drilled depth (cm)
6	R	1	12	1040	1052	1040-1280
6	R	CC	5	1052	1057	1040-1280
7	R	1	27	1280	1307	1280-1530
7	R	CC	8	1307	1315	1280-1530
8	R	1	12	1530	1542	1530-1775
8	R	CC	7	1542	1549	1530-1775
10	R	1	93	1790	1883	1790-2030
10	R	CC	6	1883	1889	1790-2030
11	R	1	60	2030	2090	2030-2280
11	R	CC	7	2090	2097	2030-2280
12	R	1	38	0	38	0-2530
12	R	CC	8	38	46	0-2530

Appendix 4: Core Descriptions MeBo continued

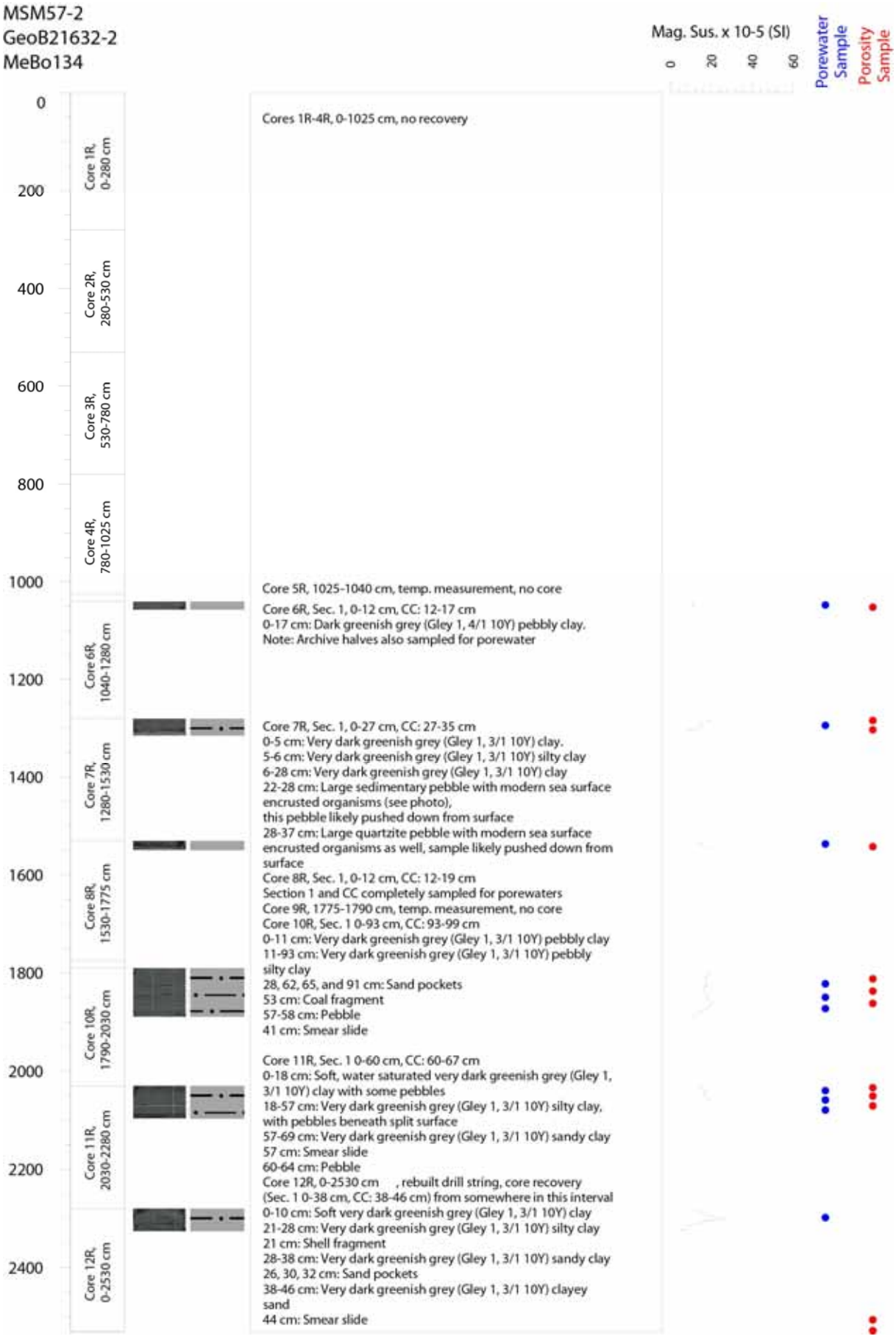

Appendix 4: Core Descriptions MeBo continued

MSM57-2
GeoB21633-1
MeBo135

Total Drilled Length: 1775 cm
Total Cored Length: 427 cm

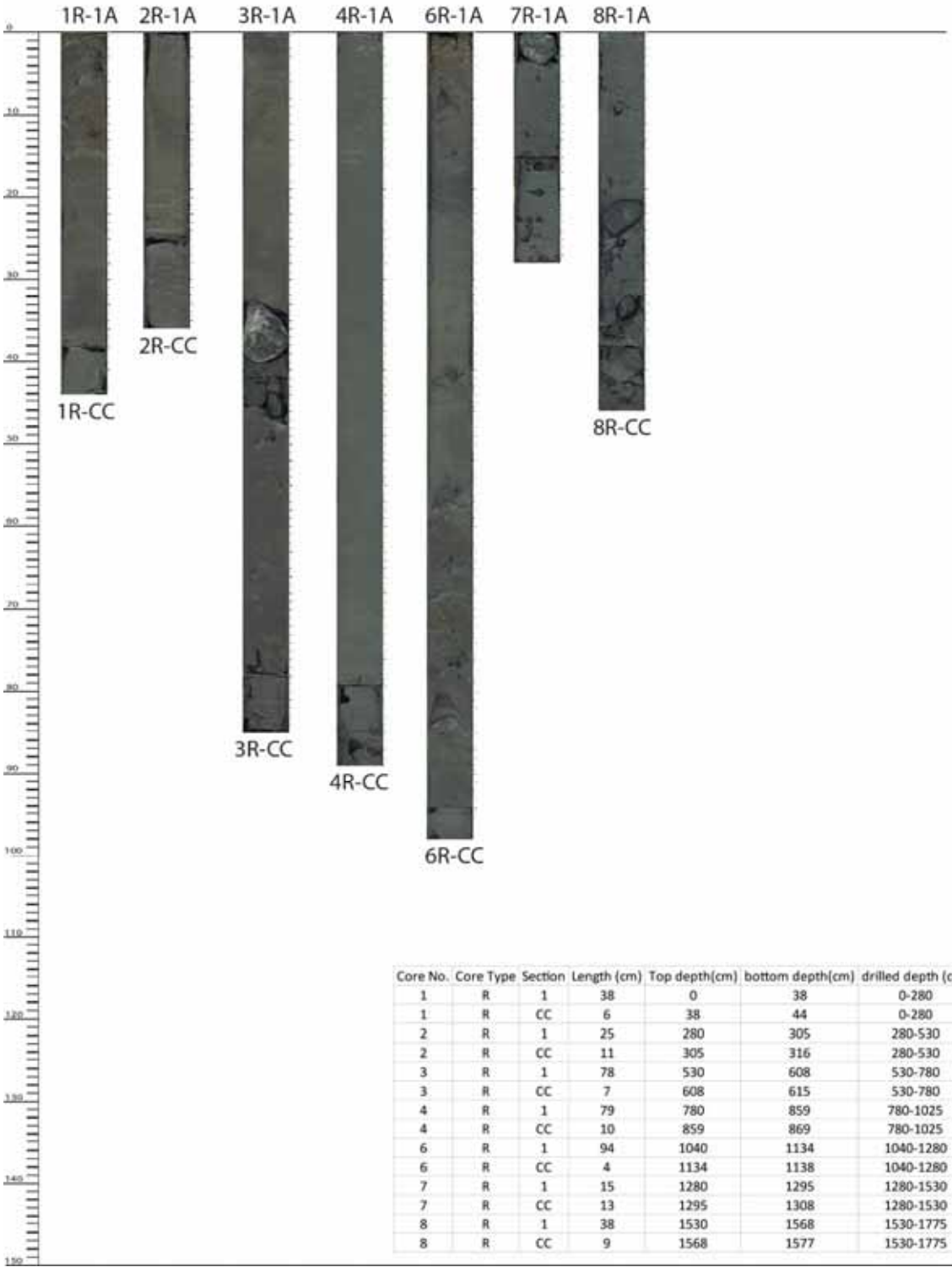

Core No.	Core Type	Section	Length (cm)	Top depth(cm)	bottom depth(cm)	drilled depth (cm)
1	R	1	38	0	38	0-280
1	R	CC	6	38	44	0-280
2	R	1	25	280	305	280-530
2	R	CC	11	305	316	280-530
3	R	1	78	530	608	530-780
3	R	CC	7	608	615	530-780
4	R	1	79	780	859	780-1025
4	R	CC	10	859	869	780-1025
6	R	1	94	1040	1134	1040-1280
6	R	CC	4	1134	1138	1040-1280
7	R	1	15	1280	1295	1280-1530
7	R	CC	13	1295	1308	1280-1530
8	R	1	38	1530	1568	1530-1775
8	R	CC	9	1568	1577	1530-1775

Appendix 4: Core Descriptions MeBo continued

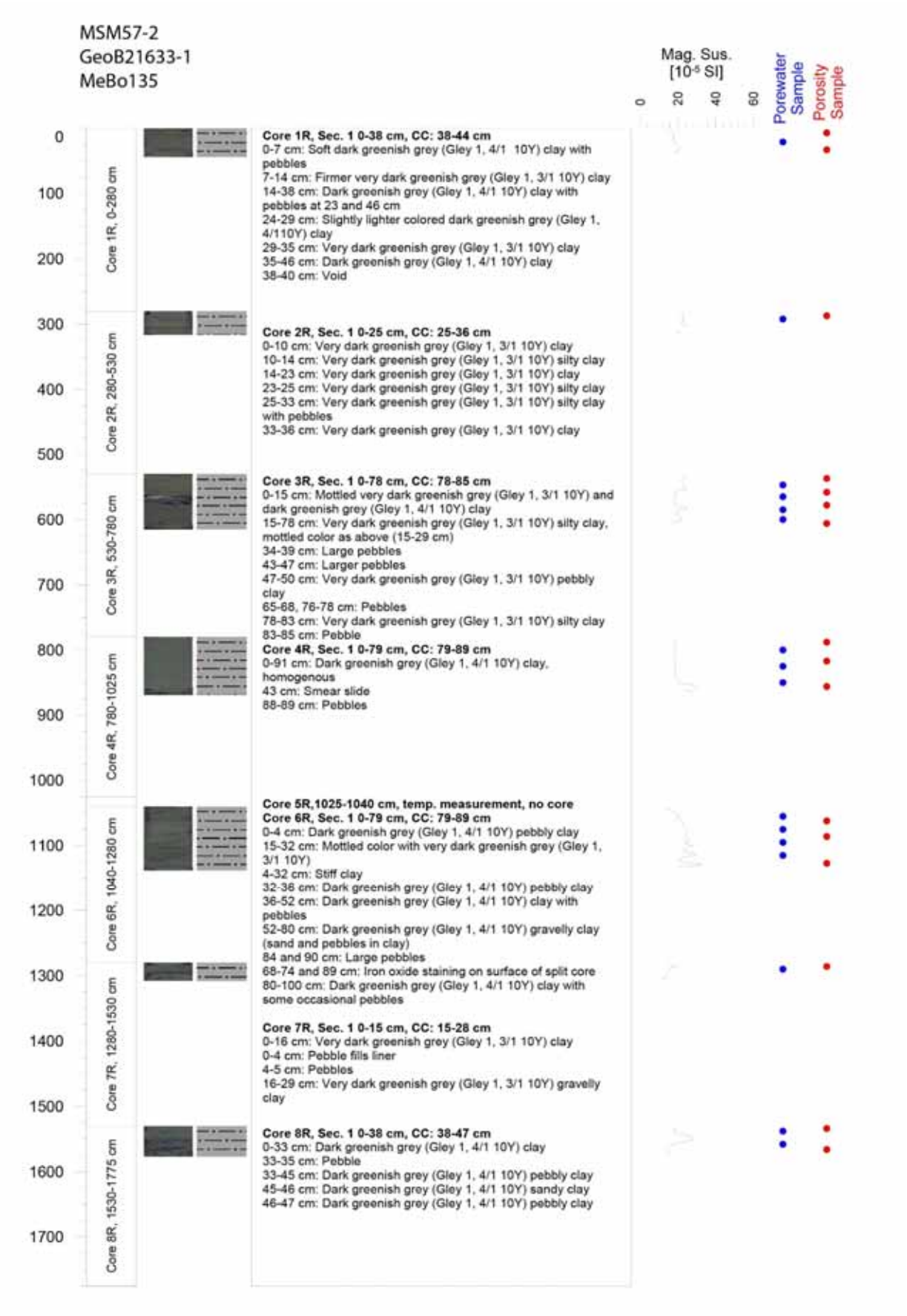

Appendix 4: Core Descriptions MeBo continued

MSM57-2

GeoB21633-3

MeBo136

Total Drilled Length: 3795 cm

Total Cored Length: 555 cm

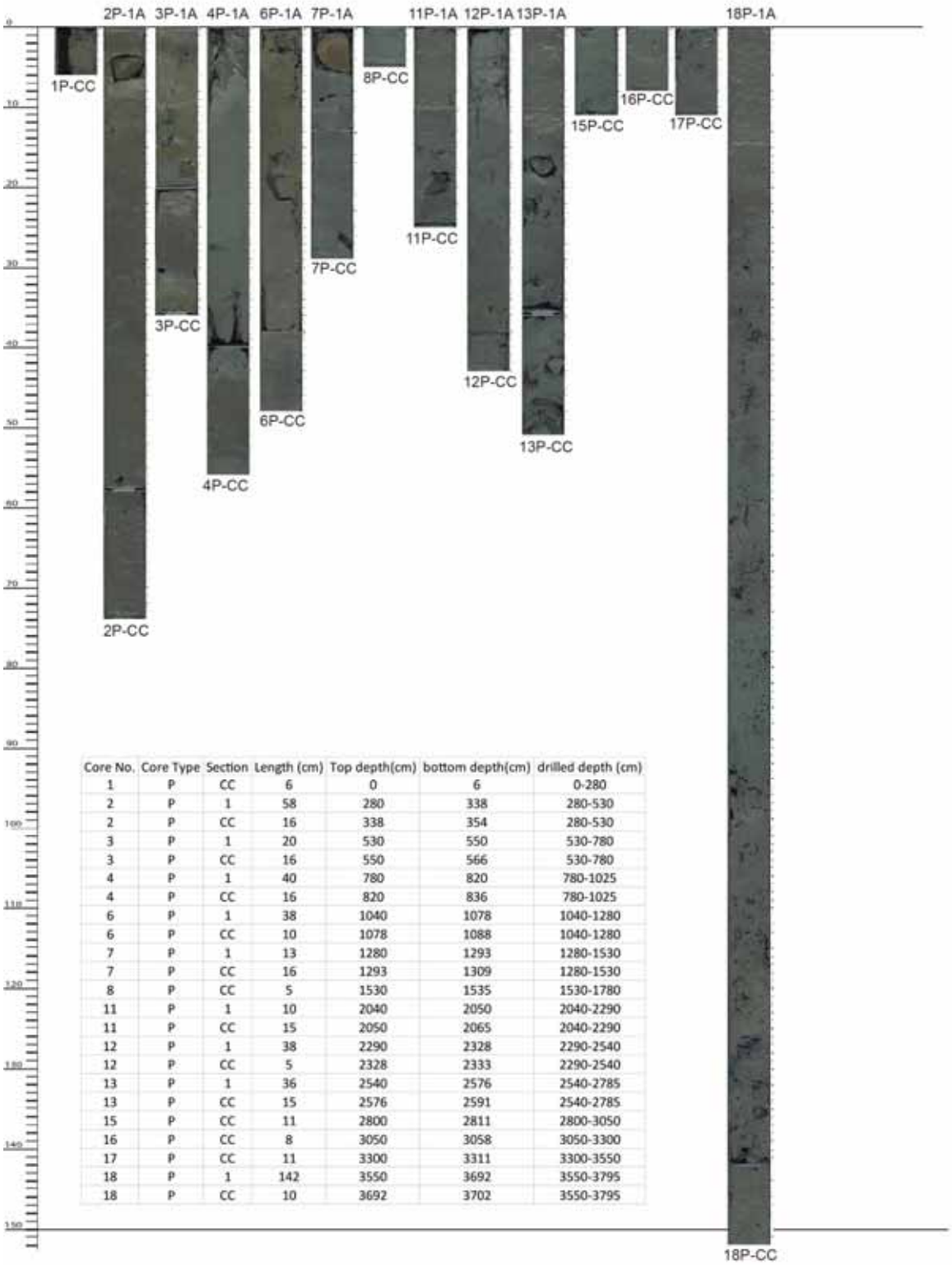

Core No.	Core Type	Section	Length (cm)	Top depth(cm)	bottom depth(cm)	drilled depth (cm)
1	P	CC	6	0	6	0-280
2	P	1	58	280	338	280-530
2	P	CC	16	338	354	280-530
3	P	1	20	530	550	530-780
3	P	CC	16	550	566	530-780
4	P	1	40	780	820	780-1025
4	P	CC	16	820	836	780-1025
6	P	1	38	1040	1078	1040-1280
6	P	CC	10	1078	1088	1040-1280
7	P	1	13	1280	1293	1280-1530
7	P	CC	16	1293	1309	1280-1530
8	P	CC	5	1530	1535	1530-1780
11	P	1	10	2040	2050	2040-2290
11	P	CC	15	2050	2065	2040-2290
12	P	1	38	2290	2328	2290-2540
12	P	CC	5	2328	2333	2290-2540
13	P	1	36	2540	2576	2540-2785
13	P	CC	15	2576	2591	2540-2785
15	P	CC	11	2800	2811	2800-3050
16	P	CC	8	3050	3058	3050-3300
17	P	CC	11	3300	3311	3300-3550
18	P	1	142	3550	3692	3550-3795
18	P	CC	10	3692	3702	3550-3795

Appendix 4: Core Descriptions MeBo continued

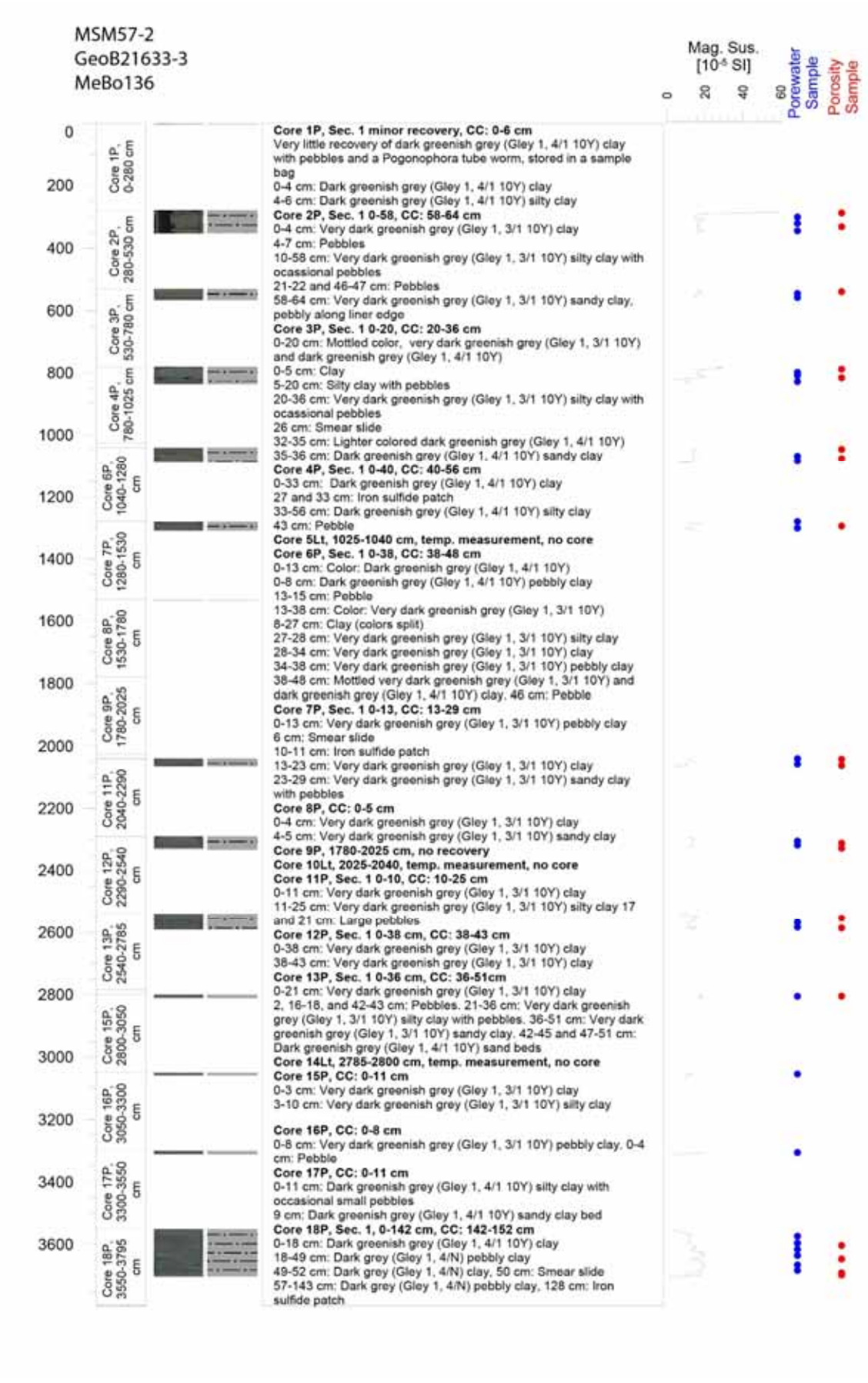

Appendix 4: Core Descriptions MeBo continued

MSM57-2
GeoB21634-1
MeBo137

Total Drilled Length: 2160 cm
Total Cored Length: 431 cm

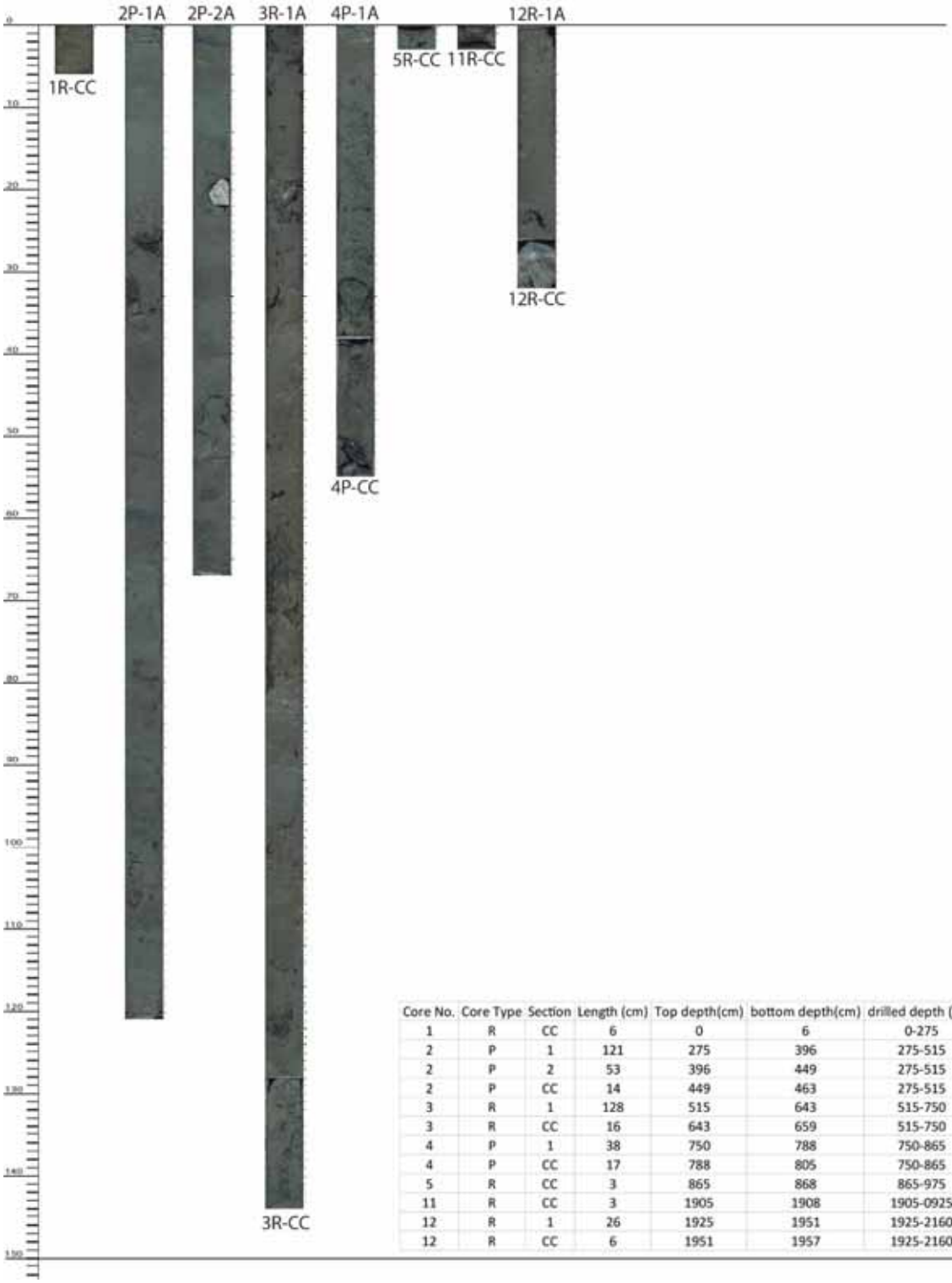

Core No.	Core Type	Section	Length (cm)	Top depth(cm)	bottom depth(cm)	drilled depth (cm)
1	R	CC	6	0	6	0-275
2	P	1	121	275	396	275-515
2	P	2	53	396	449	275-515
2	P	CC	14	449	463	275-515
3	R	1	128	515	643	515-750
3	R	CC	16	643	659	515-750
4	P	1	38	750	788	750-865
4	P	CC	17	788	805	750-865
5	R	CC	3	865	868	865-975
11	R	CC	3	1905	1908	1905-0925
12	R	1	26	1925	1951	1925-2160
12	R	CC	6	1951	1957	1925-2160

Appendix 4: Core Descriptions MeBo continued

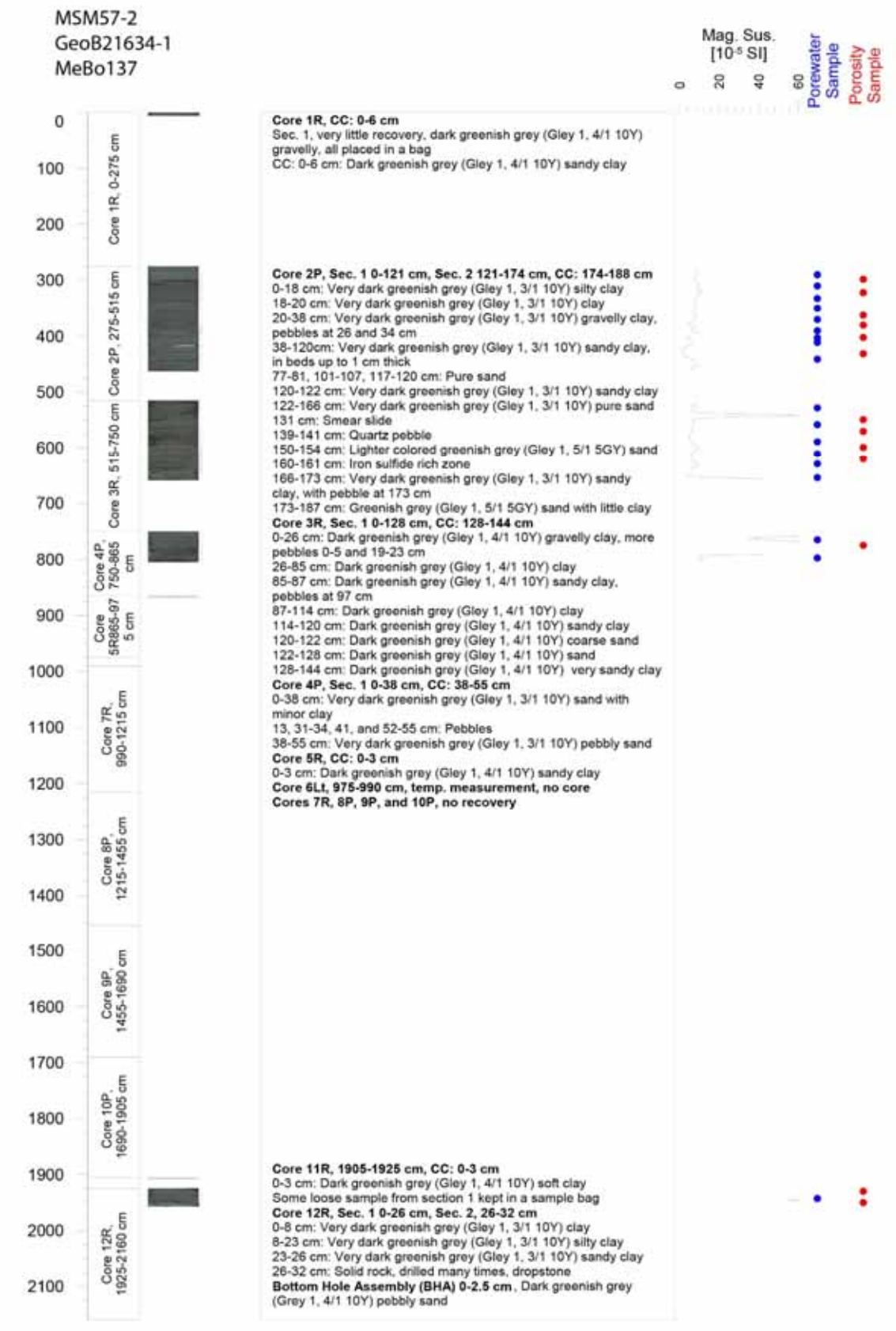

Appendix 4: Core Descriptions MeBo continued

MSM57-2
GeoB21637-1
MeBo138

Total Drilled Length: 2395 cm
Total Cored Length: 870 cm

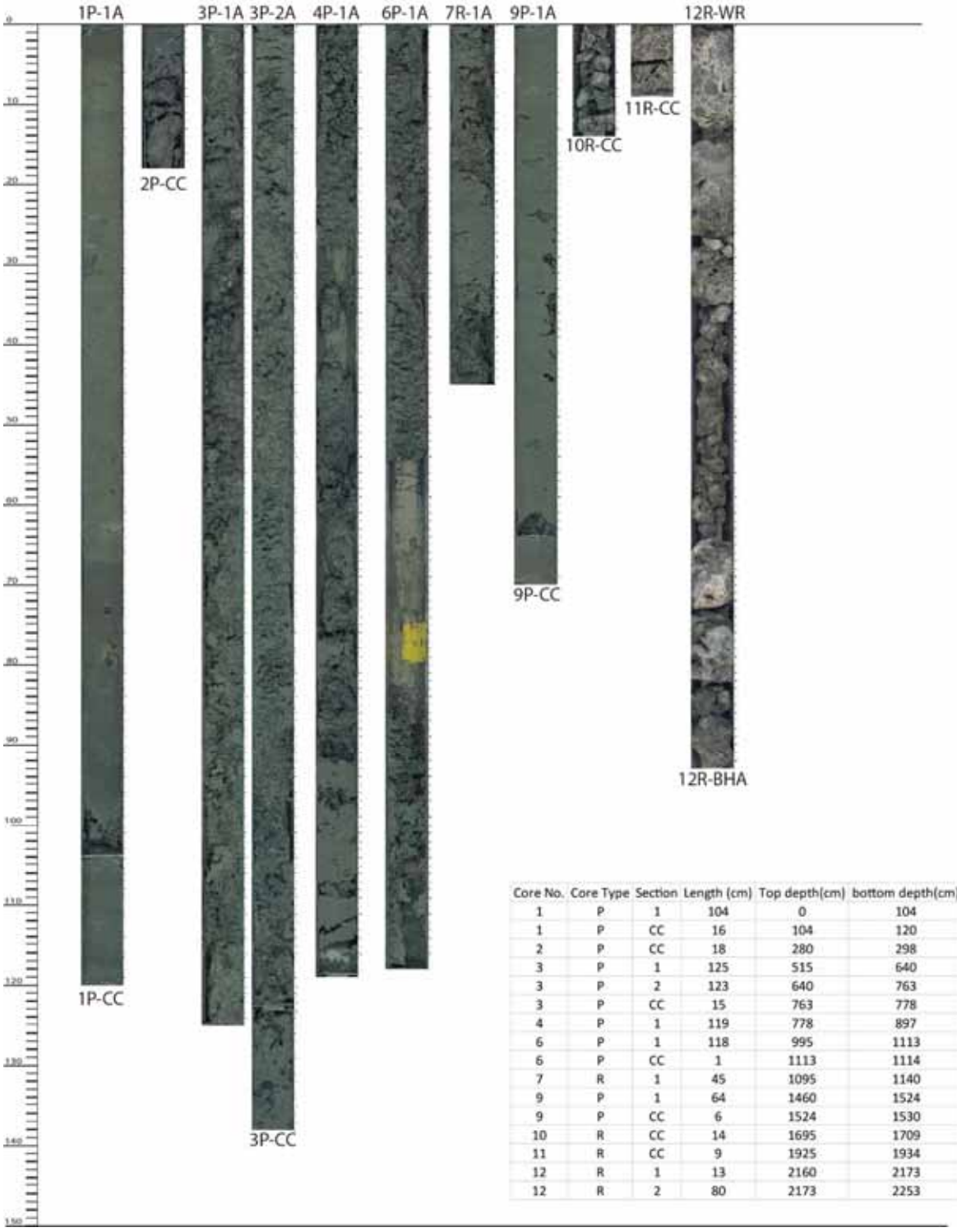

Core No.	Core Type	Section	Length (cm)	Top depth(cm)	bottom depth(cm)
1	P	1	104	0	104
1	P	CC	16	104	120
2	P	CC	18	280	298
3	P	1	125	515	640
3	P	2	123	640	763
3	P	CC	15	763	778
4	P	1	119	778	897
6	P	1	118	995	1113
6	P	CC	1	1113	1114
7	R	1	45	1095	1140
9	P	1	64	1460	1524
9	P	CC	6	1524	1530
10	R	CC	14	1695	1709
11	R	CC	9	1925	1934
12	R	1	13	2160	2173
12	R	2	80	2173	2253

Appendix 4: Core Descriptions MeBo continued

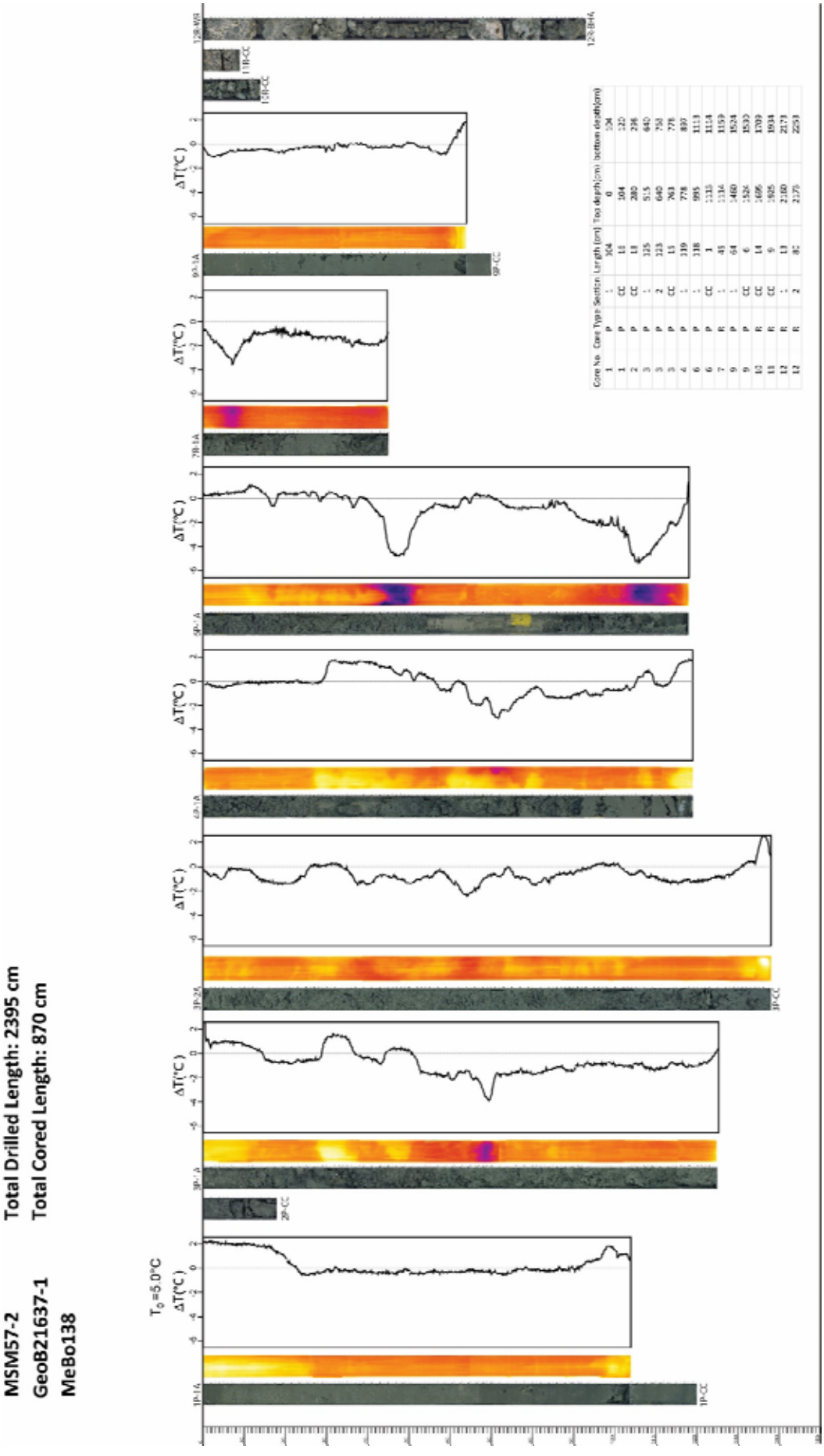

Appendix 4: Core Descriptions MeBo continued

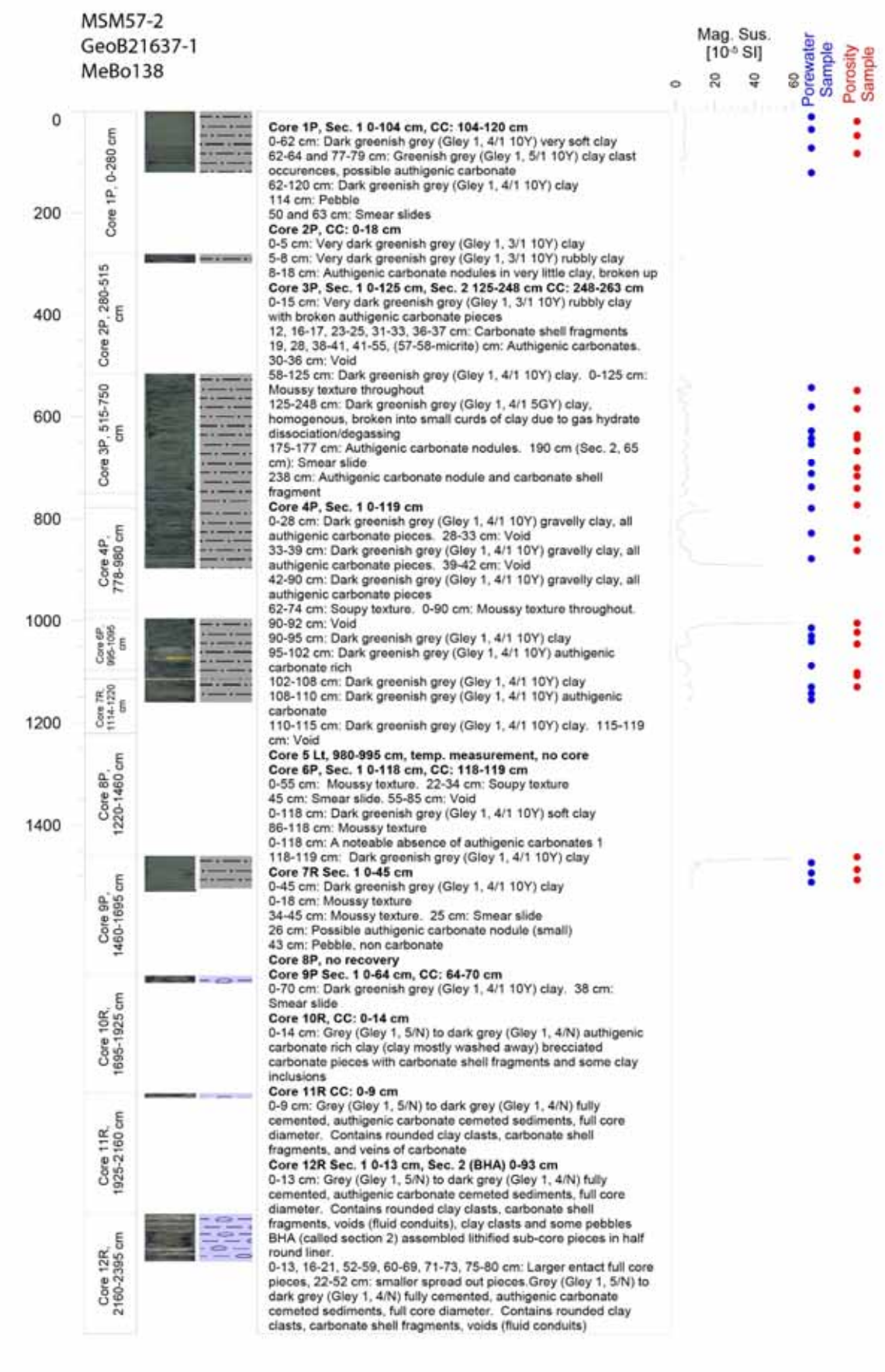

Appendix 4: Core Descriptions MeBo continued

MSM57-2
GeoB21639-1
MeBo139

Total Drilled Length: 2615 cm
Total Cored Length: 1203 cm

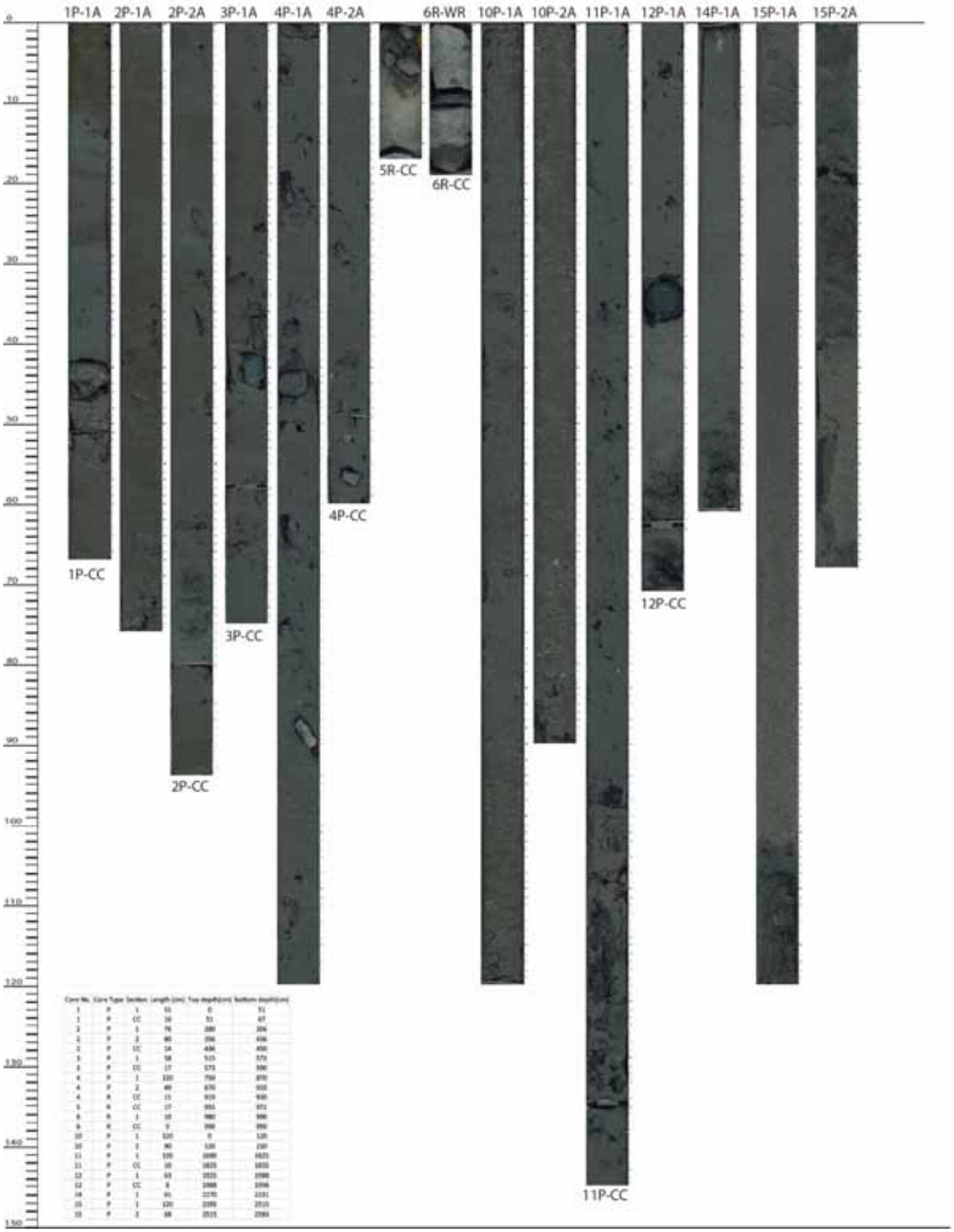

Appendix 4: Core Descriptions MeBo continued

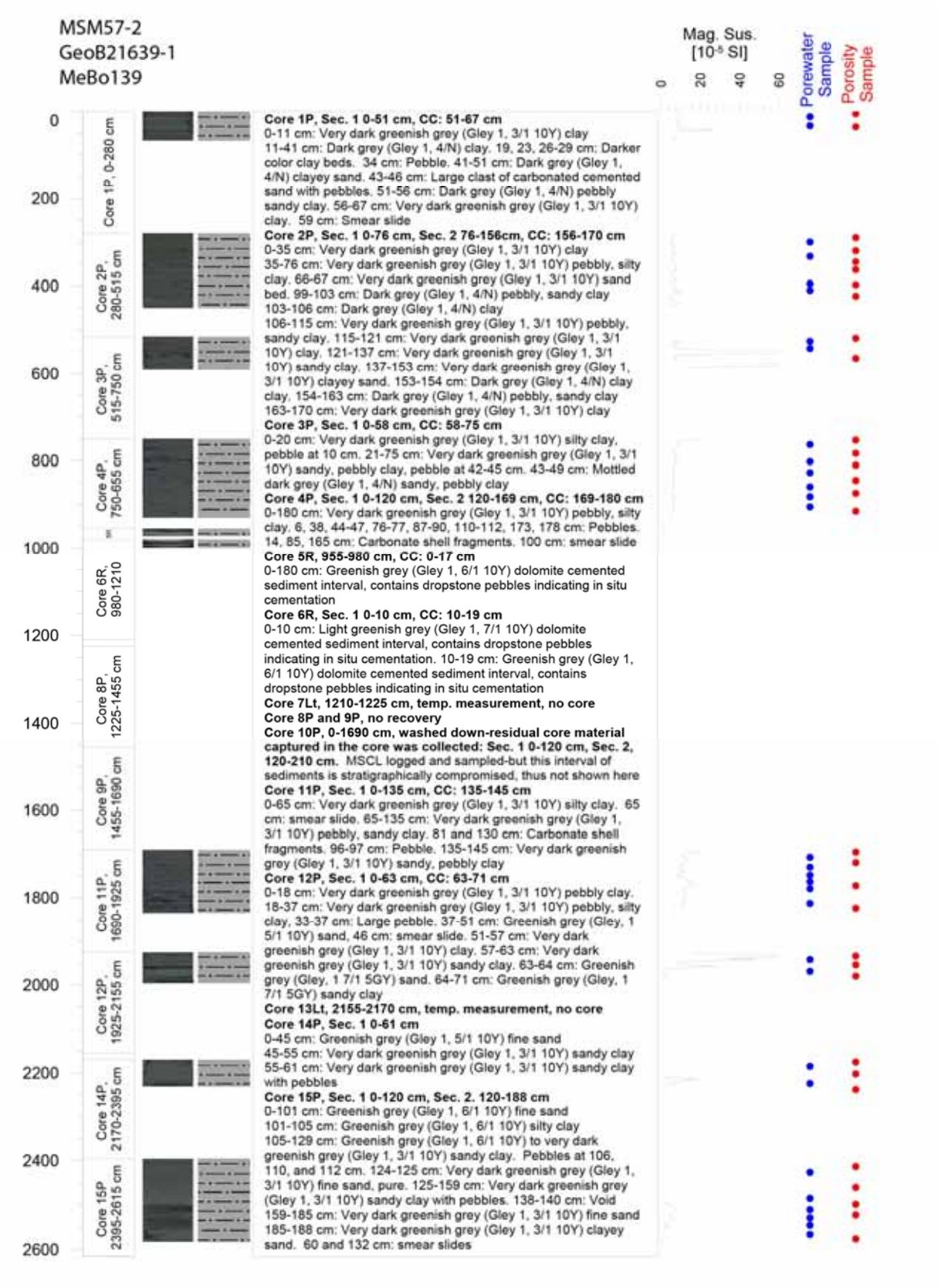

Appendix 4: Core Descriptions MeBo continued

MSM57-2
GeoB21643-1
MeBo140

Total Drilled Length: 3330 cm
Total Cored Length: 1708 cm

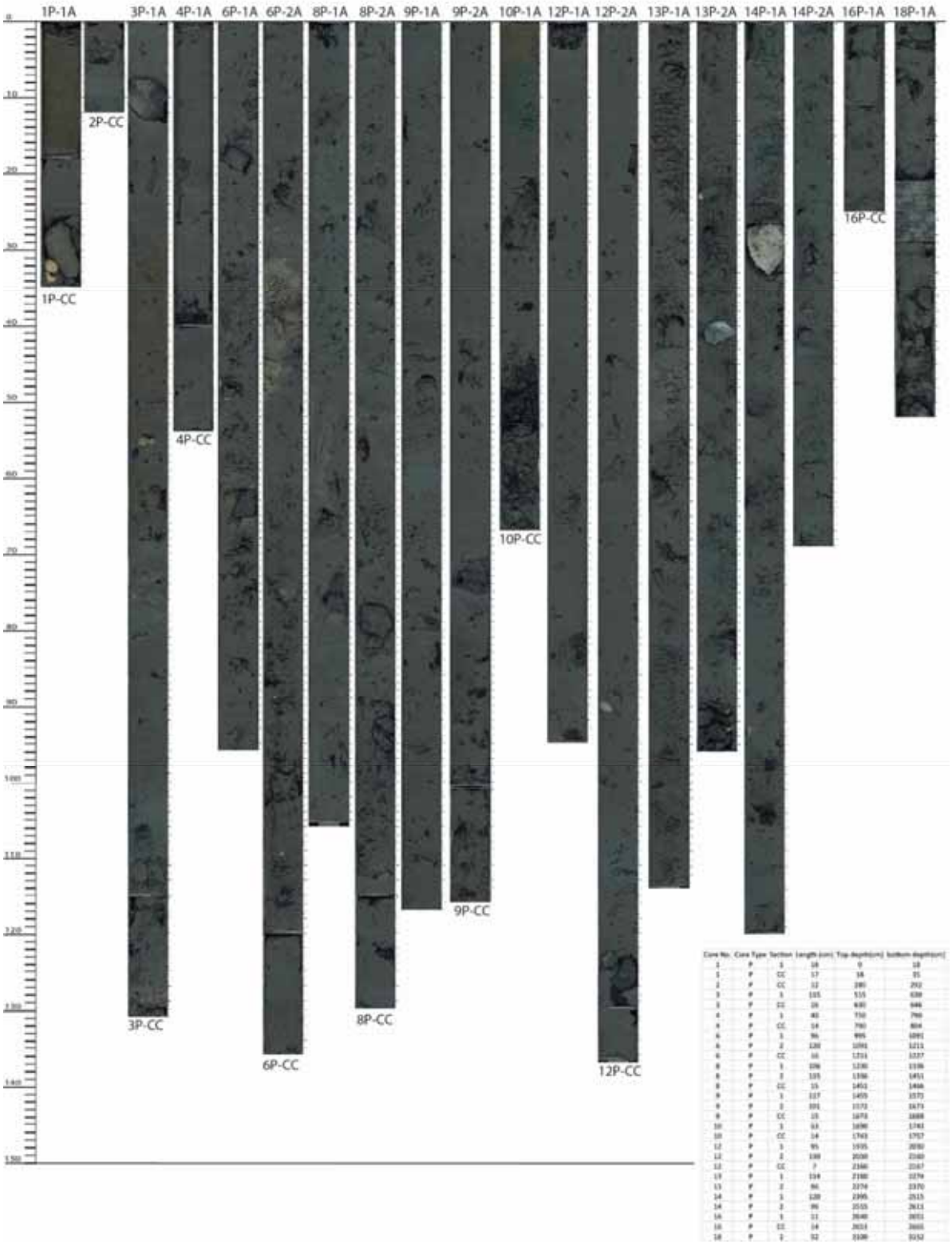

Appendix 4: Core Descriptions MeBo continued

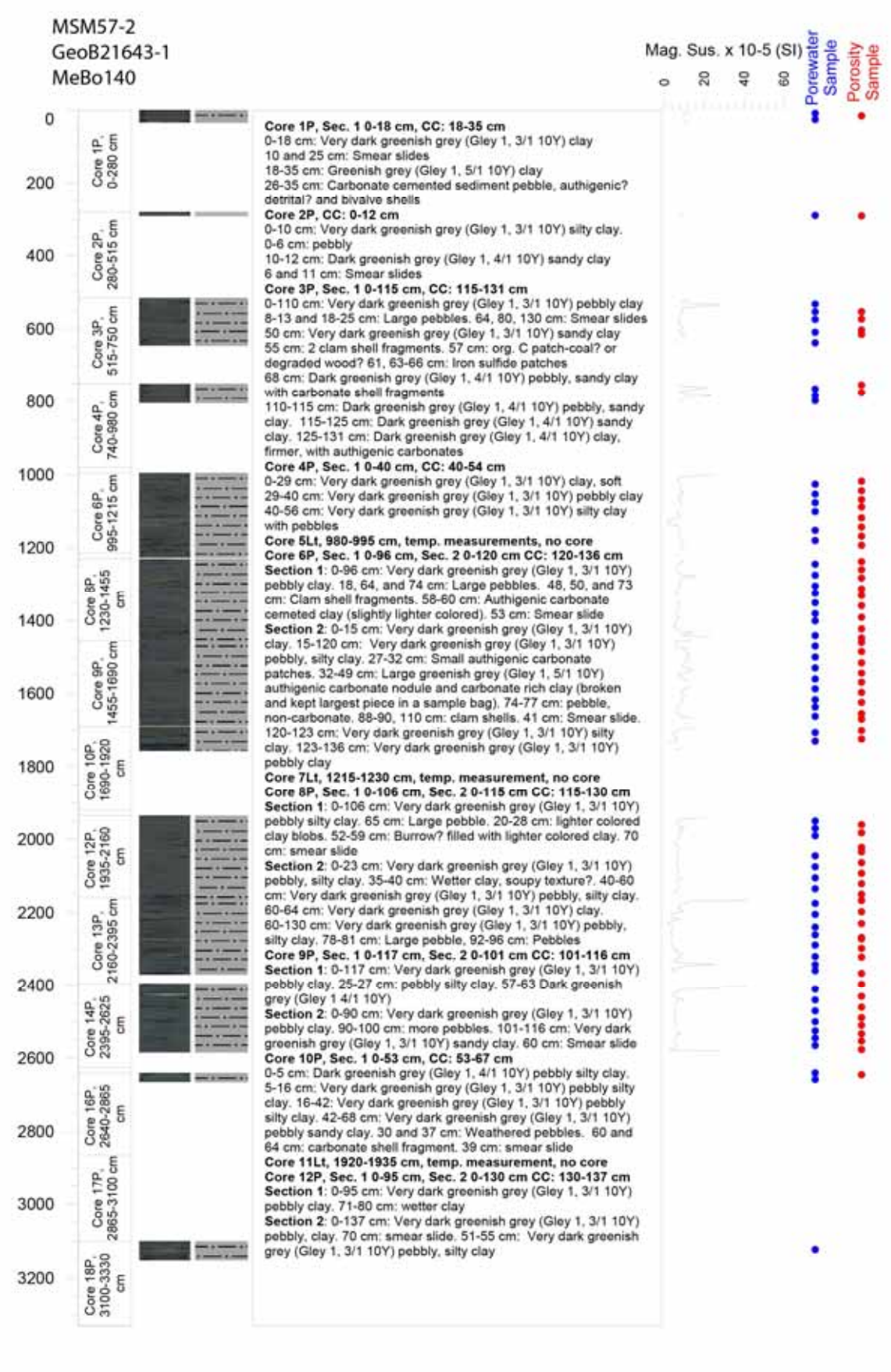

Appendix 4: Core Descriptions MeBo continued

MEBO 140 description continued

Core 13P, Sec. 1 0-114 cm, Sec. 2 0-96 cm
Section 1: 0-95 cm: Very dark greenish grey (Gley 1, 3/1 10Y) soft clay with occasional pebbles, moussy/gas texture. 44-52 cm: lighter colored (Gley 1 4/1 10Y)
78-80 cm: carbonate shell fragments. 40, 62, and 102 cm: Larger pebbles. 47 cm: smear slide
Section 2: 0-10 cm: Very dark greenish grey (Gley 1, 3/1 10Y) clay with pebbles. 10-96 cm: Very dark greenish grey (Gley 1, 3/1 10Y) silty clay with pebbles. 22, 91 and 93 cm: clam shell fragments. 40 cm: slate pebble

Core 14P, Sec. 1 0-120 cm, Sec. 2 0-69 cm
Section 1: Very dark greenish grey (Gley 1, 3/1 10Y) silty clay with occasional pebbles. 27-33 cm: Carbonate cemented sandstone-authigenic or detrital? 70 cm: Lighter colored clay patch
94, 100, 112 cm: carbonate shell fragments
Section 2: 0-69 cm: Very dark greenish grey (Gley 1, 3/1 10Y) silty clay with occasional Pebbles. 33, 38 cm: clam shell fragments.
26 cm: smear slide

Core 15Lt, 2625-2640 cm, temp. measurement, no core.

Core 16P, Sec. 1 0-11 cm, CC: 11-25 cm
0-10 cm: Dark greenish grey (Gley 1, 4/1 10Y) clay
10-25 cm: Very dark greenish grey (Gley 1, 3/1 10Y) silty clay

Core 17P, no recovery

Core 18P, Sec. 1/Bottom Hole Assembly (BHA) 0-52 cm
0-21 cm**:** Very dark greenish grey (Gley 1, 3/1 10Y) pebbly, silty clay
21-29 cm: Void
29-52 cm: Very dark greenish grey (Gley 1, 3/1 10Y) pebbly, silty clay

18.5 Appendix 5: ADCP Settings

ADCP-38kHz-settings

```
;-------------------------------------------------------------------------------\
; ADCP Command File for use with VmDas software.
;
; ADCP type:     38 Khz Ocean Surveyor
; Setup name:    Merian 56 (adapted from MSM54)
; Setup type:    Low resolution, long range profile (narrowband)
;
; NOTE:  Any line beginning with a semicolon in the first
;        column is treated as a comment and is ignored by
;        the VmDas software.
;
; NOTE:  This file is best viewed with a fixed-point font (eg. courier).
;-------------------------------------------------------------------------------/

; Restore factory default settings in the ADCP
cr1

; Set the data collection baud rate to 115200 bps,
; no parity, one stop bit, 8 data bits
; NOTE:  VmDas sends baud rate change command after all other commands in
; this file, so that it is not made permanent by a CK command.
;cb811


; Set for narrowband profile mode: broadband mode disabled (WP0),
; single-ping narrowband ensembles (NP), fifty bins (NN),
; 32 meter bin length (NS), 08 meter blanking distance (NF)
WP0
NP001
NN050
NS3200
NF0800

; Disable single-ping bottom track
BP001

; Output velocity, correlation, echo intensity, percent good
ND111100000

; Ping as fast as possible
TP000000

; Set to calculate speed-of-sound, no depth sensor,
; external synchro heading sensor, use internal
; transducer temperature sensor
EZ1020001

; Output beam data (rotations are done in software)
EX00000

; Set transducer misalignment (hundredths of degrees)
EA04500

; Set transducer depth to 65 decimeters (6.5m, info from Maggie)
ED00065

; Set Salinity (ppt)
ES35

; Save this setup to non-volatile memory in the ADCP
CK
```

Appendix 5: ADCP Settings continued

ADCP-75kHz-settings

```
;-------------------------------------------------------------------------------\
; ADCP Command File for use with VmDas software.
;
; ADCP type:     75 Khz Ocean Surveyor
; Setup name:    Merian 53
; Setup type:    Low resolution, long range profile (narrowband)
;
; NOTE:  Any line beginning with a semicolon in the first
;        column is treated as a comment and is ignored by
;        the VmDas software.
;
; NOTE:  This file is best viewed with a fixed-point font (eg. courier).
;-------------------------------------------------------------------------------/

; Restore factory default settings in the ADCP
cr1

; Set the data collection baud rate to 115200 bps,
; no parity, one stop bit, 8 data bits
; NOTE:  VmDas sends baud rate change command after all other commands in
; this file, so that it is not made permanent by a CK command.
;cb811

; Bottom track disabled (bottom track ping BP set to zero),
; Set maximum bottom search depth to 1200 meters (not needed)
BP000
;BX12000

; Disable broadband pings profile mode
WP000

; Set for narrowband profile mode (WP0 broad-band pings set to zero)
; single-ping narrow-band ensembles (NP), one hundered bins (NN),
; 8 meter bin length (NS), 8 meter blanking distance (NF)
NP001
NN100
NS0800
NF0800

; Output velocity, correlation, echo intensity, percent good
ND111100000

; Time between pings TPmmssff (m-minutes,s-seconds,f-hundredths of seconds)
; set to one second (this is faster than OS can actually ping, so it pings as fast as possible)
TP000000

; Since VmDas uses manual pinging, TE is ignored by the ADCP.
; You must set the time between ensemble in the VmDas Communication options
;TE00000100

; Set to calculate speed-of-sound,
; external synchro heading sensor (if syncro is not connected  0 is used),
; use internal  transducer temperature sensor
EZ1020001

; Set Speed of sound to 1542 m/s (not used here)
; EC1542

; Output beam data (rotations are done in software)
EX00000

; Set transducer misalignment (hundredths of degrees)
EA04500

; Set transducer depth to 65 decimeters (6.5m)
ED00065

; Set Salinity (ppt)
ES35

; Save this setup to non-volatile memory in the ADCP
CK
```

From report No. 289 onwards this series is published under the new title:
Berichte aus dem MARUM und dem Fachbereich Geowissenschaften der Universität Bremen
A complete list of all publications of this series from no. 1 to 292 (1986 – 2012) was printed at last in issue no. 292.

No. 289 – Mohtadi, M. and cruise participants (2012). Report and preliminary results of RV SONNE Cruise SO 223T. TransGeoBiOc. Pusan – Suva, 09.09.2012 – 08.10.2012. 47 pages.
No. 290 – Hebbeln, D., Wienberg, C. and cruise participants (2012). Report and preliminary results of R/V Maria S. Merian cruise MSM20-4. WACOM – West-Atlantic Cold-water Corals Ecosystems: The West Side Story. Bridgetown – Freeport, 14 March – 7 April 2012. 120 pages.
No. 291 – Sahling, H. and cruise participants (2012). R/V Heincke Cruise Report HE-387. Gas emissions at the Svalbard continental margin. Longyearbyen – Bremerhaven, 20 August – 16 September 2012. 170 pages.
No. 292 – Pichler, T., Häusler, S. and Tsuonis, G. (2013). Abstracts of the 3rd International Workshop "Research in Shallow Marine and Fresh Water Systems". 134 pages.
No. 293 – Kucera, M. and cruise participants (2013). Cruise report of RV Sonne Cruise SO-226-3. Dip-FIP - The extent and structure of cryptic diversity in morphospecies of planktonic Foraminifera of the Indopacific Warm Pool. Wellington – Kaohsiung, 04.03.2013 - 28.03.2013. 39 pages.
No. 294 – Wienberg, C. and cruise participants (2013). Report and preliminary results of R/V Poseidon cruise P451-2. Practical training cruise onboard R/V Poseidon - From cruise organisation to marine geological sampling: Shipboard training for PhD students on R/V Poseidon in the Gulf of Cádiz, Spain. Portimao – Lisbon, 24 April – 1 May 2013. 65 pages.
No. 295 – Mohtadi, M. and cruise participants (2013). Report and preliminary results of R/V SONNE cruise SO-228, Kaohsiung-Townsville, 04.05.2013-23.06.2013, EISPAC-WESTWIND-SIODP. 107 pages.
No. 296 – Zonneveld, K. and cruise participants (2013). Report and preliminary results of R/V POSEIDON cruise POS448. CAPRICCIO – Calabrian and Adriatic Past River Input and Carbon ConversIOn In the Eastern Mediterranean. Messina – Messina, 6 – 23 March 2013. 47 pages.
No. 297 – Kopf, A. and cruise participants (2013). Report and preliminary results of R/V SONNE cruise SO222. MEMO: MeBo drilling and in situ Long-term Monitoring in the Nankai Trough accretionary complex, Japan. Leg A: Hong Kong, PR China, 09.06.2012 – Nagoya, Japan, 30.06.2012. Leg B: Nagoya, Japan, 04.07.2012 – Pusan, Korea, 18.07.2012. 121 pages.
No. 298 – Fischer, G. and cruise participants (2013). Report and preliminary results of R/V POSEIDON cruise POS445. Las Palmas – Las Palmas, 19.01.2013 – 01.02.2013. 30 pages.
No. 299 – Hanebuth, T.J.J. and cruise participants (2013). CORIBAR – Ice dynamics and meltwater deposits: coring in the Kveithola Trough, NW Barents Sea. Cruise MSM30. 16.07. – 15.08.2013, Tromsø (Norway) – Tromsø (Norway). 74 pages.
No. 300 – Bohrmann, G. and cruise participants (2014). Report and Preliminary Results of R/V POSEIDON Cruise P462, Izmir – Izmir, 28 October – 21 November, 2013. Gas Hydrate Dynamics of Mud Volcanoes in the Submarine Anaximander Mountains (Eastern Mediterranean). 51 pages.
No. 301 – Wefer, G. and cruise participants (2014). Report and preliminary results of R/V SONNE Cruise SO219A, Tohoku-Oki Earthquake – Japan Trench, Yokohama – Yokohama, 08.03.2012 – 06.04.2012. 83 pages.
No. 302 – Meinecke, G. (2014). HROV: Entwicklung und Bau eines hybriden Unterwasserfahrzeugs – Schlussbericht. 10 pages.
No. 303 – Meinecke, G. (2014). Inverse hydroakustische USBL-Navigation mit integrierter Kommunikation – Schlussbericht. 10 pages.
No. 304 – Fischer, G. and cruise participants (2014). Report and preliminary results of R/V POSEIDON cruise POS464, Las Palmas (Canary Islands) – Las Palmas (Canary Islands), 03.02.2014 – 18.02.2014. 29 pages.
No. 305 – Heuer, V.B. and cruise participants (2014). Report and preliminary results of R/V POSEIDON cruise POS450, DARCSEAS II – Deep subseafloor Archaea in the Western Mediterranean Sea: Carbon Cycle, Life Strategies, and Role in Sedimentary Ecosystems, Barcelona (Spain) – Malaga (Spain), April 2 – 13, 2013. 42 pages.
No. 306 – Bohrmann, G. and cruise participants (2015). Report and preliminary results of R/V METEOR cruise M112, Dynamic of Mud Volcanoes and Seeps in the Calabrian Accretionary Prism, Ionian Sea, Catania (Italy) – Catania (Italy), November 6 – December 15, 2014. 217 pages.
No. 307 – Fischer, G. and cruise participants (2015). Report and preliminary results of R/V POSEIDON cruise POS481, Las Palmas (Canary Islands) – Las Palmas (Canary Islands), 15.02.2015 – 03.03.2015. 33 pages.
No. 308 – Wefer, G. and Freudenthal, T. (2016). MeBo200 – Entwicklung und Bau eines ferngesteuerten Bohrgerätes für Kernbohrungen am Meeresboden bis 200 m Bohrteufe, Schlussbericht. 9 pages.
No. 309 – Sahling, H. and cruise participants (2016). R/V POSEIDON cruise POS498, Recovery of Observatories at Athina Mud Volcano, Izmir (Turkey) – Catania (Italy), 18 April – 1 May, 2016. 63 pages.
No. 310 – Fischer, G. and cruise participants (2016). Report and preliminary results of R/V POSEIDON cruise POS495, Las Palmas (Canary Islands) – Las Palmas (Canary Islands), 18.02.2016 – 02.03.2016. 29 pages.
No. 311 – Bohrmann, G. and cruise participants (2016). Report and preliminary results of R/V POSEIDON cruise POS499, Calabrian Mud Volcanoes, Catania (Italy) – Catania (Italy), 04 May – 22 May, 2016. 76 pages.
No. 312 – Kopf, A., Fleischmann, T. and cruise participants (2016). Report and preliminary results of R/V POSEIDON cruise POS500, LISA, Ligurian Slope AUV mapping, gravity coring and seismic reflection, Catania (Italy) – Malaga (Spain), 25.05.2016 – 09.06.2016. 58 pages.
No. 313 – Stegmann, S. and cruise participants (2017). Report and preliminary results of R/V POSEIDON cruise POS472, NORGEotech, Geotechnical in situ investigation of slope stability in Norway, Trondheim (Norway) – Tromsø (Norway), 27.07.2014 – 12.08.2014. 103 pages.
No. 314 – Bohrmann, G. and cruise participants (2017). R/V MARIA S. MERIAN Cruise Report MSM57, Gas Hydrate Dynamics at the Continental Margin of Svalbard, Reykjavik – Longyearbyen – Reykjavik, 29 July – 07 September 2016. 204 pages.